NNT: 2016SACLC024

THÈSE DE DOCTORAT
DE L'UNIVERSITÉ PARIS-SACLAY,
préparée à Centrale-Supelec

ECOLE DOCTORALE N°575

Electrical, optical, bio-physics and engineering

Spécialité de doctorat: Génie électrique

Par:

Carmen Cardozo

Optimisation of power system security with high share of variable renewables.

Consideration of the primary reserve deployment dynamics on a Frequency Constrained Unit Commitment model

Thèse présentée et soutenue à Gif-sur-Yvette, le 10 mars 2016 :

Composition du Jury:

M. M. O'Malley	Professeur, University College Dublin	Rapporteur
M. R. Caire	Maître de conférences, Grenoble INP	Rapporteur
M. J. Malick	CR CNRS, LJK	Examinateur
M. M. Kieffer	Professeur, Université Paris-Sud	Président du jury
M. W. van Ackooij	Expert chercheur, EDF R&D	Encadrant de thèse
M. P. Dessante	Professeur, Centrale-Supelec	Directeur de thèse

A mis abuelas,
Minerva y Carmen,
A mi padre César,
A mi ahijado CJ.

Executive Summary

The Unit Commitment problem (UC) is a family of optimisation models for determining the optimal short-term generation schedule to supply electric power demand with a defined risk level. Historically, the formulation of this problem has unceasingly evolved driven by the simultaneous growth of the electrical systems and the capabilities of solving complex optimisation problems. Nowadays, the research on this topic remains a key element to address the needs of future power systems by including a more accurate representation of their practical environment in operational tools.

The UC objective function is given by the operational costs over the optimisation horizon. The constraints include, among others, technical, operational and security limits. Traditionally, the security constraints are given by the requirement of a certain volume of on-line spare capacity, which is called the reserve. The reserve is meant to handle uncertainty, such as load forecasting errors, and unit failures, while preventing the interruption of power supply. It is commonly specified following static reliability criteria, which define the acceptable risk level. The most widespread criterion for the primary reserve prescription is given by the N-1 rule, which enforces a minimal reserve requirement as a function of a reference incident, such as the loss of the largest power input. Then, the reserve constraint is meant to ensure that the system can withstand the reference incident without load disconnection. The specific allocation of the reserve is generally optimised within the scheduling procedure, although the reserve constraint does not represent the complexity of the underlying physical processes. The main reason for this choice is related to the computational tractability of the UC problem. In practice, this problem needs to be solved in a time compatible with short-term scheduling. However, depending on the nature of the objective and constraint functions, UC models may be formulated as Mixed-Integer Non-Linear Programming (MINLP) problems, which are challenging to solve and ever more so, as the size of the system grows. Hence, affine approximations have been generally used, since this hypothesis enables the employment of commercial MILP solvers that are known to be effective and reliable. In addition, the simplified security constraints, such as the reserve constraint, permit to obtain UC solutions that naturally offer an acceptable transient response in large systems. Therefore, this representation was considered to provide a good trade-off between accuracy and computational complexity. Nevertheless, in small systems the fixed, and a priori defined, reserve constraint could entail a violation of the N-1 criterion, although the reserve constraint was met.

Indeed, following a large disturbance, such as a generating unit outage, the system frequency drops due to the power imbalance. The initial gradient of this drop is limited by the inertia of the on-line synchronous generators. Then, the primary frequency control automatically (and locally) increases the power output of the units designated to provide this service, until the power balance is regained and the system frequency is stabilised.

If this process fails to keep the frequency above a certain threshold, the under frequency protection relays placed in power stations may shed some load to prevent the system collapse. This action is called Under-Frequency Load Shedding (UFLS), and it is meant to deal with events that are more severe than the reference incident. However, in small systems, with low inertia, the dynamic of the deployment of the primary reserve may be too slow to restore power balance before the frequency threshold is reached. Hence, UFLS could take place following a single contingency because the primary reserve constraint does not represent the actual needs of the system.

More recently, the increasing share of variable generation from renewable sources (V-RES), such as wind and solar, may lead to UC solutions that no longer ensure system security. On the one hand, V-RES produce a variable power output that has low controllability and is only partially predictable. On the other hand, they tend to be asynchronously connected to the grid through power electronics, which prevents them to naturally contribute to the system inertia and may deteriorate the system's dynamic behaviour. Hence, non-synchronous generation may increase the risk of UFLS.

Different impact mitigation techniques have been proposed in literature, which include the revision of UC models to provide a better representation of the system dynamics. This subfamily of UC models will be here referred to as the frequency constrained UC problem (FCUC), since they aim to keep the frequency above a certain threshold, following predefined contingencies, by adding enhanced security constraints. However, the frequency minimum, also called the frequency nadir, constraint is strongly non-linear.

In this work this issue is tackled in four parts. The first part analyses the non-linear relation between the frequency and the decision variables of the UC model through the sequential simulation of a classic UC model and a reduced order model of the primary frequency response. It is verified that the behaviour of the frequency nadir regarding the binary decision variables is hard to approximate by analytical functions. This is the reason why FCUC models are generally based on indirect constraints over certain dynamic parameters of the generating units, which in addition preserve the MILP structure of the optimisation problem.

The second part of this work assesses the impact of V-RES generation on the primary frequency response of an isolated power system. The augmentation of the UFLS risk with the share of non-synchronous generation is verified, which highlights the need for a more accurate representation of the security constraint in optimisation models.

The third part of this work examines the cost/benefit and limitation of some FCUC models that are characterised by the activation of a certain lever. A methodology is proposed that assesses the effectiveness and optimality of some existing V-RES impact mitigation techniques, such as the increase of the primary reserve requirement, the prescription of an inertia requirement, the authorisation of V-RES dispatch-down or the consideration of fast non-synchronous providers of frequency regulation services. It is shown that, although the enforcement of enhanced security constraints over certain parameters can produce secure schedules at some instants, the opposite effect may appear under different conditions. Moreover, a specific lever may be more economical than other in some instances and vice versa. Finally, this study highlights the need for new methods to properly handle the frequency nadir constraint in order to ensure optimality, without compromising the optimisation problem's tractability.

Hence, the fourth part of this work offers a new formulation of the FCUC problem following a Benders' decomposition approach. This method is based on the decomposition of an optimisation problem into two stages. The first stage, called the master problem, fixes some variables, which makes the second stage, or slave, problem easier to solve. Here, the master problem deals with the generating unit states and the slave problem handles the frequency nadir constraints through a cutting plane model. The underlying hypothesis is that the frequency nadir is supposed to be a concave function of the units' power levels, at fixed commitment decisions. Simulation results illustrate the capability of the proposed formulation to optimise the allocation of different primary frequency regulation resources. The more accurate representation of the frequency nadir in the slave problem reduces the risk of UFLS and the security cost, with respect to other FCUC models, such as those based on inertia constraints. In addition, the optimality of the global solution is guaranteed; although the convergence of the master problem is slow, due to the well-known tailing off effect of cutting plane methods.

Future developments include the implementation of stabilisation algorithms, based on bundle methods for instance, to improve the convergence properties of the proposed FCUC formulation. The industrialisation of this approach may increase the system capability of integrating non synchronous renewable generation, while ensuring an economical and secure operation.

Acknowledgements

I would like to thank Professor Mark O'Malley for reviewing this work. The work that you have conducted with your many collaborators in the study of frequency regulation issues with renewables in the Irish system has left solid foundations for other researches, such as myself, to build up our contribution on this important topic.
Au même titre, je tiens à remercier M. Raphaël Caire pour avoir apporté son regard expert et critique sur ce travail. Vos remarques ont permis d'améliorer la version finale de ce manuscrit. Je remercie aussi les autres membres du jury, professeur Michel Kieffer et M. Jérôme Malick pour avoir pris le temps d'évaluer l'ensemble de ces travaux de thèse, ainsi que pour la qualité des échanges scientifiques que nous avons eu lors de la soutenance.
Je souhaiterais ensuite exprimer ma gratitude aux équipes au sein desquels j'ai passé ces trois dernières années. D'une part, je remercie l'accueil du laboratoire GeePs, spécialement à Philippe Dessante et Marc Petit, ainsi qu'à l'ensemble des doctorants qui ont fait de ce campus en travaux un endroit d'échange et de partage. Nos pauses café et nos voyages occupent déjà une place privilégiée de mon coffre à souvenirs.
D'autre part, je remercie le groupe R12 du département EFESE (EDF R&D), car il est toujours agréable de se lever le matin sachant que l'on croisera au travail des gens compétents et ayant de grandes qualités humaines.
Dans les deux cas, j'ai une pensée qui me vient du cœur pour les secrétaires, Stéphanie Douesnard au GeePs, et Suzanne Picquenard à R12, des femmes charmantes qui rendent notre quotidien beaucoup plus simple. De plus, je remercie l'ANR pour le financement de ces travaux dans le cadre du projet APOTEOSE.
Je dois toute ma reconnaissance à Laurent Capely et Wim van Ackooij. Laurent, tu as apporté ton expertise technique et tu as su rester bienveillant pour le suivi des travaux ainsi que dans toutes les activités annexes à la thèse. Wim, j'ai été ravie de découvrir des nouveaux outils dans le domaine de l'optimisation à tes côtés, tu nous as rejoints en fin de thèse et grâce à ton engagement tu as pu nous apporter un fort contenu scientifique. Il a été un vrai plaisir de travailler avec vous, vous m'avez beaucoup appris.
Je tiens à souligner quelques personnes qui ont été impliquées dans ce projet à différents niveaux et que d'une façon ou d'une autre ont apporté leur pierre à l'édifice qui est cette thèse : Gauthier Delille, Gilles Malarange, Maria Giralt Devant, Christophe Santander, Herman Bayem, Julien Pesturi, ainsi que des personnes qui ont toujours eu leur porte ouverte pour répondre à mes questions, en apportant leur savoir-faire. Je pense notamment à Etienne Monnot, Gregoire Prime et Vera Silva, Sébastien Finet et Thomas Triboulet.

Enfin, je tiens à remercier mes proches, ma co-bureau Héloïse, à Marjorie, pour toutes ces discussions et relectures. A mon conjoint et sa famille, pour votre soutien, Merci !... A mes amis du M2R PIE, pour les voyages au ski, pour tous ces pots de thèse durant cette dernière année, et vos apports à la communauté scientifique, évidement !
A mis amigos de aquí, Maialen, Charlotte y las chicas de los brunch, a los de *longue date*, Gilbert Bergna (finalmente es por ti que estoy aquí!), Luis Diaz (por el apoyo moral esos fines de semana de trabajo) y Rafael Requena (por la fiesta, el vino y la salsa!), les digo mil gracias por su apoyo.
Para terminar, dedico estas últimas líneas a mi familia. Lo más difícil de esta tesis ha sido estar lejos de ustedes. Les agradezco por sus mensajes de apoyo y los regalitos envíados con los viajeros que me trajeron olores, sabores y sentires de casa. Por su confianza y amor, gracias!
Agradezco especialmente a mis hermanos y cuñadas por las notas de voz de mi ahijado que todavía escucho frecuentemente, y a Zaida por las incontables horas al teléfono cuando las noches se volvían muy largas. Por ultimo agradezco a mi padre por su ejemplo y apoyo incondicional a lo largo de todos estoy años, sin ti los logros que me han traído hasta aquí no hubiesen sido posibles.

Synthèse

Optimisation de la sûreté d'un système électrique en présence des énergies renouvelables intermittentes.

Intégration de contraintes de déploiement de la réserve primaire dans un outil journalier de placement de production.

1. Introduction

Dans un système électrique la fréquence doit rester aux alentours de sa valeur nominale. Cependant, elle peut subir des excursions importantes lors de certains événements, comme par exemple, l'arrêt fortuit d'un groupe de production. Dans ce cas, la fréquence du système chute car l'énergie manquante est tout d'abord compensée par la libération d'une partie de l'énergie cinétique stockée dans les masses tournantes raccordées au réseau qui ralentissent (par exemple, des générateurs synchrones).

Ensuite, la **régulation primaire de fréquence** augmente la puissance produite par les unités désignées pour fournir ce service (et ayant de la marge pour le faire) de façon automatique et locale. On appelle cette marge « réserve primaire ». La régulation primaire de fréquence permet alors de rétablir l'équilibre entre l'offre et la demande et de stabiliser ainsi la fréquence. La réserve primaire est souvent dimensionnée pour faire face à un incident de référence, tel que la perte de la plus grosse unité (critère N-1).

Dans le système interconnecté européen, par exemple, la réserve primaire est dimensionnée à 3 GW, ce qui représente la plus importante perte de production instantanée survenue sur ce système électrique (perte des deux tranches N4 à Civaux le 21 août 2000). Si la régulation primaire ne parvient pas à maintenir la fréquence dans la plage acceptable, les relais fréquence-métriques placés dans certains postes sources délestent une partie de la consommation.

Cette action, appelée **délestage par sous-fréquence** (DSF), est conçue pour éviter l'effondrement du système lorsque survient un événement plus grave que l'incident de référence comme ce fut le cas lors de la séparation du réseau UCTE (*Union for the Coordination of the Transmission of Electricity*) en trois sous-réseaux le 4 novembre 2006.

Ces contraintes de sûreté, succinctement décrites, imposent donc des besoins en **réserve de puissance active** pour assurer la continuité de service des consommateurs malgré les aléas. Selon sa fonction, et notamment sa dynamique de libération, la réserve est souvent classifiée en trois types : primaire, secondaire et tertiaire.

Ces différentes catégories de réserve servent, dans un premier temps, à stabiliser la fréquence suite aux fluctuations de la demande et aux grandes perturbations. Dans un deuxième temps, elles ont pour but de ramener la fréquence et les échanges transfrontaliers aux alentours des valeurs nominales, ainsi que de rétablir les marges de sûreté.
Toutefois, la fourniture de ces réserves a un coût pour les producteurs et pour le système et elle doit être intégrée comme contrainte dans les modèles de **placement de production** (**UC** pour *Unit Commitment*) qui déterminent l'état et la puissance de consigne des groupes de production pour satisfaire la demande électrique à moindre coût.
La **prescription d'un volume prédéterminé de réserve** permet une formulation linaire de la contrainte de sûreté, et par conséquent une résolution de l'UC dans un temps compatible avec la conduite d'un système électrique grâce aux solveurs PLNE (programmation linéaire en nombres entiers) commerciaux efficaces et fiables (comme par exemple CPLEX, GUROBI, EXPRESS, etc.). Cependant, cela implique d'une part une **perte d'optimalité** du fait du comportement fortement non linéaire de la fréquence suite à une perte de groupe, et d'autre part, cela peut entraîner un **risque** pour le système dans le cas où la contrainte de sûreté devient inefficace pour prévenir le DSF.
En effet, dans le **système interconnecté** européen, le creux de fréquence suite à l'incident de référence ne doit pas atteindre les 49,2 Hz (pour un premier cran de délestage de la consommation réglé à 49 Hz). Ceci est illustré dans la figure 1 par la courbe bleue en trait plein, qui est déterminée pour des hypothèses conservatrices. Or, le comportement attendu de la fréquence lors de la perte d'une unité de production (1.3 GW) avec des hypothèses plus réalistes est montré par la courbe verte en pointillé.

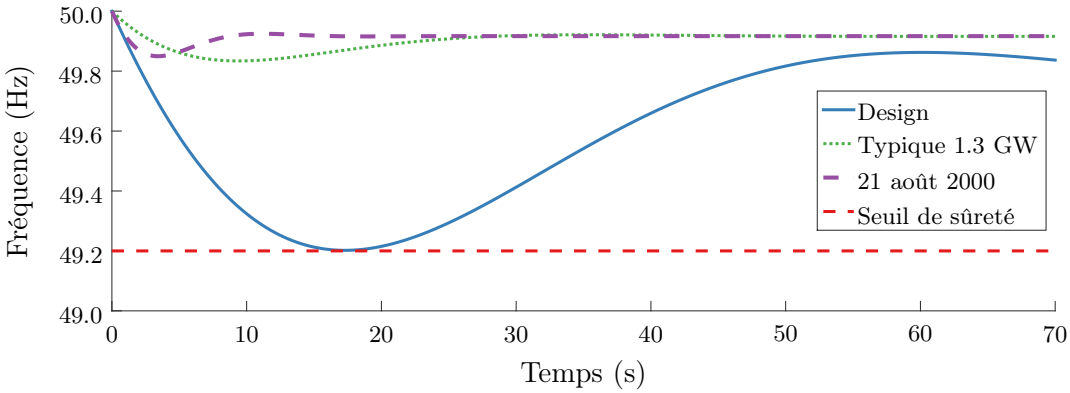

Figure 1: Comportement de la fréquence suite à un fort déséquilibre de puissance

De plus, les enregistrements des évènements graves survenus dans les dernières années montrent que la fréquence reste systématiquement bien au-dessus de ce seuil (courbe violette discontinue). Donc, la formulation d'un besoin fixe en ressource de régulation primaire de fréquence s'avère, en général, surdimensionné au regard des vitesses de réaction des groupes de production participant à la régulation primaire de fréquence et à l'auto-adaptation de la puissance appelée par les charges lors d'une baisse de fréquence.

A contrario, dans les **petits systèmes non-interconnectés**, une part importante des délestages de charge survient alors que la réserve primaire disponible est supérieure au volume de production perdu. En effet, lorsque la dynamique de libération de la réserve primaire est trop lente par rapport au gradient de fréquence, le seuil d'activation du DSF peut être atteint, avant que l'équilibre de puissance ne soit rétabli. Ceci est illustré par la courbe verte pointillé dans la figure 2 pour un seuil de sûreté défini à 49 Hz.

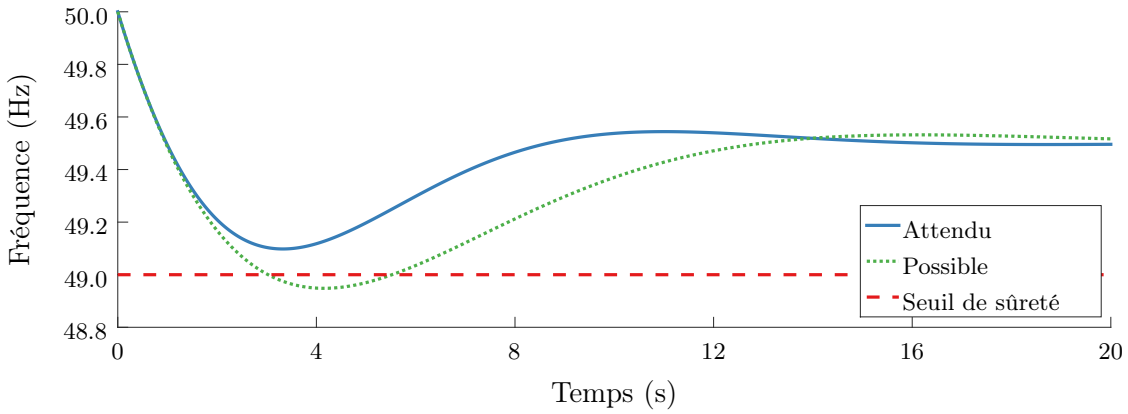

Figure 2: Comportement de la fréquence suite à un fort déséquilibre de puissance

Les productions à partir des **énergies renouvelables** (ENR) intermittentes, telles que les sources éoliennes ou photovoltaïques, produisent une puissance variable peu contrôlable et peu prévisible. Elles sont, de plus, principalement raccordées de manière asynchrone au réseau à travers une chaîne de conversion de puissance, ce qui les empêche de contribuer naturellement à l'inertie du système. Enfin, elles ne participent que très rarement à la fourniture des services système. Il est donc de plus en plus nécessaire de recourir à l'écrêtement de ces productions pour garantir la sûreté y compris dans de grands systèmes électriques. Pour faire face à ces changements dans le fonctionnement des systèmes électriques, différentes techniques d'atténuation des impacts des ENR ont été proposées dans la littérature. On s'intéresse notamment à l'amélioration des modèles de placement de la production pour inclure une représentation plus fine de la dynamique du système.

Problématique traitée et plan de la synthèse

Une contrainte de sûreté capable d'intégrer les paramètres dynamiques des groupes dans l'outil de placement de la production pourrait permettre d'optimiser le placement de la réserve tout en garantissant l'absence de recours au DSF en cas de perte unitaire de groupe. Pour désigner cette famille de problèmes UC, le terme FCUC (*Frequency Constrained Unit Commitment*) sera utilisé. Dans l'absolu, il s'agirait d'une contrainte directe sur le creux de fréquence. Malheureusement, la formulation de cette contrainte pose de nombreux défis, qui sont discutés dans la **partie 2** de cette synthèse.

En effet, le **comportement du creux de fréquence par rapport aux variables de décision du problème UC** est non-linéaire et difficile à approcher par des fonctions analytiques. Ceci est mis en évidence dans cette première partie de travaux par la formulation de différents modèles dynamiques. La relation qui lie les creux de fréquence et les variables de décision du problème de placement de la production est ensuite caractérisée à l'aide d'une chaîne de simulation séquentielle basée sur un modèle UC classique et un modèle dynamique adapté qui permet d'estimer l'évolution de la fréquence suite à des forts déséquilibres de puissance.

L'**impact des sources non-synchrones sur l'évolution de la fréquence** et la diminution de l'efficacité de la réserve primaire sont ensuite discutés dans la **partie 3**. Les processus sous-jacents qui conduisent à l'augmentation du risque de DSF sont minutieusement analysés. Le besoin de formuler des modèles de FCUC plus précis est mis en avant.

La **partie 4** porte alors sur l'**évaluation de différents modèles FCUC**, basés sur des contraintes indirectes (volume réserve, inertie minimale, etc.) permettant de préserver la structure PLNE de l'UC. Une étude paramétrique permet de tirer des conclusions sur le coût, les bénéfices et les limitations des différentes mesures palliatives proposées dans la littérature. Il est par exemple mis en évidence que, si l'ajout de contraintes indirectes permet d'atteindre le niveau de sûreté recherché dans certains pas horaires, les modifications apportées sur le plan de production peuvent induire des effets néfastes sur des pas horaires adjacents. De plus, pour limiter les risques de DSF, il peut être plus économique de placer la réserve primaire sur des groupes ayant des temps de réponse courts plutôt que d'accroître l'inertie du système ou la prescription de réserve.

Ainsi, l'efficacité des leviers proposés dépend fortement du point de fonctionnement du système et il en est de même pour le coût de la solution. Il est donc nécessaire de développer une **nouvelle formulation du problème FCUC** pour traiter correctement la contrainte sur le creux de fréquence, tout en assurant l'efficacité et l'optimalité de la solution. Une approche basée sur une décomposition de Benders, et sur la construction de modèles de plans sécants est alors proposée dans la **partie 5** afin d'inclure directement des contraintes sur les creux de fréquence dans l'optimisation du plan de production.

Bien que ces contraintes soient en principe non linéaires, cette conception innovante permet d'optimiser le placement de production à l'aide de solveurs PLNE existants. On met en évidence l'efficacité d'une représentation plus précise du creux de fréquence sur la réduction du risque de DSF et sur le coût de la sûreté par rapport à d'autres modèles de FCUC tels que ceux à base de contraintes d'inertie.

L'augmentation de la part des ENR variables à sûreté maintenue et coût maîtrisé dans les futurs systèmes électriques passe ainsi par une représentation plus fine de la dynamique de déploiement de la réserve primaire dans les outils de placement de la production. Ces travaux de thèse apportent une contribution à ce sujet.

2. Placement de production et évolution de la fréquence lors d'un incident

Cette partie présente brièvement la première étape des travaux, décrite plus en détails dans le chapitre 2 du mémoire. Après avoir introduit le modèle UC (*Unit Commitment*) classique (partie 2.1) et en ayant pour objectif la formulation du problème FCUC (*Frequency Constrained Unit Commitment*), différents modèles d'ordre réduit de détermination de l'évolution de la fréquence (ROSFR pour *Reduced Order System Frequency Response*) ont été évalués (partie 2.2). Si la démarche visant à exprimer au mieux la fonction décrivant les creux de fréquence par rapport aux variables de décision de l'UC a montré ses limites, elle a tout de même apporté des éléments de réflexion utiles pour la suite des travaux.

Des indicateurs adaptés à la caractérisation de l'évolution de la fréquence ont pu être identifiés et diverses simulations numériques ont permis d'analyser leurs relations avec des grandeurs issues de l'UC (parties 2.3 et 2.4). Les conclusions et contributions de cette partie sont résumées dans les points 2.5 et 2.6.

2.1 Problème de placement de la production

Le placement de production (UC) est une famille de problèmes d'optimisation qui détermine l'état et la puissance de consigne des groupes de production pour satisfaire la demande électrique à moindre coût. En général, la fonction objectif du problème UC représente les coûts d'exploitation des groupes tout au long de l'horizon temporel d'optimisation. Les contraintes sont notamment d'ordre techniques, opérationnelles et de sûreté.

Historiquement, la formulation du problème UC a évolué de façon continue, entraînée par la croissance simultanée des systèmes électriques et des capacités à résoudre des problèmes d'optimisation complexes. Ce sujet est abordé dans la section 2.2 du mémoire. Aujourd'hui, l'UC est souvent exprimé comme un problème PLNE (programmation linéaire en nombres entiers) qui peut être décrit de façon générique par l'équation (1).

$$\begin{aligned} \underset{x \in X}{\text{minimiser}} \quad & f_0(x) \\ \text{sous les contraintes} \quad & f_\imath(x) \leq 0 \qquad \imath = 1, \ldots, i, \\ & g_\ell(x) = 0 \qquad \ell = 1, \ldots, l. \end{aligned} \tag{1}$$

- Les variables d'optimisation $x \in X \subseteq \mathbb{R}^M$ peuvent inclure, entre autres, l'état (démarré ou arrêté, noté u), les puissances de consigne de chaque unité de production (noté g), la réserve primaire placée sur une entité de réserve (qu'on note ici r^{pr}), des variables auxiliaires, telles que les décisions de démarrage/arrêt d'une unité déjà éteinte/allumée tout au long de l'horizon d'optimisation (notées x^{up} et x^{dn} respectivement).
- La fonction objectif $f_0 : \mathbb{R}^M \to \mathbb{R}$, représente, d'une façon plus ou moins détaillée, les coûts d'exploitation du système.

- Les contraintes $f_\imath(x) : \mathbb{R}^M \to \mathbb{R} \ \ \forall \imath = 1, \ldots, i$, sont appelées les contraintes d'inégalité et comprennent, entre autres, des limites techniques, opérationnelles et de sûreté.
- Les contraintes $g_\ell(x) : \mathbb{R}^M \to \mathbb{R} \ \ \forall \ell = 1, \ldots, l$, sont appelées les contraintes d'égalité. On y trouve, par exemple, l'équation d'équilibre entre l'offre et la demande.

La dimension M est un multiple entier du produit NT, où N est le nombre d'unités de production considérées et T est le nombre d'intervalles dans l'horizon d'optimisation. Dans la suite, les indices j et h seront associés respectivement aux unités de production et aux intervalles d'optimisation. Par exemple, $u = \left[u_1^1, \ldots, u_j^1, \ldots, u_N^1, \ldots, u_j^h, \ldots, u_N^T\right]$ est le vecteur d'état du parc de production. Ces composantes décrivent l'état (démarré=1, arrêté=0) de tout groupe j à tout pas horaire (demi-horaire ou autre) h.

2.2 Évolution de la fréquence et réponse primaire des groupes

L'évolution de la fréquence dans un système électrique suite à un incident constitue un phénomène électromécanique à l'échelle de quelques secondes qui est régi par l'équation de masses tournantes. Cette équation peut être formulée pour chaque groupe synchrone raccordé au réseau de la façon suivante :

$$J_j \frac{d\omega_j(t)}{dt} = C_{m,j}(t) - C_{e,j}(t), \tag{2}$$

où $C_{m,j}$ est le couple mécanique (moteur) exercé par la turbine du groupe j et $C_{e,j}$ est le couple électromagnétique (ou résistant) exercé par la charge, les deux exprimés en N.m. J est le moment d'inertie en Kg.m2 de l'unité j, ω_j est sa vitesse de rotation en rad/s et t représente le temps. La « fréquence du système » est définie en faisant la hypothèse 1 :

Hypothèse 1 *la vitesse de rotation de tous les groupes synchrones raccordés au réseau est la même.*

Cela implique que les oscillations locales autour de la fréquence fondamentale sont négligées. Suivant quelques déroulements algébriques (décrites dans la section 2.3 du mémoire), l'équation (2) peut être réécrite comme suit :

$$\frac{df(t)}{dt} = \frac{f_0^2}{2\left(\sum_{j=1}^N H_j S_{n,j} u_j^h(t)\right) f(t)} \left(\sum_{j=1}^N g_j^h(t) - D_f^h(t)\right). \tag{3}$$

L'évolution temporelle de la fréquence est alors décrite par une équation différentielle du premier ordre. Elle dépend de la fréquence nominale du système (f_0), de la constante d'inertie (H) et de la puissance apparente nominale (S_n) de chaque unité j raccordée au réseau, de la demande (D_f^h) ainsi que du plan de production à l'intervalle h (u^h,g^h).
On rappelle que $u \subseteq X$ est l'ensemble des variables binaires qui définissent l'état des groupes de production à chaque pas de temps (démarré ou arrêté) et $g \subseteq X$ leur puissance de consigne. L'apport en inertie de la charge pourrait aussi être inclue.

Dans ces travaux, on ne traite ni des erreurs de prévision de la demande, ni des ajustements infra journaliers. On considère alors que pour un pas de temps donné (intervalle d'optimisation h) la demande est fixe et égale à sa prévision (D_f^h). Dans ce cas, en-dehors de la perte d'un groupe, la fréquence ne varie pas car sa dérivée temporelle est nulle.
Cependant, dès les premiers instants qui suivent un déséquilibre de puissance dû à la perte de groupes de production, la somme des puissances de consigne devient inférieure à la demande et le gradient de fréquence devient négatif : la fréquence chute. Toutefois, au fur et à mesure que la fréquence varie en fonction du temps, la puissance des groupes réglant $g^h(t)$, ainsi que la demande $D^h(t)$, se mettent également à évoluer. Pour simuler l'évolution de ce système bouclé, la modélisation de ces deux dernières grandeurs doit être définie.
En ce qui concerne la réponse de la régulation primaire de fréquence, on s'inspire des travaux publiés dans la littérature, qui proposent des modèles d'ordre réduit permettant de calculer l'évolution de la fréquence. Les hypothèses, avantages et limites du modèle implémenté par rapport à ceux proposés dans la littérature sont regroupés dans le tableau 1. Ces aspects sont plus amplement discutés dans la section 2.3 du manuscrit.

Table 1: Modèles d'ordre réduit pour étudier l'évolution de la fréquence

Acronyme	Nom	Avantages	Inconvénients
EM-ROSFR	*Equivalent Machine*	Expression analytique du creux de fréquence	Paramètres équivalents difficiles à déterminer
MM-ROSFR	*Multi-Machine*	Représentation différenciée des unités de production	Pas de différentiation des réserve primaire/secondaire
MMR-ROSFR	*Multi-Machine-Regulation*	+ Saturation de la régulation	Complexité

Dans la première modélisation (EM-ROSFR), le système électrique dans son ensemble est représenté par un unique groupe synchrone équivalent. La régulation est modélisée par un contrôle proportionnel et une fonction de transfert qui représente le processus physique sous-jacent. L'évolution de la fréquence est alors modélisée par un système d'équations différentielles (ODE pour *Ordinary Differential Equation*) d'ordre 2. L'intérêt de ce modèle repose sur l'obtention d'une expression analytique pour le creux de fréquence, qui représente une aide à la compréhension de certains phénomènes. Cependant, cette expression reste non-linéaire, et elle ne peut donc pas être directement exploitée dans un modèle FCUC.
Des travaux récents cherchent à contourner cette difficulté au prix de fortes hypothèses. En particulier, les constantes de temps de toutes les unités de production sont considérées comme étant identiques afin de déterminer les paramètres du système équivalent. Or, on pressent que la dynamique de libération de la réserve primaire peut être un levier intéressant à exploiter dans la formulation du problème FCUC.
De plus, les creux de fréquence sont supposés convexes par rapport aux variables d'optimisation. Or, il est peu probable que les creux de fréquence soient jointement convexes par rapport aux états et décisions de démarrage/arrêt des groupes (variables binaires).

En conclusion, l'avantage du modèle EM-ROSFR ne peut pas être exploité dans la formulation du problème FCUC. De plus, ces limites compromettent l'optimalité et l'efficacité des solutions proposées. Par conséquent, il a été envisagé, dans un second temps, d'exploiter un modèle (MM-ROSFR) qui considère une représentation individuelle de la régulation de chaque unité de production (voir figure 3, où P_a est la puissance accélérante donnée par l'écart entre la production et la consommation, qui est ici représentée par P_c).

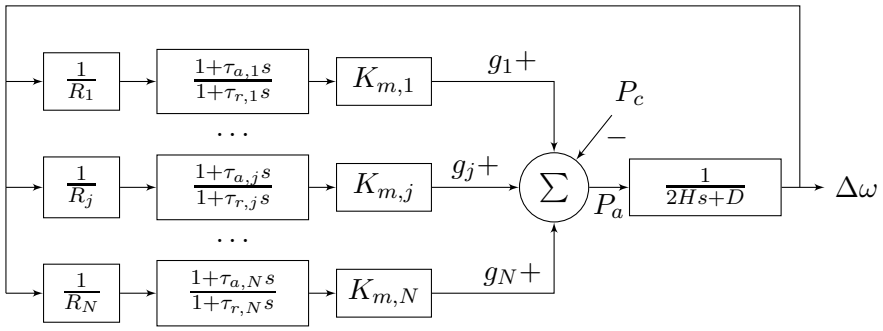

Figure 3: Diagramme général du modèle *Multi-machine ROSFR*

Les processus physiques sont identifiés par les facteurs de conversion de puissance K_m et l'auto-adaptation de la charge à la variation de fréquence D. La sensibilité de la régulation de puissance par rapport aux variations de la fréquence est déterminée par un gain proportionnel, appelé aussi statisme, représenté par le paramétré R dans la figure 3 (où toutes les grandeurs sont représentées en *per unit*).
On obtient alors un système d'équations différentielles d'ordre $N + 1$. Il ne reste plus qu'à identifier une méthode de résolution adaptée. A ce stade, l'utilisation d'une méthode d'intégration numérique devient incontournable. Cependant, ce modèle présente deux limitations majeures :

- il n'y a pas de limitation à la puissance pouvant être délivrée par une unité de production ;
- la régulation primaire de vitesse et le processus physique sont regroupés dans une seule et même cellule caractérisée par les constantes de temps τ_a et τ_r dans le figure 3.

Dans la mesure où les temps de calcul restent compatibles avec les exigences d'un futur outil opérationnel, il est souhaitable pour nos travaux de lever les deux limitations précédentes et d'utiliser un modèle dénommé MMR-ROSFR qui est illustré dans la figure 4.

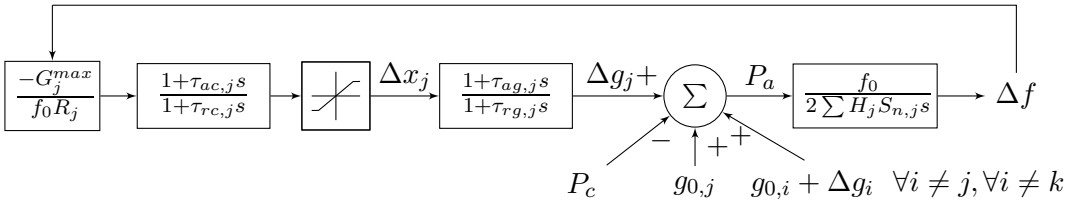

Figure 4: Diagramme général du modèle proposé (MMR-ROSFR)

L'équation (4) représente l'auto-adaptation de la charge en fonction d'un paramètre γ.

$$P_c(t) = D_f^h \left(\frac{f(t)}{f_0} \right)^{\gamma} \tag{4}$$

Le modèle proposé est un système ODE non linéaire d'ordre $2N + 1$, dont la résolution s'opère via un algorithme d'intégration numérique à pas fixe basé sur une méthode standard (Euler explicit), et implémenté sur MATLAB. Les détails de ces développements sont inclus dans l'annexe D. La partie suivante illustre le type de résultats qu'il est possible d'obtenir avec ces outils notamment dans le but d'étudier les relations entre le comportement de la fréquence et les variables de décisions de l'UC.

2.3 Relations entre l'évolution de la fréquence et l'UC

La figure 5 présente la chaîne de simulation appliquée au système test décrit dans l'annexe E. Il s'agit d'un petit système de type insulaire, ayant une demande maximale de 250 MW et disposant d'un parc de production composé de 18 unités thermiques regroupées en trois familles : les unités de base sont des centrales à charbon (groupes 11-14), les unités de semi-base fonctionnent au fioul lourd (1-10), et les unités de pointe sont des turbines à combustion au diesel (TAC, 15-18). Les unités fioul lourd sont elles-mêmes subdivisées en trois catégories selon leur taille.

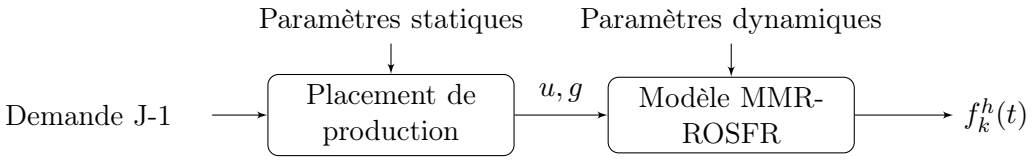

Figure 5: Chaîne de simulation

On appellera « programme d'appel » le résultat de la résolution du problème de placement de production (les deux vecteurs $u, g \in X$). Il est déterminé par un script MATLAB à l'aide d'un solveur PLNE commercial (GUROBI, avec un $MIPgap = 0.1\%$) prenant en considération les limites techniques des groupes de production telles que les puissances actives maximales (G_j^{max}), les niveaux minimaux de production stable (G_j^{min}), les limites de gradients horaires (R_j^{up} et R_j^{dn}), les temps minimaux de marche et d'arrêt (T_j^{up} et T_j^{dn}) et les allocations maximales de réserve primaire ($R_j^{pr,max}$).

De plus une allocation dynamique de réserve est considérée (éq. 5) : il s'agit de disposer à chaque pas de temps d'un volume de réserve permettant de compenser la perte de n'importe quel groupe démarré k. Ce mode d'allocation de la réserve permet à l'outil d'optimisation d'arbitrer entre une diminution de la puissance du plus gros groupe démarré et une augmentation du volume de réserve porté par les autres groupes pour faire face à sa perte.

$$\sum_{\substack{j=1 \\ j \neq k}}^{N} r_j^{h,pr} \geq g_k^h \qquad \forall k = 1, \ldots, N, \forall h = 1, \ldots, T. \tag{5}$$

Un exemple de programme d'appel est proposé figure 6c.

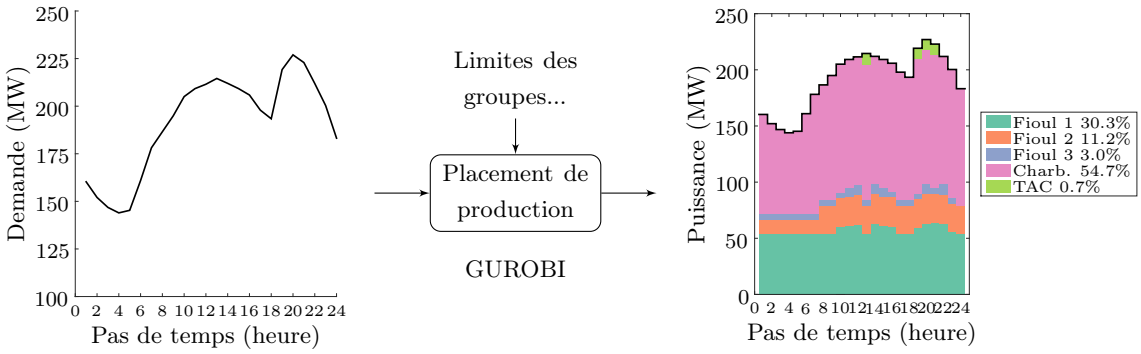

(a) Demande J-1 (b) Optimisation (c) Programme d'appel

Figure 6: Programmation de la production de la veille pour le lendemain

La figure 7a montre le détail du placement de la production, de la réserve primaire et de la marge supplémentaire pour un pas de temps spécifique (heure 13). Il est à noter que dans ce cas d'application, on considère un système insulaire où les réserves secondaire et tertiaire sont confondues (marge). De plus, aucune prescription minimale sur cette grandeur n'est imposée. Cependant, une marge involontaire est souvent dégagée dans la satisfaction des autres contraintes.

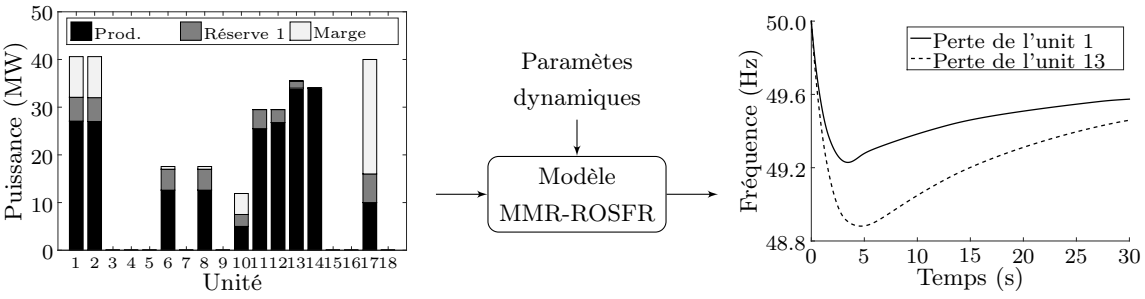

(a) Programme d'appel heure 13 (b) Modèle dynamique (c) Fréquence

Figure 7: Évolution de la fréquence suite à la perte d'un groupe de production

L'évolution de la fréquence suite à la perte de chaque unité de production démarrée k est évaluée, pour le pas de temps considéré (13 heure), à l'aide du modèle dynamique (MMR-ROSFR). Les paramètres nécessaires à la simulation incluent les limites de puissances (G_j^{max}) et de réserves actives ($R_j^{pr,max}$), les puissances apparentes nominales ($S_{n,j}$), les constantes d'inertie (H_j), les statismes (R_j), les constantes de temps des contrôleurs et des processus ($\tau_{ac,j}$,$\tau_{rc,j}$,$\tau_{ag,j}$,$\tau_{rg,j}$), ainsi que l'état initial du système (u,g). Un exemple d'évolutions de fréquence est proposé sur la figure 7c pour la perte des unités 1 et 13.

En conclusion, à partir de la détermination, par le modèle UC, d'un programme d'appel court-terme pour un certain profil de demande et un parc de production donné, le modèle MMR-ROSFR permet d'étudier le comportement de la fréquence suite à la perte d'une unité de production. La partie suivante décrit les grandeurs qui seront retenues pour caractériser plus largement ce comportement.

2.4. Caractérisation de l'évolution de la fréquence

Pour caractériser l'évolution de fréquence suite à une perte de groupe de production trois grandeurs peuvent être analysées à l'issue de la chaîne de simulation :

- le creux de fréquence (f_{min}) ;
- le gradient initial de la fréquence (*ROCOF* pour *Rate Of Change Of the Frequency*), dans les figures à venir le *ROCOF* sera représenté par sa valeur absolue ;
- les pas de temps où la fréquence est inférieure à un seuil de sûreté (*PIDR*, *Periods with Insufficient Dynamic Response*) et qui représentent donc le risque de DSF.

Afin d'obtenir une caractérisation statistique du système étudié, l'analyse peut également être réalisée sur une année calendaire par un enchaînement de 365 programmes d'appel. Puis, sur les 8760 pas horaires, le modèle MMR-ROSFR est mis en œuvre pour simuler la perte de chaque groupe démarré.
Avec l'implémentation développée dans ces travaux, pour le système test utilisé en considérant qu'il y a en moyenne entre 9 et 10 machines démarrées par pas horaire, les 80.000 simulations dynamiques peuvent être effectuées en moins d'une heure avec un ordinateur portable scientifique[1].
L'exemple proposé sur la figure 8, permet d'analyser l'impact du déséquilibre initial de puissance (*i.e.*, l'impact de la puissance de consigne de l'unité perdue, g_k), sur l'amplitude des creux de fréquence et sur le *ROCOF*. La taille du cercle indique le poids statistique de la classe. Comme attendu, les creux de fréquence deviennent plus profonds lorsque la puissance produite par l'unité perdue augmente. Le *ROCOF* augmente également avec le déséquilibre de puissance. Toutefois, pour un déséquilibre de puissance équivalent, ces deux grandeurs peuvent prendre des valeurs variées (on observe une dispersion verticale).

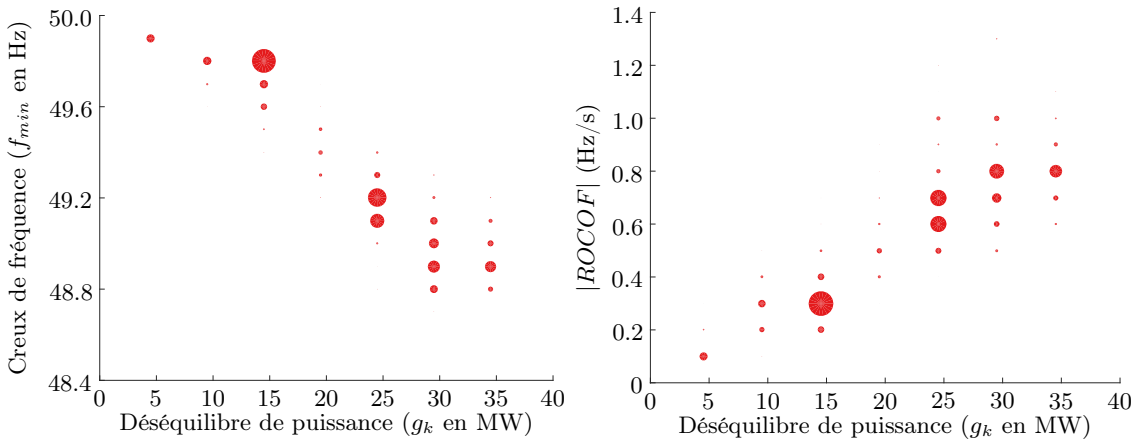

(a) Relation entre f_{min} et g_k

(b) Relation entre *ROCOF* et g_k

Figure 8: Relation entre les caractéristiques de la fréquence et les déséquilibres

[1] Hp EliteBook Workstation, Intel Core i5, 2.8GHz avec 16GB de RAM.

En général, cela est lié aux différents points de fonctionnements du système, qui se caractérisent par une demande et une inertie équivalente variables. S'il est possible d'établir une corrélation entre l'augmentation du $ROCOF$ et la baisse d'énergie cinétique disponible dans le système après la perte d'un groupe de production, il est plus difficile d'établir un lien entre la profondeur du creux de fréquence et l'inertie (voir figure 9).

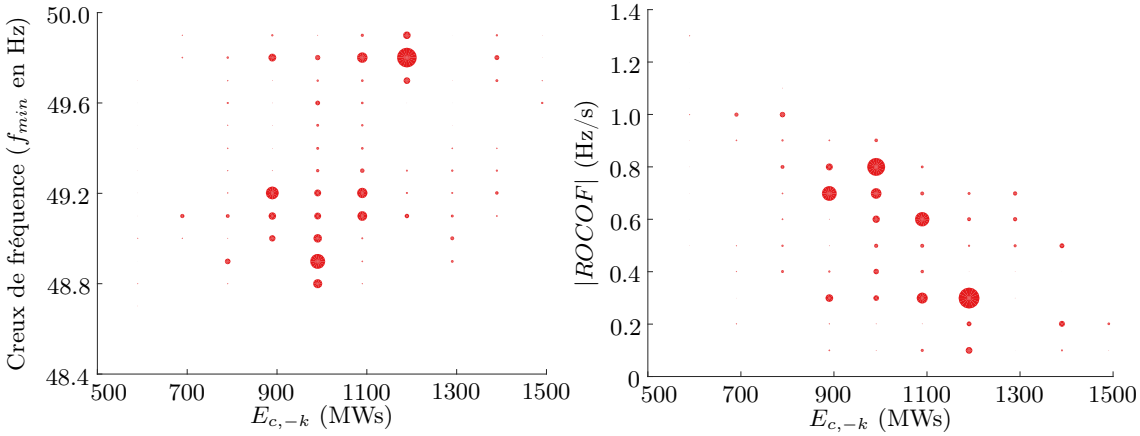

(a) Relation entre f_{min} et $E_{c,-k}$

(b) Relation entre $ROCOF$ et $E_{c,-k}$

Figure 9: Relation entre les caractéristiques de la fréquence et l'énergie cinétique

Enfin, si l'on cherche à relier $ROCOF$ et amplitude des creux de fréquence, on observe des creux de fréquence plus profonds au fur et à mesure que le $ROCOF$ augmente (figure 10). Il est à noter qu'une valeur de $ROCOF$ donnée est liée à un ratio entre le déséquilibre initial de puissance et l'énergie cinétique. Par ailleurs, on observe une dispersion verticale : pour une même valeur de $ROCOF$, la profondeur des creux peut varier de 400 mHz.

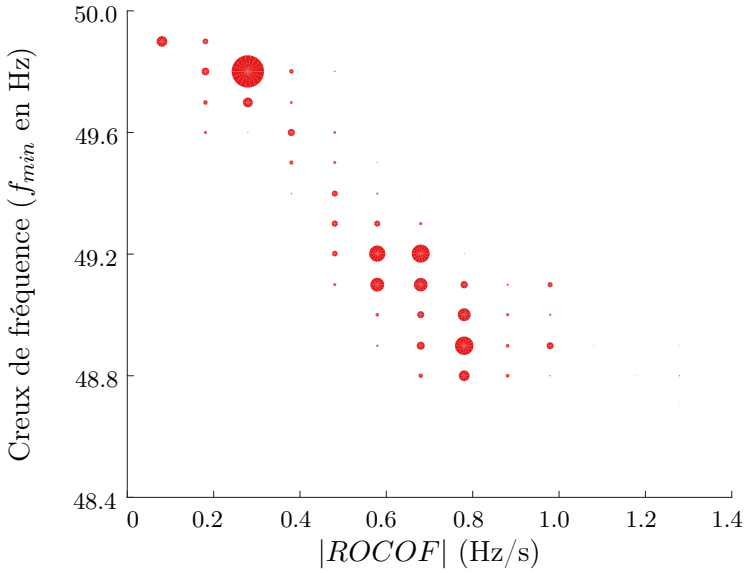

Figure 10: Relation entre les creux de fréquence et le $ROCOF$

D'autres paramètres interviennent donc dans l'évolution de la fréquence suite à une perte de groupe. En effet, $f_{min} = \mathcal{F}(u, g, D_f, \gamma, H, S_n, R, \tau, G^{max}, R^{pr,max}, f_0)$, sachant que u et g sont, à la fois, fonction des paramètres statiques et des différents coefficients de coût du parc de production. On pensera en premier lieu à la dynamique de libération de la réserve primaire, ici noté de façon générique juste τ.
Le risque de DSF, quantifié ici par l'indicateur $PIDR$, dépend évidemment du seuil de sûreté défini pour le système étudié. Dans le système test, si ce seuil était fixé en dessous de 48.75 Hz, l'indicateur $PIDR$ serait égal à zéro.

2.5. Conclusions de la partie 1

La fonction creux de fréquence est fortement non linéaire. De plus, il est difficile d'établir une expression analytique générique pour les creux de fréquence. Ceci rend le problème FCUC difficile à formuler.
Dans cette partie, trois grandeurs ont été proposées pour caractériser l'évolution de la fréquence suite à une perte de groupe. La relation entre l'amplitude des creux de fréquence, et donc le risque de recours au délestage fréquence-métrique, et les variables de décision du problème UC a été analysée au travers d'une étude empirique basée sur une simulation séquentielle des modèles UC et ROSFR. Il n'apparaît pas évident d'établir des liens directs entre ces grandeurs.

2.6. Contributions de la partie 1

1. Un modèle dynamique pour estimer l'évolution de la fréquence en cas de forts déséquilibres de puissance a été proposé. Bien que simplifié, il offre une modélisation plus fine des processus sous-jacents en comparaison avec ses prédécesseurs (EM/MM-ROSFR). Ceci permet de s'affranchir des certaines hypothèses qui limitaient auparavant la précision du modèle (voir annexe C du mémoire) par rapport aux besoins de nos travaux.
2. La relation entre le creux de fréquence et les variables d'optimisation du modèle UC a été formellement analysée. On a mis en évidence l'intérêt qu'il pourrait y avoir à exploiter d'autres leviers (comme par exemple la vitesse de libération de la réserve primaire), en plus de l'inertie pour maîtriser le creux de fréquence, et ainsi limiter le risque de DSF.
3. Un indicateur a été proposé pour quantifier le risque de délestage : le $PIDR$ (*Periods with Insufficient Dynamic Response*), donné par les pas de temps où la fréquence est inférieure à un seuil de sûreté. Ce nouvel indice permettra de quantifier la efficacité des différents modèles FCUC proposés dans la suite de travaux.

3. Impact des ENR sur l'évolution de la fréquence

L'intégration des ENR intermittentes, raccordées par le biais d'une chaîne de conversion de puissance dans un système électrique va modifier d'une part le programme d'appel des groupes conventionnels et d'autre part le comportement de la fréquence suite à une perte de groupe. Dans la mesure où, à l'heure actuelle, ces productions bénéficient dans les systèmes électriques français d'une obligation d'achat, le placement de production va évoluer de façon notable avec la puissance ENR intermittente installée. Dans cette partie, on étudie les conséquences de ces changements sur le coût de fourniture de la réserve primaire, ainsi que sur la performance de la régulation primaire de fréquence.

3.1. Impact sur les programmes d'appel

Pour différents scénarios de pénétration de la production photovoltaïque (PV) dans le système insulaire test (entre 0 et 250 MWc), les valeurs minimales, maximales et moyennes (sur l'année d'étude) du nombre d'unités démarrées par pas de temps sont proposées en figure 11a. Une représentation similaire de l'énergie cinétique stockée dans les masses tournantes raccordées au réseau est proposée en figure 11b.

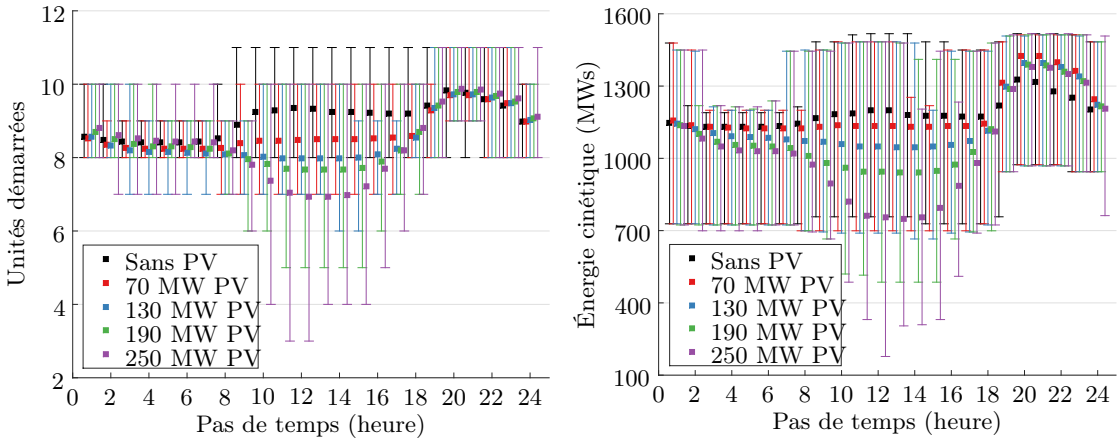

(a) Nombre d'unités démarrées

(b) Énergie cinétique stockée

Figure 11: Changement de programmes d'appel suite à l'intégration du PV

Outre la baisse attendue du nombre d'unités conventionnelles et de l'inertie pendant les heures ensoleillées, une réduction de l'inertie est observée en fin de nuit liée à l'anticipation de l'arrivée du PV. D'autres phénomènes bien connus, tels que la réduction de la marge disponible à la baisse et l'augmentation des arrêts et démarrages des groupes, sont plus largement discutés dans le chapitre 3 du mémoire.

3.2. Impact sur le comportement de la fréquence

L'impact des ENR sur le comportement de la fréquence est analysé par le biais des indicateurs définis précédemment suite aux simulations dynamiques. Les grandeurs physiques telles que les creux et les gradients de la fréquence, sont caractérisées statistiquement.

Les figures 12 et 13 présentent les valeurs minimales, maximales et moyennes des *ROCOF* et creux de fréquence respectivement. Si comme attendu, la fréquence a tendance à chuter plus rapidement avec de fort taux de PV (*ROCOF* plus élevé), la profondeur des creux de fréquence a quant à elle tendance à être, en moyenne, plus limitée, en raison de la réduction des niveaux de charge des unités de production conventionnelles. Cependant, la dispersion de cet indicateur augmente avec le taux de PV, ce qui entraîne une augmentation du risque de DSF du fait de valeurs extrêmes plus basses. Ce dernier point est illustré dans la figure 14 pour un seuil de sûreté de 48.75 Hz.

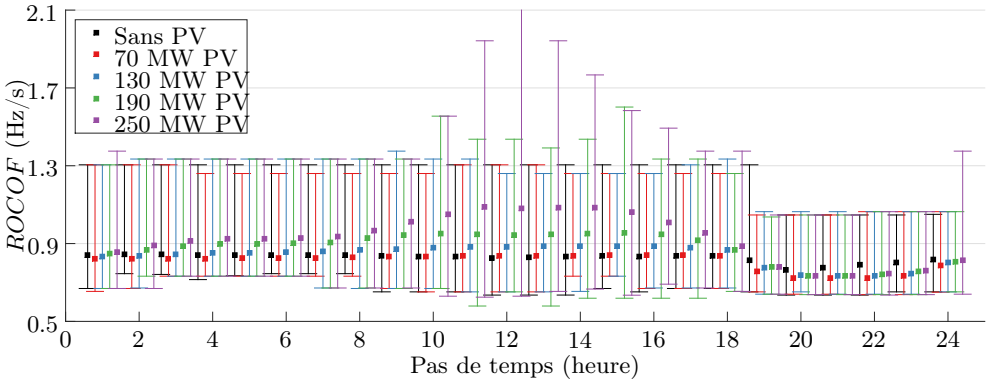

Figure 12: *ROCOF*

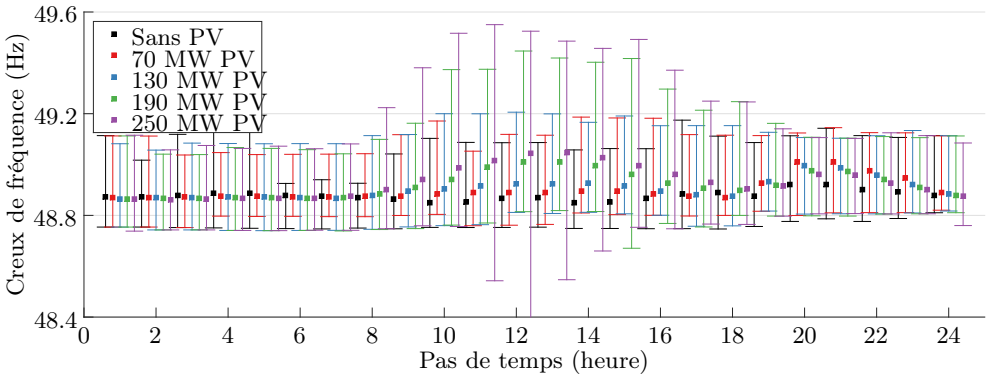

Figure 13: Creux de fréquence

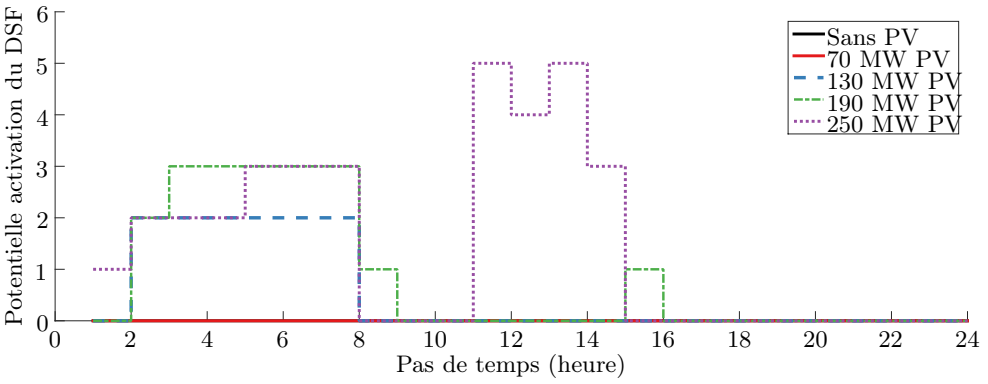

Figure 14: Potentielle activation du DSF suite l'intégration du PV

Des phénomènes moins intuitifs ont été identifiés, tels que la dégradation de l'évolution de la fréquence pendant la nuit causée notamment par une anticipation de la reprise de la production du PV et la nécessité de disposer alors de groupes plus flexibles, mais souvent de plus faible inertie.

3.3 Conclusions et tableau synthèse de la partie 2

La chaîne de simulation développée dans nos travaux permet de réaliser un placement optimisé de production au pas horaire sur une année calendaire puis d'analyser le comportement de la fréquence suite à des perte de groupe pour différents scénarios prospectifs. Ceci nous a permis de compléter les observations couramment rapportées dans la littérature concernant l'impact des ENR sur le fonctionnement des systèmes électriques.
En effet, aux changements attendus dans les programmes d'appel lors des périodes de production ENR s'ajoutent des risques accrus liés aux anticipations de reprise de production PV plus rarement évoqués, dû aux contraintes inter-temporelles, ainsi qu'une augmentation du coût de fourniture de la réserve primaire. Les résultats de simulation sont résumés dans le tableau 2 à titre d'illustration.

Table 2: Coût de fourniture et perte de performance de la réserve primaire

Scénario	Sans PV	70 MW	130 MW	190 MW	250 MW
Coût (%)	6.3	7.3	8.0	9.0	10.4
PIDR (h/an)	0	0	12	19	33

3.4 Contributions de la partie 2

1. Si les études d'impacts des ENR dans les systèmes électriques sont nombreuses dans la littérature, la très grande majorité d'entre elles se concentre sur des études statistiques visant à caractériser de nouveaux besoins en flexibilité. En ce qui concerne les études sur le comportement dynamique de systèmes électriques en présence des ENR, ils se limitent souvent à des études déterministes sur quelques points de fonctionnement précis. L'exploitation de l'outil développé dans cette partie de nos travaux offre une extension des approches méthodologiques existantes dans la littérature sur des problématiques moins profondément étudiées.
2. Les processus sous-jacents qui conduisent à l'augmentation du risque de DSF suite à l'intégration de la production non-synchrone ont été minutieusement analysés. Des phénomènes contra-intuitives ont été expliqués.
3. Le besoin de revoir les contraintes de sûreté afin d'augmenter la part des ENR variables à coût et risque maîtrisés a été mis en avant.

4. Analyse coût/bénéfices de différentes mesures palliatives

Dans cette partie, divers leviers sont évalués à travers une étude paramétrique afin de déterminer les meilleurs compromis entre l'augmentation du coût du plan de production et la réduction du risque de DSF. Cette analyse a été réalisée en ajoutant des contraintes dans l'outil de placement de production puis en analysant, comme proposé jusqu'à présent, l'évolution de la fréquence suite à la perte systématique de tous les groupes démarrés sur les 8760 pas horaires de l'année d'étude. De plus amples détails sont proposés dans le chapitre 4 du manuscrit.

Les simulations sont réalisées sur le système test retenu pour l'étude (annexe E du mémoire) et représentatif d'un petit système insulaire. Le stade d'activation du délestage fréquencemétrique est fixé à 48.75 Hz.

4.1 Augmentation de la prescription en réserve primaire

Étant donné que la réserve primaire est la principale ressource pour rétablir l'équilibre production-consommation et ainsi contenir la chute de fréquence, une première solution intuitive consiste à considérer une prescription fixe de réserve primaire puis à la faire augmenter de façon itérative jusqu'à ce que le risque de DSF soit inférieur à une limite choisie au préalable.

La figure 15 présente les coûts (ligne discontinue) et bénéfices (ligne continue) de cette mesure palliative pour différents scénarios d'intégration de PV dans le système test. Le coût a été normalisé par rapport au cas de référence, qui est défini par une allocation dynamique de réserve. Ces résultats ont été discutés dans les deux parties précédentes. Il est rappelé que pour ce cas de base le risque DSF était nul en l'absence de PV.

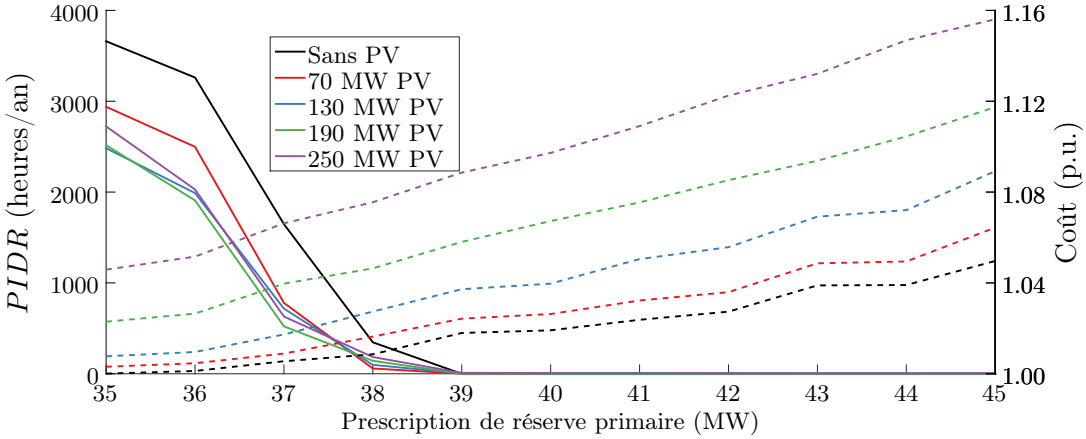

Figure 15: Coût et risque pour différentes prescriptions de réserve primaire

On constate que :

- le risque de DSF devient très important pour de faibles prescriptions de réserve même en l'absence de PV. En effet, pour des petits système, une prescription minimale

de réserve n'assure pas que cette réserve sera proprement placée pour compenser le déséquilibre de puissance produit pour les différentes situations $N-1$ possibles. En général, une allocation dynamique de réserve s'impose.

- L'intégration de PV a tendance à diminuer le risque de DSF pendant les heures ensoleillées. Ceci est dû au fait que les unités conventionnelles pourraient être appelées à faible puissance en présence de PV, et les potentiels déséquilibres de puissance deviennent donc moins significatifs.
- Le surcoût de cette mesure augmente avec la valeur de réserve prescrite et avec le développent des ENR.
- La prescription de réserve primaire devient inefficace à partir d'un certain niveau d'intégration d'ENR (voire figure 4.5 du manuscrit pour plus de détails).

Par ailleurs, pour de forts taux d'ENR et de fortes prescriptions de réserve permettant d'atteindre les risques de DSF recherchés, l'outil de placement n'est plus en mesure de proposer une solution satisfaisant l'ensemble des contraintes (cas de base sans écrêtement ENR possible). Ce manque de flexibilité dans les petits systèmes est souvent lié à la présence d'une puissance minimale démarrée sur les groupes de production. En pratique, l'écrêtement des source ENR s'imposerait avec une perte d'énergie propre et des potentielles conséquences économiques. Il semble alors nécessaire d'étudier d'autres moyens pour répondre à cette problématique en s'inspirant des travaux déjà publiés dans la littérature.

4.2 Contrainte sur l'énergie cinétique minimale dans le système

Une deuxième option consiste à ajouter une contrainte sur l'inertie, ou plus précisément sur l'énergie cinétique, dans le modèle UC. Plusieurs formulations peuvent être envisagées telles que décrites dans la section 4.2 du rapport.

De manière analogue à la contrainte de réserve fixe, il est possible de mettre en évidence un seuil à partir duquel une contrainte sur l'énergie cinétique stockée dans les masses tournantes en état $N-1$ peut devenir efficace pour maîtriser le risque de DSF.

Cette contrainte s'écrit pour chaque pas de temps h de l'horizon d'optimisation T ($h = 1, \ldots, T,$) et en cas de perte de chaque unité de production $k = 1, \ldots, N$. On observe que le coût et risque ont plutôt un comportement en marches d'escaliers pour un petit système (voir figure 4.9 du manuscrit pour plus de détails).

Si pour le système étudié cette mesure offre un meilleur compromis que la contrainte précédente, une fois encore, le coût de la sûreté augmente fortement avec le taux de pénétration d'ENR et des problèmes de faisabilité prédominent pour des prescriptions d'énergie cinétique élevées. Ceci est encore plus marqué que pour le cas de la prescription en réserve, ce qui limite fortement l'application opérationnelle d'une telle contrainte dans les petits systèmes.

Une forme plus sophistiquée de la contrainte d'inertie consiste à limiter le gradient initial de la fréquence (le *ROCOF* pour *Rate Of Change Of the Frequency*), qui dépend de l'énergie cinétique, mais aussi du déséquilibre de puissance. La figure 16 représente le coût et l'apport de cette contrainte. Dans ces travaux, le *ROCOF* est déterminé par la puissance de consigne de l'unité perdue, sachant que l'on considère la perte potentielle de chaque unité de production (voir la deuxième colonne du tableau synthèse, partie 4.5).

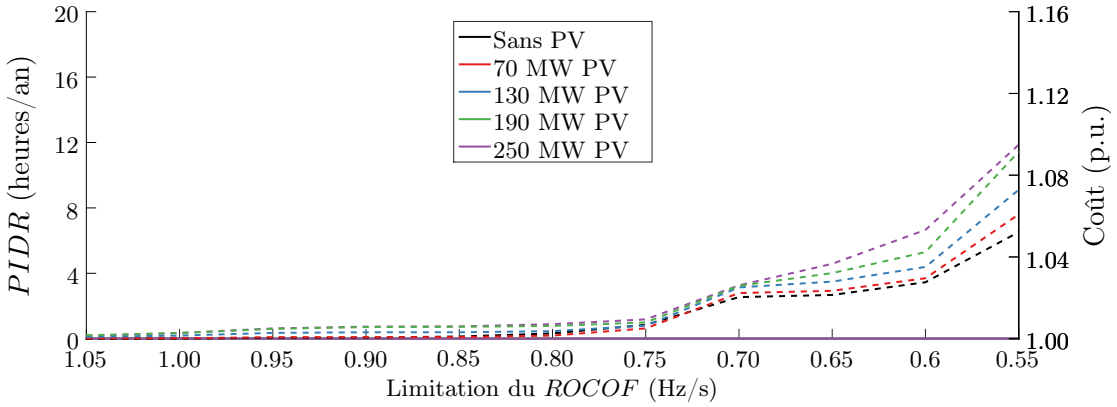

Figure 16: Coût et risque pour différentes valeurs de la limitation du *ROCOF*

Cette contrainte offre en effet une meilleure représentation du processus physique et elle permet d'atteindre un meilleur compromis coût/bénéfice que les précédentes.
Après avoir analysé l'impact des principales mesures palliatives directement liées à la contribution des groupes conventionnels, des solutions alternatives seront étudiées.

4.3 Soutien dynamique à la fréquence

La contribution de nouveaux acteurs à la régulation primaire de fréquence fait actuellement l'objet de nombreuses études et expérimentations principalement autour du stockage centralisé.
Cependant l'analyse proposée dans ces travaux peut être étendue à des sources ENR fournissant des services système, des agrégateurs de demande flexible, ou encore des véhicules électriques (*vehicule to grid*, V2G).
Pour le petit système test étudié, l'insertion d'un moyen fournissant de la réserve primaire avec une puissance minimale démarrée nulle permet de réduire de façon notable le coût annuel du plan de production (coût du stockage non inclus) et ce, quel que soit le taux de pénétration des ENR intermittentes (figure 17).
La diminution du gradient des diverses courbes avec la quantité disponible de stockage (C exprimée en MW) est en cohérence avec les diverses études mettant en évidence une diminution de la rentabilité du stockage avec son niveau de déploiement.
Après avoir mis en évidence l'intérêt économique du déploiement d'un stockage, en est-il de même vis-à-vis du comportement dynamique du système ?

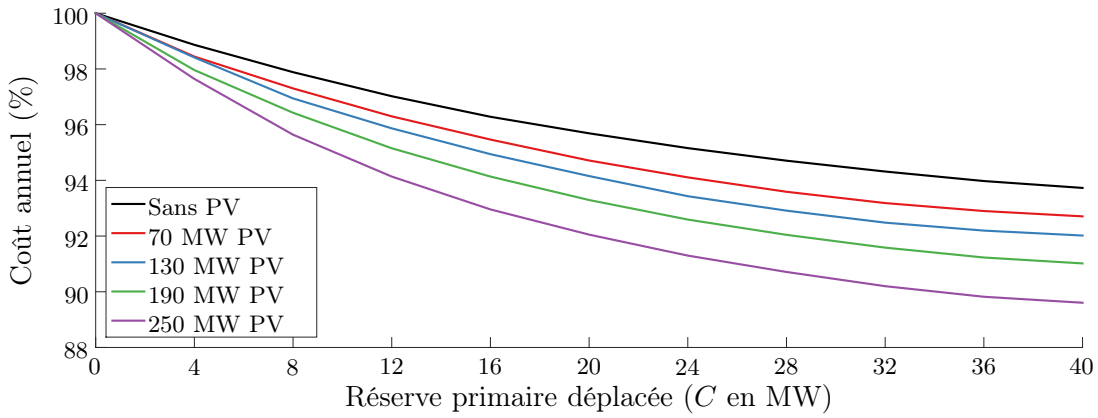

Figure 17: Réduction du coût opérationnel annuel avec du soutien dynamique

En étant raccordés par des interfaces à base d'électronique de puissance, les systèmes de stockage n'apportent pas d'inertie au système. De plus en venant se substituer aux groupes classiques de production pour la fourniture de la réserve, les systèmes de stockage contribuent à la réduction du nombre de machines connectées et à l'augmentation de la puissance produite par chacune d'entre elles. L'ensemble de ces impacts conduit donc à une augmentation des $ROCOF$ lors de pertes de groupe.

A titre d'illustration du phénomène et pour différentes valeurs de puissance nominale de stockage (C exprimée MW), les valeurs minimales, maximales et moyennes sur l'année des $ROCOF$ par pas horaire sont reportées sur la figure 18. Ces résultats correspondent à un cas sans PV dans le système test. En entraînant des chutes de fréquence beaucoup plus rapides seules des dynamiques extrêmement fortes de réponse en réglage primaire du stockage peuvent conduire à une amélioration du comportement dynamique du système.

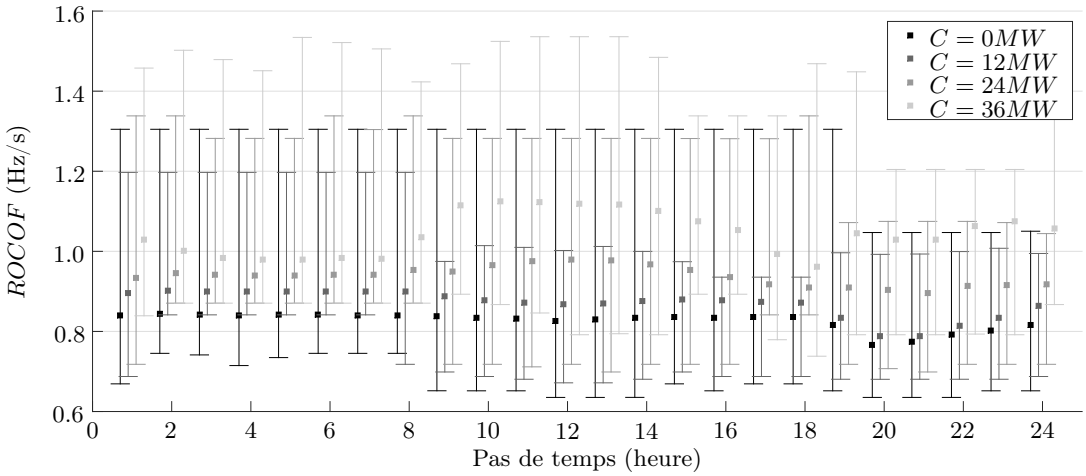

Figure 18: Évolution du $ROCOF$ par pas horaire avec soutien dynamique

Afin de déterminer le temps de réponse maximal au-delà duquel l'apport du stockage sur la dynamique du système serait insuffisant, le modèle présenté figure 19 a été retenu.

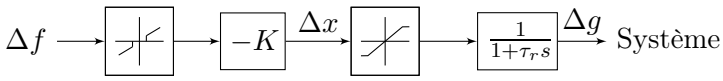

Figure 19: Diagramme général du modèle du soutien dynamique

Il s'agit d'un système avec une réponse du premier ordre, un contrôleur proportionnel, une bande morte et une saturation. Ce type de réponse a été volontairement choisi pour garder un caractère générique et permettre l'exploitation des résultats pour tout type de fournisseur potentiel de ce service de réserve primaire.

La constante K est adaptée en fonction de la puissance nominale C du stockage, de sorte à ce que toute la réserve primaire soit déployée pour une déviation de fréquence de 500 mHz. La bande morte est fixée à +200 mHz pour limiter la sollicitation du moyen de stockage, et ainsi préserver sa durée de vie. Comme le montre la figure 20, plus les constantes de temps sont faibles, moins les creux de fréquence sont profonds.

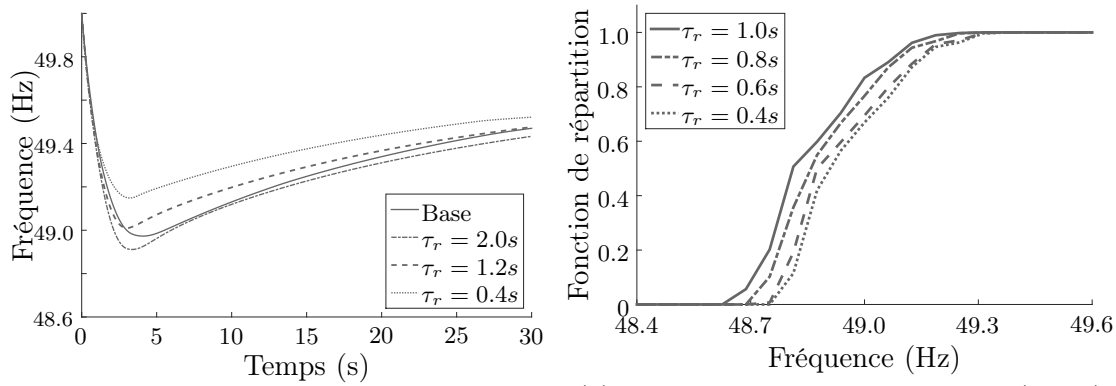

(a) Fréquence (perte de l'unité 14 à 13 h) (b) Fonction de répartition des creux (un an)

Figure 20: Fréquence pour différents temps de réponse (sans PV, $C = 12$ MW)

Pour chaque puissance nominale de stockage et d'ENR installées il est ainsi facile de déterminer la valeur maximale du temps de réponse permettant d'éliminer les risques de DSF pour un parc ENR installé. Cependant, avec l'accroissement de la puissance ENR installée, les *ROCOF* suite à des pertes de groupes deviennent plus importants (figure 21). Afin d'assurer une pérennité à l'efficacité des systèmes de stockage précurseurs, la spécification du temps de réponse maximal doit être réalisée en tenant compte d'un développement ambitieux et à long terme des ENR intermittentes.

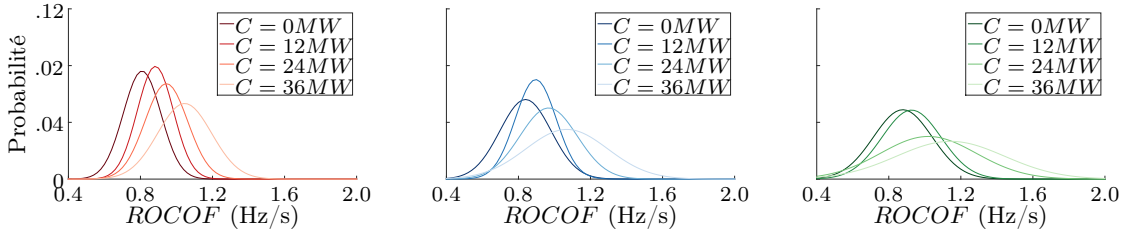

(a) Scenario 70 MW PV (b) Scenario 130 MW PV (c) Scenario 190 MW PV

Figure 21: *ROCOF* pour différentes valeurs de C suite à l'intégration du PV

4.4 Effacement de la production ENR

Dans plusieurs systèmes non-interconnectés tels que les départements français d'outre-mer (DOM), la Crête ou encore l'Irlande, et pour des raisons de sureté, les gestionnaires de ces systèmes électriques sont autorisés à déconnecter une partie des ENR intermittentes. Les modes de compensation de l'énergie non produite varient notablement d'un pays à l'autre. Il s'avère que des réductions dans les coûts de production peuvent être obtenues par un écrêtement partiel de la production ENR quand cela permet une meilleure exploitation du parc conventionnel, par exemple suite à une diminution des coûts des démarrages et d'arrêts des groupes. Ici le cas test est un petit système particulièrement flexible, pour lequel l'écrêtement devient économique dans des cas précis.
A titre d'illustration la figure 22 présente les volumes d'énergie PV effacés pour des raisons économiques. Deux cas, avec ou sans mécanisme de compensation, sont représentés pour les différents scénarios d'intégration du PV, ainsi que les réductions de coût de production obtenues grâce à cette mesure.

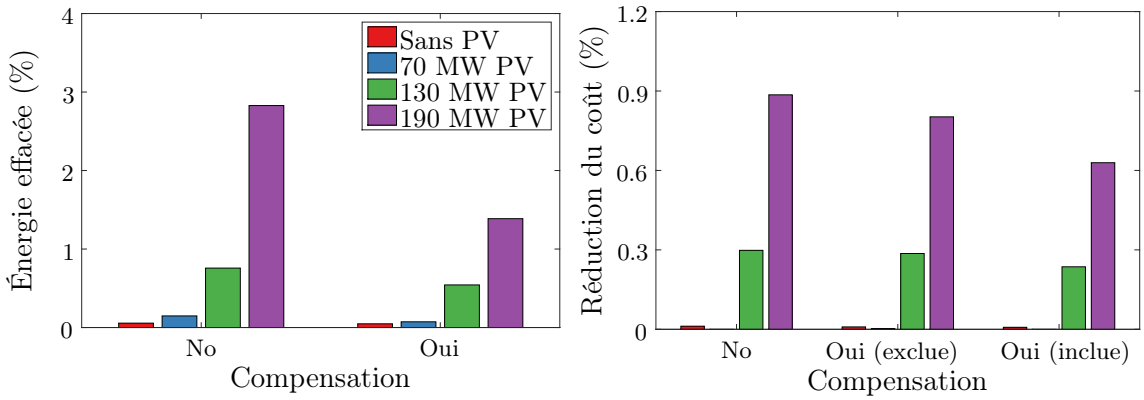

(a) Effacement de la production ENR

(b) Réduction du coût

Figure 22: Coût et bénéfice du l'effacement avec et sans mécanisme de compensation

En général, cet écrêtement que l'on appelle « économique » se concentre dans des heures à fort ensoleillement. Or il a été mis en évidence précédemment que durant les heures de production PV significative le comportement de la fréquence peut avoir tendance à s'améliorer. De plus, l'écrêtement de la production ENR dans un pas de temps génère des changements dans le programme d'appel sur les pas horaires adjacents susceptibles de dégrader le comportement dynamique en cas de défaillance d'un groupe.

4.5 Conclusions et tableau synthèse de la partie 3

L'incapacité de contraintes linéaires simples (volume de réserve primaire, énergie cinétique ou gradient initial de la fréquence) à assurer un programme d'appel présentant une réponse transitoire acceptable pour des taux élevés d'ENR s'accompagne de surcoûts importants.

Cette difficulté trouve principalement son origine dans le fait que ces contraintes ne peuvent pas traduire la grande complexité des processus physiques sous-jacents. Les principaux aspects discutés dans cette partie sont résumés dans le tableau 3.

Table 3: Analyse coût/bénéfice des contraintes indirectes

UC modifié	Contrainte	Coût	Bénéfice
Prescription de réserve	$\sum_{j=1}^{N} r_j^{h,pr} \geq R_{pr}^{min}$	€€€	✓*
Prescription d'inertie	$\sum_{\substack{j=1 \\ j\neq k}}^{N} H_j S_{n,j} u_j^h \geq KE_{-k}^{min}$	€€	✓*
Limite du $ROCOF$	$\sum_{\substack{j=1 \\ j\neq k}}^{N} H_j S_{n,j} u_j^h \geq \frac{f_0}{2ROCOF^{max}} g_k^h$	€	✓*
Effacement des ENR	$\sum_{j=1}^{N} g_j^h + VG^h = D^h$	€⋆	⚠
Soutien dynamique	$\sum_{\substack{j=1 \\ j\neq k}}^{N} r_j^{h,pr} \geq g_k^h - C^{fixe}$	€ + ?†	✓* ⚠

✓* : pour une prescription donnée, un scenario ENR, un seuil de sûreté...

€⋆ : un niveau limité d'effacement peut réduire le coût.

⚠ : effets contre-productifs liés aux contraintes inter-temporelles.

?† : coûts des moyens alternatifs non inclus.

⚠ : réduction de l'inertie, augmentation du niveau de charge et du besoin en réserve.

Pour exploiter au mieux ces divers leviers, il apparaît donc indispensable de disposer d'un outil de placement de production intégrant des contraintes directes sur le creux de fréquence, et ayant ainsi la latitude de « choisir » à chaque pas horaire l'activation de l'un de ces leviers afin d'optimiser la situation rencontrée sans perturber les situations adjacentes. Ce sera l'objet de la partie suivant.

4.6 Contributions de la partie 3

1. Les mesures palliatives d'impact des ENR sur le fonctionnement du système électrique sont souvent traitées de façon indépendante selon leur nature. Un cadre général d'analyse a été proposé pour caractériser les potentiels apports et dangers de différentes types de solutions.
2. Un étude de cas a permis de les comparer en termes de coût et efficacité.
3. On a mis en évidence les effets contre-productifs que certains leviers peuvent avoir sur le comportement de la fréquence suite à une perte de production, ainsi que les limites des formulations proposées dans la littérature pour traiter le problème FCUC.

5. Nouvelle formulation de problème FCUC

Cette partie détaille brièvement la contribution la plus innovante de ces travaux qui est décrite plus amplement dans le chapitre 5 du mémoire. Il s'agit d'une formulation du problème de placement de la production sous contrainte sur les creux de fréquence basée sur la décomposition de Benders.

5.1 Décomposition de Benders

La méthode proposée par Benders facilite la résolution de problèmes d'optimisation avec une structure appropriée par une séparation en deux sous-problèmes comme cela est présenté sur la figure 23.

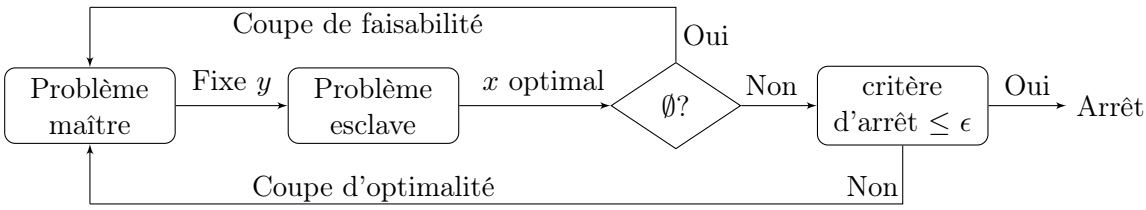

Figure 23: Schéma général de la décomposition de Benders

La première partie, appelée le « problème maître » dans la terminologie de la méthode (*Master*), fixe un ensemble de variables, qu'on note de façon générique y, rendant ainsi la deuxième partie, le « problème esclave » (*Slave*) qui est fonction des variables restantes (qu'on note x), plus facile à résoudre. Des contraintes, appelées « coupes » (*cuts*), sont alors générées au fur et à mesure que l'algorithme progresse vers la solution. Ces contraintes, sont envoyées de « l'esclave » au « maître » pour assurer que le problème original est bien résolu. Formuler le problème FCUC en suivant cette approche consiste alors à définir des deux sous-problèmes et à construire des « coupes ».

5.2 Nouvelle formulation du problème FCUC

Dans le cas du FCUC, il semble naturel de décomposer le problème en fonction du type de variable : binaires et continues. Ainsi, $x \in X \subseteq \mathbb{R}^{n1}$ est le vecteur de variables continues et $y \in Y \subseteq \{0,1\}^{n2}$ est le vecteur de variables binaires.
La fonction objectif est ensuite décomposée en deux parties, $f_1(x) : \mathbb{R}^{n1} \to \mathbb{R}$ qui inclut les coûts proportionnels qui dépendent des variables continues et $f_2(y) : \mathbb{R}^{n2} \to \mathbb{R}$ qui tient compte des coûts fixes, de démarrage et d'arrêt dépendant des variables binaires. De plus, on s'intéresse à l'inclusion d'une contrainte sur le creux de fréquence que l'on notera $q : \mathbb{R}^n \to \mathbb{R}^M$. Le problème (1) est alors récrit comme suit :

$$\begin{aligned} \underset{x\in X, y\in Y}{\text{minimiser}} \quad & f_1(x) + f_2(y) \\ \text{sous les contraintes} \quad & G(x,y) \leq 0, \\ & H(x,y) = 0, \\ & \underline{q} - q_m(x,y) \leq 0 \qquad m = 1,\dots,M, \end{aligned} \tag{6}$$

où G et H représentent les contraintes classiques et $\underline{q}$ le seuil de sûreté (en Hz). L'indice m permet d'identifier la perte d'une quelconque machine $k \in \{1,\dots,N\}$ à un pas de temps $h \in \{1,\dots,T\}$. Par conséquent, dans ces travaux $M = NT$.
En pratique, le « problème maître » propose des plans de production candidats (variables binaires, *i.e.*, états des groupes) et le « problème esclave » modifie les puissances de consigne des groupes afin que les contraintes sur le creux de fréquence soient respectées.
Dans la littérature, le problème à variables binaires fixes est appelé ED (pour *Economic Dispatch*) et il est plus facile à résoudre par des solveurs linéaires. Le « problème esclave » peut être alors assimilé à un FCED (*Frequency Constrained Economic Dispatch*). Il sera formulé dans la partie suivant.

5.2.1 Formulation du « problème esclave »

Le « problème esclave » s'écrit en principe comme suit :

$$\begin{aligned} \mathcal{V}(\bar{y}^i) := \inf_{x\in X} \quad & f_1(x) \\ \text{sous contraintes} \quad & G(x,\bar{y}^i) \leq 0 \\ & H(x,\bar{y}^i) = 0 \\ & \underline{q} - q_m(x,\bar{y}^i) \leq 0 \quad \forall m = 1\dots M, \end{aligned} \tag{7}$$

où $\mathcal{V}$ est le coût du dispatch optimal pour un plan de démarrage fixé ($\bar{y}^i$). Le « problème esclave » détermine les nouvelles puissances de consigne, x, qui minimisent le coût variable tout en respectant les contraintes classiques, ainsi que la nouvelle contrainte de sûreté. Cependant, la fonction $q_m(x,\bar{y}^i)$ reste non-linéaire et implicite. Dans la section 5.2 du manuscrit on discute le champ de validité de la hypothèse suivante :

Hypothèse 2 *les creux de fréquence sont concaves par rapport aux puissances de consigne des groupes de production x à y fixe.*

Ceci permet d'affirmer que le modèle de plans sécants de la fonction $q_m(x,\bar{y}^i)$, noté $\check{q}(x,\bar{y}^i)$ et représenté par la droite verte dans la figure 24, offre un modèle supérieure de la fonction. En effet, la tangente en tout point d'une courbe concave se situe systématiquement au-dessus de celle-ci. Le modèle de plans sécants est alors donné par l'intersection (le minimum) d'un ensemble d'approximations linéaires du premier ordre (plans sécants) et se construit de façon itérative. Ceci s'écrit mathématiquement par l'équation (8).

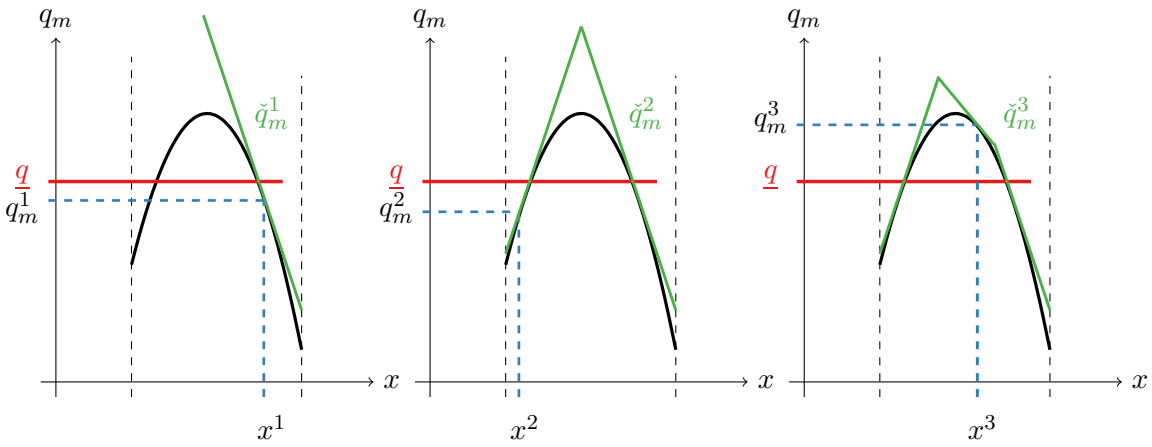

(a) Itération 1 (b) Itération 2 (c) Itération 3

Figure 24: Construction du modèle de plans sécants pour les creux de fréquence

$$\check{q}_m^L(x) = \min_{1 \leq \ell \leq L} \left\{ q_m^\ell(x^\ell, \bar{y}_{-m}^i) + \langle s_m^\ell(x^\ell, \bar{y}_{-m}^i), x - x^\ell \rangle \right\}, \tag{8}$$

où L représente l'itération en cours, q_m^ℓ est le vecteur des possibles creux de fréquence pour la solution candidate x^ℓ et s_m^ℓ son sous-gradient. On remarque que q_m est continument différentiable et de fait le sous-gradient est unique et égal au gradient classique.
Les solutions candidates x^ℓ sont obtenues par résolution successive du « problème esclave » comme illustré dans la figure 25.

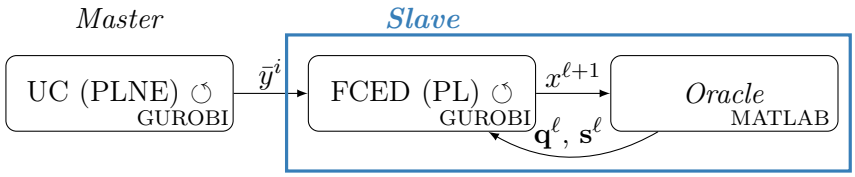

Figure 25: Schéma algorithmique du « problème esclave »

La convergence du modèle de plans sécants pour le point $(x^{\ell+1})$ est atteinte lorsque l'écart entre le modèle $(\check{q}_m^L)$ et la fonction elle-même (q_m) est inférieur à la précision recherchée ϵ (ici fixé à $1e-3$) comme exprimé dans l'équation (9).

$$\check{q}_m^L(x^{\ell+1}) - q_m(x^{\ell+1}) \leq \epsilon. \tag{9}$$

Il est ainsi devenu possible, grâce à l'identification de la concavité de la fonction, d'inclure des contraintes explicites sur les creux de fréquence dans une formulation linéaire du problème ED. De plus, la construction de cette approximation affine se fait sur la base d'un modèle dynamique du type « boîte noire », ce qui permet de prendre en compte un grand nombre de phénomènes physiques, qui étaient négligés jusqu'à présent par les contraintes indirectes. Cette boîte noire sera appelée l'*Oracle*.

Ses entrées sont les plans de production candidats dans les différents états N-1 $(x^\ell, \bar{y}^i_{-m})$, ainsi que les paramètres du parc, et ses sorties correspondent aux creux de fréquence q^ℓ_m et leurs sous-gradients s^ℓ_m pour tout $m = 1, \ldots, M$.
Il est à noter que $\mathbf{q}^\ell = \left[q(x^\ell, \bar{y}^i_{-1}), \ldots, q(x^\ell, \bar{y}^i_{-m}), \ldots, q(x^\ell, \bar{y}^i_{-M})\right]$ est le vecteur de tous les creux de fréquence considérés pour un dispatch donné (x^ℓ), sa dimension est $M = NT$.
Afin d'illustrer l'efficacité de la méthode, reprenons l'exemple du petit système de type insulaire dans lequel le premier cran de DSF est maintenant fixé à 48.9 Hz. Dans ces conditions, le plan de production optimal issu du « problème maître » (figure 26a) présente, pour la journée étudiée et à chaque pas horaire en dehors de la période 19 – 21 h, un risque de délestage suite à une perte d'au moins un groupe (figure 26b).

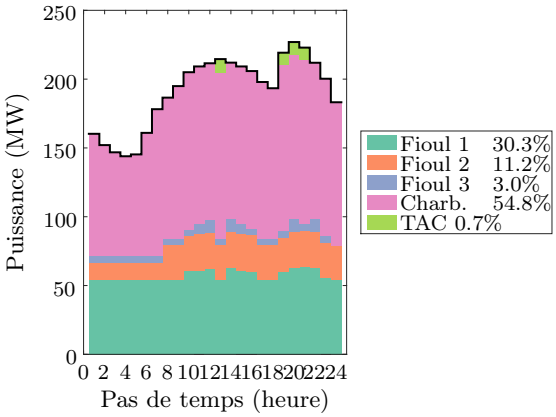

(a) Dispatch (x^1)

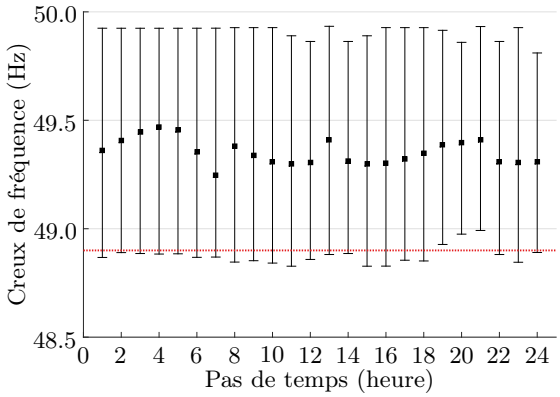

(b) Creux de fréquence (q^1)

Figure 26: Creux de fréquence avec la solution candidate initial (y^1 and x^1)

Différentes itérations successives du « problème esclave » vont permettre de faire remonter l'ensemble des creux de fréquence potentiels au-dessus du seuil de déclenchement du DSF. L'évolution des creux de fréquence les plus sévères à chaque pas de temps pour les différentes itérations du « problème esclave » est proposée sur le figure 27a.

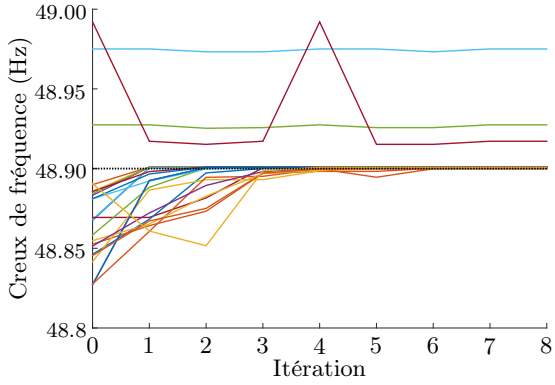

(a) Pire creux de fréquence par pas horaire

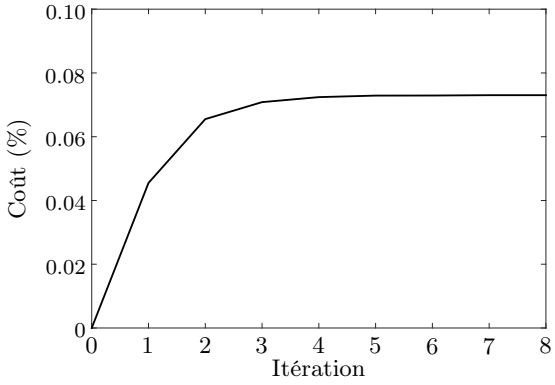

(b) Coût de la sûreté (redispatch)

Figure 27: Évolution des creux de fréquence et du coût avec les itérations

On observe que huit itérations suffisent pour améliorer la situation des pas en défaut sans dégrader le comportement sur les pas 19 -21 h qui respectaient déjà la contrainte en présentant des creux au-dessus de 48.9 Hz.
Cette réaffectation de puissance entre les divers groupes démarrés se traduit par un surcoût par rapport au plan issu du « problème maître » (figure 27b). Pour ce cas particulier, il est possible de considérer cette nouvelle solution comme optimale car le coût de la sûreté s'avère inférieur au MIP gap retenu (0.1%) dans l'optimisation du « problème maître ».

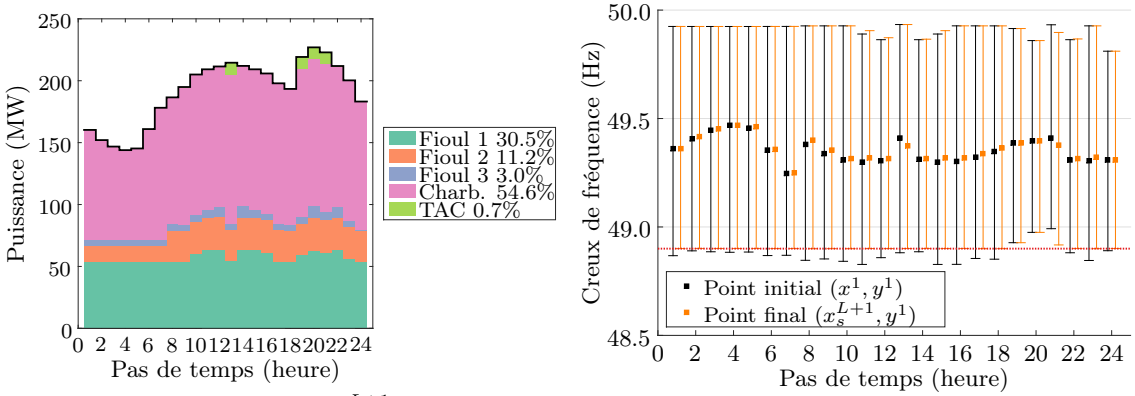

(a) Dispatch (x^{L+1})

(b) Creux de fréquence (q^{L+1})

Figure 28: Creux de fréquence (q^{L+1}) avec la solution optimale (x^{L+1})

En résumé, quelques modifications du plan de production pour la journée étudiée (figure 28a) permettent de proposer une solution sûre (figure 28b) avec un surcoût très limité. Cependant, cette approche n'est pas toujours avec succès.
D'une part il pourrait ne pas y avoir de modification envisageable de la première solution candidate y^1 issue du « problème maître » permettant de respecter les contraintes sur le creux de fréquence dans tous les pas de temps. L'algorithme doit donc imposer au « problème maître » la recherche d'un nouveau plan de démarrage via une contrainte ou « coupe de faisabilité » dont la formulation sera décrite ci-après.
D'autre part, le coût additionnel obtenu lors de la résolution du « problème esclave » pourrait être significatif. Il est donc indispensable d'inclure une garantie d'optimalité dans le « problème maître ». Cela permettra de s'assurer qu'un plan de démarrage initialement plus cher que le plan optimal initial ne puisse conduire, après résolution du « problème esclave », à la solution la moins chère dans le respect des contraintes de sureté. Cette vérification est effectuée à travers les « coupes d'optimalité ».

5.2.2 Formulation du « problème maître »

Le « problème maître » s'écrit comme suit :

$$\begin{aligned} c^* = \underset{y \in Y}{\text{minimiser}} \quad & f_2(y) \\ \text{sous contraintes} \quad & G(y) \leq 0, \\ & H(y) = 0, \\ & \text{Coupes de faisabilité,} \\ & \text{Coupes d'optimalité.} \end{aligned} \tag{10}$$

Dans le problème FCUC, la nature binaire des variables de décision (y) fournit une **coupe de faisabilité** simple, qui impose le changement de l'état d'au moins une unité de production lorsqu'il s'avère que le « problème esclave » ne peut proposer une solution respectant les contraintes de sureté. La coupe de faisabilité, exprimée comme suit, est alors ajoutée dans le « problème maître » :

$$\sum_{j \in \mathfrak{J}^i} \left(1 - y_j^h\right) + \sum_{j \notin \mathfrak{J}^i} y_j^h \geq 1 \quad \forall i = 1, \ldots, I^{fea}, \tag{11}$$

où $\mathfrak{J}^i = \{m = \{1, \ldots, NT\} : y_m^i = 1\}$. Concernant la garantie d'optimalité, il peut être démontré que les variables duales (ou multiplicateurs de Lagrange) d'une contrainte ($w = \bar{y}^i$) que l'on ajoutera au « problème esclave », notées λ^i, fournissent le sous gradient de sa fonction objectif $\mathcal{V}$ par rapport à y. Par conséquent, les **coupes d'optimalité** peuvent-être écrites à partir d'un modèle de plans sécants qui permet d'approcher $\mathcal{V}(y)$ (le coût d'un dispatch sécurisé par rapport à y):

$$\check{\mathcal{V}}^I(y) = \max_{1 \leq i \leq I} \left\{ \mathcal{V}^i + < \lambda^i, y - y^i > \right\} \tag{12}$$

De manière analogue, ce modèle de plans sécants se construit de façon itérative, comme illustré dans la figure 29.

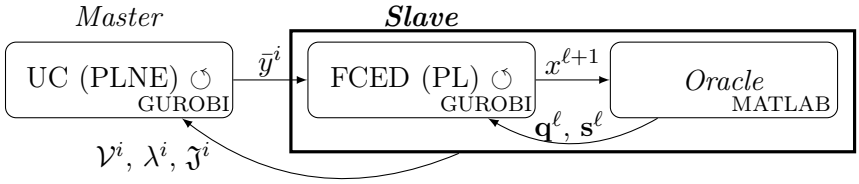

Figure 29: Schéma algorithmique complet

A l'issu du « problème esclave » une solution candidate $\bar{y}^i$ peut être déclarée « réalisable » ou « irréalisable ». Dans le premier cas, un jeu optimal $x^{\star,i}$, avec un coût $\mathcal{V}^i$, peut être déterminé, accompagné de la variable duale λ^i associée. Ces grandeurs permettent la construction d'une coupe d'optimalité. La résolution du « problème maître » avec cette contrainte additionnelle fournit une nouvelle solution candidate $\bar{y}^{i+1}$.

Si, à contrario, la solution candidate $\bar{y}^i$ est déclarée irréalisable (il n'existe aucun jeu x qui permet la satisfaction de toutes les contraintes du « problème esclave »), une coupe de faisabilité est ajoutée, à partir du $\mathfrak{J}^i$, et une nouvelle solution candidate est calculée.

L'algorithme s'arrête quand la précision du modèle de plans sécants du coût variable sera inférieure à une certaine tolérance de convergence η :

$$\mathcal{V}(y^I) - \check{\mathcal{V}}(y^I) \leq \eta. \tag{13}$$

Afin d'améliorer la convergence, des **coupes de sous-optimalité** sont également considérées dans ces travaux afin d'exploiter au mieux les résultats du « problème esclave » même s'ils s'avèrent irréalisables. On calcule alors V et λ pour $L = 0$ ce qui correspond à la solution du « problème esclave » sans contrainte sur le creux de fréquence (un ED classique est résolu).

De plus, il est indispensable d'inclure les contraintes qui dépendent des variables continues (x), telles que l'équation d'équilibre offre-demande, pour que l'algorithme ne perd pas trop de temps avec des solutions candidates y^i irréalisables. Pour éviter d'avoir une quantité importante de coupes de faisabilité, on propose la formulation d'un « problème maître » plus riche, qui inclut la variable x et ses contraintes, même si les couts variables, $f_1(x)$ ne sont pas explicitement inclus dans la fonction objectif.

En conclusion, la formulation mathématique suivante est proposée pour le « problème maître » :

$$\begin{aligned}
\mathcal{C}^* = \underset{y \in Y, \zeta}{\text{minimise}} \quad & f_2(y) + \zeta \\
\text{subject to} \quad & G(x, y) \leq 0 \\
& H(x, y) = 0 \\
& \sum_{j \in \mathfrak{J}^i} \left(1 - y_j^h\right) + \sum_{j \notin \mathfrak{J}^i} y_j^h \geq 1 \qquad \forall i = 1 \dots I^{fea} \\
& \mathcal{V}(\bar{y}^i) + \langle \lambda^i, y - \bar{y}^i \rangle - \zeta \leq 0 \qquad \forall i = 1 \dots I.
\end{aligned} \tag{14}$$

Dans l'exemple présenté dans la partie précédente, la résolution du « problème esclave » à l'issue de la première itération du « problème maître » avait conduit à une solution optimale. Supposons maintenant que le seuil de délestage ne soit plus fixé à 48.9 Hz mais à 49 Hz de façon à ce que le « problème esclave » ne soit plus en mesure de proposer une solution réalisable sur la base de la première itération (y^1) issue du « problème maître ». Une coupe de faisabilité et une coupe de sous-optimalité sont alors ajoutées au « problème maître » et une nouvelle solution candidate y^2 est proposée (voir la figure 30).

Cependant, lors de cette deuxième itération le « problème maître » ne dispose que d'une information très limitée sur les coûts variables (la fonction ζ)). En conséquence, le coût de cette solution est en pratique très élevé ($\mathcal{V}^2 \gg \mathcal{V}_0^1$). Bien que réalisable, cette solution n'est pas satisfaisante. Le critère d'arrêt est alors vérifié, mais la précision du modèle de plans sécants s'avère insuffisante à ce stade. Une coupe d'optimalité est donc ajoutée au « problème maître » et une troisième solution candidate (y^3) est calculée.

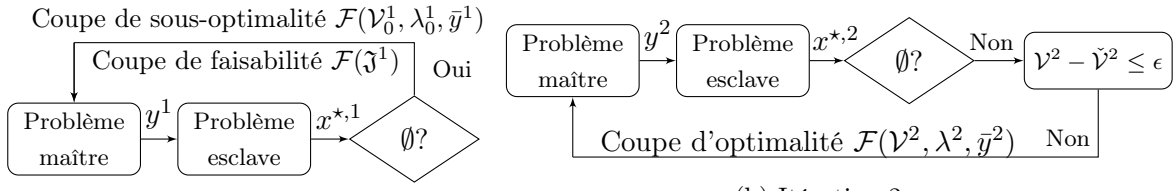

(a) Itération 1

(b) Itération 2

Figure 30: Progression de l'algorithme

Á l'issue de 500 itérations, l'algorithme développé a été capable de proposer près de 300 plans de production permettant de respecter une contrainte sur le creux de fréquence pour un seuil de sûreté à 49 Hz, ce que les FCUC plus classiques, basés sur des contraintes indirectes comme le volume de réserve ou l'inertie, n'avaient pas été en mesure de faire.
Cependant, le critère d'arrêt n'a pas été vérifié, ce qui révèle une convergente trop lente pour permettre d'atteindre l'optimalité dans des temps de calcul compatibles avec la conduite des systèmes réels. Pour améliorer cette convergence, on propose dans la partie suivante l'implémentation d'une formulation dite « stabilisée » du problème FCUC par décomposition de Benders, inspirée des méthodes de faisceaux.

5.3 Stabilisation quadratique

Dans l'optimisation convexe non-différentiable, les méthodes de faisceaux ont été proposées pour stabiliser les modèles de plans sécants. L'idée générale est d'encourager la prochaine solution candidate à rester au plus près de la meilleure solution, tout en diminuant l'objectif du modèle de plans sécants.
Dans cette partie, un « problème maître de niveau » (*Level-Master problem*), décrit par l'équation (15), est implémenté pour accélérer la convergence du problème FCUC. A cet effet, l'objectif initial est remplacé par la minimisation de la norme de la distance entre la nouvelle solution candidate (y) et le meilleur point réalisable identifié à une itération donnée ($\hat{y}^i$), appelé dans la terminologie de la méthode « centre de la stabilité ». L'ancienne fonction objectif (le coût) apparaît alors en tant que contrainte et sera minimisée à l'aide d'un paramètre de niveau, $c^{lev,i}$.

$$
\begin{aligned}
c^* = \underset{y \in Y, \zeta}{\text{minimisee}} \quad & \frac{1}{2} \left\| y - \hat{y} \right\|^2 \\
\text{sous contraintes} \quad & f_2(y) + \zeta \leq c_{lev}^i \\
& G(x, y) \leq 0 \\
& H(x, y) = 0 \\
& \sum_{j \in \mathfrak{J}^i} \left(1 - y_j^h\right) + \sum_{j \notin \mathfrak{J}^i} y_j^h \geq 1 \qquad \forall i = 1 \dots I^{fea} \\
& \mathcal{V}(\bar{y}^i) + \langle \lambda^i, y - \bar{y}^i \rangle - \zeta \leq 0 \qquad \forall i = 1 \dots I.
\end{aligned}
\tag{15}
$$

Ce paramètre est calculé comme suit :

$$\begin{aligned} c^i_{lev} =& c^i_{lb} + \gamma \Delta c, \\ \Delta c^i =& c^i_{ub} - c^i_{lb}, \end{aligned} \tag{16}$$

où :

- c_{ub} est la borne supérieure du coût de la solution, considérée dans ces travaux comme le coût de la meilleure solution trouvée jusqu'à présent (centre de stabilité),
- c_{lb} est une borne inférieure du « problème maître » calculée en résolvant un MILP rapide du « problème maître » standard (14) en limitant le temps alloué au solveur, par exemple à 5 secondes. Cette borne inférieure s'exprime comme suit : le $c^i_{lb} = \left(f_1(y^i_{fast}) + \zeta^i_{fast}\right)\left(1 - MIPgap^i_{fast}\right)$.
- le paramètre γ permet de *customiser* la formulation, ici il est fixé à 0.2.

Les principaux éléments de cette formulation sont illustrés dans la figure 31 pour une progression algorithmique équivalente à celle présentée dans la figure 30. Considérons que le premier programme d'appel proposé par un modèle UC classique (y^1) ne respecte pas le seuil de sûreté sur les creux de fréquence pour divers pas de temps lors qu'on considère la perte d'un groupe de production. Ce premier plan de démarrage est fourni au « problème esclave » qui n'ai pas été capable de trouver une solution réalisable ($\nexists \;\; x^{\star,1}$).
Dans ce cas, le « problème maître » est résolu, en incluant des coupes de faisabilité et de sous-optimalité afin de calculer une deuxième solution candidate y^2. Comme l'illustré la figure 30b, il se trouve le « problème esclave » réussit à fournir un jeu optimal ($\exists \;\; x^{\star,2}$). Maintenant qu'une première solution réalisable a été trouvée, elle peut-être utilisée pour définir le centre de stabilité de la nouvelle méthode ($\hat{y} = y^2$). De plus, le coût de cette solution candidate fournit une borne supérieure ($c^2_{ub} = \mathcal{V}^2 + f_2(\bar{y}^2)$).
Cependant, si la borne inférieure trouvée est trop faible (c^2_{lb} *petite*), le paramètre de niveau (c^2_{lev}) pourrait se trouver en dessous du modèle de plans sécants du coût ($\check{\mathcal{V}}$ représenté en rouge), tel que le montre la figure 31a.

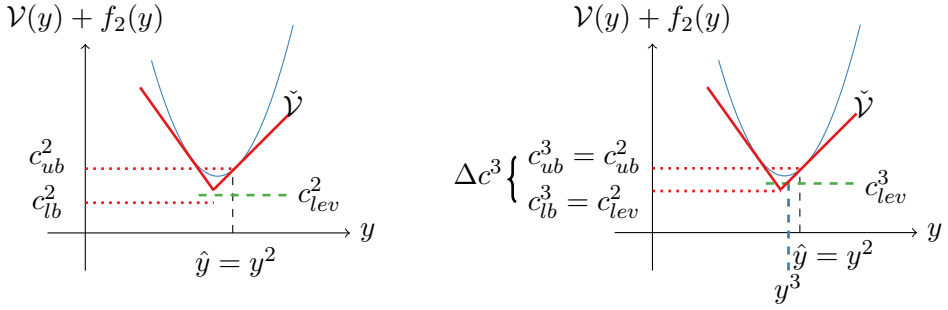

(a) Cas irréalisable (b) Cas réalisable

Figure 31: Schéma du principe du « problème maître du niveau »

Dans ce cas, le problème (15) est déclaré irréalisable et, on peut montrer que, le paramètre de niveau est une borne inférieure sur la valeur optimale du problème. Il pourra donc être actualisé afin de calculer une nouvelle solution candidate (voir la figure 31b).
L'algorithme s'arrête lorsque la distance entre les bornes inférieure et supérieure (Δc) devient elle-même inférieure à une tolérance prédéfinie (ici $\eta = 0.2\%$). A cette fin, la borne supérieure est actualisée à chaque identification d'une solution avec un coût de sûreté plus faible. La mise en évidence de l'apport de cette nouvelle formulation, concernant les propriétés de convergence, est observable dans la figure 32a. De plus, les solutions candidates présentent des surcoûts moins importants (voir figure 32b).

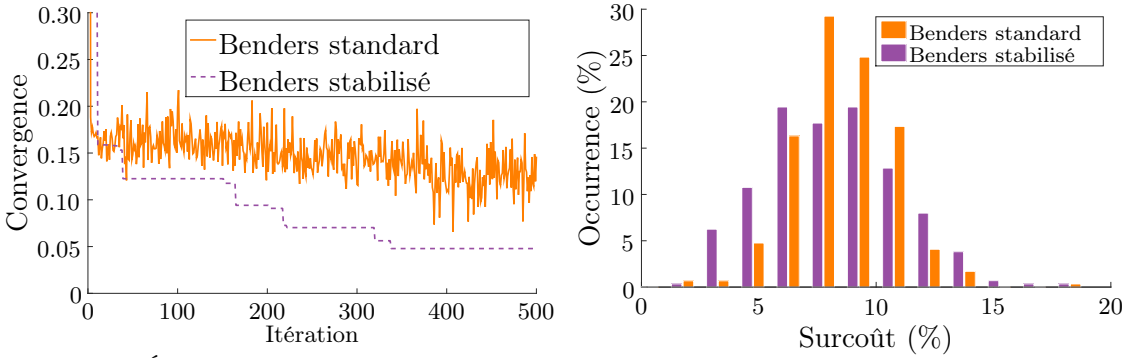

(a) Évolution du critère d'arrêt

(b) Distribution des surcoûts

Figure 32: Amélioration de la convergence par stabilisation de la méthode de Benders

5.4 Conclusions de la partie 4

La formulation du problème FCUC sur la base de la décomposition de Benders est capable de proposer en quelques itérations des plans de production qui assurent la sûreté du système, d'un point de vue du risque de DSF. Cependant, la convergence est trop lente pour permettre d'atteindre l'optimalité pour l'instant.
Pour améliorer cette convergence, une formulation stabilisée, inspirée des méthodes de faisceaux, du problème « problème maître » a été implémentée. Ceci offre des résultats prometteurs, comme l'amélioration de la qualité des solutions candidates (diminution des surcoûts), ainsi qu'une évolution plus rapide du critère d'arrêt vers le seuil prédéfini. Cependant des travaux complémentaires sur le contrôle du $MIPgap$ sont indispensables afin d'obtenir des vitesses de convergence compatibles avec une mise en œuvre industrielle. D'un point de vue pratique, le meilleur *dispatching* possible identifié dans le budget alloué (500 itérations), est en effet plus économique (1.6%) comparé à celui proposé avec la formulation standard du « problème maître » (2%) par rapport au premier programme d'appel qui ne respecte pas la contrainte de sûreté.

5.5 Contributions de la partie 4

1. Une contrainte directe sur le creux de fréquence a été formulée au travers d'un modèle de plans sécants permettant d'assurer une structure linéaire et continue du « problème esclave » facile à aborder par des solveurs linéaires commerciaux. Cette contrainte est efficace pour limiter le risque de DSF à un coût inférieur aux modèles basés sur des contraintes indirectes (volume réserve, inertie), au détriment d'une plus grande complexité et d'un temps de calcul plus élevé. Bien que le temps de calcul pour la construction des modèles de plans sécants augmente avec la taille du système, en raison du calcul des sous gradients, la parallélisation de cette procédure est simple. Pour des grands systèmes, une méthode de *clustering* pourrait également faire l'objet de développements ultérieurs.
2. Une nouvelle formulation du problème FCUC a été proposée basée sur la décomposition de Benders. Les deux parties du problème (le *Master* et le *Slave*) ont été définis, ainsi que les coupes qui permettent la communication entre les deux parties.
3. Des coupes de sous-optimalité ont été proposées pour faire face à la nature combinatoire des coupes de faisabilité et des variables binaires, et empêcher ainsi l'algorithme de rester bloqué avant de trouver une solution vraiment différente si plusieurs unités sont similaires.
4. Un algorithme de stabilisation quadratique a été mis en œuvre pour faire face aux problèmes d'instabilité de la méthode de décomposition et ainsi améliorer la convergence du « problème maître ».

6. Conclusions et perspectives

La fourniture de réserve primaire dans un système électrique désoptimise l'élaboration de programmes d'appel à court terme par rapport à la simple fourniture de la demande. Qui plus est, cette désoptimisation est accrue par le caractère indirect des contraintes utilisées et qui est lié d'une part, à la difficulté de représentation de la contrainte directe sur la profondeur du creux de fréquence à ne pas dépasser, et d'autre part, au choix des moyens de calculs actuellement retenus pour leur efficacité opérationnelle.
Cette thèse, en proposant de combiner de façon judicieuse la décomposition de Benders et diverses méthodes de plans sécants, apporte une réponse innovante et efficace permettant de prendre en compte une contrainte directe dans le problème d'optimisation. A travers un ensemble de contraintes nouvelles et compatibles avec des solveurs PL (programmation linéaire) commerciaux, il est ainsi envisageable de fournir la demande et la réserve au meilleur coût tout en maîtrisant le risque de recours au délestage fréquence-métrique.
Au préalable et dans une perspective d'accroissement du taux de pénétration des ENR intermittentes, une analyse circonstanciée des lacunes des approches actuelles tant industrielles qu'académiques a mis en avant la nécessité des développements entrepris.

6.1 Conclusions

Actuellement le placement de production (UC pour *Unit Commitment*) utilise principalement des contraintes de sûreté simplifiées sur le volume de réserve, ce qui peut amener à des solutions sous-optimales dans les grands systèmes électriques interconnectés, et inefficaces dans les petits systèmes isolés. Ceci s'explique par le fait qu'une expression analytique de la contrainte sur le creux de fréquence suppose de fortes hypothèses et reste non-linéaire.
Le problème UC devant être résolu dans un temps compatible avec la conduite du système électrique, l'utilisation d'approximations affines a été privilégiée afin de permettre l'emploi de solveurs PLNE (programmation linéaire en nombres entiers) efficaces et fiables.
Cependant, la libéralisation du secteur de l'électricité préconise aujourd'hui les réductions de coûts. De plus, les études de cas présentées dans ce rapport mettent en évidence la fragilisation du système avec l'intégration des ENR variables du fait de leurs caractéristiques intrinsèques. Enfin il apparaît qu'un modèle plus précis de la contrainte de sûreté est nécessaire pour l'obtention de programmes d'appel garantissant pour tout point de fonctionnement une réponse transitoire acceptable et avec des ressources de régulation primaires optimisées.
Le coût, les avantages et les limites des contraintes de sûreté améliorées proposées dans la littérature ont été étudiés. Il est démontré que l'utilisation de contraintes fixes sur des paramètres spécifiques n'offre pas de bons compromis coûts/bénéfices pour garantir la sûreté suite à l'intégration des sources non-synchrones.
D'une part, l'application de ces contraintes, qui augmentent évidemment le coût opérationnel, produit des solutions sous-optimales. D'autre part, ces techniques d'atténuation des impacts peuvent échouer à contenir le risque de DSF en raison de leur faible représentativité des processus sous-jacents. En outre, la dépendance inter-temporelle des variables d'optimisation peut produire des actions involontaires dans des pas de temps adjacents ayant des effets contreproductifs. Enfin, certaines solutions ont tendance à encourager l'écrêtement des sources ENR, ce qui va à l'encontre des politiques écologiques.
Devant ces divers constats, une formulation linéaire explicite de ce type de contrainte compatible avec l'utilisation de solveurs PLNE commerciaux a donc été entreprise. Une nouvelle formulation du problème FCUC (*frequency constrained UC*) basée sur la décomposition de Benders a été proposée.
Cette approche permet de surmonter un ensemble de limitations des modèles existants. Par exemple, une contrainte explicite sur le creux de fréquence est écrite grâce à la construction de son modèle de plans sécants, et ceci malgré sa non-linéarité, mais sous l'hypothèse de concavité par rapport aux variables continues de l'UC. Le modèle de plans sécants est construit sur la base d'une fonction du type boîte noire, appelée l'*Oracle*, ce qui permet de prendre en compte des phénomènes physiques négligés jusqu'à présent, tels que la dynamique de libération de la réserve primaire par chaque unité.

Il est à noter que grâce à la décomposition nous nous affranchissons des hypothèses sur la relation entre la fonction creux de fréquence et les états (binaires) des groupes. Cela se fait sans compromettre la capacité à déterminer une solution, puisque la structure linéaire du problème est conservée à chaque itération du « problème esclave ».

Les résultats de simulation montrent que le modèle de plans sécants du creux de fréquence est précis, efficace à 100% (à la précision de l'*Oracle*, tant que la solution candidate est réalisable). De plus, il converge rapidement pour des centaines de solutions candidates, ce qui entraîne de faibles coûts de sûreté supplémentaires.

Enfin, une coordination est mise en œuvre au niveau du « problème maître » visant à assurer la résolution du problème initial (FCUC). Une fois encore, un modèle de plans sécants est proposé, cette fois-ci pour représenter l'objectif du « problème esclave », qui est calculé grâce à la solution d'un problème d'optimisation plus simple.

L'optimalité est assurée et ce bien que la convergence du « problème maître » soit lente. Ceci s'explique par des problèmes de stabilité bien connus des méthodes de décomposition. En effet, l'algorithme semble converger asymptotiquement au début, mais au fil des itérations la qualité des solutions candidates baisse, ce qui empêchent le « problème maître » de converger rapidement.

Pour apporter des éléments de réponse à cette limitation, un « problème maître » stabilisé a été formulé sur la base d'une méthode de faisceaux. Les résultats préliminaires sont prometteurs, et ouvrent la voie à des travaux complémentaires afin d'aboutir à une convergence de l'algorithme global compatible avec les contraintes opérationnelles.

La nouvelle formulation proposée permet d'optimiser toutes les ressources de régulation primaire de fréquence disponibles au niveau de l'optimisation des programmes d'appel de façon simultanée grâce à une représentation explicite directe des contraintes sur les creux de fréquence. Une industrialisation de cette approche permettrait d'augmenter la part de la production non-synchrone, dont les sources renouvelables, tout en garantissant la sûreté de fourniture d'électricité et en maîtrisant le coût.

6.2 Perspectives

Ces travaux ont apporté des éléments de réponse à de nombreuses questions, mais ils laissent ouverts plusieurs champs d'investigations. A ce stade, nous identifions quatre axes principales de recherche :

1. **Amélioration de la convergence du « problème maître »**. La convergence lente du « problème maître » ne permet pas d'envisager une mise en œuvre opérationnelle immédiate. Cependant divers travaux sur l'amélioration de la convergence de problèmes de décomposition pourraient être exploités pour aboutir à une industrialisation de cette approche.

2. **S'affranchir d'hypothèses dans l'outil de placement de production**. Certaines hypothèses simplificatrices utilisées dans ce travail pourraient être revues sans que l'efficacité de la méthode innovante développée ne soit a priori remise en cause. Par exemple à :

   - la prise en compte d'une prescription de réserve primaire à la baisse en complément de la seule réserve primaire à la hausse retenue dans cette étude pour faire écho à la pratique actuelle dans les systèmes insulaires français ;
   - la prescription des réserves pour faire face à la variabilité infra-horaire de la production intermittente ;
   - la prise en compte d'une compensation imparfaite de la variabilité des ENR intermittentes par les moyens dédiés à cette effet dans le but d'améliorer la représentativité des états initiaux des systèmes au moment des simulations de pertes de groupe ;
   - les contraintes liées au réseau.

   Plus de détails sur la révision de ces hypothèses sont présentés dans le chapitre 6 du mémoire.

3. **Modélisation plus fine de la régulation des groupes**. Un modèle multi machine d'ordre réduit (MMR-ROSFR) a été proposé dans ce travail pour estimer l'évolution de la fréquence suite à un fort déséquilibre de puissance. Plusieurs processus ont été modélisés, comme par exemple :

   - la réponse inertielle agrégée des unités qui restent raccordées suite à la perturbation,
   - l'auto-adaptation de la charge avec les variations de fréquence ;
   - les paramètres de la régulation primaire de fréquence des différentes unités thermiques. Ce dernier point inclus: (i) un contrôleur proportionnel (statisme), (ii) une fonction de transfert du premier ordre pour représenter la dynamique de réponse du moyen de production, (iii) un compensateur *lead-lag*, et (iv) une saturation du signal de commande que ce soit pour respecter des limites de capacité de l'installation ou un volume alloué de réserve primaire.

   Cette représentation beaucoup plus détaillée que dans les travaux existants sur le sujet, pourrait être enrichie par une modélisation encore plus fine des moyens de production dont la réponse dynamique n'est pas toujours assimilable à un premier ordre. On pense par exemple à la production hydraulique, où la chute de pression consécutive à l'ouverture des organes de régulation dans les premiers instants suivant une perte de groupe conduit à une baisse de la puissance fournie par certains groupes hydrauliques en régulation primaire de fréquence.

Enfin, pour les systèmes à grande échelle, la nécessité pour les calculs dynamiques de regrouper des unités similaires par famille devra s'accompagner de développements particuliers pour tenir compte de l'hétérogénéité au sein de chaque famille des points de fonctionnement des unités.

4. **Réduction du temps de calcul dans le modèle dynamique**. La révision de certaines considérations de modélisation et de simulation pourrait apporter des améliorations dans les performances de calcul de certaines parties des outils proposés.
   - **Méthode de solution du modèle MMR-ROSFR**. Dans ce travail, une méthode d'intégration numérique à pas fixe a été mise en œuvre afin de prendre en compte facilement les processus de saturation. Toutefois, il est bien connu que l'évolution de fréquence a un comportement lisse, ce qui incite à utiliser des méthodes d'intégration numérique à pas variable. Ces méthodes réduisent généralement les exigences de calcul en termes de mémoire et nombre d'opérations.
   - **Dans la simulation séquentielle**. Une approche séquentielle a été utilisée pour l'analyse de l'impact d'ENR sur le comportement de la fréquence, et l'efficacité des techniques d'atténuation des impacts (chapitres 2-4). La parallélisation accrue des calculs dynamiques offrent certainement des perspectives intéressantes pour la réduction des temps de calcul.

     Enfin, dans les systèmes où de nombreux groupes sont identiques et exploités sur des points de fonctionnement proches, il pourrait être envisageable de ne considérer la validation du respect du critère de sécurité que sur un seul d'entre eux par exemple.

Contents

List of Tables

List of Figures

Chapter 1

Introduction

Contents

1.1 Context and challenges

The operational environment of power systems has not ceased to evolve in the last decades. On the one hand, the deregulation of the energy industry generated profound structural changes in the electricity sector, increasing the amount of actors, products/services and interactions required to reliably supply the demand. On the other hand, following environmental policies, renewable energy sources (RES), such as wind and solar, have been taking an important share of the electricity mix, displacing conventional units. These facts have brought new challenges to conciliate economics with security in the electricity supply.

Section 1.1.1 describes some specific mechanisms and resources used by system operators to ensure a reliable electricity supply, with emphasis on the frequency control. Sections 1.1.2 discusses the two main drivers of recent power system evolution: deregulation and RES integration (excluding hydro). Finally, section 1.1.3 analyses the impacts of these changes on the frequency regulation of different power systems, establishing the bases that motivate the research questions addressed in this thesis, and detailed in sections 1.2-1.5.

1.1.1 Power system operation and security

Electrical power system management is done over different time horizons and multi-level decision coordination is essential to ensure a reliable and cost effective energy supply, as illustrated in figure 1.1. Under-investments in generation and grid infrastructure can have severe consequences on the operation and on the electricity prices of the future system. An accurate mid-term estimation of the demand and the resources needed to supply it, allows generating companies to define asset use and maintenance as well as better negotiate long-term contracts.

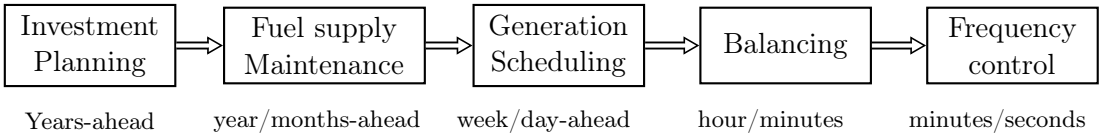

Figure 1.1: Main tasks by time horizons in power system operation

Then, different mechanisms exist to guarantee that generation will meet the load in real-time. In a vertically integrated system, where an utility owns the power plants and the networks, one entity centralises the decision of short-term unit scheduling considering the most accurate prevision of the load and generation availability. This process is more complex in deregulated systems and can differ from one system to another. Roughly speaking, the system operators establish the generation schedules through a day-ahead market clearing mechanism based on the bids submitted by the energy suppliers [1]. Then, real-time uncertainties are handled by intra-day markets and intra-hour balancing mechanisms.

Power system security and ancillary services

Power system security will be understood here as the ability of the power system to withstand plausible contingencies without interruption of customer service [2]. Power system security is ensured by system operators through a set of resources that includes, among others, ancillary services such as the voltage and frequency control.

These services have been traditionally provided by generating units. Voltage control is related to the local provision of reactive power [3], while frequency control is achieved by keeping the balance between the load and generation [4]. In practice, these are based on the implementation of different hierarchical control schemes, which require the provision of certain amounts of spare capacity, called reserves.

This thesis is about the optimal allocation of active power reserve for primary frequency regulation purposes. Thus, the focus is placed on the last two time scales between the day-ahead and the real-time decision making processes. The goal is to ensure that the amount and quality of a scheduled resource, the primary reserve, is sufficient to ensure security when facing large disturbances in real-time operation.

Active power reserves

Spinning reserve is defined here as the difference between the power ratings of all the operating units and the actual load plus losses [5]. Its activation ensures the power balance following forecasting errors and unit failures. Different criteria can be used to classify the reserve: its response time, its main function, its mode of activation, etc. Nowadays, it also depends on the country and the electricity market design [6].
In Europe, the reserve is traditionally split into primary, secondary and tertiary reserves. In general, the primary reserve is meant to avoid load shedding after sudden disturbances and stabilise the power system frequency in some seconds. It is also called the frequency containment reserve by the ENTSO-E [7]. Then, slower reserves are used to automatically bring the frequency back to its nominal value in some minutes, to restore interconnection power flows, and to compensate for very short term demand variability, by following a centralised signal [8]. Finally, tertiary reserve is deployed to improve the economical performance of the dispatch, to manage congestions and to restore faster reserves. Quick-start units may form part of the tertiary reserve, and they are called standing reserves or, by opposition, non-spinning reserve, and are usually deployed manually.

Frequency control

The frequency in a synchronous power system is an indicator of the instantaneous power balance between generation and demand. When the load exceeds the power generation, the lacking energy is extracted from the kinetic energy stored in rotating machines and their speed is reduced, and vice-versa. The frequency control historically consists in maintaining the balance between the production and the consumption of active power by using the value of the frequency as a signal to adapt conventional generator power outputs [9]. The frequency control operates in both normal and contingency conditions.

Primary frequency control

Following a large disturbance, such as a unit outage, the power system frequency drops due to the power imbalance. The inertia of the rotating masses connected to the system will limit the gradient of this drop. Then, the primary frequency control will automatically (and locally) increase the power output of the units designated to provide this ancillary service, until the power balance is regained and the system frequency is stabilised. In addition, frequency sensitive loads, such as synchronous motors, will reduced their power consumption as the frequency drops.
If this process fails to maintain the frequency over a certain threshold, the under frequency protection relay placed in power stations may automatically shed load to prevent system collapse. This action is called Under-Frequency Load Shedding (UFLS) [10, 11].

1.1.2 Evolution of power systems

Deregulation of the electricity industry

In the 90's, a profound structural transformation started in some power systems, driven by the deregulation of the electricity industry, to potentially improve the economical efficiency of the sector. Among others, this transformation implied important changes on the way ancillary services were provided. In a vertically integrated structure, the utility, responsible for the system security, owned the means to ensure it, *i.e.*, the generating units capable to provide ancillary services. After the deregulation of the electricity markets, the generation, transmission and distribution were separated, and the responsibility of the power system security was assigned to the transmission system operator (TSO), while the property of power plants was associated to independent generating companies (GENCOs).
Therefore, ancillary services became products provided by some participants to the system operators. Over the last decades, significant research was devoted to the definition of a suitable market design to exchange these services [3, 4, 12]. The provision of some of these services was declared mandatory and/or negotiated via bilateral contracts. This is the case of "basic" voltage control in Europe and USA [13], while other services are now traded in dedicated markets, depending on the system.
In this context, the simplest way of maintaining the performance of the frequency regulation is to contractually oblige specific GENCOs to accept a control signal as if they were owned by the system operator [4]. The advantage of this approach is that load following can be ensured while the share of controlled units in the energy mix remains high enough. Although, further discussion on this topic is beyond the scope of this work, it should be noted that, in practice, it is unlikely that this structure is implemented due to some drawbacks, such as the underlying economic "inequities" and the risk of over-dimensioning the provided services, which might entail unnecessary cost to the suppliers.
Hence, the implementation of specific structures over time produced different operational responses in various systems.

Integration of renewable sources

In 1997 an international treaty, the Kyoto protocol, was adopted by several countries to face global warming by reducing greenhouse gas emissions [14]. Thereafter, strong support policies for renewables were deployed in different countries, which have attracted significant investment on new technologies, first wind and then photovoltaic (PV). Therefore, the installed capacity of generation based on renewables is growing worldwide. In this section hydro power will not be considered since it has been deployed for many years, and it does not entail the operational changes caused by the integration of variable RES (V-RES).
Figure 1.2a presents the installed capacity of RES in 7 countries at the end of 2014 [15].

Figure 1.2b depicts the worldwide progression of the wind and solar over the last decade. It is observed that the sector was launched initially by the wind power, and then followed by PV, which exhibited a more significant growth from 2007 onwards.

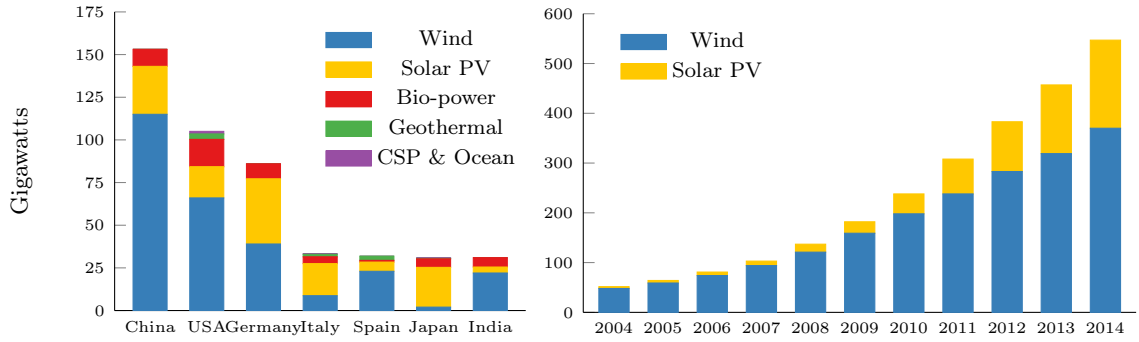

(a) RES by country in 2014

(b) Main RES progression

Figure 1.2: Installed capacity of renewable energy sources

By the end of 2014, 370 GW of wind power and 177 GW of PV have been installed, representing 4% of the global energy mix [15]. Main factors driving this trend are:

- Environmental concerns and high fuel prices.
- Regulatory incentives, such as subsidies (ex. feed-in tariffs, etc.).
- Technological advancement, regarding efficiency and/or nameplate capacity.
- Reduction of investment cost.
- Better knowledge on operation due to the development of pilot projects.

Indeed, the European Parliament adopted in 2008 the European Union (EU) climate and energy package, which consist on a set of binding legislation to meet three specify targets for 2020 [16]:

- 20% reduction in EU greenhouse gas emission from 1990 levels,
- 20% increase of the share of EU energy consumption from renewable resources,
- 20% improvement in the EU's energy efficiency.

This targets will be succeeded by the EU 2030 framework for climate and energy policies, where the emission reduction objective has risen up to 40% and the energy efficiency and renewables participation goals have increased up to at least 27% for 2030 [17]. In addition, different initiatives has been taken to define global objectives on renewable energy use and energy efficiency such as the Sustainable Energy for All (SE4ALL) [18]. Finally, these targets, measures and recommendations have been declined into national policies.

By the end of 2014, at least 164 countries had renewable energy targets, and an estimated of 145 countries had renewable energy support policies in place [15]. In France, the energy transition for green growth law has recently been adopted [19]. Nevertheless, depending on the characteristics, size and available resources of each system, the local targets are more or less ambitious, and the road to attain them will be more or less long. Smaller systems, for instance, may reach higher share of renewables in their mix with lower global investments, at the expense of facing more technical challenges. Figure 1.3 presents the V-RES share in the electricity generation of some countries for 2014 [20, 21, 22, 23, 24, 25].

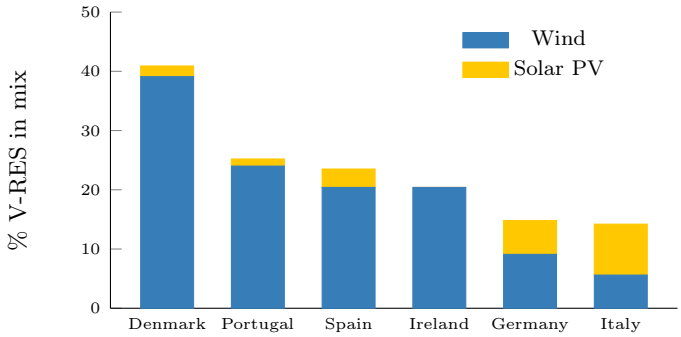

Figure 1.3: V-RES share by country in 2014

France

In France, the deployment of RES has been more modest than in some neighbouring countries. The share of wind and PV represented 4.2% of the total electrical energy consumption of 2014 [26]. One of the reason is that France already has a low carbon mix due to the high share of nuclear and hydro, as shown in figure 1.4a. The evolution of the installed wind power and PV capacity in France is shown in figure 1.4b.

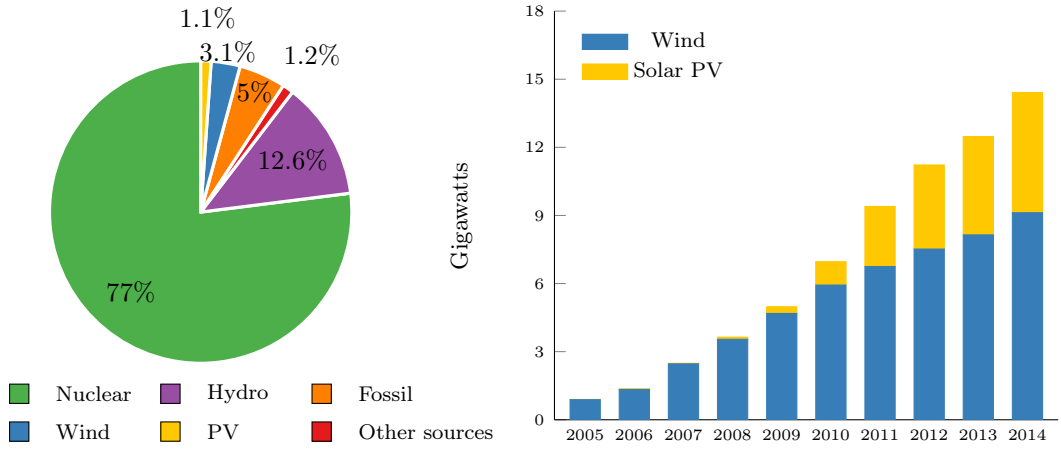

(a) Energy Mix France 2014

(b) RES progression in France

Figure 1.4: Energy mix and installed capacity of Wind and PV in France for 2014

French overseas departments

The overseas departments, or DOM (french acronym for *Départements d'Outre-mer*), are French-administered territories outside of the European continent. They are constituted by French Guiana and four islands: Guadeloupe, Martinique, Reunion and Mayotte. These territories are non interconnected, and, except for French Guiana with a high share of hydro, their electricity generation is highly dependent on imported fossil fuels, which are expensive and induce a significant carbon content in the energy mix. Therefore, the DOM are also affected to some extent by the energy transition law. In addition, due to the high fuel cost, RES may become competitive faster than elsewhere.
A similar situation occurs in Corsica, a French island in the Mediterranean sea, despite of the existing interconnection with Sardinia. Hence, the installed capacity of RES, especially PV, have experienced an important growth in these regions, as presented in figure 1.5.

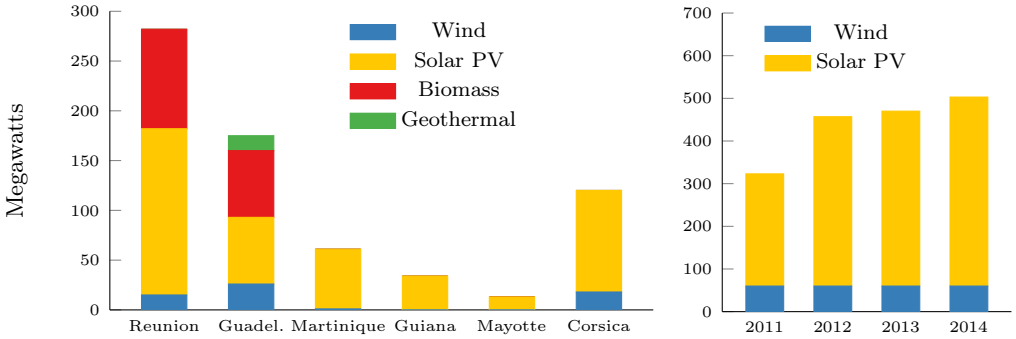

(a) RES in DOM and Corsica for 2014 (b) Main RES in DOM and Corsica

Figure 1.5: Installed capacity of renewable energy sources in DOM and Corsica

The PV installed capacity in DOM for 2013 was 317 MW and produced 442 GWh, which represented 5,8% of the total energy mix [27]. Nevertheless, V-RES technologies have some fundamental differences with respect to conventional power plants, which has slowed down their development as the concerns about their impact on power system planning and operation raise [28].

RES integration challenges

Wind speed and solar irradiation cannot be controlled; therefore, they produce a variable power output that has low controllability (only curtailment or spilling) and is only partially predictable, increasing the level of uncertainty in power systems operations. In addition, they tend to be asynchronously connected to the grid by power electronics, which prevents them to naturally contribute to the system inertia and may deteriorate dynamic behaviour of the system. Moreover, they may interfere with the effectiveness of contingency measures, such as the automatic UFLS, or the normal operation of protection devices, like distance relays, since they are generally connected to the distribution network .

Furthermore, according to environmental policies, they are prioritised in dispatch, even though in many cases they do not participate to the provision of ancillary services. These specificities of V-RES have motivated an exhaustive review of power system optimisation, analysis and control principle and models from planning to real-time operation [29, 30]. A significant amount of work has been published on examining the impact of V-RES at different levels (generation, transmission and distribution), in systems of diverse sizes, from small and isolated to large-scale interconnected [31, 32]. Literature on this topic is extensive, specially considering wind power, and it covers a wide range of time scales.

Although an exhaustive state of the art on this topic is beyond the scope of this work, it should be noted that some issues received more attention than others. For example, the impact of the hourly variability and increased uncertainty is the focus of several works [33, 34, 35, 36], and some trend can nowadays be identified: these V-RES features may be handled with higher flexibility requirement (*i.e.*, ramp rates) and larger margins (*i.e.*, reserves) [37, 38, 39, 40, 41, 42]. In addition, a handful of stochastic and robust approaches, and improvement on forecasting techniques have been proposed to deal with the high cost incurred when covering for unlikely extreme scenarios [43, 44, 45]. Some recent works may be cited here for illustrative purposes:

- In 2014, Mai *et. al* [46] stated that renewable electricity generation from technologies that are commercially available today, in combination with a more flexible system, is adequate to supply 80% of the total U.S. electricity generation in 2050. This implies an appropriate mix of renewable technologies, the establishment of mechanisms to ensure adequate contribution to planning and operating reserves, as well as the expansion of transmission infrastructure.
- In 2015 a technical report published by EDF [47] concluded that the short-term variability of wind and PV generation is highly reduced at the European scale by the geographical smoothing effect, although some issues remain for handling intermittency at the distribution level. Moreover, the mid and long term variability poses an actual challenge due to the coupling of climate regimes. Regarding investments in transmission capacity, the need of coordination between the development of RES and network infrastructure is highlighted. Furthermore, it is stated that the conventional generation mix should evolve towards a higher share of peaking units against a lower share of base units in order to manage the increased variability coming from V-RES. From a operational point of view, the main challenge appears at high V-RES instantaneous penetration rates, since traditional flexibility sources are no longer available and there are limited providers of the ancillary services. In this context, the contribution of V-RES and new providers such as active demand, to ancillary services, is declared essential to ensure power system security.

- In 2010, the Irish TSOs EirGrid and SONI commissioned the “Facilitation of Renewable studies" in order to examine the technical challenges of integrating significant volumes of wind power generation onto the power system of Ireland and Northern Ireland [48]. Main issues were classified into four categories: fundamental issues, fundamental issues that need further analysis, issues that can be mitigated, and non-issues according to modelling. They conclude that certain aspect of the power system behaviour will not be significantly affected by the integration of V-RES, such as the small system stability, although it was acknowledged that a comprehensive quantitative analysis was not carried out due to model limitations. However, it is also stated that other technical issues may jeopardise stable system operation for certain operational conditions. Hence, some operational strategies are suggested, such as the definition of limits over predefined metrics. For instance, two proposed metrics are the V-RES instantaneous non-synchronous penetration (SNSP) level and the ratio of kinetic energy stored in conventional generators plus load and the dispatched power of the largest in-feed. Moreover, the report proposes possible directions for power system adaptations in order to further increase the V-RES integration capabilities without compromising security. Some examples include the increase of network capacity, the deployment of alternative protection schemes and the extension of reactive power sources.
- In 2014, the French Environment & Energy Management Agency (ADEME), published a study on the optimal conditions for a 100% renewable electricity mix (80% V-RES) in 2050 [49], where four scenarios were considered depending on RES technology evolution, network reinforcement and social acceptability. It is concluded that interconnections, flexibility resources (demand side management and short/long-term storage) and technological diversity are essential to maintain system adequacy. The proposed mixes are based on at least 20% of hydro and renewable thermal, and a complementarity between wind (in and off shore) and solar (rooftop and ground-mounted).

Nevertheless, many challenges remain regarding social acceptance, the feasibility of adding enough transmission capacity, and the compatibility between grid codes and markets [50], as well as, in the development of scheduling, regulation, and stabilisation methods and algorithms [51]. More recently, these latter topics have received some attention as the concerns about power system security have increased [52, 53, 54, 55]. For example, the decline of frequency regulation as the share of non-synchronous generation increases has become an active research field [56], especially following some recent frequency stability events [57, 58]. According to [48] the frequency stability following large disturbance remains indeed a fundamental issue in V-RES integration.

1.1.3 Emerging frequency regulation issues

First, modern discussions on frequency regulation issues were related to the deregulation of the electricity sector. The main concern at the moment was related to load following (secondary frequency control) [59]. In 2000, the California electricity market crisis revealed that the reliability standard were no longer respected under this new structure [60].

Nowadays, most of the liberalised systems have switched to competitive procure methods [13], that ensure adequate means to the TSO to maintain reliability in load following, at least at the operational level. The challenge remains in addressing investment incentives to ensure power system security in the long run [61]. Further discussion on this matter is beyond the scope of this work.

Second, some attention was given to the problem of cascading outages after the frequency incident in Europe the night of November 4, 2006 [57]. In fact, first wind turbines were equipped with tight protection schemes, which disconnects them when deep voltage sags or frequency deviation occur due to short-circuits or large power imbalances. In 2006, the European transmission grid split into three independent parts for a period of two hours following a line switching manoeuvre that produced the cascade tripping of some overloaded lines. The imbalance between supply and demand as a result of the splitting was further increased due to a significant amount of tripped resources connected to the distribution grid. More than 15 million European households were affected.

This incident exposed the need for more standardization regarding the connecting condition of DG, especially about their expected performance during and following a disturbance on the grid. In France, for instance, all DG facilities with a capacity greater than 5 MW must comply with a low voltage ride through (LVRT) specific characteristic, as any conventional generator [62].

Regarding frequency deviations, distributed generation (DG) facilities should disconnect below a certain threshold to avoid islanding, which might cause some system-wide drawbacks as DG share increases. Following large disturbances, as the loss of a generating unit, frequency deviations may reach this threshold and generate cascading outages of RES distributed plants. In order to limit the risk of such events, a frequency range for normal and continuous operation has been established, usually from 49.5Hz to 50.5Hz in Europe. Beyond this range, the generating units are required to remain connected for at least a predefined time. In France, for instance, all DG facility with a capacity greater than 5 MW must remain connected to the grid for at least 3 minutes if the frequency drops between 49-48 Hz and 48-47.5 Hz [63]. In addition, the effectiveness of load shedding emergency schemes may be compromised to some extend if DG units are lost after the breaker operation. Isolated systems are more likely to suffer from these side effects, as described in the next section.

Isolated power systems

A isolated power system is defined here as an electrical system with a limited or in-existent connection with other power systems. They are characterised by certain features:

- They have a limited geographical extension and relatively low peak demand, therefore they are equipped with a reduced amount of small size power plants.
- Production costs are usually high and the active power reserves are difficult and costly to provide.
- They have low short-circuit power and are more sensitive to disturbances.

Indeed, in the case of the loss of a generating unit, the power imbalance is very large with respect to the size of the system. For example, in the French DOM, it can exceed 15% of the connected capacity at a given instant. For a large interconnected system such as the European continental synchronous area, the reference incident (loss of two units of 1.5 GW) will not exceed a ratio of 2% of the connected capacity, even at its lowest demand level (150 GW). In addition, the frequency in an isolated power system is less robust than in an interconnected one. These systems are subject to larger frequency deviations and gradients. Following a power imbalance, the maximum rate of change of the frequency (ROCOF) depends on the imbalance itself and on the *equivalent inertia* of the system. Therefore, it depends on the number and size of synchronous units that remain connected after the contingency. As aforementioned, in an isolated system, the number and size of the production units are considerably smaller than in interconnected system such as continental Europe.
Regarding the integration of RES, the reduced geographic extension of isolated systems makes them even more vulnerable to the intrinsic variability and uncertainty of these sources. This is due to the limited contribution of the spatial smoothing effect to the reduction of the aggregated output power variations and prediction errors. The secondary frequency control, called automatic generation control (AGC) or load-frequency control (LFC), meant to handle short-term demand variability, tends to be absent in such systems since no interchange schedules need to be restored after a large disturbance. Instead, the former function is generally fulfilled by fast, but usually manual, tertiary control.
For those reasons, V-RES integration challenges in isolated power systems may slightly differ from those of larger systems and often appear for lower shares, because high instantaneous penetration rates are reached after installing a few gigawatts (or some megawatts) of capacity. This is the case in different European overseas territories (autonomous community or regions), such as the Canary Islands (Spain) [64, 65], the Madeira and Azores archipelagos (Portugal) [66, 67], Sardinia (Italy) as well as the DOM and Corsica (France) [68, 69] and even in larger system such as Great Britain and Ireland [32, 70].

In general, the generation mix of isolated power systems is composed of small thermal units without technical hourly ramping constraints. Flexibility is not the main concern, however, increasing reserve requirements might be costly or even infeasible at some time steps with high penetration rate of RES, and frequency regulation may become a challenging task. As a consequence, some system operators have established a cap on the instantaneous penetration rate of sources connected through power electronics in order to maintain security levels. These are not in strict relation with uncertainty or variability management.
For example, the relevant Greek legislation framework explicitly defined a threshold for the wind power instantaneous penetration in order to maintain the system stability and power quality [71]. For medium- and large-size isolated systems (such as the ones of Crete and Rhodes), the wind power instant penetration value was limited to 30%, while in smaller systems (small Aegean Sea islands), the corresponding value may be lower than 20%.
In the DOM, the system operator EDF SEI (*Systéme Électrique Insulaire*), is authorised to disconnect V-RES facilities larger that 100 kVA when the sum of the active power injected by such facilities reaches 30% of the total active power flowing on the network [63]. However, in some cases, the system security is already compromised below this threshold, while in other cases the system could be operated at higher penetration levels without increasing the risk of load shedding. In this context, one challenge consists of proposing suitable solutions for raising this technical limit and further integrate RES generation, while ensuring the proper functioning of the primary frequency control.
In the Ireland system, studies suggested the SNSP level most not exceed the 50% given the current operational environment of the power system, although this threshold may be pushed following major adaptations [48]. Moreover, it is stated that the integration of the system conditions in the real time system monitoring tools (state estimator) will help to maximise the allowable value for the V-RES instantaneous penetration rate in operation. These limits are usually verified at the dispatch or UC level and a curtailment decision may be send to the energy supplier before real-time if a violation is foreseen.

1.2 Motivation and problem statement

Nowadays, technical regulations are evolving in different systems to anticipate security issues as the installed capacity of RES continues to grow. Some of them start to require at least constructive capability of RES to provide certain ancillary services or considering dedicated providers. Services related to voltage regulation and reactive power seem more straightforward to implement in units with fully-controlled converters. However, the provision of active power reserves and frequency regulation services could be more challenging to prescribe for non-dispatchable resources, although different alternatives have been proposed. Some of them are listed below:

- Participation of V-RES to the provision of active reserve by injecting a derated power [72, 73, 74].
- Participation of V-RES to the inertial response, by extracting kinetic energy for the shaft in wind turbines [75, 76], or by adding storage systems to PV plants.
- Provision of dynamic support by dedicated facilities, such as centralised storage systems (pumped-storage [66], batteries [68], flywheel [77], etc.) or demand side management systems (DSMS) [78, 79, 80].

Regarding frequency control, EirGrid for instance requires that all wind farms with a nominal power greater than 5 MW must be able to reduce their power in case of over-frequency, while wind farms with a capacity greater than 10 MW should be able to contribute to the primary reserve by controlling its generation to a level below the maximal available power in normal operation, and injecting the remaining power in case of under-frequency following a frequency/power characteristic [81]. The main drawback of this technique is that part of the wind energy (the reserve) is constantly spilled.

In order to address this setback, another solution has been considered, referred to in the literature as “synthetic" or “virtual" inertia, which enables wind turbines to inject part of the kinetic energy stored in rotating masses to the grid when the frequency drops. Some arguments have been given against this technology, such as the increase on the costs of the converter and some mechanical parts due to the current response and the constraints applied to the turbine. In addition, the effectiveness of this measure alone might be partially compromise in practice. Indeed, it is challenging to build a firm offer since it is affected by both forecast and variability.

Finally, the provision of dynamic support by dedicated storage facilities starts to become a cost effective solution in isolated systems with high share of V-RES [64, 66, 68], although these technologies imply a high investment cost, which prevents them to be implemented in larger systems.

As a conclusion, no consensus has yet emerged on the suitable measures to ensure power system security while maximising the share of renewable energy in the mix at reasonable cost. Moreover, it is not straightforward to think that there will be a consensus at all, given the characteristics on the dynamic responses of different systems, until more adequate methods and algorithms are conceived.

Indeed, the limits of the existing impact mitigation techniques should be investigated, while the development of advance tools to optimise the dispatch of the frequency regulation resources is essential to tackle some operational challenges with high share of V-RES. This thesis aims to make a contribution to this field.

Problem statement

The Unit Commitment problem (UC) is defined here as a family of optimisation models for determining the optimal short-term generation schedule to supply electric power demand with a defined risk level [82]. In general, the objective is to minimise the production costs over a predefined time horizon (ex. 48-24 hours ahead) and across all generating units, while respecting their technical constraints. In general, reserve allocation is also optimised within this procedure. However, the reserve constraints are usually deeply simplified, and, as a consequence, they are not able to catch the complexity of the underlying processes and the regulation services are not fully optimised.

Reserve requirements are traditionally specified following a static reliability criterion, usually given by a reference incident, such as the loss of the biggest unit or the largest power input. Historically, for a conventional generation mix, this security constraint allowed one to obtain UC solutions that naturally provided an acceptable transient response.

However, the increasing share of V-RES, such as wind and solar, can lead to UC solutions that no longer ensure system security. Some mitigation techniques have been proposed. As aforementioned, one option is to make V-RES participate to the primary frequency regulation or to install dedicated facilities. Another option is to tighten the transient response expected from the conventional park that will remain committed. Thus, enhanced security constraints have been proposed to consider the power system dynamics when optimising the day-ahead generation schedule [83, 84, 85, 86].

In general, these contributions are based on linear approximation of the units dynamic response to maintain the Mixed-Integer Linear Programming (MILP) structure of the UC formulation and apply classic optimisation techniques. Nevertheless, this approach has some limitations in terms of effectiveness and optimality, even though its implementation is rather straightforward. Indeed, the use of fixed constraints on inertia, for example, will over-schedule primary regulation resources for some time steps, and nothing guarantees that the security threshold will always be respected. In fact, the relation between inertia and frequency minimum, also called nadir, at the commitment decision level is not necessary, or at all, linear.

In this work, the Frequency Constrained Unit Commitment problem (FCUC) is defined as the family of UC optimisation models, where, in addition to the classic power balance equation and units technical limits, a set of enhanced constraints is added on the inertial response and/or on the quantity and quality of the primary reserve, such that the frequency is kept above a certain threshold following a set of pre-defined (plausible) contingencies.

Finally, the key element of this research line is the choice of a suitable set of enhanced constraints for the FCUC problem. It must be noted that this approach is rather complementary with respect to all the innovating solutions discussed before.

The idea is to compute for each time step (ex. 1 hour-30 minutes) of the optimisation horizon (ex. 48-42 hours) the minimum primary frequency regulation resources needed to ensure security, reduce cost and maximise the energy produced by RES. The next section list the steps followed to achieve this goal.

1.3 Objectives and scope

The general objective of this dissertation is to investigate the effectiveness and cost of different FCUC models in limiting the impact of V-RES on real-time system security, more specifically, on the primary frequency response following large power imbalance, such as the lost of any generating unit. The more effective the tool is, the higher is the share of RES the system can accommodate.

Objectives

In order to achieve this goal, different steps should be taken. These are:

1. Investigate the correlation between day-ahead commitment decisions and primary frequency response.
2. Define an indicator to assess the impact of the increasing share of asynchronous V-RES on the primary frequency response of a conventional power system.
3. Assess the effectiveness and optimality of different FCUC models by examining the capability and over-cost incurred to maintain primary frequency response over different scenarios of RES integration.
4. Identify the set of constraints that more accurately represent the system dynamic behaviour, regarding the frequency trajectory following a large disturbance, in order to propose a new formulation for the FCUC model that ensures optimality.
5. Assess the generalisability and computational tractability of the proposed approach.

Scope

As aforementioned, this work concerns the FCUC problem in a short-term basis. Since the focus is placed on the definition of the set of enhanced security constraint that characterised the FCUC, related to the primary reserve allocation, the departure optimisation model will be a classic and deterministic UC model.
The main hypotheses are linear cost coefficients, typically used for thermal plants, no hydro power consideration and the demand is considered as perfectly known (forecast). This means that the secondary and tertiary reserve are supposed to cover for short-term variability and forecasting errors.

Regarding the modelling of the frequency-related constraints, the representation of certain aspects of the transient response of a power system will be privileged while some hypothesis on other phenomena shall be made. In the first place, it will be considered that the primary reserve can be allocated over different providers, not only conventional units. Furthermore, V-RES curtailment is possible at a certain penalty cost. The impact of this parameter will be assessed.
In addition, the heterogeneous dynamic parameters of the different providers, specially conventional units, must be represented with some detail to catch the notion of "quality" of the contribution to the primary frequency response at the day-ahead scheduling level. This quality notion combines at least three different aspects. The first one, maybe the more common, is the inertia, more specifically, the contribution of a certain energy provider to the kinetic energy stored in the system. The second one is droop parameter, the sensitivity of the power output signal to the frequency changes. And the third, maybe the less common one, is the response time of the regulation. In addition, the reduction of the possible power imbalance itself is also considered as a mechanism to limit UFLS risk.
Finally, network constraints, voltage regulation issues, and frequency regulation issues driven by market structure or by the mislead action of protection scheme are out of the scope of this work. The acronym FCUC is specifically defined for this security problem, since the term security constrained UC (SCUC) is already used in literature to designate the day-ahead scheduling problem with network constraint (power flow and voltage limits) [87], which are not considered here, but could be included in the proposed formulation.

1.4 Thesis outline

Beyond the introduction, this dissertation is organised in five chapters as follows:

Chapter 2: Formulation of classic models to study the primary frequency response

This chapter presents a first attempt to formulate the frequency nadir constraint. First, section 2.2 details the implemented classic UC model, as well as the selected solution method and assumptions. Second, section 2.3 thoroughly examines the relation between the frequency nadir and the UC decision variables through the analytical formulation of different reduced order system frequency response (ROSFR) models. In addition, it describes the proposed ROSFR model to estimate the average frequency trajectory after a unit outage, which includes additional features with respect to its predecessors available in literature. Lastly, section 2.4 proposes a sequential simulation tool to numerically analyse the relationship between the frequency nadir and the generation schedules and reveal the interest, from a technical point of view, of better formulating the security constraint.

Chapter 3: Impact of PV generation on the primary frequency response

The evolution of the UFLS risk with the installed capacity of PV in an isolated power system is quantified. Simulation results of a day-ahead schedule are extensively analysed to examine the impact of the PV integration on the commitment decisions, and their consequences on the primary frequency response of the system under concern. Then, hourly stepped time series of one year demand and PV generation are used the get an statistical representation of the primary frequency regulation performance. Finally, the relation between the frequency nadirs and some parameters, such as instantaneous penetration rates or system stored kinetic energy, is investigated. The need for a more accurate representation of the primary frequency regulation process in the UC is highlighted.

Chapter 4: Limiting UFLS risk with high share of non-synchronous generation

This chapter examines the effectiveness and cost of different impact mitigation techniques by running a set of primary reserve & energy co-optimisation models. More specifically, seven FCUC models are implemented, based on linear approximations of dynamic constraints and the deployment of dynamic support resources, such as a centralised storage. Then, 365 day-ahead schedules are obtained for each one of them, corresponding to a one year demand and PV load factor time series. This procedure is repeated for different parameter associated to each model and for four scenarios of PV installed capacity. Afterwards, dynamic simulations are performed for every conceivable outage in order to quantify the risk of UFLS. It is shown that enforcing a fixed reserve, inertia, or maximal frequency slope constraint is not cost/effective to limit the dynamic risk as the share of RES raises, since the system's need for frequency regulation capabilities depends on the operating point, exposing the need for new approaches to properly account for the frequency regulation underlying processes in optimisation models.

Chapter 5: A convex formulation for the FCUC problem

This chapter develops a Benders' decomposition approach for the FCUC problem, where the frequency minimum constraints are included in the slave problem, a frequency constrained multi-temporal economic dispatch (FCED) model, through a cutting plan model. The underlying hypothesis is that the frequency minimum is a concave function of the power level of the generating units, at fixed commitment decisions. Therefore, the binary variables defining the unit states are optimised by the master problem, while the continuous power output variables for a candidate solution are adjusted at the slave problem level to ensure that the frequency constraints are respected. If the slave problem is feasible an optimality cut is generated, otherwise a feasibility cut is send to the master problem to prevent the infeasible candidate solution to reappear.

The proposed methodology is able to ensure optimality (to a predefined confidence interval), which means that the primary frequency regulation resources are optimally allocated at each time step to keep the frequency minimum over the specified threshold, considering the available provides: conventional generator (with different inertia, regulation parameters and primary reserve deployment dynamics), RES curtailment, storage, interruptible loads, etc. Nevertheless, this first formulation, based on a standard Benders' method, presented poor convergence properties. Therefore, a second version, called stabilised FCUC by Benders' decomposition, was proposed, based on a Level bundle method, to handle the inherent instability of cutting plans-based methods that lead to slow convergence. Preliminary results are encouraging but additional work is still needed.

Chapter 6: General conclusions and perspectives

This chapter summarises the main achievements of this research work and proposes some recommendations for future developments.

Appendices

A certain number of appendices completes the presentation of this dissertation. First, appendixes A-D include additional details regarding the ROSFR models presented in chapter 2. These sections provide some numerical illustrations and algebraic manipulation, as well as the algorithm of the solution method. Appendix E describes the test system and the characteristics of the different RES scenarios considered in the case studies. Appendix F offers a comprehensive analysis of the primary reserve deployment of the different regulating units considering the simulation results presented in chapter 2.

1.5 Main contributions and originality claim

The main contributions of this work are:

1. The relation between the frequency nadir and the UC decision variables is formally analysed and a upgraded ROSFR model was proposed that account for saturation processes of the regulation. The importance of this feature is thoroughly discussed.
2. The limits of enforcing a fixed reserve, inertia, or maximal frequency slope constraint are highlighted. These measures are not cost effective to limit the UFLS risk, since the system's need for frequency regulation depends on the operating point.
3. A FCED model based on a cutting plane model of the frequency minimum is formulated. Simulation results show good convergence properties. Therefore, a first feasible solution, in term of the frequency constraints, can be easily obtained for fixed commitment decisions. If the FCUC is not feasible, the feasibility cuts will enable the computation of a new candidate commitment vector.

Although, the computational time of building the CP rises with the size of the system, due the sub gradient calculation, the parallelisation of this procedure is straightforward. However, due to the nature of the feasibility cuts (no-good cuts), the algorithm can lose some time before finding a really different solution if several units are similar.

4. A FCUC formulation by Benders' decomposition is proposed and proves to be effective in limiting the risk of UFLS while integrating RES, at lower cost than the models discussed in chapter 4. This is at the expense of a higher complexity and computational time and this formulation suffers from a slow convergence. Thus, a quadratic stabilisation algorithm, based on a level-bundle method, was implemented to tackle the instability issues of the decomposition method and improve the convergence of the master problem.

This dissertation provides a theoretical and rigorous formalisation of the FCUC by Benders' decomposition method that was missing in the field of operational research and power systems optimisation. Decomposition methods has been applied to power systems problems for a while and they have proven their value. The Benders' method has been used before for handling non-linear constraints in the MILP formulation of the SCUC model [88], while strong hypothesis have been made on the primary frequency response for day-ahead scheduling purposes [85]. Thanks to this original work, a set of restrictive assumption, such as the convexity (even local) of the frequency minimum regarding the commitment decision variables or the equality on the response times of all system governors, can be raised. In addition, the limitations of indirect constraints, such as those on the inertia, have been revealed, although they are easier to implement.

Publications

1. C. Cardozo, L. Capely, P. Dessante. Frequency constrained unit commitment. *Energy Systems*, pages 1-26, 2015 [89].
2. C. Cardozo, L. Capely, P. Dessante. Increasing the integration capabilities of photovoltaic generation in a small and isolated power system. In *EPEC*, London, Ontario, Octobre 2015 [90].
3. C. Cardozo, L. Capely, J. Lacoste, P. Dessante. A statistical analysis of the frequency response in an isolated power system with an increasing share of photovoltaic generation. In *PowerTech*, Eindhoven, June 2015 [69].
4. C. Cardozo. Impact des énergies renouvelables sur le fonctionnement dynamique d'un système électrique. In *JCGE*, Cherbourg, France, Juin 2015.
5. C. Cardozo. Unit Commitment with Uncertainties - State of the art. In *JCGE*, Saint-Louis, France, Juin 2014.

Chapter 2

Formulation of classic models to study the primary frequency response

Contents

2.1 Introduction

This chapter describes the two main models implemented in this thesis to study the evolution of the primary frequency response following the integration of renewable energy

sources (RES) connected through power electronics. Section 2.2 discusses the state of the art of unit commitment (UC) models and details the UC model implemented in this work. Section 2.3 provides a theoretical analysis of the frequency behaviour with respect to the UC decision variables and presents the simplified dynamic model implemented in this work to estimate the average frequency trajectory after a unit outage. Section 2.4 examines the relation between day-ahead schedules and the primary frequency response through simulation. Conclusions are drawn in section 2.5.

2.2 Unit commitment model

The Unit commitment (UC) can be defined as a family of constrained optimisation problems that defines the generation units' schedules to supply the electrical demand of a power system over a specific time period, while respecting technical limits, as well as operational and security constraints at every interval of the optimisation horizon. This can be written in a generic form as follows:

$$\begin{aligned} \underset{x \in X}{\text{minimise}} \quad & f_0(x) \\ \text{subject to} \quad & f_\imath(x) \leq 0 \qquad \imath = 1, \ldots, i, \\ & g_\ell(x) = 0 \qquad \ell = 1, \ldots, l, \end{aligned} \tag{2.1}$$

where, $f_0 : \mathbb{R}^m \to \mathbb{R}$ is called the objective function, $f_\imath : \mathbb{R}^m \to \mathbb{R}$ for $\imath = 1, \ldots, i$, are the inequality constraints, $g_\ell : \mathbb{R}^m \to \mathbb{R}$ for $\ell = 1, \ldots, l$, are the equality constraints, and $x = (x_1, \ldots, x_m) \in X \subset \mathbb{R}^m$ is the optimisation vector. The components of this vector are the optimisation variables, also called decision variables, which, for the UC problem, are usually given by the generating units' states (on/off) and their power output.

In general, the UC objective function f_0 is a more or less detailed representation of the cost of supplying the demand for the optimisation horizon, which in short-term scheduling is typically 24 to 48 hours, composed of discrete time steps of 30 minutes or 1 hour.

Several variants of the general UC problem exist considering different sets of constraints and/or terms in the objective. For example, the security constrained UC (SCUC) problem includes network constraints, such as limits on the power flows, bus voltages, transformer taps, power losses, etc. [87, 88], which can be modelled with different degrees of detail, from linear approximations (DC power flow) to full non-linear equations [91].

Moreover, significant effort has been devoted to the consideration of detailed constraints specific to hydro power valleys [92, 93, 94, 95]. Fuel or emission (*e.g.*, CO2) considerations can be also added to the UC model [96, 97, 98, 99, 100].

Therefore, depending on the power system specificities, which define the size and the nature of the objective and constraint functions, a detailed UC model can become a large-scale Mixed-Integer Non-Linear Programming (MINLP) problem, difficult to solve.

However, this problem needs to be solved in a time scale compatible with short-term scheduling in order to be used in operation. Thus, different approximations have been used and a lot of research has been done on effective solution methods for the UC problem.

2.2.1 Background

The optimal short-term schedule of generation to supply the electric power demand with a reasonable risk level has been a matter of concern in utilities for at least five decades, and has been widely addressed in literature [82, 101, 102, 103, 104, 105, 106]. Intuitive methods such as Exhaustive Enumeration (EE) [107] and Priority List (PL) [108] were initially applied to small power systems. Afterwards, the simultaneous growth of the electrical system infrastructure and computational power drove the application of formal optimisation techniques such as Dynamic Programming (DP) approaches [109] to solve the UC problem. Since then, its mathematical formulation has not ceased to evolve.

Until 2000 two main evolution trends could be identified: the modelling of new or more accurate operating constraints and the application of different optimisation techniques. Indeed, the simplifications traditionally made in the modelling of generating units' constraints were reviewed as the tractability of the initial versions of the UC problem progressed with the methodological and technological advances. Nowadays, efficient and reliable MILP solvers, suited for parallel execution, are commercially available [110, 111, 112], and are capable of solving certain relativity large MILP problem (with a few thousands of variables and constraints) in a matter of seconds, even on a personal computer.

Although these research fields remain active, recent developments in UC models are more related to the transformation of the power system operational environment, following the deregulation of the energy industry and the integration of variable RES (V-RES). In this section, some published literature reviews will be discussed to identify the suitable formulation and solution method for addressing the frequency constrained UC (FCUC) problem. Nevertheless, a detailed description of all considered solution techniques is beyond the scope of this work.

In 1987 Cohen *et al.* [101] discussed the scope of the short-term UC problem, with emphasis in hydro-thermal constraints. The available solution methods for the UC problem at that time were: DP, Lagrangian Relaxation (LR), branch-and-bound methods and Benders' decomposition.

Then, in 1994 Sheble *et al.* [102] analysed 80 available references on the solution of the thermal UC problem and concluded that LR was the most promising technique in short-term scheduling, since some drawbacks were identified regarding the use of DP approaches to solve the complete UC problem. In fact, this technique suffers from dimensionality issues due to the combinatorial nature of the UC problem. Certain simplifications were proposed but, they entailed a suboptimal treatment of inter-temporal units' constraints.

As a consequence, the optimality principle may be violated when considering minimum up/down time constraints, which impose an on-line/off-line time once a unit has been started/shut down [113]. Nonetheless, the DP is still used, but to solve sub-problems following decomposition approaches, such as LR.

A review by Padhy in 2004 [103] covered 35 years of research on UC including over 150 published papers. Three topics were discussed: UC cost minimisation vs. profit maximisation firsts' formulations, the integration of network constraints (SCUC) and suitable optimisation methods to solve the UC problem. The first point is related to the deregulation of the energy sector, while the two others correspond to the aforementioned traditional research branches, *i.e.*, constraint modelling and solution methods.

In a market-based power system, the generating companies (GENCOs) objective is revenue maximisation, which created a new family of scheduling problem that are referred to as bidding strategies in the literature [114]. Then, the cost of energy purchases is minimised (or the social welfare is maximised) through Market Clearing (MC) mechanisms, whether by the Transmission System Operator (TSO) [115] or a Power Exchange. These topics represent nowadays a research field on its own that lies outside the scope of this work.

Regarding the solution methods, a new trend was identified towards the implementation of hybrid methods, based on a combination of classic techniques with heuristic algorithms. This review work has been updated in [105] and [106], with a focus on meta-heuristic methods such as simulated annealing [116], particle swarm [117], genetic algorithm [118], neural networks [119], taboo search [120], etc. applied to the UC problem. Nevertheless, these methods on their own have some recognised downsides, such as the inability to provide qualified bounds. In addition, they have been applied to small and theoretical test systems to prove feasibility, but are still outperformed by other techniques based on mathematical programming, which have also known significant improvements.

Finally, a comprehensive literature survey, with more than 400 references, on optimisation methods applied to large-scale UC, with special attention on uncertainty consideration following V-RES integration, has been recently published [82]. Indeed, the use of deterministic UC models in a uncertain environment may lead to schedules that are in practice significantly more costly than predicted, or even infeasible. Research on this topic has followed two main approaches. On the one hand, uncertainty is handled in a implicit way through an advance calculation of reserve requirements and flexibility constraints [36, 44]. On the other hand, the explicit representation of uncertainties, specially those coming from the V-RES forecast errors, in the UC model formulation has been proposed. This sub-family of UC model has been referred to as the uncertain UC (UUC) problem [82]. In the last ten years some UUC formulations have been focussed on the modelling of the demand addressed to the conventional park (the net or residual demand) as a random variable [32, 35, 45, 121, 122, 123].

In 2015 Tahanan *et al.* [82], categorised this approach in three families: stochastic optimisation (SO), robust optimisation (RO), and chance constrained optimisation (CCO), which are based on mathematical programming techniques, considered to be the most relevant for the UUC formulation.
Finally, the simplest UC model can still be difficult to solve when the size of the system, represented by m in equation (2.1) is too large (a few hundreds of thousands variables) or when the technical and operational constraints are represented to a certain level of detail, which makes the feasible space (where the constraints are satisfied) a complex set.
In both cases, decomposition methods offer an interesting research line and will be further discussed in chapter 5. In general, dealing with uncertainties in UC models implies at least one of the two aforementioned features, which makes it a challenging task. For example, in SO approaches, the scenario dimension is added, while CCO approaches are based on the inclusion of probabilistic constraints that can be nonconvex and hard to evaluate.
It must be noted that even in the deterministic case, certain constraints may be harder to take into account than others depending on the specific considered mix.

A suitable approach for the FCUC problem

Figure 2.1 illustrates the different aspects of the UC problem discussed in this section and position the work carried out in this dissertation, which is focussed on the formulation of new operating constraints regarding the allocation of primary reserve to efficiently limit the risk of under-frequency load shedding (UFLS), referred to here as the FCUC problem.

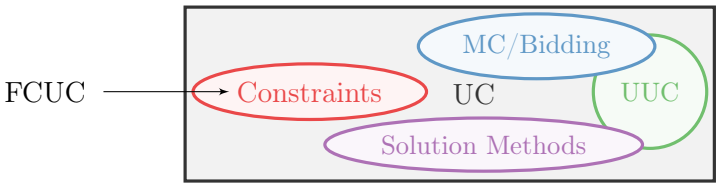

Figure 2.1: Main research fields for the UC problem

It should be noted that the more recent fields (deregulated environment and UUC) are not exclusive, since uncertainty is also present in the electricity prices, which are an input parameter in the strategic bidding models [124].
In addition, the modelling of complex constraints has been represented as a dissociated problem from the uncertainty management and the search of solution methods, which might not be the case in practice. In fact, the need for taking into account complex constraints in short-term scheduling have motivated the application of new optimisation approaches to the UC problem, from both mathematical programming and meta-heuristic areas. Hence, some works propose the development of ad-hoc methods. A second option consists in reformulating the initial problem to apply standard optimisation techniques.

In this work this second path is taken. The frequency constraints will be formulated in a way that enables the use of established solution methods, based on mathematical programming techniques, and leave the road open to their integration in the other sub-families of the UC problem, such as MC mechanisms or the UUC.
Thus, without loss of generality, a classic MILP deterministic formulation is chosen as a starting point to address the FCUC problem [125]. Until now, some published works on this topic use linear approximations that neglect relevant features of the committed units dynamics [83, 84, 85, 86].
Moreover, the use of a MILP deterministic formulation enable a statistical study of the primary frequency response for different V-RES integration scenarios (see chapter 3), since it limits the computational burden. Then, the limitations of existing FCUC formulation based on indirect linear constraints will be examined in chapter 4.
Afterwards, the effort will be placed on overcoming these limitations, which is a challenging task because, as it will be shown in section 2.3, the frequency nadir is extremely non linear with respect to the decision variables. Moreover, it is not obvious how to obtain an analytical expression capable of taking into account the heterogeneous characteristics of different units and emerging providers of frequency regulation services. Therefore, an alternative path way will be explored in chapter 5, following a decomposition approach.

2.2.2 Notation

Integer and indexes

N	number of units
T	optimisation horizon, number of time steps (of duration Δh hours each)
h	index of time step
j	index of unit

Optimisation variables

u_j^h	binary state of unit j at time step h ($off = 0$, $on = 1$)
g_j^h	continuous output power of unit j at time step h in MW
$r_j^{h,pr}$	continuous primary reserve of unit j at time step h in MW
$r_j^{h,sl}$	continuous slow upward reserve of unit j at time step h in MW
$r_j^{h,dn}$	continuous slow downward reserve of unit j at time step h in MW
$x_j^{h,up}$	binary up auxiliary variable of unit j at time step h (started up=1)
$x_j^{h,dn}$	binary down auxiliary variable of unit j at time step h (shut up=1)

Parameters

R_{pr}^{min}	minimal primary reserve in MW
R_{sl}^{min}	minimal slow upward reserve in MW
R_{dn}^{min}	minimal slow downward reserve in MW

D_f^h	demand forecast (including losses) for time step h in MWh
G_j^{max}	maximal power output of unit j in MW
G_j^{min}	minimal stable generation (MSG) of unit j in MW
R_j^{up}	hourly upward ramping limit of unit j in $MW \cdot h^{-1}$
R_j^{dn}	hourly downward ramping limit of unit j in $MW \cdot h^{-1}$
T_j^{up}	minimum running time of unit j in hour
T_j^{dn}	minimum down time of unit j in hour
$R_j^{pr,max}$	maximal primary reserve allocated on unit j in MW
$R_j^{sl,max}$	maximal slow upward reserve allocated on unit j in MW
$R_j^{dn,max}$	maximal slow downward reserve allocated on unit j in MW
$a_{0,j}$	fixed linear cost coefficients of unit j in €
$a_{1,j}$	variable linear cost coefficients of unit j in €$\cdot MW^{-1}$
$a_{r1,j}$	linear cost coefficients of unit j primary reserve in €$\cdot MW^{-1}$
$a_{r2,j}$	linear cost coefficients of unit j slow reserve in €$\cdot MW^{-1}$
$a_{rdn,j}$	linear cost coefficients of unit j downward reserve in €$\cdot MW^{-1}$
$a_{up,j}$	start up cost of unit j in €
$a_{dn,j}$	shut down cost of unit j in €

Functions

C_j^h	fixed and variable cost of unit j at time step h in €
S_j^h	start up and shut down cost of unit j at time step h in €

2.2.3 Deterministic UC model

The objective function of the classic deterministic UC problem is given by equation (2.2) as the sum of the operating cost over all N units through the optimisation horizon T. The components of this cost are the energy (C), start up and sometimes shut down costs (S), which depend on the state and power output of each unit j at each time step h, denoted by u_j^h and g_j^h respectively.

$$f_0(u,g) = \left\{ \sum_{h=1}^{T} \sum_{j=1}^{N} C_j^h \left(u_j^h, g_j^h\right) + S_j^h \left(u_j^h, u_j^{h-1}\right) \right\}. \tag{2.2}$$

In addition, auxiliary variables are generally defined for the start up ($x_j^{h,up}$) and shut down ($x_j^{h,dn}$) operations, as expressed in equation (2.3).

$$\begin{aligned} x_j^{h,up} - x_j^{h,dn} - u_j^h + u_j^{h-1} &= 0 \qquad && \forall j = 1,\ldots,N, \forall h = 1,\ldots,T, \\ x_j^{h,up} + x_j^{h,dn} &\leq 1 \qquad && \forall j = 1,\ldots,N, \forall h = 1,\ldots,T. \end{aligned} \tag{2.3}$$

As discussed in chapter 1, the reserve is commonly split in three types: primary, secondary and tertiary reserve and is often symmetrical but not always. Here only upward primary, and slow (upward and downward) reserves are represented, for the sake of simplicity. This is a current practice in small and isolated system. They are denoted by $r_j^{h,pr}$, $r_j^{h,sl}$ and $r_j^{h,dn}$ respectively.

Cost functions

In this work a linear cost approximation is used as this is a well accepted assumption [125]. Different cost coefficients may be then defined: $a_{0,j}$ represents the fixed cost, if any, $a_{1,j}$ is the variable cost coefficient, $a_{up,j}$ and $a_{dn,j}$ account for start up and shut down costs, if considered separately.

$$\begin{aligned} C_j^h &= a_{0,j}u_j^h + a_{1,j}g_j^h + a_{r1,j}r_j^{h,pr} + a_{r2,j}r_j^{h,sl} + a_{rdn,j}r_j^{h,dn} && \forall j = 1,\dots,N, \forall h = 1,\dots,T, \\ S_j^h &= a_{up,j}x_j^{h,up} + a_{dn,j}x_j^{h,dn} && \forall j = 1,\dots,N, \forall h = 1,\dots,T. \end{aligned} \tag{2.4}$$

Finally, a cost might be explicitly defined for each reserve type through coefficients $a_{r1,j}$, $a_{r2,j}$ and $a_{rdn,j}$. In this work, these last three coefficients are set to zero for conventional units, and reserve provision cost is quantified by the loss of opportunity cost (LOC).

Main constraints

The UC problem is commonly subject to three types of constraints: the power balance (2.5), the generators' technical limits (2.6)-(2.11), and the security constraints (2.12).
The deterministic UC problem supposes a perfect knowledge of the load profile, therefore the power balance equation can be written as a function of the average forecasted demand addressed to the dispatchable units at each time step h (D_f^h).

$$\sum_{j=1}^{N} g_j^h = D_f^h \qquad \forall h = 1,\dots,T. \tag{2.5}$$

The sum of the generated power and the reserves allocated on each unit must respect its up and down capacity limits given by G_j^{max} and G_j^{min} respectively.

$$\begin{aligned} g_j^h + r_j^{h,pr} + r_j^{h,sl} &\leq u_j^h G_j^{max} && \forall j = 1,\dots,N, \forall h = 1,\dots,T, \\ g_j^h + r_j^{h,dn} &\geq u_j^h G_j^{min} && \forall j = 1,\dots,N, \forall h = 1,\dots,T. \end{aligned} \tag{2.6}$$

The reserves, as defined here, must be positive.

$$\begin{aligned} r_j^{h,pr} &\geq 0 && \forall j = 1,\dots,N, \forall h = 1,\dots,T, \\ r_j^{h,sl} &\geq 0 && \forall j = 1,\dots,N, \forall h = 1,\dots,T, \\ r_j^{h,dn} &\geq 0 && \forall j = 1,\dots,N, \forall h = 1,\dots,T. \end{aligned} \tag{2.7}$$

In addition, an operational limit is generally defined on the maximal primary reserve that can be allocated in a specific unit ($R_j^{pr,max}$), since it must be deployed in some seconds. The same can be done for slower reserves ($R_j^{sl,max}$ and $R_j^{dn,max}$). These values are set to zero for the units that do not participate to the frequency regulation.

$$\begin{aligned} r_j^{h,pr} &\leq R_j^{pr,max} && \forall j = 1,\dots,N, \forall h = 1,\dots,T, \\ r_j^{h,sl} &\leq R_j^{sl,max} && \forall j = 1,\dots,N, \forall h = 1,\dots,T, \\ r_j^{h,dn} &\leq R_j^{dn,max} && \forall j = 1,\dots,N, \forall h = 1,\dots,T. \end{aligned} \tag{2.8}$$

In some case a generating unit may not be able to modify its output power above a certain value from one time step to another. This is known in the literature as the ramping limits, which constraint the power that can be generated at some instant with respect to the power scheduled for the previous time step.

$$\begin{aligned} g_j^1 - g_j^0 &\leq R_j^{up}\Delta h && \forall j = 1,\dots,N, h = 1, \\ g_j^h - g_j^{h-1} &\leq R_j^{up}\Delta h && \forall j = 1,\dots,N, \forall h = 2,\dots,T, \\ g_j^0 - g_j^1 &\leq R_j^{dn}\Delta h && \forall j = 1,\dots,N, h = 1, \\ g_j^{h-1} - g_j^h &\leq R_j^{dn}\Delta h && \forall j = 1,\dots,N, \forall h = 2,\dots,T. \end{aligned} \tag{2.9}$$

Analogously, a unit might or not be available for commitment in a certain time step depending on its state at the previous one. On the one hand, minimum up time constraints represent the minimal time that a unit must remain on-line once it has been committed.

$$\begin{aligned} &\sum_{\tau=1}^{(T_j^{up}-T_j^{0,up})} u_j^\tau \geq u_j^0(T_j^{up} - T_j^{0,up}) && \forall \tau = 1,\dots,T, \forall j = 1,\dots,N, h = 1, \\ &\sum_{t=\tau}^{min(t+T_j^{up}-1,T)} u_j^\tau \geq T_j^{up} x_j^{h,up} && \forall \tau = 1,\dots,T, \forall j = 1,\dots,N, \forall h = 2,\dots,T, \end{aligned} \tag{2.10}$$

On the other hand, minimum down time constraints prevent the commitment of a unit that has just been shut down in order to limit cycling processes.

$$\begin{aligned} &\sum_{\tau=1}^{(T_j^{dn}-T_j^{0,dn})} (1 - u_j^\tau) \geq (1 - u_j^0)(T_j^{dn} - T_j^{0,dn}) && \forall \tau = 1,\dots,T, \forall j = 1,\dots,N, h = 1, \\ &\sum_{t=\tau}^{min(t+T_j^{dn}-1,T)} \left(1 - u_j^\tau\right) \geq T_j^{dn} x_j^{h,dn} && \forall \tau = 1,\dots,T, \forall j = 1,\dots,N, \forall h = 2,\dots T. \end{aligned} \tag{2.11}$$

All uncertainty is covered by enforcing security constraints in order to ensure a certain volume of on-line spare capacity. The simplest representation of these constraints are based on a set of deterministic (pre-defined) minimal requirements (R_{pr}^{min}, R_{sl}^{min} and R_{dn}^{min}).

In general, the required primary reserve (R_{pr}^{min}) is set to the capacity of the largest unit following the static $N-1$ criterion.

$$\begin{aligned}
\sum_{j=1}^{N} r_j^{h,pr} &\geq R_{pr}^{min} && \forall h = 1,\ldots,T, \\
\sum_{j=1}^{N} r_j^{h,sl} &\geq R_{sl}^{min} && \forall h = 1,\ldots,T, \\
\sum_{j=1}^{N} r_j^{h,dn} &\geq R_{dn}^{min} && \forall h = 1,\ldots,T.
\end{aligned} \tag{2.12}$$

Dynamic primary reserve requirement

Another way of writing the $N-1$ criterion is presented in equation (2.13), which ensures that enough primary reserve is provided by the *surviving* units to stand the loss of any *committed* unit k. This enables a better economical performance of the dispatch by limiting the committed primary reserve to the actual needs of the system at each time step.

$$\sum_{\substack{j=1 \\ j\neq k}}^{N} r_j^{h,pr} \geq g_k^h \qquad \forall k = 1,\ldots,N, \forall h = 1,\ldots,T. \tag{2.13}$$

The basic deterministic UC model with dynamic primary reserve requirement, given by equations (2.2)-(2.13) will be referred to as model $\mathfrak{M}_0$, while the UC model with static primary reserve requirements, given by expressions (2.2)-(2.12) will be denoted by $\mathfrak{M}_1$.

2.2.4 Hypotheses, computational complexity and solution method

The selected methodological approach has one structural hypothesis, which supposes that the cost functions are convex and the constraint functions are jointly convex with respect to the continuous relaxation. Then, some simplification hypotheses have been made to limit the computational complexity of the optimisation problem, however, raising them is quite straightforward. For instance:

1. Variable generation costs are considered linear, but a piece-wise linear or even a quadratic model could be used. In the latter case the problem becomes a Mixed-Integer Quadratic Programming problem (MIQP) that can be handled by efficient and reliable commercial software (such as GUROBI [110]) at a (significantly) higher computational cost.
2. Single bus model (no network consideration) is used, but DC power flow or quadratic formulation of AC constraints could be included. In the latter case the problem becomes Mixed-Integer Quadratically Constrained Quadratic Program (MI-QCQP).

3. Conventional units are considered to be thermal, but different terms can be added to the objective function to account for other types of power plants.
4. Only units operational constraints, power balance equation and three types of reserve are modelled, but differentiated variables can be used for the secondary and tertiary reserves and additional constraints, such as emission, fuel, must run units, modulation etc., can be added as long as they preserve the MILP problem structure.

Computational complexity

The dimension of the optimisation vector for the both UC models described in section 2.2.3 is $7 \times N \times T$. Model $\mathfrak{M}_0$ includes $15 \times N \times T + 4 \times T$ constraints, while model $\mathfrak{M}_1$ considers $14 \times N \times T + 4 \times T$ constraints. If a small test system of 18 generating units is optimised for a time horizon of 32 hourly time steps, the solution contains 2304 continuous variables, 1728 binary variables, and the optimisation must deal with 8768 (or 8192) constraints. This problem is in fact easy to solve with the available methods and computational power.

Solution method

As aforementioned, MILP optimisation problems are a specific class that can be solved by mathematical programming, or exact, methods. However, standard algorithms able to solve this kind of problems in a polynomial time have not been identified, reason why the are referred to as *NP-hard* according to the computational complexity theory.
In this work, the UC models are implemented in MATLAB 8.4.0 (R2014b) [126] and are solved with a commercial MILP solver (GUROBI [110]), which is mainly based on the simplex and the branch and bound (B&B) algorithms. Indeed, the most widespread way of dealing with MILP problems consists in removing the constraints containing integer variables and solving the remaining continuous linear program (LP). Then, the integer variables are obtained by rounding the solution to the continuous LP relaxation.
However, this first retuned solution may not be optimal or even feasible at all, since the suppressed constraint may be violated. Therefore, other algorithms, such as the cutting plane, the branch and bound, and the branch and cut, are used to obtain integer solutions. Roughly speaking, these methods are based on an iterative procedure that includes linear constraints at each step in order to provide more information to the relaxed problem about the real one.
More specifically, the B&B method uses the solutions of the LP relaxations to provide *lower bounds* (LB), and estimate the worst-case distance from optimality of the returned solution through the $MIPgap$. This metric is in fact the normalised value of the objective at a certain integer feasible point (f_0^i) minus the LP relaxation objective at the given iteration i of the B&B algorithm (LB^i) as indicated in equation (2.14).

$$MIPgap^i = 100\frac{f_0^i - LB^i}{f_0^i}. \tag{2.14}$$

The algorithm will stop at iteration I, if the $MIPgap^I$ meets a certain predefined requirement, which ensures that the returned solution is *at least* to the given distance of the optimal one. In addition, this method may return a “solution" as long as at least one feasible integral point has been found. For instance, MILP solvers, such as GUROBI can get a certain time limit as an entry and return the best point found in the allocated time.

2.3 Reduced order system frequency response model

This section analyses different models proposed in literature to characterise the primary frequency response in an electrical power system. Their pros and cons in view of the construction of suitable frequency nadir constraints for the FCUC problem are discussed. The need of modelling some additional features is highlighted and a improved reduced order system frequency response (ROSFR) model is proposed.

In power systems, different dynamic phenomena can be categorised according to their time scale; from wave phenomena (microseconds) to thermodynamic phenomena (hours), passing through electromagnetic and electromechanical phenomena [2, 9]. On the one hand, electromagnetic interactions occur within the generator at a time scale of some milliseconds after a disturbance appears on the system. In this case, the interest is placed in the fault current, internal voltages and fluxes, while the rotor speed is considered to be constant. On the other hand, electromechanical dynamics analysis includes the variation of the rotor speed, and the action of the turbine and generator control systems.

In this work, the interest is place in the latter. Then, different hypotheses can be made to achieve a trade off between the complexity of the generator model and the accuracy of the overall system model. A “detailed" or “complete" electromechanical model of a generator is composed by a system of ordinary differential equations (ODE) that may reach several orders (4-8) to include its internal dynamics, as well as the inertial and controllers response. In transient stability analysis, where the attention is placed on the rotor angular position following a sudden disturbance, reduced order models tend to be used. In fact, following a large power imbalance the angular speed of generating units varies since part of the kinetic energy stored in the rotating masses is injected into the network, making the system frequency evolve. This evolution can be studied with the torque (couple or moment of force) equation of rotating masses, referred in the transient stability terminology as the swing equation, and represented by equation (2.15).

$$J_j \frac{d\omega_j(t)}{dt} = C_{m,j}(t) - C_{e,j}(t), \tag{2.15}$$

where, J_j is the moment of inertia of unit j in kgm^2, ω_j is the angular velocity of unit j in rad/s, t stands for the time in seconds, $C_{m,j}$ is the mechanical torque applied by the primary driver of unit j, and $C_{e,j}$ is the electrical torque applied by the generator j, both in Nm. Then, knowing that:

$$\omega_j(t) = \frac{2\pi f_j(t)}{p_j},$$

where, f_j is the electrical frequency of generator j in Hz and p_j is the amount of magnetic poles of generator j, and that the power generated by unit j (P_j) can be defined as follows:

$$P_j(t) = C_j(t)\omega_j(t).$$

Equation (2.15) can be rewritten as follows:

$$J_j \frac{2\pi}{p_j} \frac{df_j(t)}{dt} = \frac{p_j}{2\pi f_j(t)} \left(P_{m,j}(t) - P_{e,j}(t)\right), \tag{2.16}$$

where $P_{m,j}$ is the mechanical power injected by the primary driver and $P_{e,j}$ is the electrical power produced by the generator j, both in watts (W).
In practice, the rotating speed of each unit may be different, but solving a detailed dynamic model may be computationally expensive. Therefore, some works have been published on building ROSFR to determine the average frequency trajectory [127, 128], which are based on hypothesis 1.

Hypothesis 1 *All generators connected to the grid will have the same frequency. Thus, the local oscillations around the fundamental frequency are neglected.*

Then, the inertia of a synchronous generating unit is characterised by a parameter called the *inertia constant* (H), which is defined by equation (2.17):

$$H_j = \frac{E_{c0,j}}{S_{n,j}} = \frac{\frac{1}{2} J_j \omega_{0,j}^2}{S_{n,j}} = \frac{\frac{1}{2} J_j \left(\frac{2\pi f_0}{p_j}\right)^2}{S_{n,j}}, \tag{2.17}$$

where f_0 is the system nominal frequency in Hz ($50Hz$ in Europe), $E_{c0,j}$ is the kinetic energy stored in unit j at nominal frequency in Ws, and $S_{n,j}$ is the nominal apparent power of unit j in VA. Afterwards, the average evolution of the system frequency f can be written as the sum of equation (2.16) over all connected units.

$$\frac{df(t)}{dt} = \frac{f_0^2}{2\left(\sum_{j=1}^{N} H_j S_{n,j}\right) f(t)} \left(\sum_{j=1}^{N} P_{m,j}(t) - \sum_{j=1}^{N} P_{e,j}(t) \right), \tag{2.18}$$

where N is the total amount of generating units. In order to express (2.18) as a function of the decision variables and parameters of the UC model at a specific time step h (state u_j, scheduled power g_j and forecasted demand D_f), a second hypothesis can be made:

Hypothesis 2 *The power conversion and transmission system losses are included in the demand forecast ($D_f(t)$), such that the sum of the active power produced by all generating units can be approximated by the total system power load.*

Finally, the swing equation is rewritten in expression (2.19):

$$\frac{df(t)}{dt} = \frac{f_0^2}{2\left(\sum_{j=1}^{N} H_j S_{n,j} u_j(t)\right) f(t)} \left(\sum_{j=1}^{N} g_j(t) - D_f(t) \right). \tag{2.19}$$

Therefore, when the generation and demand are in balance, the system frequency is stabilised. Traditionally, the evolution of the frequency is divided into a few stages that are analysed separately. In this work, the interest is placed on the primary frequency response, which takes place in the first seconds, and includes the inertial and the governor responses. More specifically, the objective is to characterise the risk of UFLS as a function of the frequency nadir for different operating points and contingencies, and identifying the conditions that entail a security threshold violation.

Then, it is necessary to determine the frequency trajectory as a function of the system initial state (the demand and the UC decision variable for a fixed h), and, of course, the time, following a large disturbance of power P_{step}, this is $f(t, P_{step}, \mathbf{u}^h, \mathbf{g}^h, D_f^h)$. Hence, models for $g_j(t)$ and $D_f(t)$ need to be built, which are given by the dynamic of the deployment of the active reserves and the load damping respectively.

This section discusses different simplified electromechanical models used to estimate the first stage of the frequency response following unit outages in order to identify the best compromise between simplicity and accuracy for the purposes of this work. Section 2.3.1 presents the notation used to describe the ROSFR models. Section 2.3.2 introduces the simplest ROSFR model, where the whole system is reduced to an equivalent machine (EM-ROSFR). This first model provides an analytical expression for the frequency nadir, which is the natural first step when formulating the FCUC problem, and offers helpful insights on the relationship between the frequency nadir and some system parameters.

However, the EM-ROSFR model exhibits some limitations that motivate the consideration of a more detailed multi-machine ROSFR model (MM-ROSFR) described in section 2.3.3.

The nature of these downsides is formalise and thoroughly discussed, since such an analysis seems to be lacking in literature, while the EM-ROSFR model may still be (too) widely used [85]. Finally, section 2.3.4 proposes a new ROSFR model, which is inspired on the latter but integrate additional features, such as the saturation of the regulation by capacity limits, that are considered to be relevant in the formulation of the FCUC problem.

2.3.1 Notation

Parameters

f_0	system nominal frequency in Hz (here $50Hz$)
P_{sp}	incremental power set point in MW
K_m	mechanical gain factor in per unit
F_H	fraction of the total power generated by the turbine (not delayed)
D	load damping factor
H_j	inertia constant of unit j in $MWs \cdot MVA^{-1}$
R_j	droop parameter of unit j in % (sensitivity of the regulation to the frequency)
τ_r	time constant of the equivalent unit process in seconds
τ_1, τ_2, τ_3	smaller time constant of the equivalent unit process (ex. servo motors) in seconds
τ_{ag_j}	time constant of the process (lead) of unit j in seconds
τ_{rg_j}	time constant of the process (lag) of unit j in seconds
τ_{ac_j}	time constant of the regulation (lead) of unit j in seconds
τ_{rc_j}	time constant of the regulation (lag) of unit j in seconds
ω_n	system natural oscillation frequency in $rad \cdot s^{-1}$
ω_r	damped or ringing frequency in $rad \cdot s^{-1}$
ξ	damping ratio (dimensionless)

Variables

s	complex Laplace transform variable in s^{-1}
f	system frequency in Hz
P_a	accelerating power in MW
P_e	electrical power (demand) in MW
P_m	turbine mechanical power in MW
g_j	power output of unit j in MW
x_j	regulation signal of unit j in MW
Δg_j	deviation of the power output of unit j in MW
Δx_j	deviation of the regulation signal of unit j in MW
$\Delta\omega$	incremental angular speed in $rad \cdot s^{-1}$
Δf	frequency deviation in Hz

2.3.2 Equivalent machine ROSFR model

The model presented here was proposed by P.M. Anderson and M. Mirheydar in 1990 [127]. It is based on the representation of the whole system as one single equivalent machine in order to estimate the frequency behaviour considering an equivalent inertial and governor response by computing the deviation of the equivalent unit speed ($\Delta\omega$). The advantage of this model is that the system frequency response can be computed in closed form.
Therefore, analytical expressions can be derived for the frequency and time domain response of the frequency, as well as for many essential metrics of the frequency transient, such as its minimum value (nadir) and the time when it happens. Hence, their behaviour may be formally analysed and/or integrated in other models. Moreover, their values can be computed for free in terms of computational cost.

Hypotheses of the equivalent machine ROSFR model

Aforementioned hypotheses 1 and 2 hold, and additional ones, specific to the representation of the generating units' dynamics are discussed below.

Hypothesis 3 *The generation is dominated by reheat steam turbine generators.*

Hence the inertia and reheat time constants predominate the system average frequency response. Therefore, all but the largest time constants in the equations of the generating units of the power system are neglected. In addition:

Hypothesis 4 *The regulation is constituted by a proportional controller.*

Hypothesis 5 *Non-linearities, such as saturation processes, are neglected.*

Hypothesis 6 *The disturbance is small compared to the total rating of the system. Therefore, it is supposed that the equivalent machine will be able to absorb this change.*

Model of the conventional power plant

Figure 2.2 presents a general diagram of an individual thermal power plant. As aforementioned, in this study, the electromagnetic transient is considered too fast and the thermal system dynamics is considered too slow with respect to the phenomena of interest.

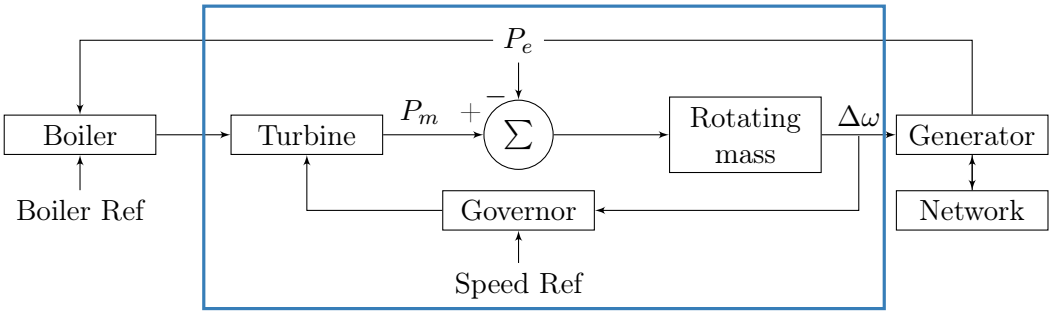

Figure 2.2: General diagram of the generating unit frequency control

Figure 2.3 presents a typical model for a governor-turbine system. The notation used is consistent with [127], where all quantities were expressed in per unit. The variable of interest is the output power of the plant (P_m) as a function of its parameters, initial generation and angular speed variation.

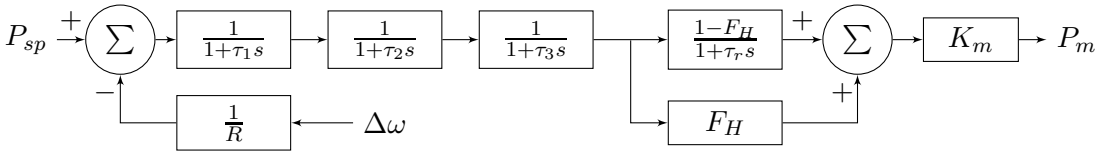

Figure 2.3: Typical reheat turbine governor model

where P_{sp} is the power set point, K_m is the mechanical power gain factor, R is frequency droop (the inverse of the gain of the proportional controller), τ_r is the re-heater time constant, τ_1, τ_2 and τ_3 represent servo-motors and other parts of the power plant.
Finally, the parameter F_H measures the fraction of the shaft power developed by the high pressure turbine on a single reheat system. This is the fraction of the shaft power that is not delayed by reheating. This last two blocks transfer function can be rewritten in one block by adding a zero in $\tau_a = F_H \tau_r$. Then, it is considered that the re-heater time constant (τ_r) is the most significant in the system and it tends to dominate the response of the largest portion of the power output (hypothesis 3). Therefore, the other smaller time constants will be neglected. Figure 2.4 includes these assumptions, as well as, the load damping (D) and the equivalent inertia (H).

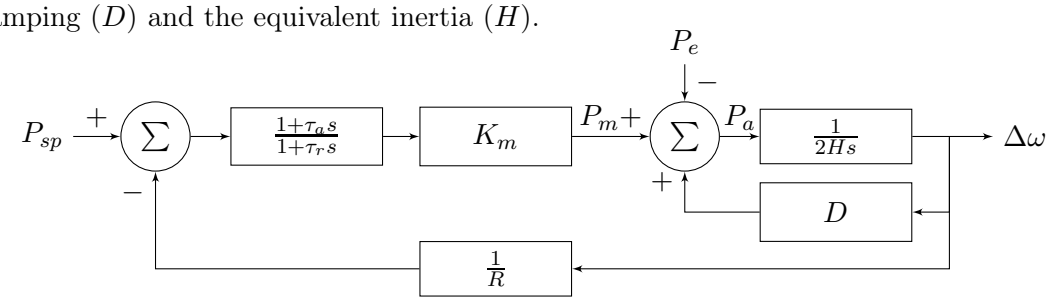

Figure 2.4: The equivalent machine ROSFR model

Frequency evolution following sudden disturbance

By direct analysis of figure 2.4, the analytic expression of the frequency deviation can be obtained in the Laplace domain as a function of the the natural system frequency (ω_n) and the damping ratio (ξ).

$$\Delta\omega(s) = \left(\frac{R\omega_n^2}{DR + K_m}\right)\left(\frac{K_m(1+\tau_a s)P_{sp} - (1+\tau_r s)P_e}{s^2 + 2\xi\omega_n s + \omega_n^2}\right), \tag{2.20a}$$

$$\omega_n^2 = \frac{DR + K_m}{2HR\tau_r}, \tag{2.20b}$$

$$\xi = \frac{2HR + DR\tau_r + K_m\tau_a}{2(DR + K_m)}\omega_n. \tag{2.20c}$$

Equation (2.20a) indicates that the response to a change in the power set point (P_{sp}) or the electrical demand (P_e) has the same form, but different sign and phase. The generation and load upsets are aggregated in a variable called disturbance power (P_d) in order to obtain the expression of the primary frequency response. Figure 2.5 shows the resulting simplified ROSFR model.

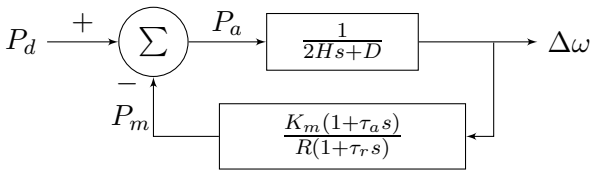

Figure 2.5: Equivalent machine ROSFR model with disturbance input

For a sudden disturbance, P_d is represented by a step function ($P_d < 0$ for a load increase or generation lost, $P_d > 0$ for a generation increase):

$$P_d(s) = \frac{P_{step}}{s}, \tag{2.21a}$$

$$\Delta\omega(s) = \left(\frac{R\omega_n^2}{DR + K_m}\right)\left(\frac{(1 + s\tau_r)P_{step}}{s(s^2 + 2\xi\omega_n s + \omega_n^2)}\right). \tag{2.21b}$$

Time domain solution of the frequency

The time domain expression of equation (2.21b) can be found using the inverse Laplace transformation as detailed in appendix A. The result is given by equation (2.22).

$$\Delta\omega(t) = \left(\frac{P_{step}R}{DR + K_m}\right)\left[1 + \alpha e^{-\xi\omega_n t}\sin(\omega_r t + \phi')\right], \tag{2.22}$$

where,

$$\alpha = \sqrt{\frac{1 - 2\tau_r\xi\omega_n + \tau_r^2\omega_n^2}{1 - \xi^2}}, \tag{2.23a}$$

$$\phi' = \phi_1 - \phi_2 = \tan^{-1}\left(\frac{\omega_r\tau_r}{1 - \xi\omega_n\tau_r}\right) - \tan^{-1}\left(\frac{\sqrt{1 - \xi^2}}{-\xi}\right). \tag{2.23b}$$

As aforementioned, the EM-ROSFR model provides an analytical expression for the frequency evolution after a large power imbalance, which, in this case, is given by a damped sinusoidal function. Indeed, the system frequency can be computed from equation (2.22) as follows:

$$f(t) = f_0 + \frac{\Delta\omega(t)}{2\pi}. \tag{2.24}$$

For illustrative purposes, figure 2.6 presents the evaluation of equation (2.24) for different values of the disturbance power. The parameters of the test system are taken from [127], and included in appendix B. Then, the frequency trajectory may be characterised by at least four metrics. The value of the initial (and maximal) frequency gradient referred to as the *ROCOF* in the literature (for Rate of Change of the Frequency), the steady state frequency (ω_{ss}), the maximal frequency deviation $\Delta\omega_{max}$ and the time when it occurs (t^z).

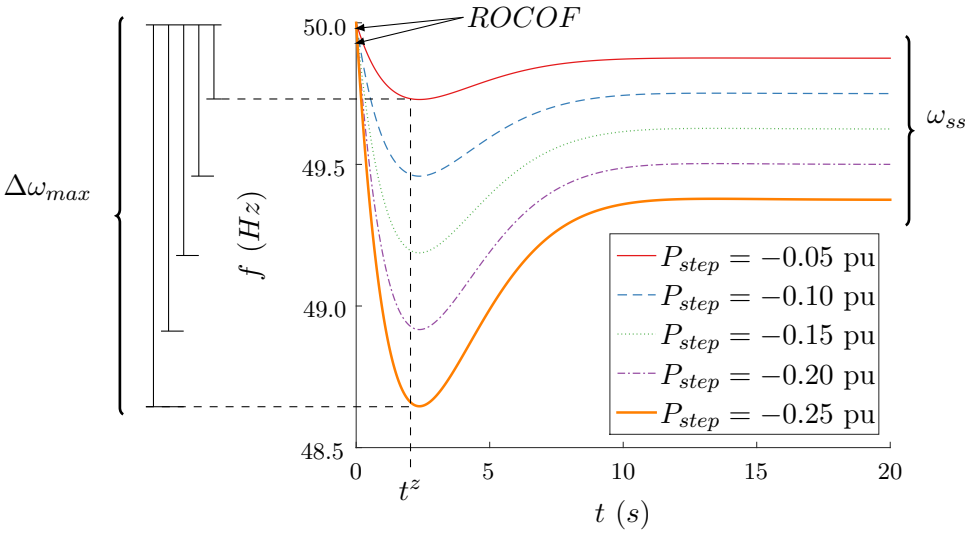

Figure 2.6: Frequency for different disturbance power

It is observed that all but the latter metric depend on the severity of the contingency (the size of the power imbalance). In this work, the interest is placed on two of these values:

- The *ROCOF* or initial slope of the frequency given by $\frac{d\omega}{dt}|_{t=0^+}$.
- The frequency nadir, or the maximal frequency deviation $\Delta\omega(t^z), t^z = t|_{\frac{d\omega}{dt}=0}$.

It must be noted that the steady state frequency deviation ($\Delta\omega_{ss}$) can be also determined by $\lim_{t\to+\infty}\Delta\omega(t)$, but is not of interest in this work.

Maximal frequency gradient and the minimal frequency

In order to obtain the *ROCOF*, equation (2.22) must be differentiated. Its initial value is given by equation (2.25), which is obtained by evaluating the derivative at $t = 0$. Some details on the analytical developments can be found in appendix A.

$$ROCOF = \frac{d\Delta\omega}{dt}|_{t=0^+} = \frac{P_{step}}{2H}. \tag{2.25}$$

The maximal frequency deviation is determined by evaluating equation (2.22) in t^z, which can be determined when the derivative is equal to zero (for more details see appendix A).

$$t^z = -\frac{\phi_1}{\omega_r} = -\frac{1}{\omega_r}\tan^{-1}\left(\frac{\omega_r\tau_r}{1-\xi\omega_n\tau_r}\right) = \frac{1}{\omega_r}\tan^{-1}\left(\frac{\omega_r\tau_r}{\xi\omega_n\tau_r-1}\right). \tag{2.26}$$

Consequently, the maximal frequency deviation is related to an exponential function when the certain conditions (given by equation A.5) are satisfied.

$$\Delta\omega_{max} = \frac{P_{step}R}{DR+K_m}\left(1+e^{\frac{\xi\phi_1}{\sqrt{1-\xi^2}}}\sqrt{\omega_n^2\tau_r^2-2\omega_n\tau_r\xi+1}\right). \tag{2.27}$$

Finally, for negative power imbalances (load increase or loss of generation) the frequency nadir, which is given by $\omega_{min} = \omega_0 + \Delta\omega_{max}$, tend to be used. Appendix B presents a numerical implementation that illustrates the sensibility of the frequency nadir to the parameters of the EM-ROSFR model. It is shown that the droop parameter (R) has the most significant impact on the frequency nadir, while the mechanical gain (K_m) has a limited influence. Then, the inertia and time constants (H, τ_r and τ_a), as well as the load damping have a comparable effect on the minimal frequency.

Relation with the UC optimisation variables

According to this model, the time of the minimum (t^z, eq: 2.26) does not depend directly on the size on the disturbance (P_{step}), while the maximal gradient of the frequency drop ($ROCOF$, eq. 2.25) and the maximal frequency deviation ($\Delta\omega_{max}$, eq. 2.27) are linearly dependent of the size of the power imbalance. Now, let us try to express the frequency nadir as a function of the equivalent machine parameters:

$$\Delta\omega_{max} = \frac{P_{step}R}{DR+K_m}\left(1+e^{\frac{\xi\phi_1}{\sqrt{1-\xi^2}}}\sqrt{\frac{K_m(\tau_r-\tau_a)}{2HR}}\right), \tag{2.28}$$

where the exponent of the exponential function is given by:

$$\frac{\xi}{\sqrt{1-\xi^2}} = \frac{(2HR+\tau_rDR+\tau_aK_m)}{\sqrt{8HR\tau_r\left(DR+K_m\right)-\left(2HR+\tau_rDR+\tau_aK_m\right)^2}}, \tag{2.29}$$

$$-\phi_1 = \tan^{-1}\left(\frac{\omega_r\tau_r}{\xi\omega_n\tau_r-1}\right) = \tan^{-1}\left(\frac{\sqrt{8HR\tau_r\left(DR+K_m\right)-\left(2HR-\tau_rDR+K_m\tau_a\right)^2}}{\tau_rDR+K_m\tau_a-2HR}\right). \tag{2.30}$$

If the system must withstand the outage of any single unit, g_k^h, the set of possible disturbances is given by the schedule powers of each on-line unit, which means that the frequency constraint could be written as follows:

$$\frac{g_k^hR}{DR+K_m}\left(1+e^{\frac{\xi\phi_1}{\sqrt{1-\xi^2}}}\sqrt{\frac{K_m(\tau_r-\tau_a)}{2HR}}\right) \leq \Delta\omega_{th} \quad \forall k=1,\ldots,N, \forall h=1,\ldots,T, \tag{2.31}$$

where $\Delta\omega_{th}$ is the maximal acceptable frequency deviation. It is observed that the frequency nadir constraint is strongly non-linear on the decision variables of the UC model, such as the binary ones, since the equivalent inertia of the system (H), for instance, depends on the inertia constant (H_j) and size ($S_{n,j}$) of committed units ($u_j = 1$). Thus, although the EM-ROSFR model does provide analytical expressions for the metrics of main interest, the FCUC MILP formulation cannot take advantage of this feature.

Moreover, according to the rigorous investigation on the nature of this non-linearity presented in this section, it is concluded that a linearisation method is not suitable for the purpose of this work. Indeed, it is not clear how to calculate (formally express) the equivalent machine parameters as a function of the parameters of each unit. This would prevent the FCUC model of optimally allocating the primary reserve by considering the potential contribution of each units to the frequency response. Therefore, the next section considers a more detailed ROSFR model.

2.3.3 Multi-machine ROSFR model

The model presented here was proposed by D.L. Hau in 2006 [128] and tackles some of the aforementioned issues. In this case, the individual response on each unit to the frequency variation is represented in a separate way, which enables the consideration of the heterogeneous characteristics of different units. As a consequence, the contribution (and impact) of individual units to the frequency response can now be examined.

Nevertheless, hypothesis 1-5 of the previous model are still required for the MM-ROSFR. In this case, the response of the overall system is given by the addition of different first order subsystems as shown in figure 2.7.

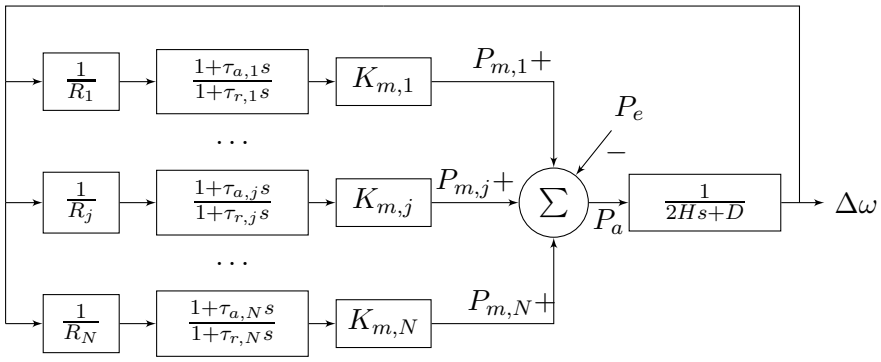

Figure 2.7: Multi-machine ROSFR model

If the procedure followed in the previous section to determine an analytical expression of the frequency evolution for the EM-ROSFR model is applied to the MM-ROSFR; the Laplace domain expression presented in (2.32) is obtained.

$$\Delta\omega(s) = P_d \left(\frac{\prod_{j=1}^{N}(1+s\tau_{r,j})}{(2Hs+D)\prod_{j=1}^{N}(1+s\tau_{r,j}) + \sum_{k=1}^{N}\left[\frac{K_{m,k}}{R_k}(1+\tau_{a,j}s)\prod_{j=1,j\neq k}^{N}(1+s\tau_{r,j})\right]} \right). \tag{2.32}$$

It is observed that the numerator is of order N and the denominator is of order $N+1$. In [128] is stated that for a step function ($P_d = P_{step}/s$), equation (2.32) can be expressed as a sum of partial fractions:

$$\Delta\omega(s) = P_{step} \sum_{j=1}^{N+1} \frac{A_j}{p_j} \left(\frac{1}{s} - \frac{1}{s-p_j} \right), \tag{2.33}$$

where, A_j is real or complex and p_j is a pole of the denominator of (2.32) that can be real or a complex conjugated pair. Thus, the time domain frequency response is given by:

$$\Delta\omega(t) = P_{step} \sum_{j=1}^{N+1} \frac{A_j}{p_j} \left(1 - e^{p_j t}\right) U(t). \tag{2.34}$$

However, it is not possible to determine the root of the characteristic polynomial p_i, or the coefficient A_i, in a generic way, as a function of the individual units parameters. Thus, the implementation of a numeric integration method becomes inevitable to achieve a differentiated representation of individual units' contributions to the primary frequency regulation. In the next section, an upgraded MM-ROSFR model is proposed in order to integrate a more accurate representation of the primary reserve deployment dynamics.

2.3.4 Proposed ROSFR model

In this work a test system is built based on existing units in different French Non Interconnected areas (ZNI, by its French acronym), to ensure representativeness of the results. A simplified model of their regulation includes, at least, a proportional controller (the power/frequency droop) and a lead-lag compensator, typically used to improve the frequency response of a feedback loop in a control system. Therefore, the MM-ROSFR is improved for taking into account:

1. The inertial response of surviving synchronous production units.
2. The primary frequency regulation characteristics and limits of the units providing this ancillary service; this is their governor droops, lead-lag compensators, maximal power outputs and the saturation of the regulations.
3. The load damping following frequency drop.

The model of the primary frequency regulation of a unit j is depicted in figure 2.8. In this representation, the outage of unit k has been considered as the disturbance ($P_{step} = g_k$).

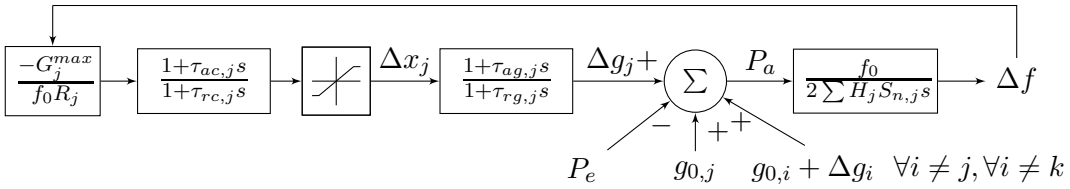

Figure 2.8: Proposed MMR-ROSFR model

Each unit is represented by two first order transfer functions, which gives a $2N + 1$ order ODE system. The first one accounts for the control system (lead-lag compensator), and the second one represents the physical process (power plant). This model is referred to as the MMR-ROSFR model and has been implemented in MATLAB 8.4.0 (R2014b) [126]. Table 2.1 summarises the hypotheses that hold for the various ROSFR models.

Table 2.1: Hypotheses by ROSFR model

ROSFR model	Hyp. 1	Hyp. 2	Hyp. 3	Hyp. 4	Hyp. 5	Hyp. 6
Equivalent machine (EM)	✓	✓	✓	✓	✓	✓
Multi-machine (MM)	✓	✓	✓	✓	✓	✗
Proposed (MMR)	✓	✓	✓	✗	✗	✗

It is observed that assumptions 1 and 2 (on the disregard of local oscillation and network losses) are inherent to the selected approach. Then, the MM-ROSFR model raises hypothesis 6 on the aggregated system response, while the proposed MMR-ROSFR model also raises hypotheses 4 and 5, on the regulation and saturation. Lead-lag controllers are modelled in addition to the proportional droop. Moreover, the implemented model accounts for saturation of the control signal due to capacity limits. The importance of this choice is illustrated in appendix C, where it is shown that the deployment rate of the primary reserve may be overestimated otherwise.

Finally, hypothesis 3, regarding the exclusive consideration of steam turbine generators, can be easily relaxed to some extent. Indeed, the model of different types of units, such as hydro power or nuclear, can be included, as well as other parts of the process. The latter can be modelled by adding more first order transfer functions, in which case the model becomes a $3N+1$ order ODE system that can be solved with the same numeric integration method described below.

In conclusion, the proposed MMR-ROSFR model includes a more accurate and flexible representation of the primary frequency response underlying processes, which have a significant impact on the frequency nadir, but it does not support a formal (analytical) study of the relation between the frequency nadir and the UC decision variables.

Alternatively, the next section proposes an empirical (numerical) analysis of this dependency. Instead of formally characterising the risk of UFLS by an analytical condition, the frequency nadirs are computed for different operating points and contingencies, and the scenarios in which the security threshold is not met are identified.

Solution method and computational complexity. In this work a customised fixed step numeric integration method (Euler) was implemented to capture the saturation process of individual units. The Euler method is a standard numerical procedure for solving ODE systems with a given initial value. More details can be found on appendix D. It is acknowledged that the average frequency exhibits a smooth behaviour, which makes variable steps methods more suited. However, the representation of saturation processes (events) becomes more challenging under this framework. This is the reason why they have been disregarded at this point. In addition, the computational requirements of the frequency nadir calculation are relatively low compared to the UC model resolution, as it will be shown in the next section. Therefore, no further efforts were devoted to this aspect. As aforementioned, all primary reserve must be deployed before 30 seconds for large systems [129], or even less for smaller ones [130], hence the simulation time is set to 30 seconds. The integration step can be fixed to 5 milliseconds, which will entail 6000 iterations to build the frequency curve. However, since the interest is placed on the frequency nadir, the simulation is interrupted once the minimum is reached to limit the computational burden. For the small test system, this happens between 2-5 seconds.

2.4 Numerical analysis

In this section a numerical implementation provides an insight on the relation between the UC decision variables and the primary frequency response for different load profiles, through the sequential simulation of the implemented UC and ROSFR models (figure 2.9).

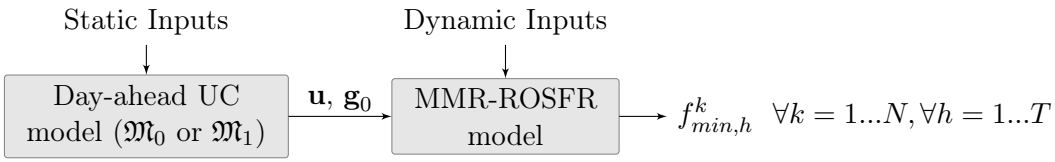

Figure 2.9: Diagram of the sequential simulation approach using the proposed models

Section 2.4.1 describes the test system and discusses the results obtained by solving models $\mathfrak{M}_0$ and $\mathfrak{M}_1$ in terms of commitment decisions and dispatch cost. Then, section 2.4.2 compares the primary frequency response for different contingencies and generating unit dispatches. Finally, section 2.4.3 investigates the relation between some frequency metrics and the UC optimisation variables, while section 2.4.4 discusses computational features.

2.4.1 UC solution

As aforementioned, a MILP solver (GUROBI [110]) is used to solve the models detailed in section 2.2 ($\mathfrak{M}_0$ and $\mathfrak{M}_1$), which were implemented in MATLAB 8.4.0 (R2014b) [126]. Both model minimise generation cost (2.2), while respecting constraints (2.3)-(2.11). The difference between these two models lays in the security constraint as recalled in table 2.2.

Table 2.2: Different primary reserve constraints

Model	$\mathfrak{M}_0$	$\mathfrak{M}_1$
Security criterion	Dynamic requirement	Static requirement
Constraint	$\sum_{j\neq k}^{N}{}_{j=1} r_j^{h,pr} \geq g_k^h$	$\sum_{j=1}^{N} r_j^{h,pr} = max(G_j^{max})$
Equation	(2.13)	(2.12)

The considered test system is composed of 18 thermal units and has a peak load of $250MW$. Figure 2.10 illustrates two typical day-ahead load forecast curves that are used to compute day-ahead schedules.

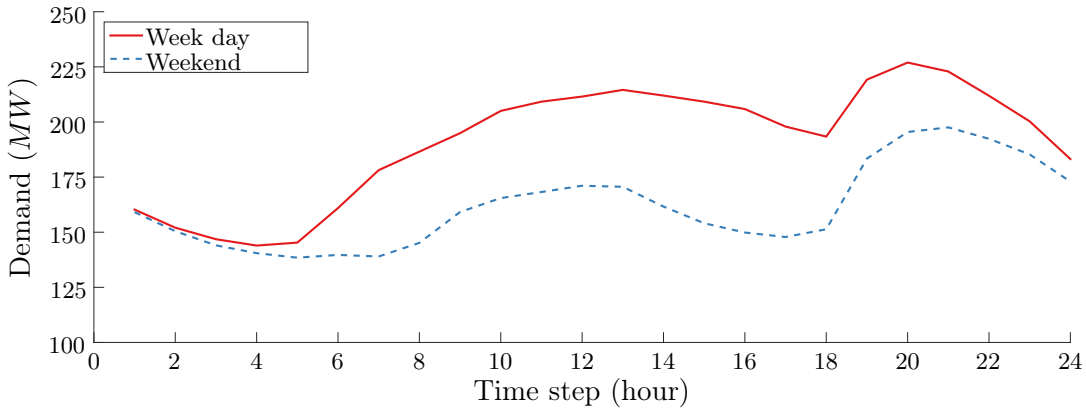

Figure 2.10: Day-ahead load forecast

The generation portfolio includes 4 base coal units (ID numbers 11 to 14), 10 semi-base heavy fuel units (ID numbers 1 to 10) and 4 diesel peaking units (ID numbers 15 to 18). More details are provided in appendix E.

Model $\mathfrak{M}_0$: dynamic primary reserve requirement.

In this paragraph no static reserve requirement are considered, *i.e.*, R_{pr}^{min},R_{sl}^{min},R_{dn}^{min} in equation (2.12) are set to zero and constraint (2.13) is enforced. Figure 2.11 presents the results obtained regarding the binary variables u_j^h for both typical days. The abscissa represents the hourly time steps, and the ordinate indicates the unit ID number. A coloured circle indicates that the specific unit is committed (the binary variable is 1).

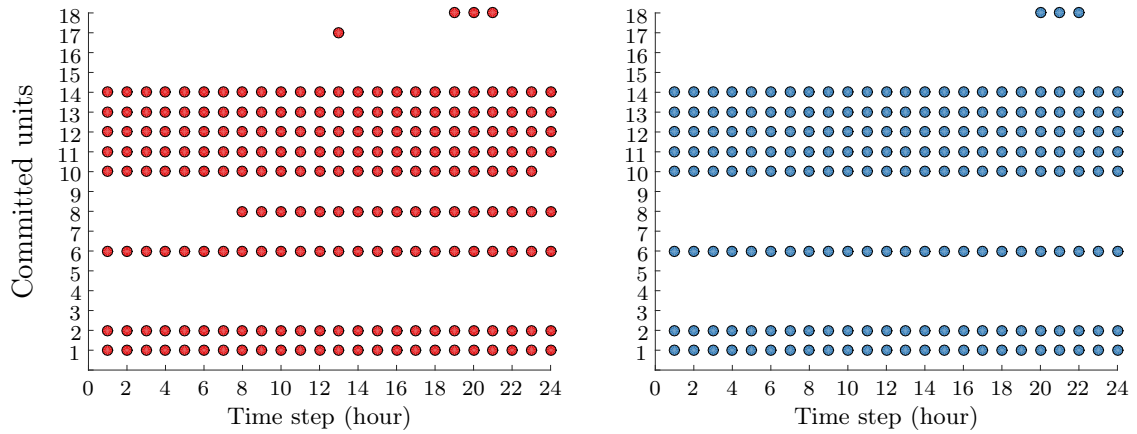

(a) Week day (b) Weekend

Figure 2.11: Day-ahead schedules with dynamic primary reserve requirement (model $\mathfrak{M}_o$)

Figure 2.12 illustrates the results obtained for the continuous power output variables g_j^h, *i.e.*, the dispatch, where the 18 units have been grouped by technology. Units 1 and 2 are heavy fuel units of type 1 (HF 1), units 3-8 and 9-10 are grouped in HF type 2 and 3 respectively. The abscissa represents the hourly time steps, and the ordinate indicates the stacked power outputs. It is observed that the coal units have the largest share on the energy mix since they are the cheapest ones. They are followed by the heavy fuel units, while the diesel units have the lowest share (used only to supply the load peaks).

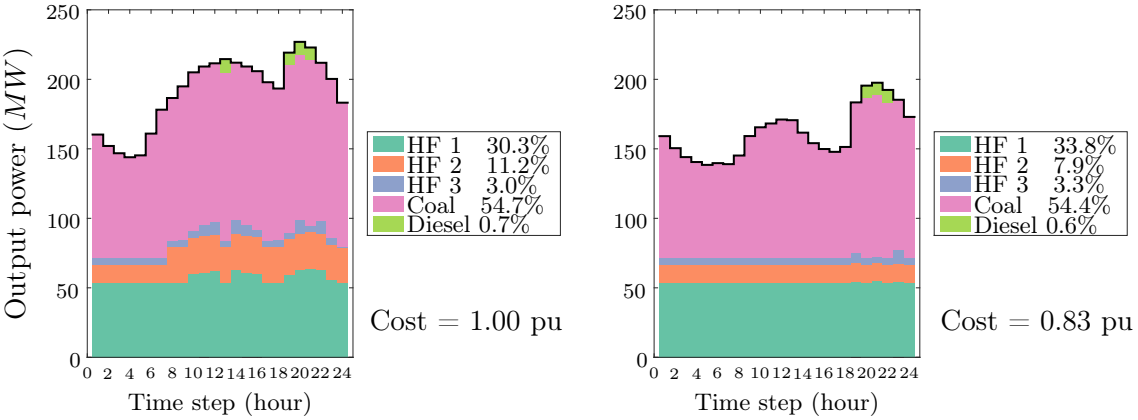

(a) Week day (b) Weekend

Figure 2.12: Day-ahead dispatches with dynamic primary reserve requirement (model $\mathfrak{M}_o$)

The week day dispatch is set as a reference and the cost of the different considered dispatches will be indicated in per unit (pu). Absolute production costs will not be provided due to industrial secret. Figure 2.13 shows the primary reserve effective requirements by hourly step ($\sum_{j=1}^{N} r_j^{h,pr}$), and it is observed that the need for primary reserve depends on the specific operational point of the system.

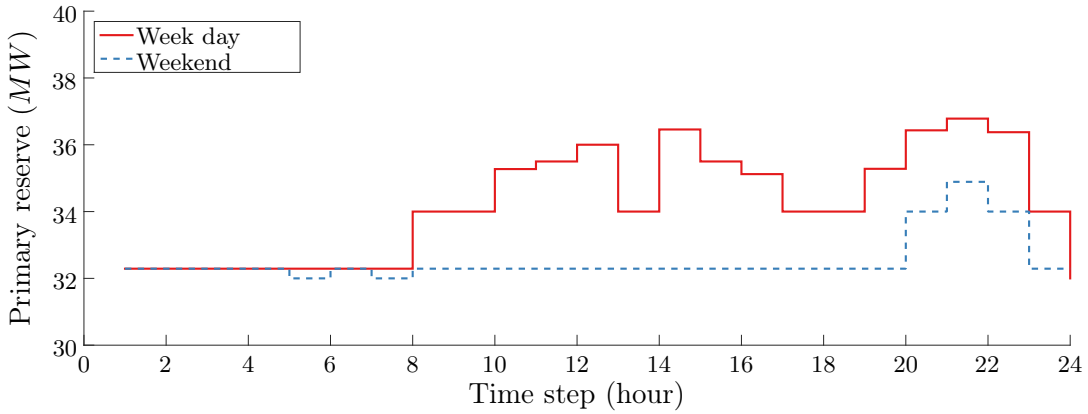

Figure 2.13: Scheduled primary reserve

The results obtained with model $\mathfrak{M}_0$ will be used as a benchmark. Next paragraph considers the enforcement of a static $N-1$ security criterion (model $\mathfrak{M}_1$).

Model $\mathfrak{M}_1$: static primary reserve requirement

In this paragraph, the primary reserve is required to be larger or equal to the capacity of the largest unit ($40.6MW$). Figure 2.14 illustrates the results obtained regarding the binary variables u_j^h for both selected typical days. Once more, the abscissa represents the hourly time steps, and the ordinate indicates the unit ID number.

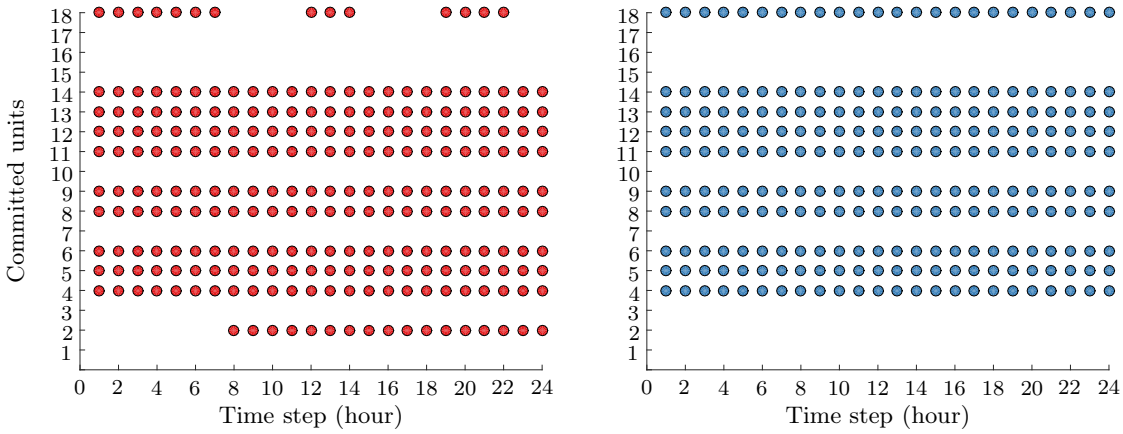

(a) Week day (b) Weekend

Figure 2.14: Day-ahead schedules with static reserve requirements (model $\mathfrak{M}_1$)

Figure 2.15 illustrates the results obtained for the continuous power output variables g_j^h. The dispatch costs are referred to the model $\mathfrak{M}_0$ week day dispatch. It is observed that the share of the cheap heavy fuel units (HF 1) is reduced. In fact, constraint (2.12) enforces a certain amount of committed primary reserve, which obliges the selection of smaller semi-base units, in order to satisfy the $N-1$ security criteria.

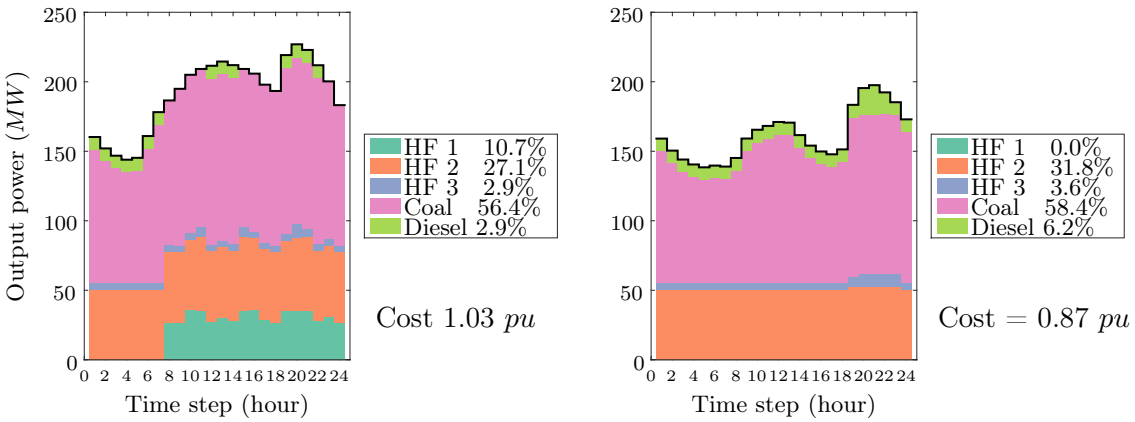

(a) Week day (b) Weekend

Figure 2.15: Day-ahead dispatches with static reserve requirement (model $\mathfrak{M}_1$)

As a consequence, the economical performance of the dispatch is degraded. This effect is accentuated when the load is low (weekend). For the week day, the dispatch presented in 2.12a (dynamic primary reserve requirement) is 3% cheaper that the one depicted in figure 2.15a (static primary reserve requirement). For the low load weekend, the cost saving reaches 5%. The annual production cost can be reduced by up to 1.9% when enforcing the $N-1$ criterion dynamically.

Remark 1: A static primary reserve requirement may be uneconomical, at least for an isolated system. On the one hand, the actual need of the system evolve with the operational point. On the other hand, sometimes it may be more economical to limit the value of the maximal possible contingency (g_k^h) by reducing the power output of some base units than carry on the reserve to compensate for the loss of those units.

In this work, the scheduling over-cost due to the provision of the primary reserve will be referred to as the *security cost*. For the purposes of this study, slow reserve requirements are not considered. The next paragraph estimates the net security cost for the test system by comparing the annual production cost with and without the reserve constraints.

Primary reserve provision cost

Results for the day-ahead schedules without any reserve requirement are presented in figure 2.16. Here, all reserve requirements (R_{pr}^{min},R_{sl}^{min},R_{dn}^{min}) in equation (2.12) are set to zero when solving model $\mathfrak{M}_1$. In this case, the load is almost completely supplied by base units, and fewer units would be committed. The cost difference between the dispatches presented in figure 2.16a and 2.12a is 7%, while this value can reach 11% for the low load weekend (figure 2.16b vs. 2.12b). The annual security cost of the test system was estimated to 6.3% of the total production cost when considering a dynamic primary reserve requirement (model $\mathfrak{M}_0$).

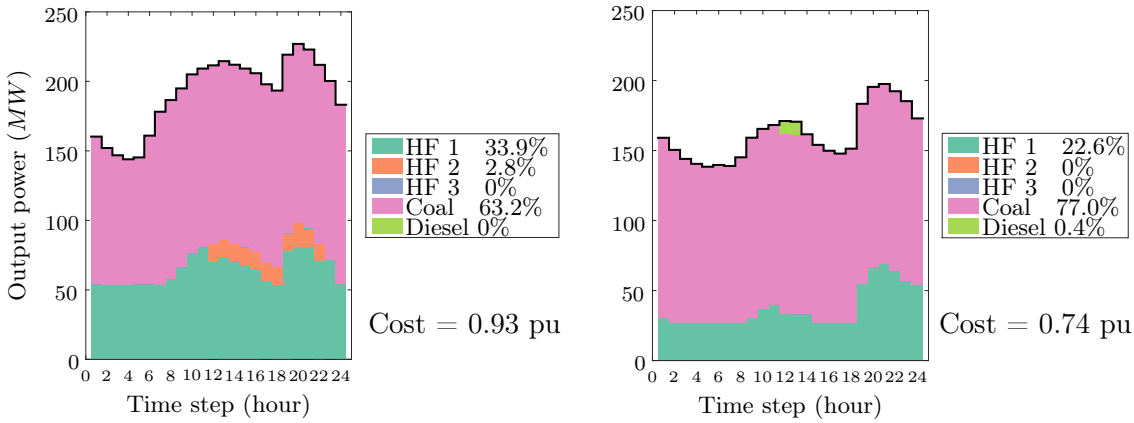

(a) Week day (b) Weekend

Figure 2.16: Day-ahead dispatches without reserve requirements

Table 2.3 compares the security cost obtained with the different formulations of the $N-1$ security criterion. It is observed that the static $N-1$ criterion (model $\mathfrak{M}_1$) increases the annual generation cost by 2% for the test system with respect to the dynamic primary reserve requirement (model $\mathfrak{M}_0$). This explains why in small and isolated power systems the primary reserve requirement tends to be computed with in the optimisation.

Table 2.3: Test system annual security cost due to the provision of the primary reserve

Model	$\mathfrak{M}_0$	$\mathfrak{M}_1$
Security criterion	Dynamic requirement	Static requirement
Security cost (%)	6.3%	8.1%

Remark 2: The reserve in an isolated power system is costly to provide, and the security cost may rise as the load profile decreases. Therefore it should be optimised.

Comparison of the UC solutions with different load levels

The dashed blue curve in figure 2.10, corresponding to a weekend day, exhibits a lower load level that the red curve (week day). Therefore, in the latter case more units were committed. Figure 2.17 compares the amount of committed units and the resulting kinetic energy stored in the system by time step ($E^h_{c,0}$), which is calculated as the sum of the inertia constant multiplied by the nominal apparent power of on-line units, this is:

$$E^h_{c,0} = \sum_{j=1}^{N} H_j S_j u^h_j \qquad \forall h = 1, \ldots, T. \tag{2.35}$$

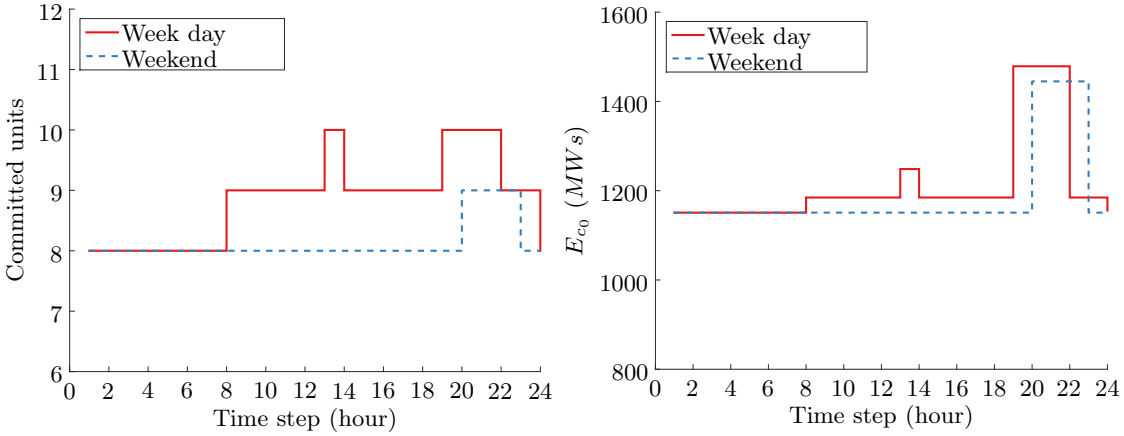

(a) Amount of committed units

(b) Stored kinetic energy

Figure 2.17: UC results for different load levels (model $\mathfrak{M}_0$)

It is observed that indeed, as the load increases, more units shall be committed, for instance, unit 8 is brought on-line from hour 8 on the week day (see figure 2.11). In addition, unit 18 is committed in both typical days at 19-20 hours to anticipate the load peak. In general, the increase of committed units entails an increase of the kinetic energy stored in the system, but this is not always true.

A close look on hour 22 shows that for the same amount of committed units, more kinetic energy is available in the system when considering the weekend dispatch. This is explained by looking at figure 2.11, where unit 18 has been shut down one time step before on the week day due to the presence of unit 8, with a lower contribution of kinetic energy to the system than unit 18. This type of phenomena may be less notorious in larger systems.

Remark 3: Load, committed units and kinetic energy are not necessarily correlated.

Another initial parameter that evolves with the committed regulating units is the K factor, which is defined by:

$$K^h = \sum_{j=1}^{N} \frac{G_j^{max}}{R_j f_0} u_j^h, \tag{2.36}$$

where G_j^{max} is the capacity of unit j in MW, R_j is the droop parameter of unit j (dimensionless) and f_0 is the nominal system frequency in hertz. It is expressed in MW/Hz and its evolution is depicted in figure 2.18.

Figures 2.17 and 2.18 might suggest that the performance of the primary frequency response on the week day would be better than on a weekend day, since more regulating units are committed and the stored kinetic energy in the system is higher. In addition, the scheduled primary reserve and K factor are lower in the weekend example. The next section will examine the truthfulness of this preliminary conclusion.

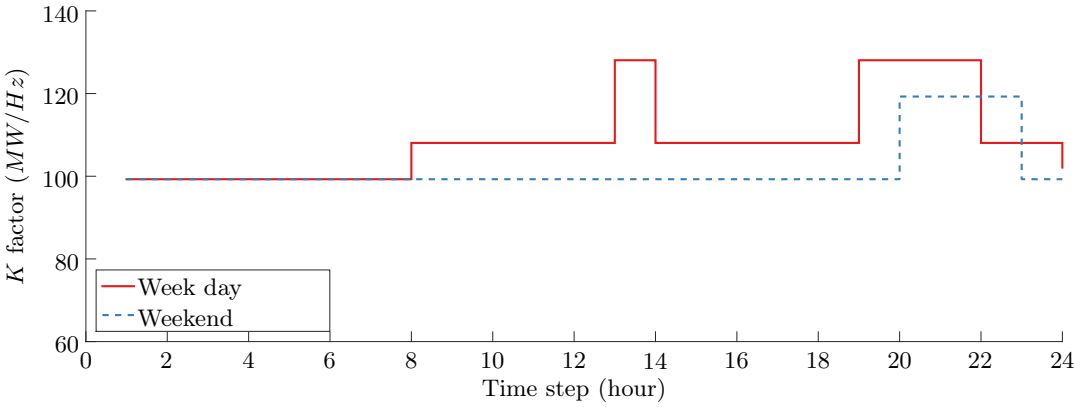

Figure 2.18: K factor for different load levels (model $\mathfrak{M}_0$)

2.4.2 Primary frequency response

Let us consider the schedules presented in figure 2.12. Figure 2.19 provided a closer look at hour 13, where the load is $214.6MW$ on the week day and $170.6MW$ on the subsequent weekend. In this case, the time step h is fixed, the abscissa represents the units and the ordinate the power. Three colours are used to identify the scheduled power, the primary reserve and the remaining slower reserve. The size of the bars represents the units' capacity.

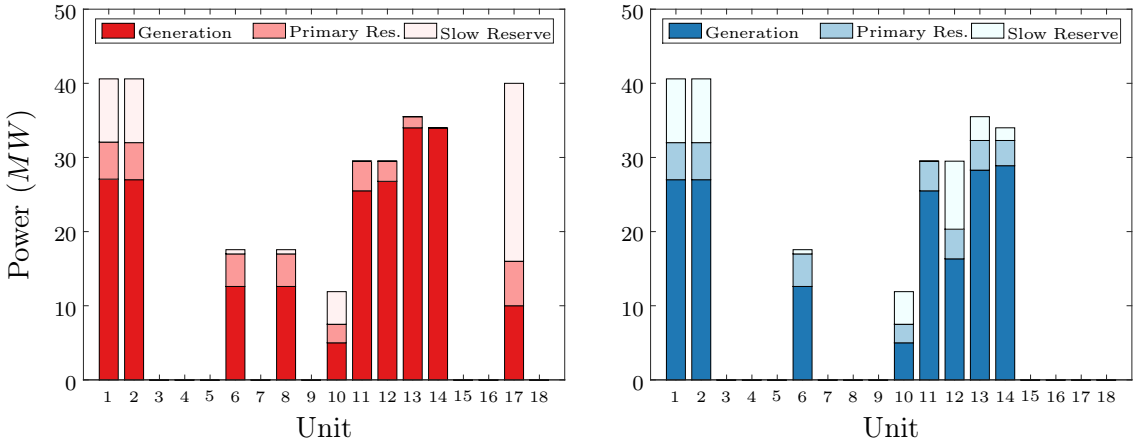

(a) Week day (b) Weekend

Figure 2.19: Detailed dispatch with dynamic primary reserve requirement at hour 13

It should be noted that, for the purposes of this section, no requirement was enforced for the slow reserves ($R_{sl}^{min} = 0$), however, in order to satisfy the primary reserve a certain capacity is committed, which entails some unintended slow reserve, represented in pale color in figure 2.19.

Figure 2.20 compares the frequency evolution of both typical days when considering the outage of unit 1 at hour 13, which generates a power imbalance of $27MW$ (according to the solution of the UC model $\mathfrak{M}_0$ for the load profiles given in figure 2.10).

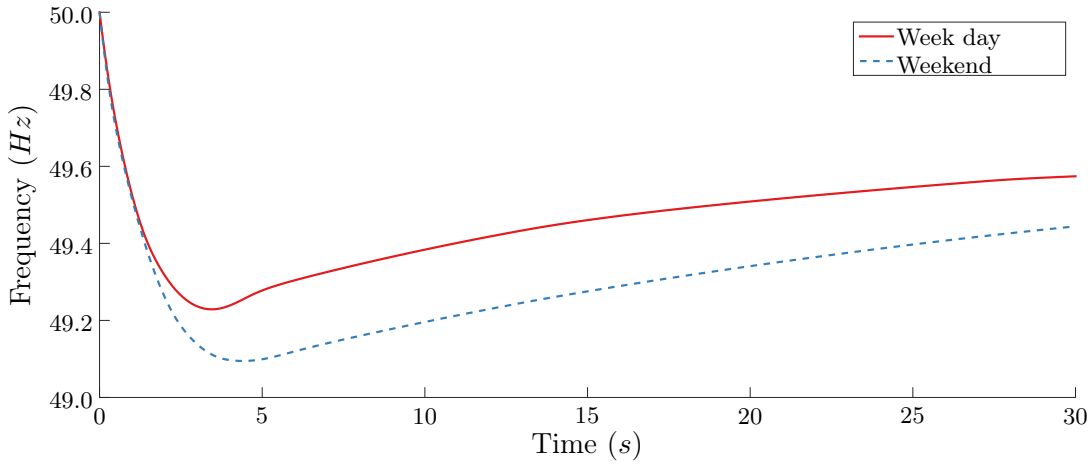

Figure 2.20: Frequency evolution following the outage of unit 1

For an equivalent power imbalance, the primary frequency regulation exhibited a better performance on the week day, since more regulating units were committed. The initial frequency gradient increased from 0.68 Hz/s (week day) to 0.75 Hz/s (weekend). This procedure is repeated for all possible unit outages, over all times steps (24 hours). Figure 2.21 shows the distribution of the frequency nadirs for the two typical days.

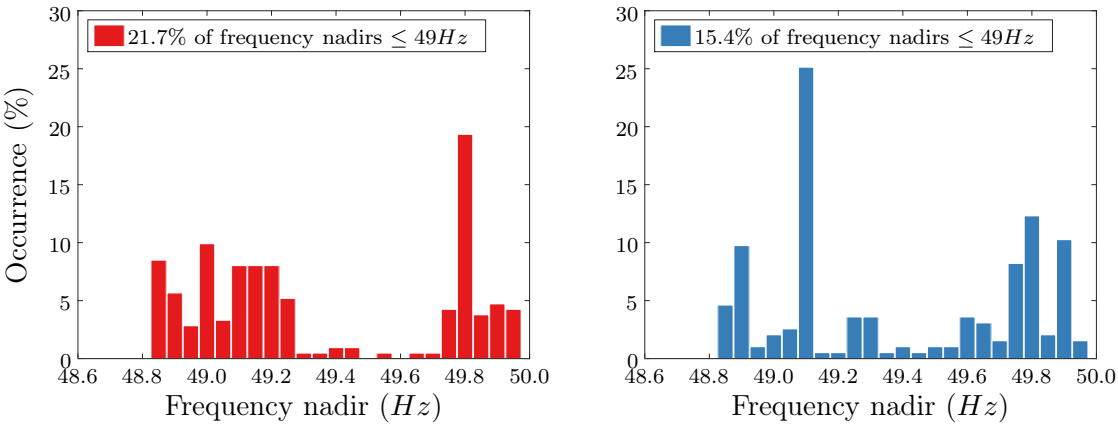

(a) Week day (b) Weekend

Figure 2.21: Frequency nadir distribution for the two typical days

Let us suppose that the frequency threshold for the operation of the under frequency load shedding (UFLS) relays is set at $49Hz$. It is observed that 21.7% of possible unit outages may entail load shedding on the week day, whereas this value is reduced to 15.4% on the weekend example. In fact, the units tend to be partially loaded in days with a low demand level. Therefore, in average, possible unit outages represent lower power imbalances, and the actual available reserve may exceed the enforced requirements.

Remark 4: In days with a low demand profile units might be committed in a partially loaded state, which may have a positive effect on the primary frequency response.

Primary reserve deployment

Figure 2.22 illustrates the different deployment dynamics of the regulating units. Figure 2.22a shows that unit 14 does not participate to the frequency regulation, since it has been committed to its maximal power output. Similarly, units 11-13 reach their capacity limits before the power balance has been restored and the frequency drop contained.

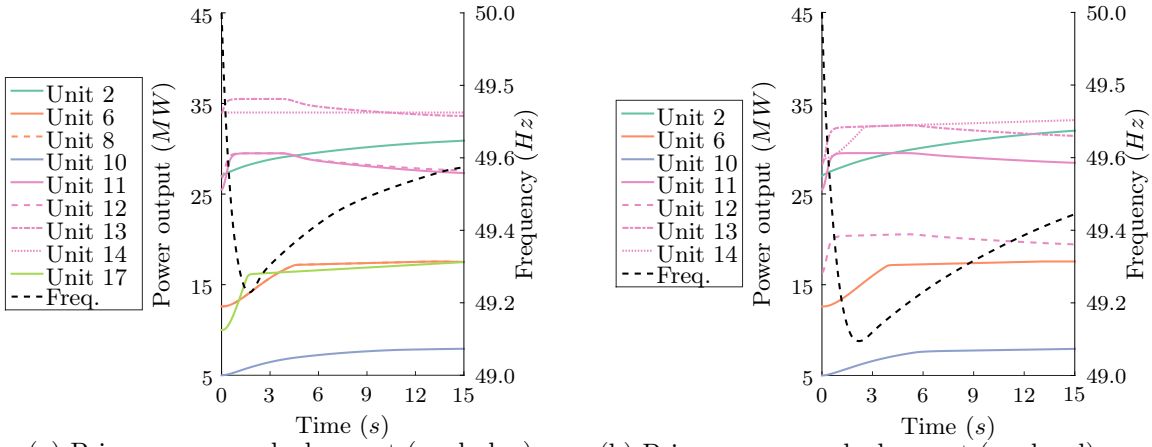

(a) Primary reserve deployment (week day) (b) Primary reserve deployment (weekend)

Figure 2.22: Deployment of the frequency containment reserve by unit

Alternately, peaking unit 17, has been committed at its minimal stable generation level (MSG), hence, it disposes of plenty of headroom capacity, nevertheless, it can not ramp up to its capacity limit in a matter of seconds. In that case, the saturation limit of the control system is reached at the maximal allocation of primary reserve (R_j^{max}). Then, the unit may still be able to further increase its power output, but at a lower rate.

Remark 5: The number of units that contribute to the regulation may vary as the transient evolves, depending on the initial dispatch of regulating units. As a consequence, the aggregated deployment rate of the reserve may decrease before the nadir is reached.

Appendix F offers a comprehensive analysis of the primary reserve deployment of the different regulating units presented in figure 2.22 and the parameters determining their behaviour. It is explained that depending on the lead-lag parameters ($\tau_{ac,j}$ and $\tau_{rc,j}$) the deployment of the primary reserve may be quite different from one unit j to another.
Units 2 and 10 exhibit similar behaviours, a slow and no saturated first order shape given by their lag compensator ($\tau_{rc,j} > \tau_{ac,j}$). On the other hand, units 6, 8 and 17 ($\tau_{ac,j} = 0$) respond as a second order system, the initial tangent is zero. Any overshoot is limited by the saturation. Finally, base coal unit have a lead compensator ($\tau_{ac,j} > \tau_{rc,j}$), which offers them a faster initial dynamic. Then, their output power slowly decreases after the nadir has been reached and the frequency gradient has become positive (details on equation D.15).

2.4.3 Relationship between frequency nadirs and generation schedules

In this section, the relation between the frequency nadirs and certain decision variables of the UC model is empirically examined by a graphic representation of statistical classes. First, 365 day-ahead schedules are computed for the hourly stepped demand profile presented in appendix E. Then, some frequency metrics, such as the nadir and the *ROCOF* are computed for every possible single outage by exhaustive simulation, using the implemented ROSFR model described in section 2.3. Finally, the scenarios having the same metric and decision values are put together. Hence, the sizes of the circles represent the statistical weights. For example, figure 2.23 presents the relation between the frequency nadirs and ROCOF with respect to the power imbalance, given by the scheduled output power of any unit k.

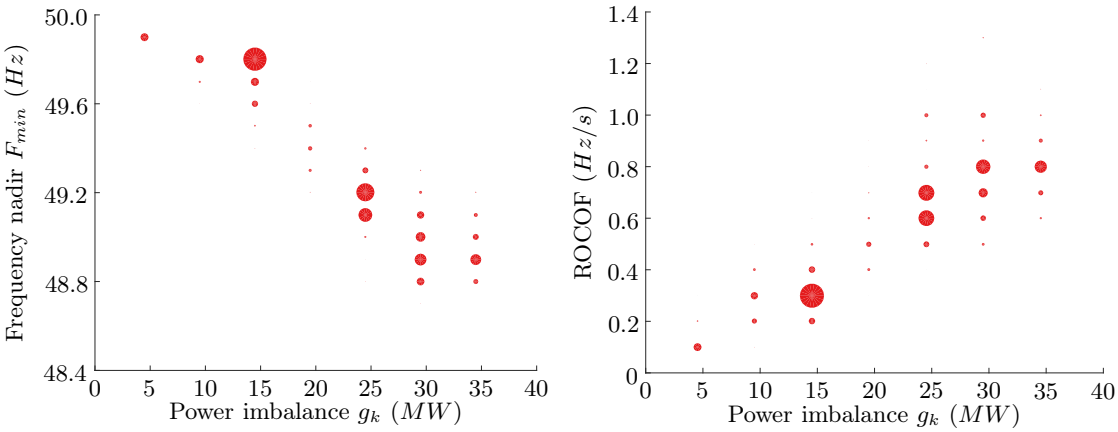

(a) Relation between F_{min} and g_k

(b) Relation between ROCOF and g_k

Figure 2.23: Relation between frequency metrics and power imbalance

In section 2.3.2 analytical expression were found for the frequency nadir and the ROCOF using the EM-ROSFR model. It was stated that these metrics are linearly dependent on the power imbalance for a given system. Figure 2.23 shows that indeed, there is a tendency: the frequency deviation and ROCOF tend to increase with the power imbalance.

However, in a year, different hourly time steps may be characterised by a set of specific parameters, which produce a vertical dispersion, *i.e.*, for an equivalent power imbalance, produced by the outage of unit k, the frequency nadir can vary more that $0.5Hz$ for the test system. For instance, at $g_k = 30MW$ the nadirs vary from less than $48.8Hz$, to more than $49.3Hz$, depending on the system post-contingency state. Analogously, for the same contingency size the ROCOF can vary form 0.5 to $1.3Hz/s$.

These results support the preliminary conclusion provided in section 2.3.2: the EM-ROSFR is not suited for formulating the frequency constraint in the FCUC model. Moreover, they highlight the need for an advance representation of the underlying processes to achieve optimality in the allocation of frequency regulation resources.

Figure 2.24 illustrates the relation between the two frequency metrics of main interest, and the post-contingency stored kinetic energy ($E_{c,-k}$). The inertia constant of the loss unit k is not included in the computation of these metrics.

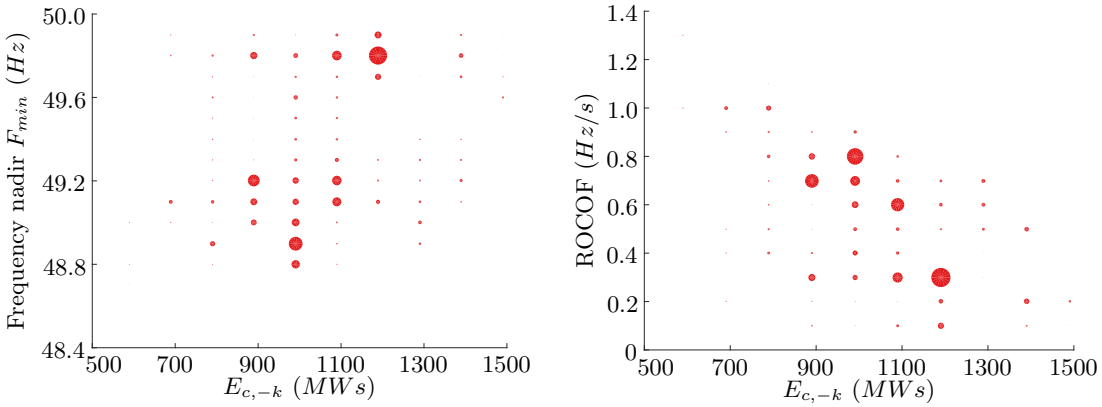

(a) Relation between F_{min} and $E_{c,-k}$

(b) Relation between ROCOF and $E_{c,-k}$

Figure 2.24: Relation of frequency metrics with the post-contingency kinetic energy

It is observed that the frequency initial gradients tend to decrease as the post-contingency kinetic energy increases. However, once more, for a fixed stored kinetic energy, several ROCOF values are possible over a year, depending this time on the size of the contingency. Regarding the frequency nadir, it is difficult to establish a clear relation with the kinetic energy stored in the system, a large range of combinations are possible. Finally, figure 2.25 examines the relation between the maximal frequency deviation and the ROCOF.

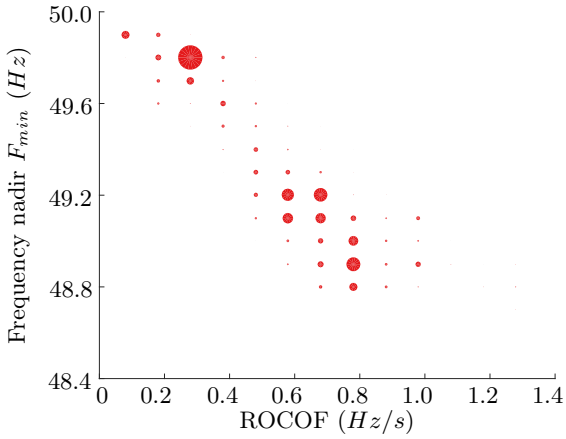

Figure 2.25: Relation between F_{min} and ROCOF

The relation between the frequency nadirs and the ROCOF is more narrowed, although some dispersion remains. In general, slow frequency initial variations lead to a proper primary frequency regulation response. In this case, the frequency nadir is kept above the security threshold (here defined at $49Hz$) for ROCOF values lower than $0.5Hz/s$. However, for higher ROCOF, both secure and load shedding scenarios appears. For those points, the dominant factor seems to be the dynamic of the primary reserve deployment.

2.4.4 Computational details

Optimisation with the classic UC models

The results presented in this section were obtained with a 2x8 cores Intel(R) Xeon(R) CPU E5-2690 @ 2.90GHz and 64Gb of RAM computer. As aforementioned, the optimised models include a few thousands of binary and continuous variables, and even more linear constraints. A primal method was set to the MILP solver (GUROBI) and the required MIP gap was specified to 0.1%.

The computational time of the presented two instance of the UC problem (week day and weekend) were 1 minute and 35 seconds respectively when using model $\mathfrak{M}_0$. This times are drastically reduced when considering a static reserve requirement ($\mathfrak{M}_1$). In this case, the week day schedule was computed in 7.8 seconds, while the weekend day took 8.9 seconds. Hence, constraint (2.13) does allow a better representation of the primary reserve requirements and the reduction of the security cost. However, this improvement on the economical performance of the dispatch is associated to an increased complexity of the optimisation model. In fact, this constraint is enforced for all time steps h when considering static reserve requirements (dimension T), while the security constraint must be defined for all units k and time step h (dimension NT) when using model $\mathfrak{M}_0$. As a consequence, the computational time increases.

Finally, it should be noted that considering different load profiles (different instance of the same optimisation problem) might entail quite different CPU times. For the time series presented in appendix E (a year of hourly stepped demand), 365 day-ahead schedule were computed. The distribution of the CPU times by day-ahead schedule is presented in figure 2.26. The average computing time over 365 day-ahead schedules, where only the load profile varied, was 25 seconds, and ranges between 4.3 and 132.5 seconds, when using model $\mathfrak{M}_0$. These values are reduced to 0.3-16 seconds, with a mean value of 5.88 seconds and a standard deviation of 2.47 seconds for $\mathfrak{M}_1$.

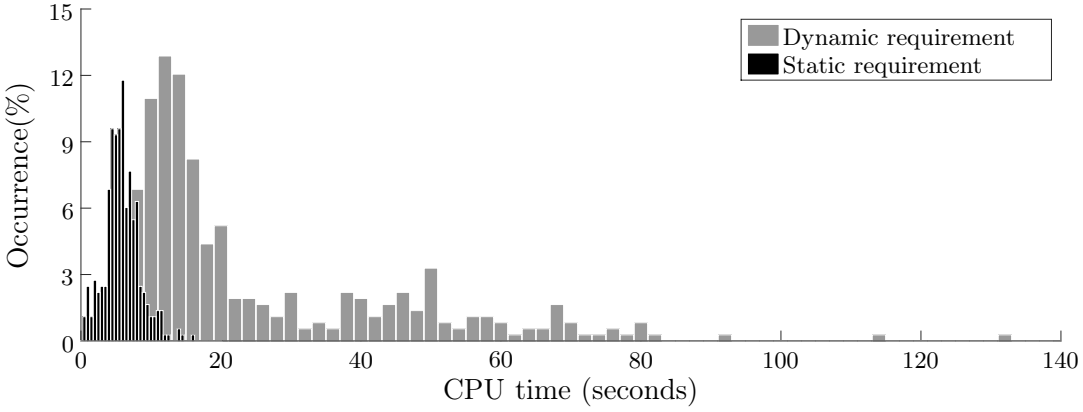

Figure 2.26: CPU times distribution

Dynamic simulation with the proposed MMR-ROSFR model

It must be noted that 212 dynamic simulations were run for the week day, while 195 possible unit outages were considered for the weekend example. The total computational time of the full frequency trajectories is less than 1 minute in both cases using a sequential execution[1]. Some rudimentary parallel execution can be easily implemented through a parallel loop even in MATLAB (*parfor* function, up to 12 workers).
In this work, dynamic simulations were stopped after the frequency minimum is reached. The total computational time is brought down to less than 7 seconds, without parallel execution. The CPU time of the computation of all possible frequency nadirs for a whole year (8760 hourly steps and about 80000 ROSFR model runs) was 40 minutes.

2.5 Conclusion

The day-ahead scheduling represents a difficult optimisation problem that must be solved in some minutes. As a consequence, significant simplification has been historically made to ensure computational tractability. Nevertheless, the vertiginous advances in optimisation methods and computational power have enabled the revision of certain assumptions that compromise the feasibility and optimality of the obtained solutions. This trend has been recently boosted by the transformation of the power system operational environment.
For instance, the nature of different uncertainties are generally overlooked when scheduling the resources needed to handle them in real-time (the reserves). In practice, deterministic security criteria, based on a specific volume of spare capacity, are used to ensure the secure operation of power systems. Nevertheless, this approach may overschedule frequency regulation resources, which leads to higher production costs (sub-optimal solutions).
This effect may become more relevant as the uncertainty rises due to the V-RES forecasting errors. Therefore, new formulations are being proposed to schedule frequency regulation resources accordingly to the actual system needs. In this context, UC formulations based on mathematical programming techniques have received more attention. In this work, the interest is placed on the optimal scheduling of the primary frequency reserve, which is usually specified following a static $N-1$ deterministic criterion.
First, the cost of allocating the primary reserve was assessed by the computation of day-ahead schedules for one year using different primary reserve criteria. The different schedules were computed by solving deterministic MILP UC models. Then, the cost of providing the primary reserve in a test system was estimated by comparing the annual production cost with and without the reserve constraints. For the test system, a dynamic primary reserve requirement entailed almost 2% of generation cost saving.

[1] Hp EliteBook Workstation, Intel Core i5, 2.8GHz with 16GB of RAM.

Second, different ROSFR models proposed in literature were analysed in a attempt to formulate an explicit frequency constraint suited for the FCUC problem. It was shown that the primary frequency response of a power system is highly non-linear with respect to the commitment variables, even at its simplest representation as an unique equivalent unit. The downsides of the EM-ROSFR model, which include a limited representativeness of the underlying processes, were thoroughly discussed.
Alternatively, a enhanced MM-ROSFR model was proposed in order to take into account certain phenomena that are quite relevant for the allocation of the primary reserve, such as the regulation saturation by capacity limits. Following to this, an empirical approach was proposed to examine the relation between certain metrics, such as the frequency nadir and the $ROCOF$, with respect to some parameters related to the decision variables, such as the amount of committed units and the stored kinetic energy.
Numerical implementations showed that small variations on the commitment decisions may modify the primary regulation frequency performance, at least for the test system. Furthermore, it was shown that some parameters of the primary frequency response, such as the inertia, depend on the binary UC variables, *i.e.*, whether a unit is committed or not. In addition, the capacity of a certain unit to participate to the frequency regulation depends on its scheduled power outputs, since once the capacity (or deployed reserve) limit is reached, the output power is saturated. Finally, the outage of heavily-loaded units may entail larger power imbalances. Therefore, two main questions need to be addressed in order to formulate a FCUC model that maximises the integration of V-RES without compromising power system security at minimal cost:

1. What is the impact of the V-RES on the commitment decisions, and what are the consequences on the primary frequency response?
2. How to introduce a more accurate model of the regulation in the UC model to maintain the performance of the primary frequency regulation?

These questions will be addressed in the remaining chapters. First, chapter 3 assesses the impact of V-RES on power system security. Second, chapter 4 examines the effectiveness and optimality of different impact mitigation techniques, regarding the primary frequency regulation performance. Finally, chapter 5 proposes a new FCUC formulation based on the MMR-ROSFR proposed in this chapter.

Chapter 3

Impact of PV generation on the primary frequency response

Contents

3.1 Introduction

Chapter 2 described the classic unit commitment (UC) model and the simplest reduced order system frequency response (ROSFR) model, *i.e.*, the equivalent machine ROSFR model (EM-ROSFR). This latter model enabled the formulation of the frequency nadir as an explicit function of the equivalent unit parameters. However, this expression is strongly non-linear and does not exhibit a direct dependency on the *individual* unit's optimisation variables. Therefore, it was found unsuited for the frequency constrained UC problem (FCUC) and an enhanced multi-machine ROSFR (MMR-ROSFR) model was proposed.

Then, the sequential simulation of the implemented UC and ROSFR models provided an insight on the complex relation between the primary frequency response and the day-ahead decision variables.

This chapter studies, in a similar way, the evolution of the primary frequency response of an isolated power system, following the progressive integration of photovoltaic generation (PV). This section, discusses some recent works dealing with the integration of variable renewable energy sources (V-RES), and provides a description of the proposed methodology. Section 3.2 investigates the impact of the PV integration on the UC solutions through a numerical implementation over two typical days. Afterwards, section 3.3 analyses the consequences of the commitment decision changes on the primary frequency response. Section 3.4 comments on the aggregated results of the day-ahead schedules and dynamic simulations for one year of hourly stepped data (demand and PV load factor forecasts), considering four scenarios of installed PV capacity. The relation between the commitment decisions, the declining behaviour of the frequency and the V-RES penetration rates is examined. Finally, conclusion are drawn in section 3.5.

3.1.1 Background

The analysis of the impacts of V-RES on power systems planning and operation is quite a broad topic, and it has been widely addressed in the literature, especially for wind power [28, 51]. This work is focussed on system-wide frequency regulation issues. Thus, the impacts of V-RES distributed generation on local voltage profiles, and transmission/distribution line overloads are out of the scope of this work. As discussed previously, concerns in large-interconnected systems regarding frequency regulation are more related to flexibility (maintaining margins) and load following problems (secondary control), which are not the main issues addressed in this dissertation. Nevertheless, some methodological aspects of those studies are highlighted below as they inspire the simulation approach proposed here. For illustrative purposes, let us briefly describe two of them:

- In 2009 Makarov *et al.* [31] proposed a methodology to identify the new regulation and load following requirements of the Californian power system, considering a growth on the installed wind power capacity. For this, forecasts of the minute-to-minute load and wind generation variations, involved in the scheduling, real-time dispatch and regulation processes, were modelled. Expected wind and demand profiles were obtained from a commercial forecasting tool (AWS Truewind) and by scaling up historical data, respectively. Historical forecast errors were injected into the expected time series. Then, the actual Californian Independent System Operator (CAISO) practices were simulated to mimic different markets, with and without wind generation, in order to determine the load following requirements due to the additional wind

power. Finally, certain metrics, such as the maximal capacity, ramp and duration of the deployed load following resources were computed, with the aim of ensuring the reliable integration of additional wind generation.

- In 2010 Doherty *et al.* [84] studied the impact of wind generation on the frequency control of the Irish All-Island electricity system in order to characterise the evolution on the frequency behaviour and identify upcoming challenges. In this case, simplified frequency control models and extensive simulations of wind penetration scenarios based on a time series sampling methodology over an extended multiyear timeframe were proposed. The scenarios were defined by a set of generation portfolios with different wind penetration levels, types of wind turbine technologies and external HVDC interconnections. Time series of wind generation were obtained from historical data. The system frequency response was characterised by the rate of change of frequency ($ROCOF$) and the frequency nadir.

Despite these research works address specific topics with different techniques, they have some common elements with many others published papers [28]. On the one hand, they share several hypotheses, such as the consideration of a copper plate network, which is a standard assumption when the interest is placed on power balancing issues. In addition, availability and investment considerations are, in general, disregarded. On the other hand, they are based on some similar settings, such as the use of sequential time-series to represent the load and V-RES generation, since, due to their variability, snapshots are not suitable to characterise the overall impact of V-RES on power system security.
The next paragraph lists and describes some key elements that appear in several V-RES impact assessment studies, and positions the analysis proposed in this chapter with respect to some recent works. Indeed, the identification of certain widespread considerations provides a general framework for the V-RES impact assessment. It will be shown that this general framework is suited for the evaluation of the primary frequency response following the integration of V-RES, and enables the subsequent cost/benefit analysis of some impact mitigation measures presented in chapter 4. Moreover, the formalisation of these key elements brings forward the specific features of different contributions.

Key elements of V-RES impact assessment

In a very general way, the bases of a V-RES impact assessment are (1) the construction of scenarios, (2) the sequential simulation of market structures and real-time operation, and (3) the definition of suitable performance indicators or metrics. Moreover, these performance metrics are in general compared with respect to (4) a predefined reference scenario. Furthermore, the sequential simulation tool should be run over different operational conditions to get (5) an statistical representation of the performance metrics and provide meaningful conclusions.

It must be kept in mind the each one of these elements has been (and should be) customised depending on the aspect of the system operation that is analysed and the time frame of main interest. Then, different trade-offs between accuracy and computational time can be achieved, which makes literature on this topic so extensive. Main features of these elements are discussed below:

1. **Scenarios**. A scenario is a set or sequence of operational points. The latter is usually referred to as a time or chronological series. It commonly defines a load and/or a V-RES generation profile, that can represent a forecast or a realization. When it is considered that the a posteriori observed realization is identical to the forecast, the scenario may be called a "perfect forecast scenario" [123]. The size of a scenario depends on the particular study, for instance:

   - The trivial case is an operational point, the length of the time series is one. It is traditionally used for dynamic and security analyses.
   - In day-ahead scheduling, a scenario is an hourly (or 30 minutes) stepped time series covering 24 to 48 hours ($\approx 10^2$ points).
   - This time step needs to be tightened to a few minutes to evaluate the performance of the load frequency control (LFC), thus a time series (scenario) consists of a few thousand points.

   In general, a scenario may be deterministic or stochastic. A **deterministic scenario** only considers one possible future. A **stochastic scenario** is defined here as a representation of a deviation from the deterministic scenario. It represents a possible realization of the underlying stochastic process.

   Different approaches can be used to define time series for load and V-RES generation. One option is to use historical data. The advantage of this approach is its simplicity, while its main drawback would be the limited representation of possible outcomes. The second option consists in building models to *artificially* generate time series.

   In general, historical realizations are used to define deterministic scenarios. Then, different models can be used to simulate the uncertain future, *i.e.*, to generate the stochastic scenarios, from simple random sampling to autoregressive–moving-average (ARMA) models. One of the challenges that appears when using these models is the parameter identification process, which may entail a certain number of hypotheses. For instance, it is commonly supposed that the wind speed errors are normally distributed [131], although more complex models have been proposed, such as the Cauchy, Beta and Weibull distributions [132]. Moreover, some published works consider different data fitting techniques [133].

Therefore, an V-RES impact assessment may include a few deterministic scenarios and consider a certain number of stochastic scenarios around each one of them, at the expense of a high computational cost [32]. In order to avoid this, scenario reduction techniques for stochastic scenarios have been proposed [134, 135, 136]. Moreover, these studies are typically conducted separately:

- Some works are interested in the impact of the V-RES capacity increase, based on the definition of a set of perfect forecast (deterministic) scenarios with longer time series (*e.g.*, single or multi-year) [84].
- Other works deal with the impact of uncertainty, therefore only one or a limited number of V-RES integration scenarios are defined, with several possible realizations. This latter approach is common in stochastic scheduling, where one can imagine hundreds of possible realizations of one unique day-ahead forecast.

Finally, other parameters may, in practice, define a scenario, and bring uncertainty into it. For instance, the geographic location of the installed capacity and the technologies associated to this new generation have an impact on the operation of the power system, and may be modelled as a random variable. The former may impact power flow and introduce network constraints.

Moreover, the spatial distribution of V-RES may impact the correlation factor between different local profiles, which makes the aggregated time series more or less smooth. Lastly, different technologies may exhibit different transient behaviours.

2. **Sequential simulation of different decision making and/or real-time processes**. Research works on V-RES impact assessment showed the interest, which has become a trend, of developing mathematical models able to simulate the actual System Operator (SO) scheduling, real-time dispatch and regulation processes. In practice, a sequential simulation approach is generally used since these processes take place at different time scales. For instance:

   - the day-ahead scheduling defines the generating unit states;
   - (re)dispatch models adjust generation in an hour-ahead basis every few minutes;
   - finally, automatic regulation processes, such as the primary frequency control and load following occur in some seconds/minutes respectively.

   Figure 3.1 illustrates some main decision making processes in power system planning and operation, and their time scale. The generic terminology used in theoretical model is preferred considering the wide range of classifications that can be found across the world. In practice, UC decision may be modified during the day following the realization of a certain uncertainty (*e.g.*, for quick start units), such as the outage of a generating unit. This is represented here as the “hour-after" time scale.

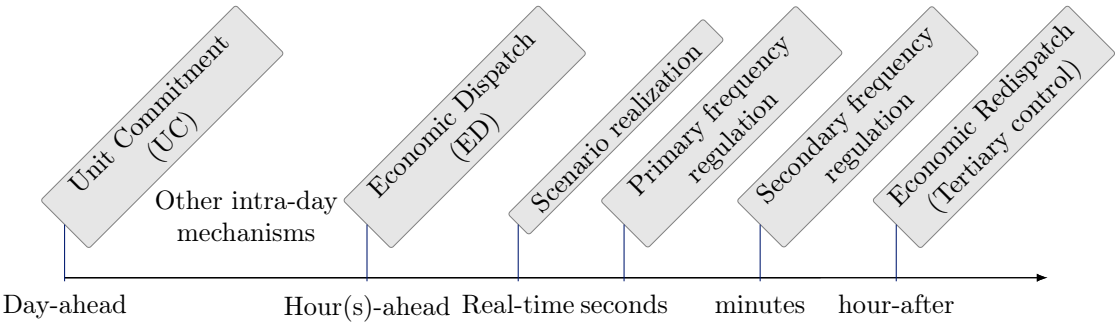

Figure 3.1: Decision making processes

Then, the level of detail of each layer varies from one study to another, depending on the topic of main interest. Once more, the uncertain dimension is very important. As discussed in chapter 2, a lot of research has been done recently in the formulation of uncertain versions of the unit commitment model (UUC) [82]. A significant share of those works is based on stochastic programming, where the load and/or the V-RES generation are considered to be uncertain parameters at the scheduling level. The use of sequential simulation to quantify the robustness of the obtained solutions remains a widespread approach under this framework.

3. **Definition of performance metrics**. V-RES impact studies attempt to quantify the ability (and the cost) of an initial system to perform a specific task after the integration of V-RES. The time window, variables and performance metrics of interest may vary depending on the considered task. For instance:

   - At the scheduling level (day-ahead), the task is to supply the demand at minimal (expected) cost, while respecting operational and security constraints. The variables of main interest are the commitment decisions, and the metrics examined are usually flexibility ones. The concern is generally placed on the capability of conventional units to balance the variable power while maintaining reliability, which involves, among others, reserve availability and ramping requirements.
   - At the dispatch level (intra-day), the attention may be placed on the power output fluctuation, generator loading levels and their ability to provide ancillary services, despite of the intra-hour variability and forecasting errors.
   - At the regulation level, different processes can be modelled and a cost/benefit analysis tends to be proposed. The performance metrics are physical magnitudes or binary ones, *i.e.*, whether the system is capable or not of maintaining power balance under different scenarios (ramp event in load following, or step events in primary frequency regulation).

Then, the notion of severity, duration or frequency may appear, for instance, in the case of load shedding, the risk (or probability) of occurrence characterises the level of system inability to perform the task (regulation), while the (expected or cumulative) value of the loss load may indicate the dimension of the potential consequences.

4. **Reference scenario**. The evaluation of the performance of a power system by itself can be tricky. Certain performance metrics may be standardised, in which case the analysis consists in determining if the requirement is met or not. In Europe, for instance, the volume of reserve i given by the reference incident ($3GW$). Then, it can be stated that the system is able to fulfil this requirement if a volume of reserve can "always"[1] be ensured.

   However, as discussed in chapter 1, the power system is evolving fast, and certain relevant performance metrics are not standardised, for instance the ramping capabilities, or the robustness of the UC solutions. Therefore, in order to asses the impact of V-RES from a certain operational view, it is easier to approach the topic in terms of a comparison. For this, one scenario is generally used as a benchmark.

   In deterministic studies, this "zero" scenario usually represents the system "before", without V-RES (or with a lower share). Then, deterministic scenario(s) of V-RES integration, with a specific installed capacity for instance, will define the system "after". In stochastic approaches, the reference case is the system without uncertainty (perfect forecast scenario). Finally, the same set of simulation are run for all the predefined scenarios, and the performance metrics of the system "after" and/or with uncertainties are compared with the reference scenario to quantify the consequence of the (uncertain) V-RES development.

5. **At least some statistics**. As aforementioned, the trivial representation of a scenario is an unique operational point, *i.e.*, a snapshot of the power system. There are some published works that do consider this case [53]. They compare the performance (of certain aspects) of the system operation for two deterministic scenarios (with and without V-RES) at a specific operational point, given by a load level. However, one can imagine that taking one unique load level may not be the best way to characterise a power system behaviour, especially considering the increasing variability and uncertainty following a high level of V-RES integration.

   Therefore, nowadays it is more common to use time series, that represent a more complete set of possible system states. Then, the aforementioned performance metrics can be computed for a large number of instances, which give a significant amount of results that need to be aggregated to provide meaningful information.

[1] A standard can also define the acceptable duration or condition in which the requirement can be violated.

The more intuitive metrics are the mean, maximal and minimal values of the performance indicator. In addition, q-quantiles, or even cumulative distribution function (CDF) can be examined. Other standard metrics include probabilities and expected values of some quantities, as well as the duration and frequency of certain events. When the notion of probability is absent, the expected duration can be replaced by the number of periods that exhibit an insufficiency of a certain resource, such as generation (similar to adequacy studies), a certain ancillary service (*e.g.*, reserves), flexibility or even inertial response.

Although main features of V-RES impact assessment studies were discussed, it is acknowledged that alternative schemes have been proposed in the literature, with some pros and cons. For instance, network constraints are relevant to study the impact of V-RES on congestion and quality of electricity. For this reason, they are included to some extents in certain scheduling and dispatch models [30]. In addition, some studies propose the use of non sequential Monte Carlo instead of time series to reduce computational requirements, when inter-temporal dependencies can be neglected or at least approximated [137].
Nevertheless, this general framework enables the characterisation of published (and forthcoming) works by the proposed formulation of the key elements, *i.e.*, the scenario, the sequential simulation tool (and the time frames involved), the performance metric, etc.

Positioning this work

Table 3.1 summarises the main characteristics of some studies proposed in literature for assessing the impact of V-RES on the scheduling of frequency regulation resources. Attention is placed on the three first key elements in order to ensure readability. Exhaustiveness is not claimed, but the selected works suffice to highlight the main features and contributions of the proposed approach, which is further detailed in the next section.
In general, some studies such as [31, 34] analysed the operational changes of the conventional power system with deterministic formulations of scheduling models. Then, uncertainty may (or not) be considered a posteriori through stochastic scenarios.
Other authors proposed the use of stochastic approaches to take into account uncertainty at the optimisation level [32, 35]. Then, a year of load and V-RES time series may (or not) be used to get an statistical representation of the performance metrics and the robustness of the solutions. These latter contributions are more related to the scheduling of tertiary reserve and other flexibility levers from load or V-RES sources.
This work addresses an aspect of the **frequency regulation** that has received less attention in the literature by **adapting a widespread simulation approach** used in the **assessment of V-RES impacts on power system operation**.

Table 3.1: Characteristics of some V-RES impact studies

Reference	Scenario		Sequential simulation tool		Performance
	Deterministic	Stochastic	Time lines	Ability	metric
[31]	✓	✓	2 day-ahead (UC) min-ahead (LFC)	Load following	LF capacity, duration and ramps
[32]	✓	✓	1 day-ahead (UUC)	Supply net demand	Lack of capa- city and reserve
[34]	✓	✗	2 day-ahead (UC) hour-ahead (ED)	Thermal generation for compensating wind variability	Regulation power, needed, duration, cost, emissions
[35]	✗	✓	1 day-ahead (UUC)	Flexibility levers for increasing V-RES integration	Security cost V-RES spillage Load shedding
[48]	✓	✗	1 day-ahead (UC)	Supply net demand	Kinetic energy SNSP level
[84]	✓	✗	hour-ahead (ED) seconds	Ensure primary frequency control	*ROCOF* nadir
This work	✓	✗	2 day-ahead (UC) seconds (ROSFR)	avoid UFLS	*ROCOF* nadir PIDR

Indeed, statistical studies related with frequency regulation issues due to the V-RES integration are more focussed on static considerations (provision of active reserves) and load following [31]. The declining behaviour of the system stability and primary frequency regulation has been addressed in some published works [84], however, these studies are usually based on snapshots of the system and/or are treated in a decorrelated fashion regarding scheduling models [53, 55].

In this work network constraints are not considered and, in this chapter, V-RES generation does not participate to the system inertial response (non-synchronous generation) and does not provide ancillary services (no frequency control loops). This latter assumption permits taking into account the impact of no-controllable distributed generation. The case study considers PV integration scenarios, while the majority of the published works in the field deal with wind power.

3.1.2 Methodology

In this section, the five key elements identified before are customised to fit the assessment of the V-RES impact on the primary frequency response and the risk of under frequency load shedding (UFLS).

1. **Scenarios:** in this work a deterministic approach is adopted, which supposes that the system operational condition is perfectly known within the simulation. Then, a reduced number of deterministic scenarios is defined by the development of V-RES. For instance, a given per unit (or load factor) V-RES time series can define several deterministic scenarios by changing the considered installed capacity.

   Time series for load and V-RES generation are built from historical measurements in the French oversea departments or DOM (*Départements d'Outre-mer*) systems. Four scenarios of PV integration, with different installed capacity, are considered as described in table 3.2.

   Table 3.2: PV development scenarios

Scenario	PV capacity (MW)	Share on total capacity (%)	Max. Instantaneous rate (%)
1	70	13	24
2	130	22	45
3	190	29	65
4	250	35	86

   A unique hourly-stepped load factor time series is used, which is built from normalised measurements of more than a hundred facilities in a DOM system. This curve is presented in appendix E. The maximal load factor is about 0.65, which means that the maximal PV generation in scenario 4 (with $250MW$ of installed PV), for instance, is around $162,5MW$ (0.65×250). It must be noted that for the test system (see appendix E), with a peak load of $250MW$, this entails a maximal instantaneous penetration rate of 85.8% at one specific hour. This value is larger than 80% for 5 hours of the year.

2. **Sequential simulation tool:** the proposed methodology is based on the sequential simulation of the day-ahead scheduling ($\mathfrak{M}_0$) and the reduced order system frequency response models (MMR-ROSFR) following unit outages (both described in chapter 2). For the purposes of this work, the intra-hour variability is not represented, hence the dispatch adjustment after the day ahead schedule is not modelled. Consequently, the intra-day time-line depicted in figure 3.1 is not simulated. The performance of the primary frequency regulation will be assessed by running the implemented models for 365 days, as represented in figure 3.2.

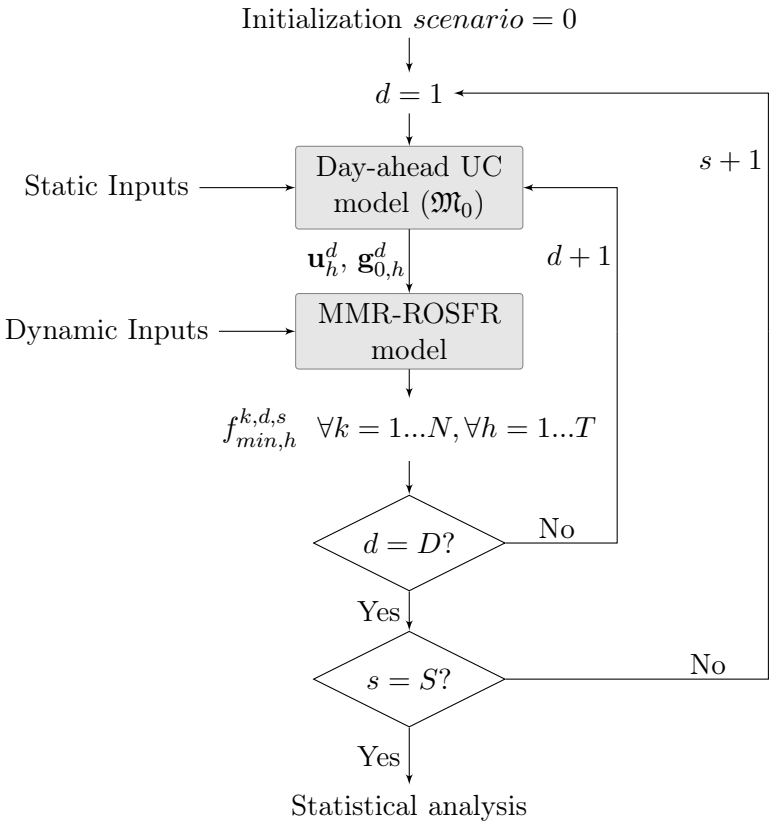

Figure 3.2: General diagram of the proposed methodology

N	number of units	k	index of the loss unit
T	optimisation horizon	h	index of time step
D	amount of days (in this study 365 for one year)	d	index of the day
S	amount of PV integration scenarios (in this work 4)	s	index of the scenario

Although, the use of stochastic UC models and the sequential simulation of intra-day and load following processes may be relevant in this framework, it would be prohibitive for the subsequently study of the V-RES impact mitigation techniques (chapter 4) in terms of computational cost.

3. **Performance metrics:** the physical variables used to examine the evolution of the primary frequency response are the frequency initial gradient ($ROCOF$) and the frequency minimum (nadir) as proposed in [84]. In addition, a security metric is defined: the periods with insufficient dynamic response (PIDR), given by the time steps where the UFLS is potentially activated, *i.e.*, when the frequency nadir following a unit outage goes below a certain security threshold.

4. **Reference scenario:** the reference scenario considers the test system without any PV, and will be called scenario 0 .

5. **Statistical approach:** a year of day-ahead schedules will be computed for each scenario, followed by an exhaustive contingency analysis. This represent 8760 operational points and about 80000 possible unit outages for each scenario. The evolution of the conventional units schedules as the share of PV increases will be examined, with especial attention on the primary reserve allocation. Mean, maximal and minimal values, as well as CDF will be computed.

3.2 Understanding generation scheduling changes with PV

In this section, the impact of different levels of installed PV on the day-ahead commitment decision and dispatch for the two typical days considered in section 2.4 will be investigated.

3.2.1 Day-ahead demand and PV generation forecast

The demand day-ahead forecasts presented in figure 2.10 are recalled in figure 3.3a. Then, different PV generation profiles can be defined depending on the meteorological conditions, two possibilities are illustrated in figure 3.3b.

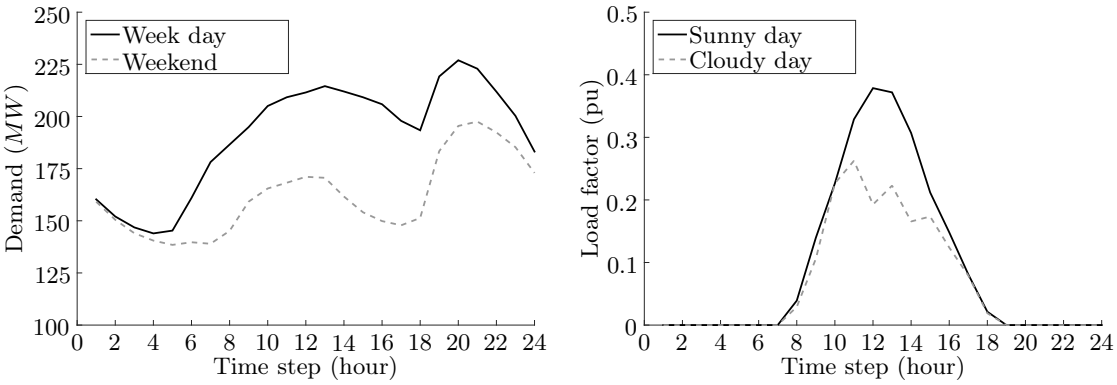

(a) Day-ahead load forecasts

(b) PV load factor forecasts

Figure 3.3: Two typical demand and PV load factors daily profiles

3.2.2 PV integration scenarios and residual demand

Depending on the PV installed capacity, different residual demand profile can be obtained. The residual demand is defined as the load minus the V-RES generation. Figure 3.4 shows the residual demand of the two chosen typical days for different scenarios of PV integration, considering a sunny day (PV load factor in black solid line on figure 3.3b).
These figures are referred to in literature as the duck curves because of their shape. They show the evolution of the gap between the total demand that conventional units used to supply, and the residual demand after the PV has served part of the load.
It is observed that:

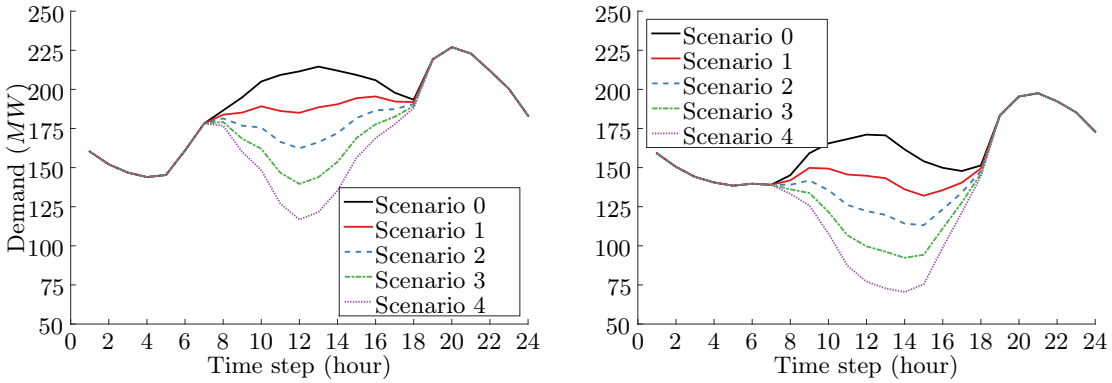

(a) Week day (b) Weekend

Figure 3.4: Residual demand for the two typical days and different PV integration scenarios

1. The minimal load is dramatically reduced as the share of PV increases.
2. The load variations within one optimisation period, a day, become more important.

The next paragraph discusses the effect of these features on the UC solutions.

3.2.3 Optimisation results

The optimal dispatches obtained by solving model $\mathfrak{M}_0$ described in chapter 2, for the different residual demand curves presented in figure 3.4, are shown on figure 3.5. The results for the week day are shown on the left side and the those for the weekend are depicted in the right side. In both cases, a sunny load factor profile was considered. The different scenarios are presented from **top to bottom** (**from scenario 0 to 4**).
It is observed that the share of the base unit HF 1 is highly reduced. This change is more notorious on the weekend day, where these units start to cycle. It must be noted, that in practice additional modulation is required to face intra-hour variability and uncertainty, which may entail further flexibility requirements.

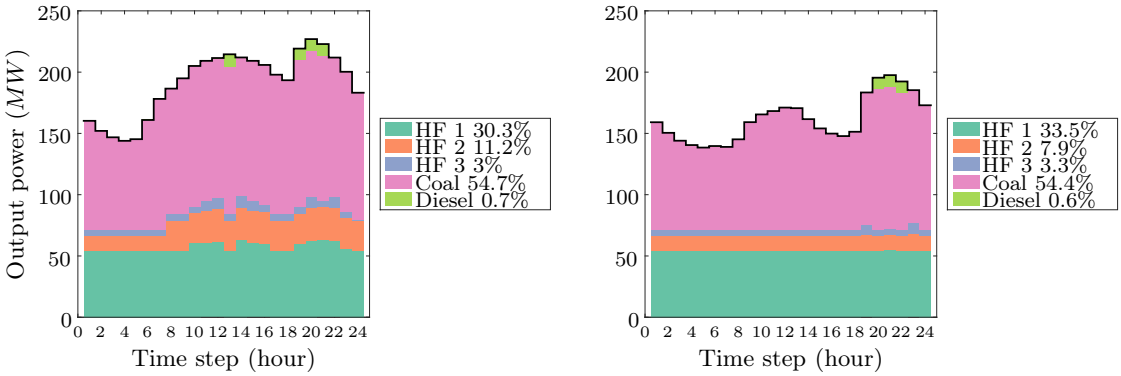

(a) Weekday (b) Weekend

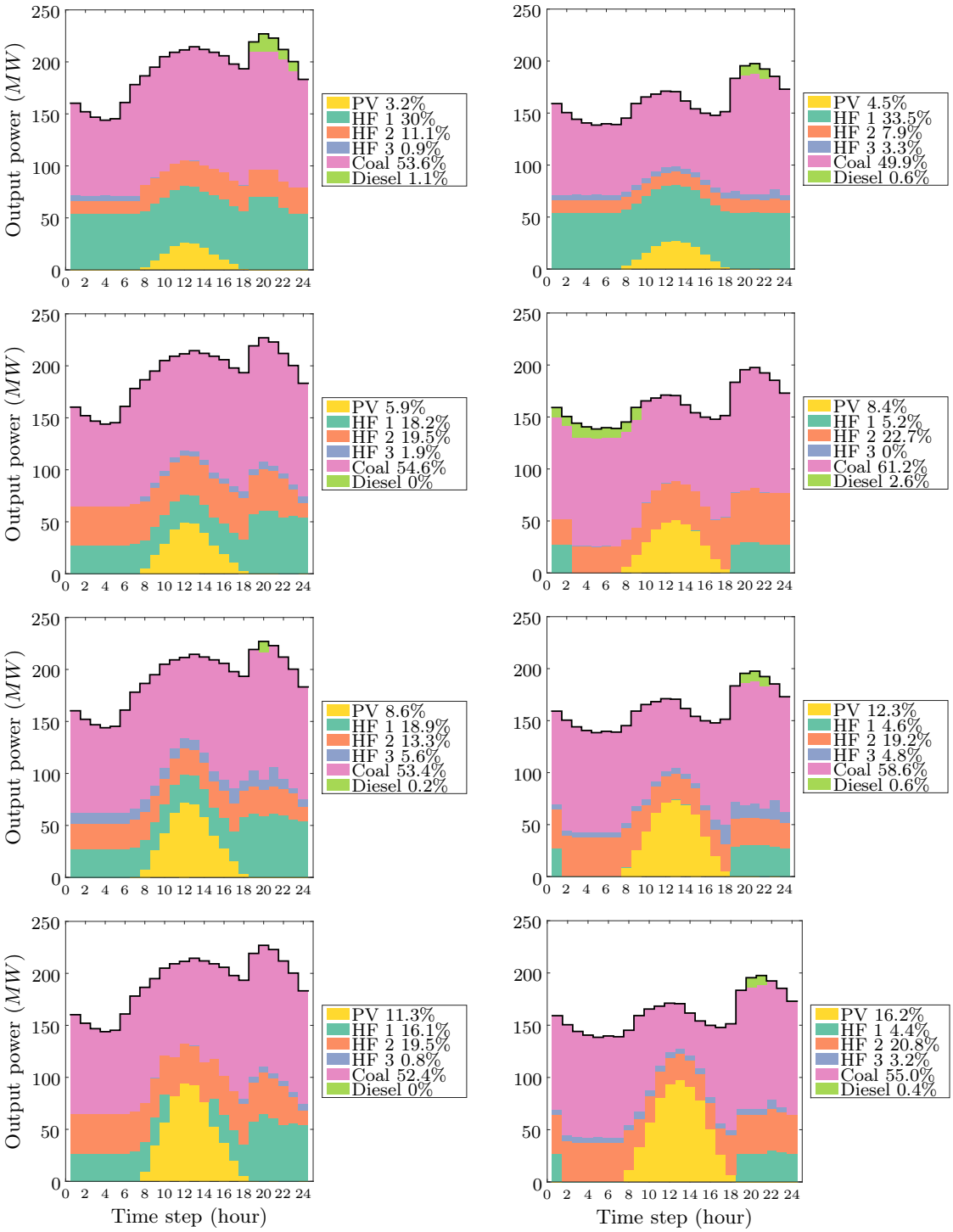

(a) Weekday (b) Weekend

Figure 3.5: Dispatch evolution for the different PV integration scenarios

Figure 3.6 compare for both days the evolution of the amount of committed unit as the PV generation increases. As expected, the amount of committed units tends to decrease whenever PV is present, but attention must be paid to three less intuitive observations:

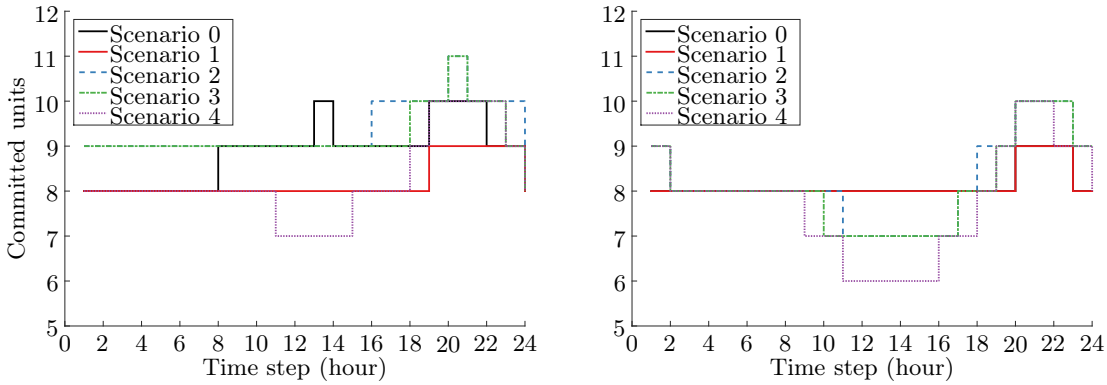

(a) Week day (b) Weekend

Figure 3.6: Amount of committed units for the different PV integration scenarios

1. Even though PV produces only in day hours (from 6 to 18), **commitment changes also occur in night hours to anticipate PV arrival**. For the flexible test system, with low minimum up/down times, this is related to the limitation of start-up cost. For less flexible systems, this feature may be accentuated by the activation of inter-temporal constraints (*e.g.*, ramping limits and minimum up/down times).
2. **The changes are more or less notorious depending on the load and penetration level**. For instance, in a working day (left) 8 conventional units were started during the day instead of 9 units when comparing scenario 1 to 0. However, in a low demand day (right), there is no difference between both scenarios.
3. In some particular cases, **an increase on the PV share may entail the start up of more, but smaller, conventional units** (compare scenario 2 to 1 in the left at hour 22). To have an insight on this last aspect, figure 3.7 compares the kinetic energy stored in the rotating masses at nominal frequency (50 Hz) for the two typical days and different PV integration scenarios.

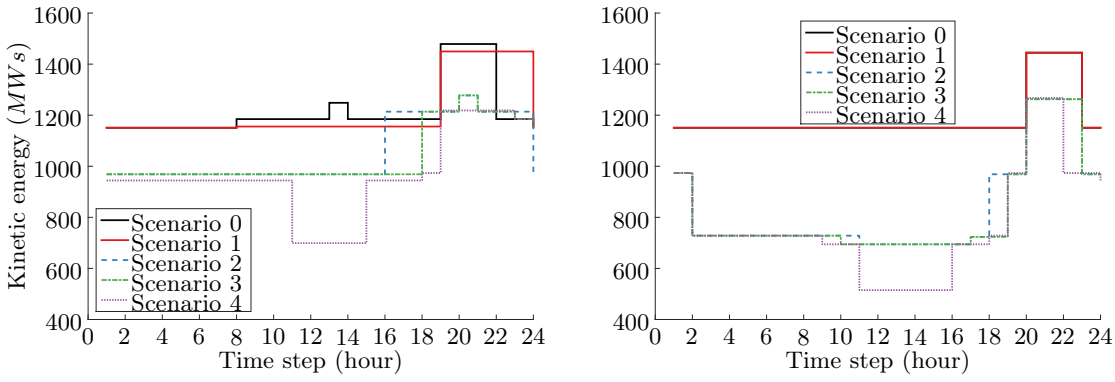

(a) Week day (b) Weekend

Figure 3.7: Stored kinetic energy for the different PV integration scenarios

It is observed that as the PV installed capacity increases, the kinetic energy available in the rotating masses is reduced, but not in a linear manner. For the specific test system, minor changes are observed when passing from scenario 0 to 1 (0 up to 70 MW of installed PV). However, the equivalent system inertia seems to be more impacted from scenario 2. This effect is amplified for the low demand day. The next section discusses the consequence of these changes on the resources and response of the primary frequency regulation.

3.3 Evolution of the primary frequency response

This section investigates the evolution of the primary frequency response following the integration of PV generation in a isolated power system. For illustrative purposes, the results computed for the specific instances of the test system, discussed in the previous section, will be provided. However, the interest is not placed on the results themselves, which are strongly system dependent, but in the understanding of the underlying phenomena.

As aforementioned, the primary frequency response will be characterised by two metrics: the initial $ROCOF$, which depends on the system equivalent inertia and power imbalance, and the frequency nadir that also depends on the primary reserve deployment dynamics. Then, the risk of UFLS, *i.e.*, when a certain security threshold is violated, is determined.

In addition, some features of the required and allocated primary reserve will be examined in order to assess the relation between the commitment changes due to the PV integration and the power system security. For instance, figure 3.8 compares the maximal power input (the power output of the largest or most loaded unit, g_k) for different levels of PV integration, which determine the required primary reserve by equation (2.13).

These figures illustrate a well known issue: in low demand day conventional units tend to be dispatched at their minimum stable generation (MSG) level, in order to provide enough ancillary services by committing more units.

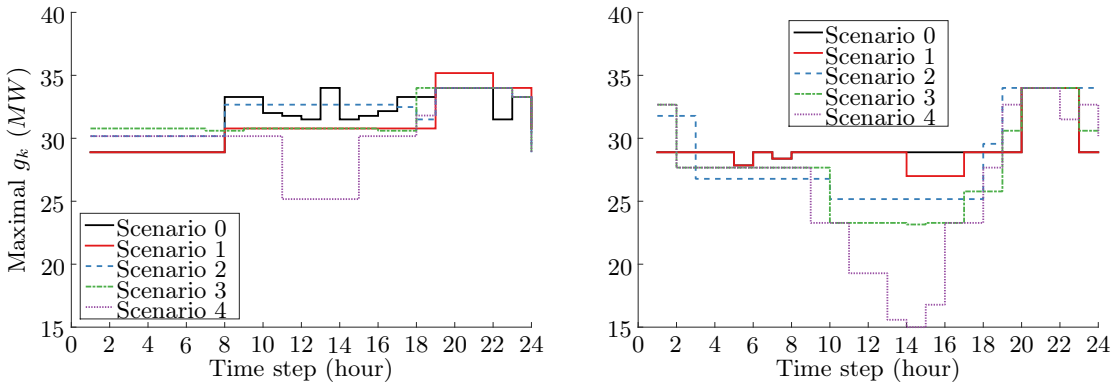

(a) Week day (b) Weekend

Figure 3.8: Maximal power input for the different PV integration scenarios

In small system, the binding constraint tends to be the primary reserve requirement, which enforce a certain committed synchronous capacity. However, this phenomenon may entail a new regulation issue due to the lack of downward reserves at some instants. This topic will be discussed in the next section.

Regarding the primary frequency response, having partially-loaded units may reduce the risk of UFLS, since the power imbalance following generating unit outages are reduced. Nevertheless, one must bear in mind that the system equivalent inertia was also diminished, which limits the system frequency robustness. Figure 3.9 compares the maximal initial $ROCOF$ by time step of the two typical day for the different PV integration scenarios.

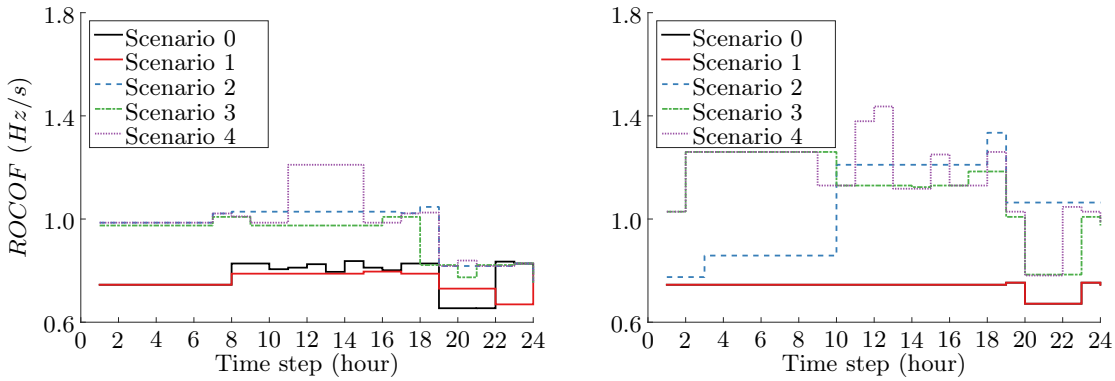

(a) Week day (b) Weekend

Figure 3.9: Rate of change of the frequency for the different PV integration scenarios

It is observed that as the PV share increases and the equivalent inertia is reduced, the initial gradient of the frequency following unit outages increases, despite the reduction of the power imbalances in sunny hours. It is worth noticing that this last feature is in general disregarded in published works, which consider a fixed power imbalance (typically given by a reference incident [138], such as the loss of the largest unit).

Once more this effect is not limited to sunny hours, since units with lower inertia are committed at night to anticipate PV arrival, the $ROCOF$ is also higher at night. The low demand weekend exhibits a larger $ROCOF$ increase.

Finally, the evolution of the K factor is depicted in figure 3.10. It is observed that this parameter tends to diminish with the integration of non-synchronous generation. The increase of the $ROCOF$ and the decrease of K factor indicate that the frequency evolves faster, and that the regulation capacity of the system declines as the V-RES share increases.

In order to analyse the consequence of these changes on the risk of UFLS, the frequency nadirs must be computed for different unit outages and scenarios of V-RES integration. Let us choose, for illustrative purposes, a specific time step with high PV generation, such as hour 13 for the week day (with a total demand of $214.6MW$).

Figure 3.11 shows a closer look of the dispatch for the different scenarios of PV for the week

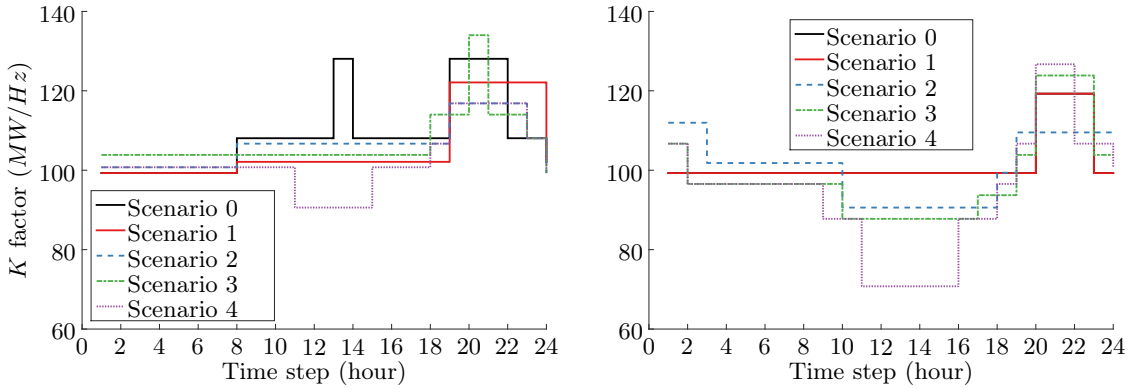

(a) Week day (b) Weekend

Figure 3.10: Available regulating energy for the different PV integration scenarios

day. The abscissa represents the units and the ordinate the power. Different colors are used by scenario, a three colour shades identify the scheduled power, the primary reserve and the remaining slower reserve of each scenario. The size of the bars represents the units' capacity. The main commitment changes are the shut down of unit 17 from scenario 1 and substitution of unit 2 for smaller ones from scenario 2, which explains the inertia and K factor reductions.

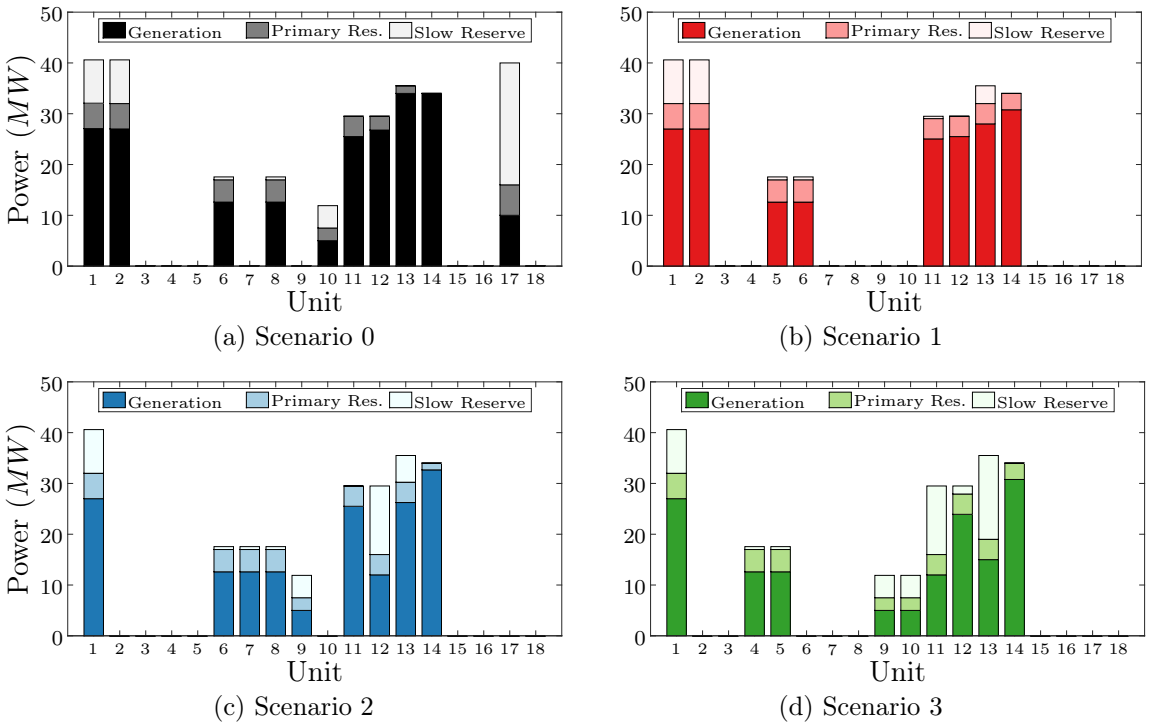

(a) Scenario 0 (b) Scenario 1

(c) Scenario 2 (d) Scenario 3

Figure 3.11: Detailed dispatch at hour 13 (week day) for different PV integration scenarios

However, looking back to figure 3.10b at hour 13, it can be noticed that the K factor for

scenarios 2 and 3 is larger that in scenario 1, due to the participation of units 8-9 and 9-10 (respectively) to the primary frequency regulation, which possess lower droop constants (see appendix E). Afterwards, the consideration of equivalent power imbalances provides an insight on the impact of these changes on the frequency nadir.

In all but scenario 4 (see figure 3.5a), unit 1 is committed to produce 27 MW. Therefore, for illustrative purposes, it is desirable to consider the outage of this unit when computing the average frequency trajectories for scenarios 0 to 3, although unit 14 is the most heavily loaded unit and would probably produce the largest frequency deviation. Results are showed in figure 3.12. It is observed that indeed the frequency drops faster and lower with the increasing share of PV for an equivalent load level, unit outage and power imbalance.

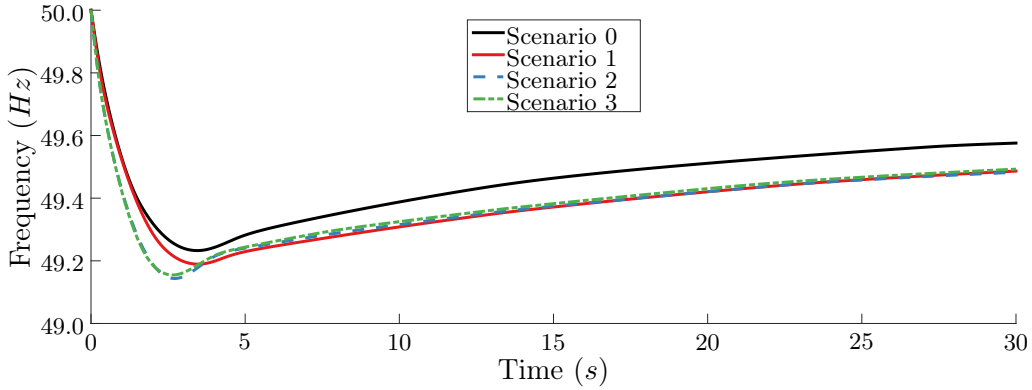

Figure 3.12: Frequency following the outage of unit 1 at hour 13 of the week day

Regarding others metrics, the steady-state frequency (f_{ss}), for instance, depends on the power imbalance, the K factor and the load damping. For the specific cases represented in figure 3.12, the power imbalance is the same for all scenario, and the K factor is similar for scenarios 1-3, and considerably higher for scenario 0 (see figure 3.10), which explain the behaviour of the f_{ss}. In order to examined the risk of UFLS, all possible single outages are simulated. Figure 3.13 presents the lower frequency nadir (among all possible unit outages) by time step for both typical days and the defined PV integration scenarios.

Results for the week day are less dispersed than those for the weekend day from 0 to 20 hours. Therefore, for an equivalent V-RES share, the frequency nadir, and the risk of UFLS, are less affected when the load is higher. This is the reason why, as discussed in chapter 1, some limits have been set to the V-RES instantaneous penetration rate, because in low loaded day the actual V-RES power that can be securely accommodated tend to be reduced when compared to operating conditions with high demand. However, it is possible that for an equivalent instantaneous penetration rates, different frequency nadir are obtained depending on other factors already discussed here related to the system specific operational point. Similar findings are reported in recent works [138].

To improve readability figure 3.14 shows these results normalized to the case with no PV.

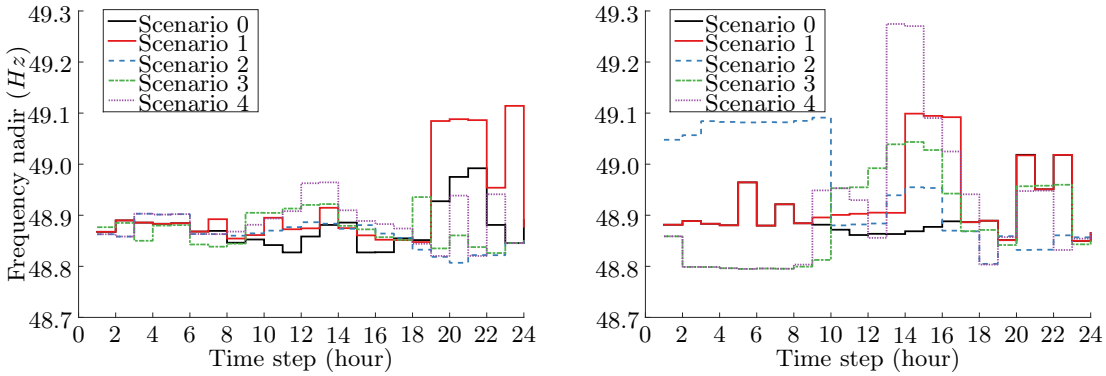

(a) Week day (b) Weekend

Figure 3.13: Minimum frequency nadirs for the different PV integration scenarios

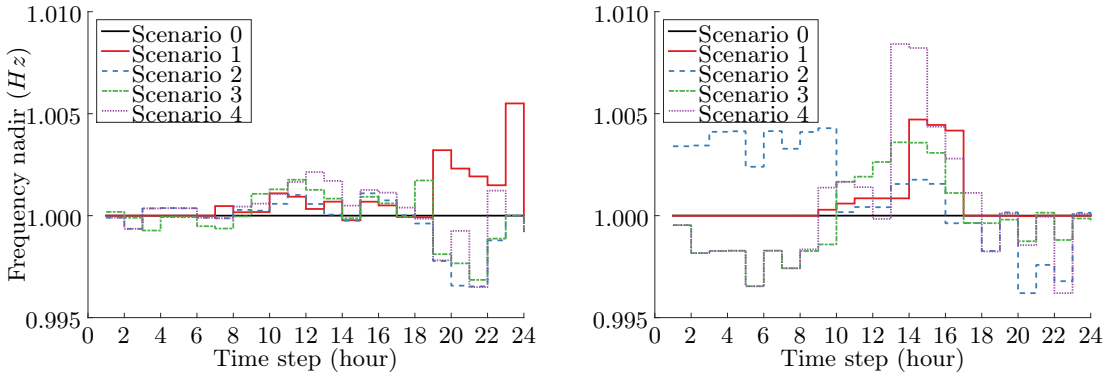

(a) Week day (b) Weekend

Figure 3.14: Normalized minimum frequency nadirs for the different PV scenarios

It is observed that:

1. **Scenario 1:** a certain (reduce) level of V-RES may slightly improve the performance of the primary frequency response at some instants, when enough conventional units remain at a partially-loaded state, making available more primary reserve than actually needed. In the illustrative example, the commitment changes between scenarios 0 and 1 are negligible, and units tend to be partially loaded during sunny hours since part of the demand is supplied by the PV generation.
2. **Scenario 2:** the performance of the primary frequency response is improved during sunny hours due to the same reason given for scenario 1. The nadirs are also less deep in early hours when considering the weekend load profile, but they decline at night because the peaking diesel unit is not longer committed.
3. **Scenario 3 and 4:** the decline of the primary frequency response is observed during night hours. Smaller units were chosen to anticipate PV arrival reducing the system inertia and the available headroom capacity in early and late hours.

In general, for the selected days, the primary frequency regulation security does not seem

to be compromised during sunny hours. The effect of having partially loaded units prevails over the inertia and regulating capacity reduction. In order to draw more general conclusions, a statistical analysis is proposed through the year time series of demand and PV generation load factor. The data set used for the case study is described in appendix E.

3.4 Case study

Analysing two typical days of the test system, described in appendix E, may illustrate the impact of the PV on the operation of a conventional generation mix. However, these results do not allow one to characterise the performance of the primary frequency response, since the impact of PV is strongly dependent on the specific operational point of the system. Therefore, in this section a larger set of load levels and PV load factors will be considered, taken from a hourly stepped year time series (8760 points).

Computational details

The simulation results presented in this section respond to the following considerations:

- The solution of 365 instances of the model $\mathfrak{M}_0$, given by equations (2.2)-(2.13) and described in section 2.2, which corresponds to one year of day ahead schedules. The instances differ on the residual demand profile $\mathbf{D}_f$.
- The optimisation horizon is a moving window of 32 hours, where only 24 hours are kept. This is a common practice in industry to anticipate the morning load raise.
- The state and up/down times at the end of the day (24 hour) are considered to be the initial condition for the optimisation of the following day.
- The $MIPgap$, which represent the quality of the optimisation as explained in section 2.2.4, is specified to 0.1%. The MILP solver (GUROBI) takes this parameter as an input.
- In order to prevent the solver of spending too much time on a given instance, a time limit of 10 minutes is also specified. As discussed in section 2.2.4, the selected MILP solver takes this parameter as an input and returns the best feasible point found so far when the elapsed time reaches this value, even though the $MIPgap$ is larger than the predefined threshold. In the optimisation terminology, the returned feasible points are considered to be upper bounds of the solutions. In practice, this means that a schedule is indeed computed for these cases, but the quality of the solution is lower than expected.
- Computer: 2x8 cores Intel(R) Xeon(R) CPU E5-2690 @ 2.90GHz, 64Gb of RAM.

Table 3.3 indicates the amount of instances, or days, stopped by the time limit, which means that after 10 minutes the predefined $MIPgap$ (0.1%) was not attained, but a lower quality solution is still provided.

Table 3.3: Days stopped by time limit

Scenario 0	Scenario 1	Scenario 2	Scenario 3	Scenario 4
0	1	3	12	49

For scenario 0 (without any PV), all the instances were solved in less than 3 minutes. However, as the PV capacity is added, the amount of instances that do not reach the specified $MIPgap$ in the predefined time increases.
Hence, the addition of PV makes the optimisation problem harder to solve, which may entail *optimality issues* if the $MIPgap$ of the returned solution is too high. This feature must be kept in mind when comparing the cost between scenarios. A cost difference within the solution gap will not be significant enough to provide meaningful conclusions.
Table 3.4 presents the maximal (worst) and mean $MIPgap$ reported for the 365 solved instances. It is observed that, even in the worst case the $MIPgap$ is lower than 0.75%, and that this value remains acceptable in average, even for scenario 4, which enables a comparison between the security cost over the year among scenarios.

Table 3.4: Mixed integer programming gap ($MIPgap$)

$MIPgap$	Scenario 0	Scenario 1	Scenario 2	Scenario 3	Scenario 4
Maximum	0.10%	0.25%	0.55%	0.56%	0.74%
Mean	0.05%	0.04%	0.06%	0.07%	0.12%

Moreover, it is possible that there is no schedule satisfying all the constraints considered by model $\mathfrak{M}_0$ for certain instances. In this case, it is said that the feasible set is empty and the MILP solver returns an *infeasible* status. For the purposes of this work, a day a-head schedule is computed even for these cases, by loosing some constraints. Therefore, **different modified UC models** can be proposed, allowing the partial violation of a certain constraint, while penalising its activation in the objective function.
In this chapter, **two variations of model $\mathfrak{M}_0$** have been considered, and are referred to as $\mathfrak{M}_2$ and $\mathfrak{M}_3$. The former is given by a relaxation of the reserve constraint (2.13) and represents the fact of accepting the risk of UFLS, while the latter is given by a relaxation of the demand constraint (2.5) and, as defined here, represents the dispatch-down of some V-RES. Other versions exist depending on the goals of the study.
For implementing $\mathfrak{M}_2$, an auxiliary variable R^h_{ns} is defined, which represent the no supplied primary reserve, and its value is penalised in the objective function by a high loss of load cost (VOLL). Therefore, the objective function (2.2) and constraint (2.13) are

rewritten as indicated in equation (3.1), while all other constraints of model $\mathfrak{M}_0$ given by equations (2.3)-(2.12) are maintained.

$$\begin{aligned} \underset{\mathbf{u},\mathbf{g},\mathbf{R}_{ns}}{\text{minimise}} \quad & \left\{ \sum_{h=1}^{T} \sum_{j=1}^{N} C_j^h \left(u_j^h, g_j^h \right) + S_j^h \left(u_j^h, u_j^{h-1} \right) \right\} + VOLL \sum_{h=1}^{T} R_{ns}^h, \\ \text{subject to} \quad & \sum_{\substack{j=1 \\ j \neq k}}^{N} r_j^{h,pr} + R_{ns}^h \geq g_k^h \qquad \forall h = 1, \ldots, T, \end{aligned} \tag{3.1}$$

Analogously, a V-RES dispatch-down variable, VG_{dn}^h, can be defined by time step in order to build $\mathfrak{M}_3$, by including it in the objective and power balance equations, given by expressions (2.2) and (2.5) respectively, as indicated in equation (3.2).

$$\begin{aligned} \underset{\mathbf{u},\mathbf{g},\mathbf{VG}_{dn}}{\text{minimise}} \quad & \left\{ \sum_{h=1}^{T} \sum_{j=1}^{N} C_j^h \left(u_j^h, g_j^h \right) + S_j^h \left(u_j^h, u_j^{h-1} \right) \right\} + a_{vg,dn} \sum_{h=1}^{T} VG_{dn}^h, \\ \text{subject to} \quad & \sum_{j=1}^{N} g_j^h - VG_{dn}^h = D_f^h \qquad \forall h = 1, \ldots, T. \end{aligned} \tag{3.2}$$

where $a_{vg,dn}$ is the cost associated to the dispatch-down of V-RES in €/MW. Once more, constraints (2.3)-(2.13) are included in $\mathfrak{M}_3$. This model will be further discussed in the next chapter (section 4.2.2). Simulation results exhibited only one infeasible day when considering scenario 4, but a schedule was still computed by relaxing the primary reserve constraint and penalising its violation in the objective function (model $\mathfrak{M}_2$).

It must be noted that *feasibility*, from an optimisation point of view, may become a real issue in systems with a less flexible mix. Furthermore, the increase of infeasible instances may be interpreted as a V-RES integration limit due to a flexibility shortage. In practice, V-RES dispatch-down is nowadays the more widespread solution for these cases [139]. In small power systems other sources of flexibility, such as centralised storage systems are being considered to tackle this issue [68].

Finally, table 3.5 presents the average computational times for one instance and the total CPU time for the whole year day-ahead schedule computation. The total CPU time is multiplied by 8 from scenario 0 to 4. The next paragraph shows that this is related to the difficulty of providing primary reserve.

Table 3.5: CPU times for model $\mathfrak{M}_0$

CPU time	Scenario 0	Scenario 1	Scenario 2	Scenario 3	Scenario 4
Mean (s)	25.1	24.4	45.4	100.7	200.8
Whole year (hour)	2.5	2.5	4.6	10.2	20.4

Primary reserve provision cost

Section 2.4.1 presented day-ahead schedules for one year of hourly step demand with and without the primary reserve constraints, and showed that this resource is difficult and costly to provide in an isolated power system. In this paragraph, the same procedure is repeated for the different scenarios of PV integration described in 3.1.2. Results are presented in table 3.6. It is observed that the primary reserve provision cost, referred to here as the security cost, increases with the share of PV. Similar results have already been reported for larger systems with high share of V-RES [140].

Table 3.6: Primary reserve constraint impact on schedules

Results	Scenario 0	Scenario 1	Scenario 2	Scenario 3	Scenario 4
Cost due to reserve (%)	6.32	7.32	8.01	9.02	10.43

Remark 1: The cost of providing the primary reserve increases with the V-RES development, at least for PV generation in a isolated power system.

In addition, the average computational time of one day-ahead schedule, without the reserve constraints, is less than 1 second regardless of the scenario, which gives total CPU times for the 365 day-ahead schedules of some minutes.

3.4.1 Energy mix

The obtained annual energy mixes are presented in Fig. 3.15. It must be noted that for the test system, the instantaneous penetration rates can go beyond 23, 42, 61 and 80% for 5 hours a year, to achieve an annual energy contribution of only 4, 8, 12 and 16% respectively. It is observed that the share of coal units is only slightly reduced, while the participation of large heavy fuel 1 is significantly impacted (a reduction of 40% at scenario 4). This is indeed an interesting feature, but additional information is needed to understand the evolution of the conventional park operation.

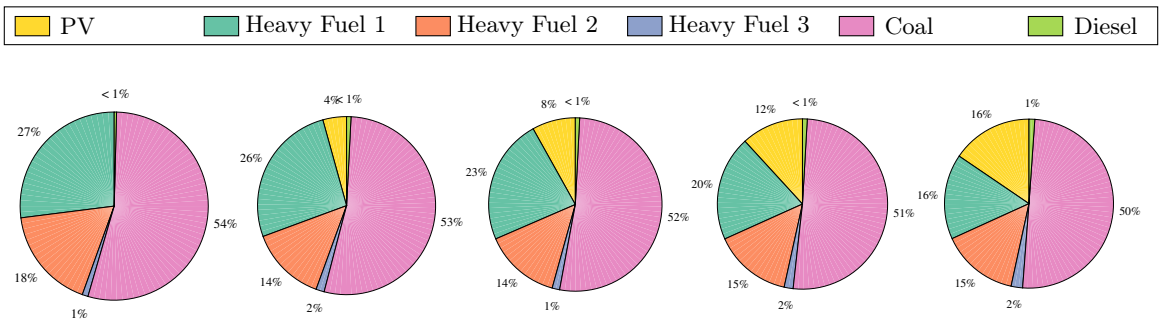

(a) Scenario 0 (b) Scenario 1 (c) Scenario 2 (d) Scenario 3 (e) Scenario 4

Figure 3.15: Energy Mix for different scenarios of PV integration

Fig. 3.16 shows the start up cost by unit type as the PV integration progresses, normalised with respect to the base case total start up cost. It is observed that scenario 1 exhibits a reduction of the start ups, related to diminished share of heavy fuel 2 in the energy mix.

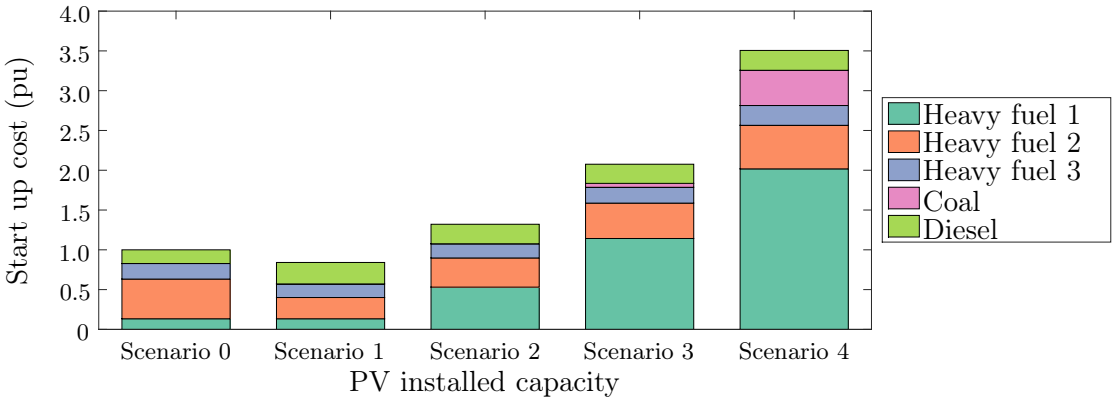

Figure 3.16: Start-up costs by technology for different scenarios of PV integration

In fact, these units were used to supply demand peak on the day; since the PV production is correlated with human activity, less semi-base units are called during working hours. However, more peaking units are needed to supply the primary reserve. From scenario 2, the start up costs increase, specially for the heavy fuel 1 units as more PV is installed. Base units start to behave as semi-base units. From scenario 3 even base coal unit start to cycle, which is consistent with the increase of the security cost. Finally, from scenario 3 the total system cost of supplying the residual demand also increases (average of €/MW)

Committed units and kinetic energy

Figure 3.17 depicts the schedule results by time step and scenario in box plots. The box represents the average value and the lines extending vertically from the boxes (the whiskers) indicate the minimal and maximal values, which are defined over the 365 days of the year. This kind of graph gives information about the degree of dispersion (spread) and skewness of the represented variables. Since the statistical population remains small, neither quartile or quantile definition seems relevant.

More specifically, figure 3.17a shows the amount of committed conventional plants and figure 3.17b represents the stored kinetic energy. The abscissa defines the time steps. As expected, the amount of committed units and the stored kinetic energy tends to decrease on average as the share of no synchronous generation increases. Moreover, these variables are more spread, which gives place to new extreme cases. Similar results are reported in [47] for the interconnected European system with high share of wind power generation. For example, comparing scenarios 2 and 3 (with a higher share of PV), the average amount of committed units decreases only slightly, while extreme cases are more dispersed.

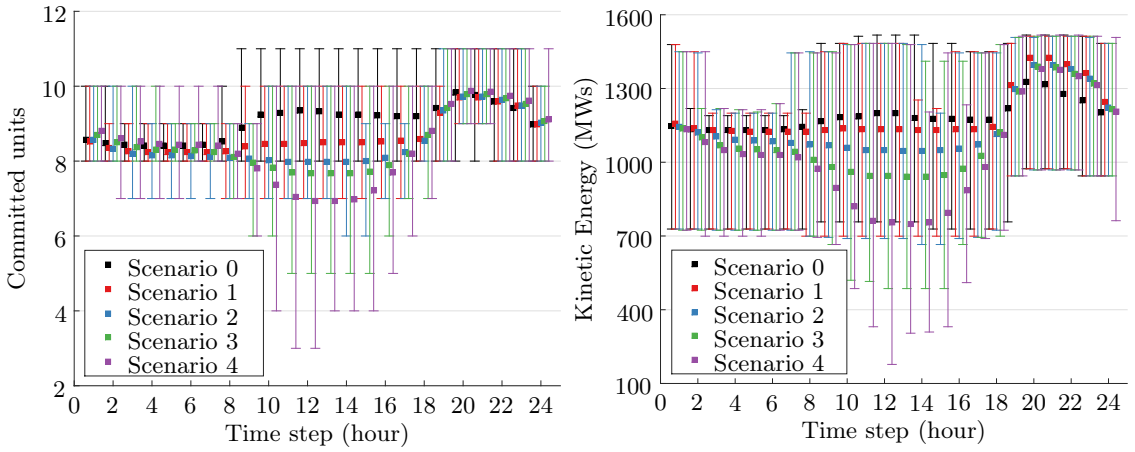

(a) Amount of committed units

(b) Stored kinetic energy

Figure 3.17: Comparison of schedules by time step between PV integration scenarios

Scenarios 3 and 4 exhibit a significant drop in the average and minimal stored kinetic energy, during sunny hours. Some reduction on the average is observed from hour 2 to anticipate PV arrival. Cases with high stored kinetic energy remain in all scenarios, which could be explained by the presence of cloudy days.

Headroom capacity and unit loading

As discussed in chapter 2, the relation between the kinetic energy and the primary frequency response is not direct. Other factors, such as the loading state of the lost unit and the available reserve allocated on the surviving units will play an important role in the frequency stabilisation. Figure 3.18 shows equivalent box plots for the headroom capacity and the load level of the largest (or most loaded) committed unit.

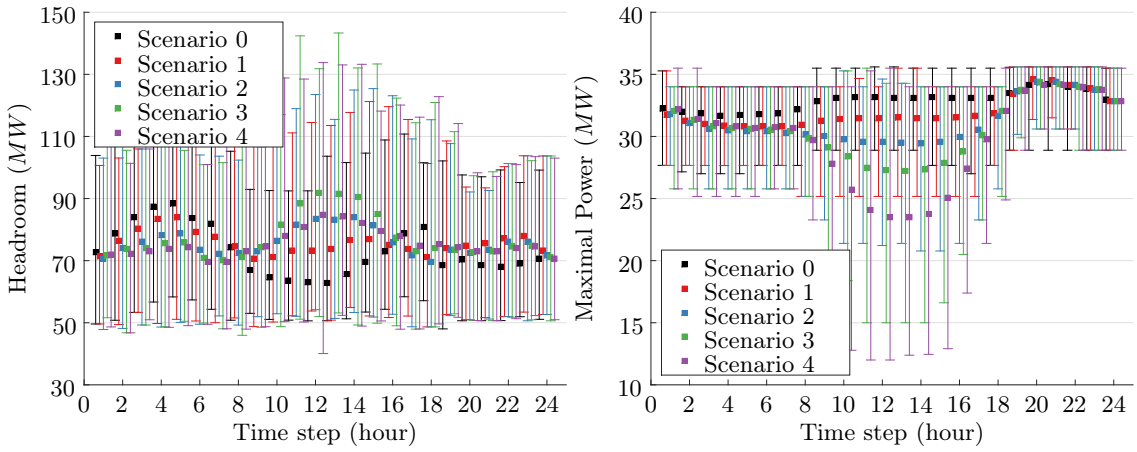

(a) Headroom capacity

(b) Maximal output power

Figure 3.18: Headroom and maximal output power for different PV integration scenarios

It is observed that the PV generation in the sunny hours increases the available headroom capacity. It must be noted that all the reserve can not be deployed fast enough to help stabilising the frequency. Therefore, what it is observed is that a lot of unintended slow reserve has been scheduled, because the units tend to be lowly-loaded. Nevertheless, this increase is not linear with the installed capacity of PV. Scenarios 2 are 4 are almost overlapped during sunny hours in figure 3.18a, while intermediate scenario 3 is above.
Figure 3.18b shows how the loading level of units is heavily reduced when the PV installed capacity is increased. In practice, this may entail an unacceptable dispatch cost when considering efficiency curves. It is recalled that in this work linear cost were supposed. An additional drawback is the lack of downwards reserves in those cases, when all units are committed at their minimal stable generation (MSG) as shown in the next paragraph.

Lack of downwards reserve

Figure 3.19 shows a box plot of the downward reserves over the year for the different scenarios, when considering no requirement at the optimisation level. As aforementioned, in small power system an unintended supplementary margin is often available. However, generation schedules with almost no downward reserves may appear as the share of V-RES.

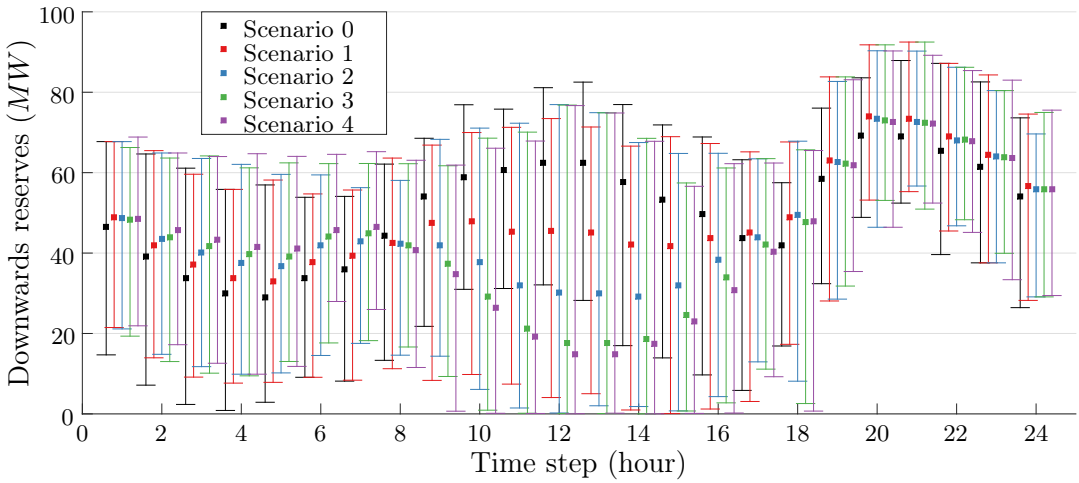

Figure 3.19: Downwards reserves for different PV integration scenarios

In practice, the dispatch-down of V-RES could be used as downward reserve. In this paragraph, the prescription of downward reserve, provided by conventional units is examined. For this, the set of simulation already discussed in this section (365 day-ahead schedules for 5 scenarios of PV integration, including scenario 0) are repeated enforcing a minimum requirement of downwards reserves (R_{dn}^{min}). Some simulation results are given in table 3.7 where the amount of instances that were stopped by time limit are indicated.
It is recalled that for those cases the specified $MIPgap$ is not reached, therefore the returned solution is only an upped bound, which may entail some optimality issues.

Table 3.7: Day stopped by time limit for different downward reserve requirements

R_{dn}^{min}	0 MW	5 MW	10 MW	15 MW	20 MW
Scenario 0	0	0	0	0	0
Scenario 1	1	1	1	1	2
Scenario 2	3	7	10	13	18
Scenario 3	12	42	34	42	61
Scenario 4	49	93	68	86	127

In general, the problem becomes harder to solve as the PV share and downward reserve requirement increase, and the computational time tends to increase. For a predefined maximal time (10 minutes) the quality of the returned solution declines.
Table 3.8 presents the average $MIPgap$ reported over the 365 solved instance for different the downward reserve requirements.

Table 3.8: Average $MIPgap$ for different downward reserve requirements

R_{dn}^{min}	0 MW	5 MW	10 MW	15 MW	20 MW
Scenario 0	0.05%	0.05%	0.06%	0.06%	0.06%
Scenario 1	0.04%	0.04%	0.04%	0.05%	0.06%
Scenario 2	0.06%	0.05%	0.06%	0.07%	0.08%
Scenario 3	0.07%	0.10%	0.10%	0.11%	0.16%
Scenario 4	0.12%	0.18%	0.17%	0.17%	0.32%

Moreover, the additional cost due to the downward reserves requirement can be computed by comparing the schedules with and without this requirement. Results are presented in table 3.9.

Table 3.9: Extra cost due to the downward reserve requirements

R_{dn}^{min}	5 MW	10 MW	15 MW	20 MW
Scenario 0	$< 0.1\%$	$< 0.1\%$	$< 0.1\%$	$< 0.1\%$
Scenario 1	$< 0.1\%$	$< 0.1\%$	$< 0.1\%$	0.2%
Scenario 2	$< 0.1\%$	$< 0.1\%$	0.2%	0.3%
Scenario 3	0.2%	0.5%	0.9%	1.4%
Scenario 4	0.5%	1.1%	1.6%	3.0%

Once more, the cost of providing frequency regulation services increases with the share of no synchronous generation. Finally, feasibility issues were encountered only for scenario 4, and they became more significant as the downward reserve requirement was increased.

Therefore, it could be stated that the test system generation mix reached its V-RES integration capabilities. Some complementary measures need to be deployed. For the purposed of this section the dispatch-down of the V-RES is considered with a high penalty cost, which means that for the instance that are infeasible with model $\mathfrak{M}_0$, the schedules are computed using model $\mathfrak{M}_3$. Table 3.10 summarizes the obtained results.

Table 3.10: Infeasible days for Scenario 4 with different downward reserve requirements

R_{dn}^{min}	0 MW	5 MW	10 MW	15 MW	20 MW
Instances	1	1	3	16	30
Total VG_{dn}	$< 0.1\%$	$< 0.1\%$	$< 0.1\%$	0.1%	0.3%

It is observed that some V-RES dispatch-down allows one to tackle *feasibility issues*. In chapter 4, the contribution of this and other V-RES mitigation techniques to deal with *optimality issues* will be discussed.

Optimal primary reserve

Figure 3.18b showed that as the V-RES integration progresses, the conventional units tend to be operated at low load factors, which in practice may reduce the primary reserve requirements. This phenomenon is illustrated in figure 3.20, which shows the cumulative distribution function of the total allocated primary reserve by scenario.

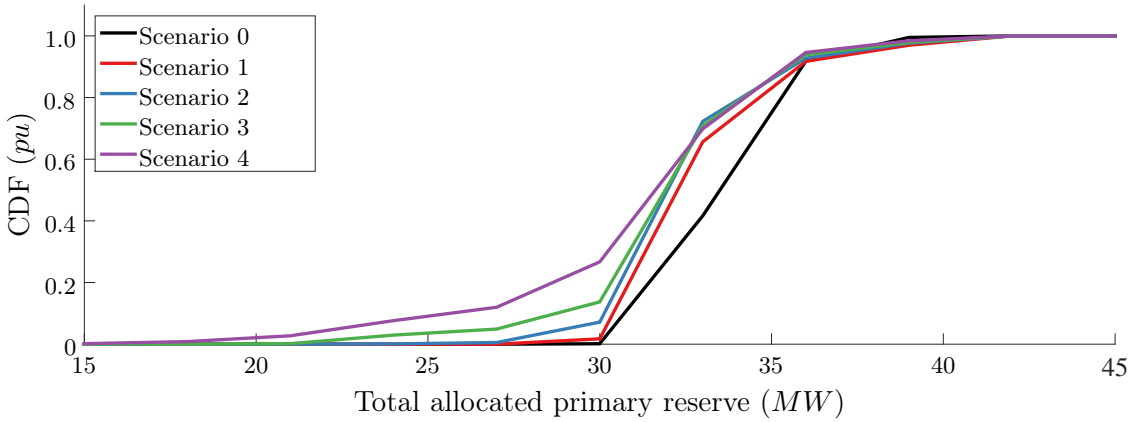

Figure 3.20: Cumulative distribution of the allocated primary reserve with model $\mathfrak{M}_0$

It is observed that for scenario 0 almost all 8760 time steps required at total primary reserve of at least 30 MW. This value is reduces to less than 20 MW for scenario 4.

Remark 2: The optimal primary reserve requirement, from a static point of view, tends to decrease with the PV share, since the potential power imbalances due to conventional unit outages g_k, are reduced. However, the reserve gets harder to place.

3.4.2 Primary frequency response

On the one hand, the amount of committed units and the stored kinetic energy tend to diminish as the integration of V-RES progresses. On the other hand, the headroom capacity in daily hours increases and the possible power imbalances due to a unit loss are reduced. These observations have, respectively, detrimental and beneficial impacts on the frequency regulation response.

This section discusses the outcome of a contingency analysis in order to identify the dominating factors in the long run. Once more, simulation results for the considered test system are provided for illustrative purposes, but the interest is placed on the understanding of the observed phenomena. The average, maximal and minimum value of the frequency nadir and the $ROCOF$ by time step for the 365 days under study, are presented in figures 3.21 and 3.22 respectively by box plots.

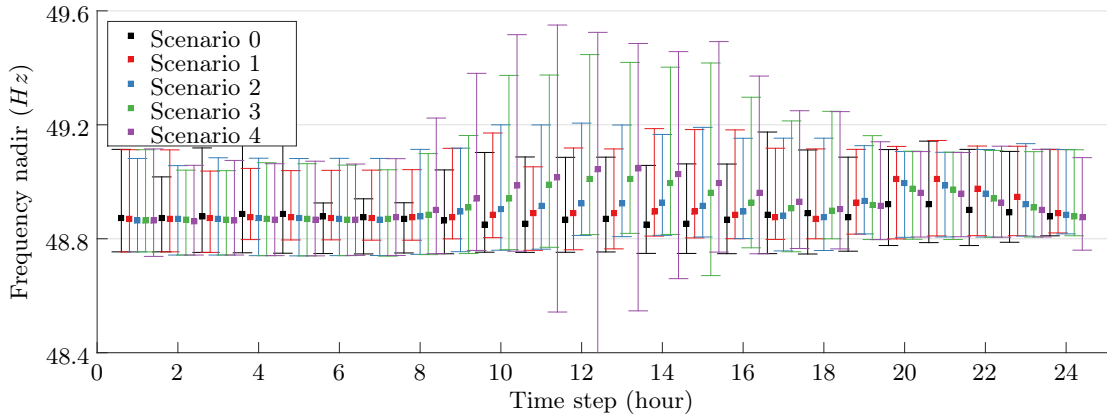

Figure 3.21: Frequency nadirs for different PV integration scenarios

It is observed that the frequency minimum after a unit outage is, in average, higher in sunny hours as the PV installed capacity is increased since committed units tend to be smaller and partially loaded, increasing the reserve actually available, and above all, reducing the simulated power imbalance. This metric is also more spread. Indeed, small frequency deviations are produced by the outage of small and low loaded units that become more common as the share of PV increases, while the analysis of extreme cases shows that new lower values can be achieved.

In scenario 4, at hour 12, the only infeasible hour appears (the bar goes below $48.4Hz$ and beyond $2.1Hz/s$). This specific operational point will be further discussed below. Moreover, the initial frequency gradients or $ROCOF$ increase, which means that the frequency tend to drops faster. For the test system the absolute value this metric passes in average from $0.8Hz/s$ without any PV, to $1.1Hz/s$ for scenario 4 during sunny hours as shown in figure 3.22.

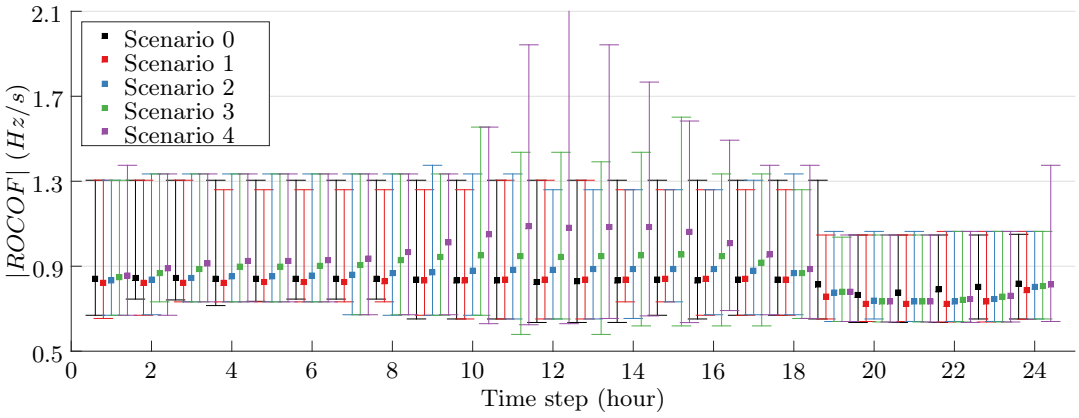

Figure 3.22: $|ROCOF|$ for different PV integration scenarios

Furthermore, from scenario 3 the maximal initial $ROCOF$ values exhibit a significant increase. Some small $ROCOF$ does appear but the dispersion in this sense is less significant. In fact, even though simulated power imbalances tend to be smaller with PV, the respective inertia reduction prevents the $ROCOF$ of being slower. It must be noted that for the purposes of this section no cascading outages were considered, the consequence of such events will be briefly discussed in the next paragraph.

Frequency regulation for the infeasible instance of scenario 4

For illustrative purposes, this paragraph offers a close look on the infeasible instance encountered when computing the day-ahead schedules for scenario 4. As expected, this happened at the lowest residual load point ($\approx$ 23 MW) and highest instantaneous V-RES penetration level of the year ($\approx$ 85%), which for the test case, does not correspond to the lowest total demand point of the year ($\approx$ 130 MW). Figure 3.23 presents the obtained dispatches for the specific instance by solving the corresponding UC models.

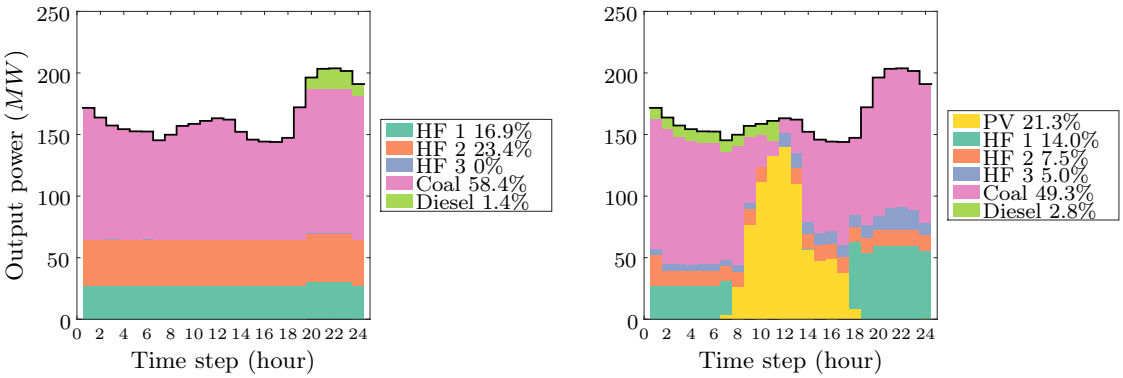

(a) Scenario 0 (**model** $\mathfrak{M}_0$) (b) Scenario 4 (**model** $\mathfrak{M}_2$)

Figure 3.23: Extreme dispatch change with high share of PV

In addition to the high PV generation, this specific 24 hour load profile is characterised by large ramping requirements. As aforementioned, the schedule presented in figure 3.23b is computed by allowing the violation of the reserve constraint (model $\mathfrak{M}_2$). Figure 3.24b shows the detailed dispatch for hour 12, where the primary reserve is not fully provided.

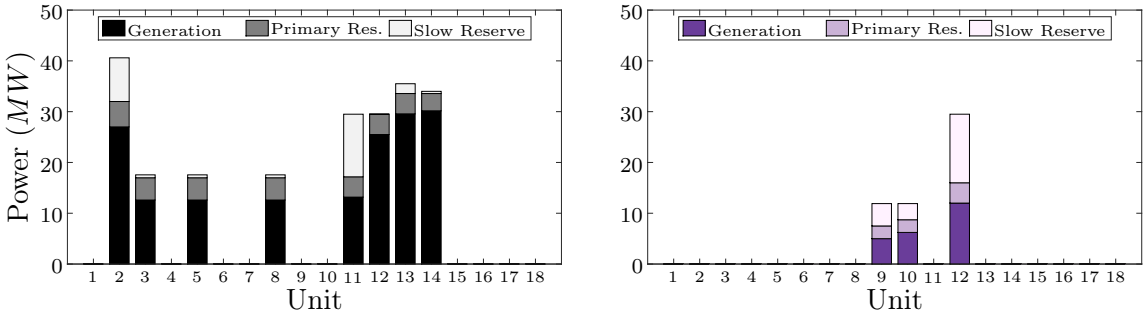

(a) Scenario 0 (model $\mathfrak{M}_0$) (b) Scenario 4 (model $\mathfrak{M}_2$)

Figure 3.24: Detailed dispatches at hour 12 for the scenario 4 infeasible instance

It is observed that due to the low demand and MSG limitations only three units are committed, which are not able to provide all frequency regulation services, such as the primary and downward reserves, although there is enough headroom capacity. Moreover, in this specific case the $ROCOF$ following the outage of unit 12 exceeds the 5.1 Hz/s because of the low rating and inertia constants of units 9 and 10 (see appendix E).

Furthermore, the allocated primary reserve in units 9 and 10 is only $5MW$, which entails a shortage of $7MW$ when unit 12, committed to its MSG level ($12MW$), is lost. For the purposes of illustration let us imagine that such event is produced. The resulting frequency trajectory is showed in figure 3.25a. For a load of approximately $160MW$ and a load damping factor of around $1.75MW/Hz$, this shortage could be theoretically covered by the natural demand reduction associated to frequency dependent loads for a frequency deviation of $4Hz$, which means that the power balance would be regained at a frequency value of about $46Hz$.

However, such a frequency behaviour would compromise the safety of a real power system, since conventional synchronous generator are not meant to operate under this condition. Therefore, the operation of UFLS relays will shed some load in order to the regain power balance and avoid system collapse, as depicted in figure 3.25b.

Then, the effectiveness of this kind of security measures may be compromised as the share of distributed generation increases. Indeed, as discussed in chapter 1 some V-RES sources may disconnect following frequency deviation to prevent islanding operation. Moreover, part of the distributed generation could be lost after the breaker operation. If these events are considered, the $ROCOF$ may increase in the seconds following the first outage entailing significantly larger frequency deviation (deeper nadirs).

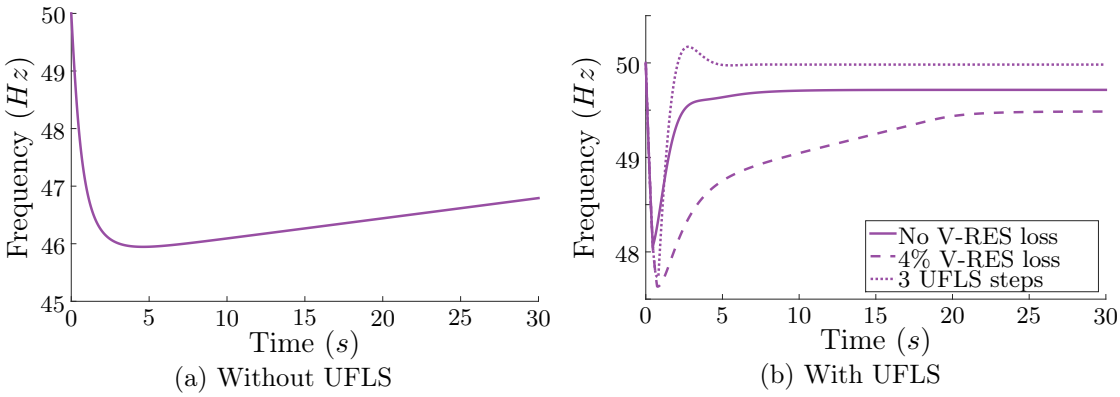

(a) Without UFLS (b) With UFLS

Figure 3.25: Frequency following the outage of unit 12 - extreme case scenario 4

The average behaviour of the frequency following the operation of UFLS relays is illustrated in figure 3.25b, for a load shedding of 5% of the total demand, with and without considering the loss of 4% of the power generated by distributed sources after the breaker operation. It is observed that after the activation of the first UFLS step (set at $48.75Hz$ in the test system), the frequency is not stabilised when some PV is also lost. In this case, a second UFLS step is activated (set at $48.5Hz$ in the test system), interrupting the power supply to another 5% of the load. Finally, it is worth discussing at least one last case, corresponding to the consecutive operation of three UFLS steps as a consequence of the high $ROCOF$. Depending on the configuration of UFLS protections, their operational delays for instance, the third UFLS step (set at $48.0Hz$ in the test system) may be also activated. Then, depending on the disconnected power (in this example another 7.5% of the load is disconnected for the third UFLS step), a rapid pick up of the frequency may appear. Here, it was considered that each breaker operation entailed an additional V-RES lost of 4%.

As a consequence, even though a system operator may be willing to accept some risk in order to maximise the share of renewables in the energy mix, the severity of the contingency may conduct to a system collapse due to the rapid evolution of the frequency (low inertia) and the uncontrolled disconnection or tripping of distributed generation. Hence, different measures are proposed in literature to deal with the impact of V-RES on the primary frequency regulation, and will be thoroughly discussed in the next chapter.

For the moment, let us introduce the potential contribution of some V-RES dispatch-down to limit this kind of security issues. Figure 3.26 shows equivalent results obtained for the same instance already discussed. This time, the day-ahead schedule is obtained by solving model $\mathfrak{M}_3$, which authorises the V-RES dispatch-down. For the purposes of this section a high penalty cost ($a_{vg,dn} \approx 3max(a_{1,j})$) is used. The dispatch-down of 4% of the V-RES generation enable the commitment of more and larger conventional units, which ensured the provision of the primary frequency resources, along with some extra inertia.

As a consequence, the $ROCOF$ following the outage of unit 12 is reduced to $0.68Hz/s$, the

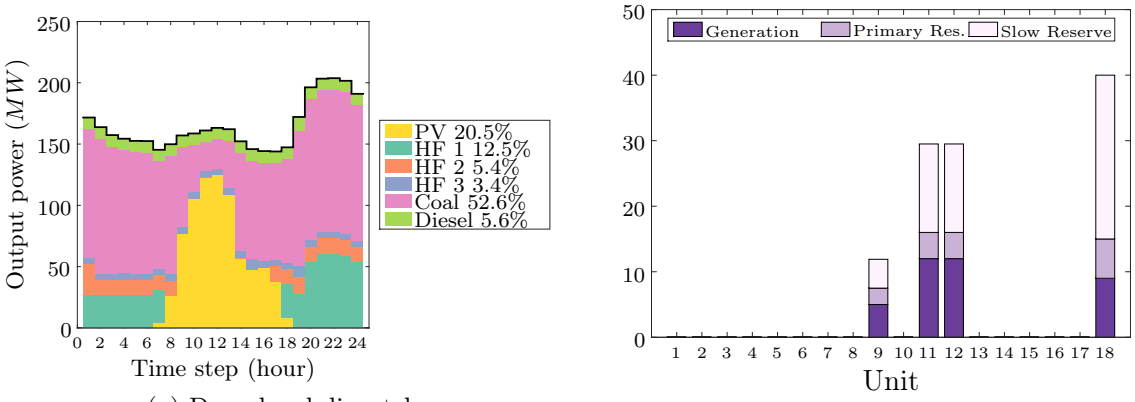

(a) Day-ahead dispatch

(b) Detailed dispatch at hour 12

Figure 3.26: Dispatch for extreme instance for scenario 4 with model $\mathfrak{M}_3$

frequency minimum is limited to $49.3Hz/z$, and no UFLS step is activated. In addition, the dispatch showed in figure 3.26a is 3.4% cheaper than the one presented in figure 3.23b, due to a reduction on start-up cost and a better operation of base units.

Remark 3: Security issues may be contained with a punctual renewable energy lost, that have limited impact in the energy mix, and in some cases this may also reduce costs.

3.4.3 Periods with an insufficient dynamic response

In this work, a security indicator is proposed, given by the amount of time steps with a risk of UFLS, *i.e.*, where at least one simulated unit outage entailed a frequency deviation larger than the predefined security threshold. This metric is denoted PIDR for periods with an insufficient dynamic response.

For the purposes of illustration, let us fix the first UFLS threshold at $48.75Hz$. The previous section showed that for scenario 4, one instance required complementary measures to compute the day-schedule while respecting the security constraint ($N-1$ dynamic primary reserve requirement). In that case, some dispatch-down enable the satisfaction of the security criterion. However, other instances presented deep frequency nadirs, although the required primary reserve was provided. Table 3.11 summarises the amount of PIDR by scenario.

Table 3.11: Periods with insufficient dynamic response (hour/year)

Scenario 0	Scenario 1	Scenario 2	Scenario 3	Scenario 4
0	0	12	19	33

Remark 4: The risk of UFLS increases with the PV installed capacity even if enough primary reserve can be allocated, since the dynamic of its deployment is too slow to restore power balance before the frequency reaches the UFLS limit.

Figure 3.27 represents the total amount of PIDR over the year by daily time step. It is observed that from scenario 2 the risk of UFLS appears, first at early hours, then for sunny hours.

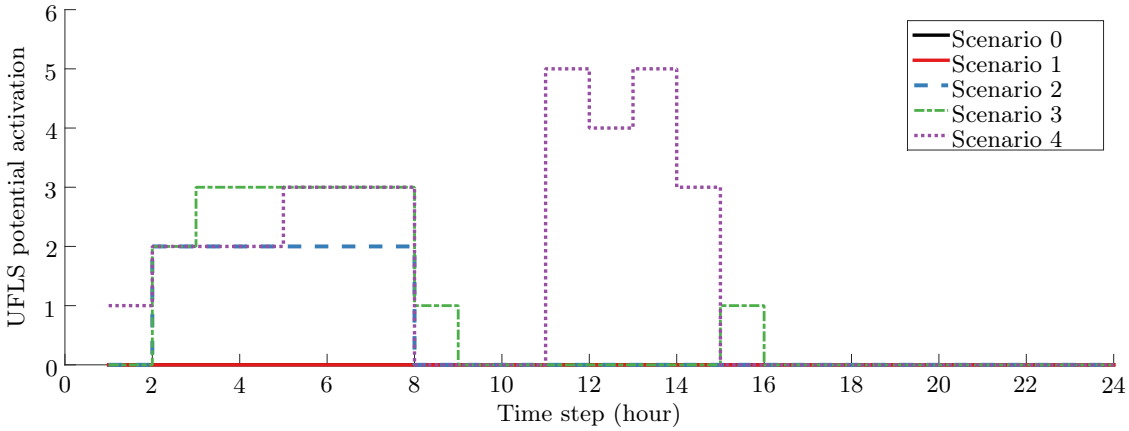

Figure 3.27: Potential activation of UFLS for different PV integration scenarios

Remark 5: The additional UFLS does not necessarily appears in high instantaneous V-RES penetration instants. The inter-temporal dependency of commitment decisions may produce scheduling changes around those hours affecting the primary frequency response.

3.4.4 Relation between the frequency and the PV generation share

In this section, the relation between some frequency metrics, such as the nadir and the *ROCOF* with respect to the PV instantaneous penetration rate is examined. The statistical classes will be used in similar way as done it in chapter 2, where two variables are fixed and all simulation results having these characteristics are gathered such that the size of the circle represents the occurrence (*i.e.*, the statistical weights).
For instance, figure 3.28 presents the relation between the frequency nadirs and the PV instantaneous penetration rates for scenario 4. It is observed that it is not straightforward to establish a relation between the frequency nadirs and the V-RES instantaneous penetration rates when considering a large variety of operating points (load level) and power imbalances (units outages).
Therefore, figure 3.29 offers a different scatter plot where at least three variables can be represented. In this case, the abscissa represents the load level, the ordinate the PV instantaneous penetration rate, and the color indicated the frequency nadir.

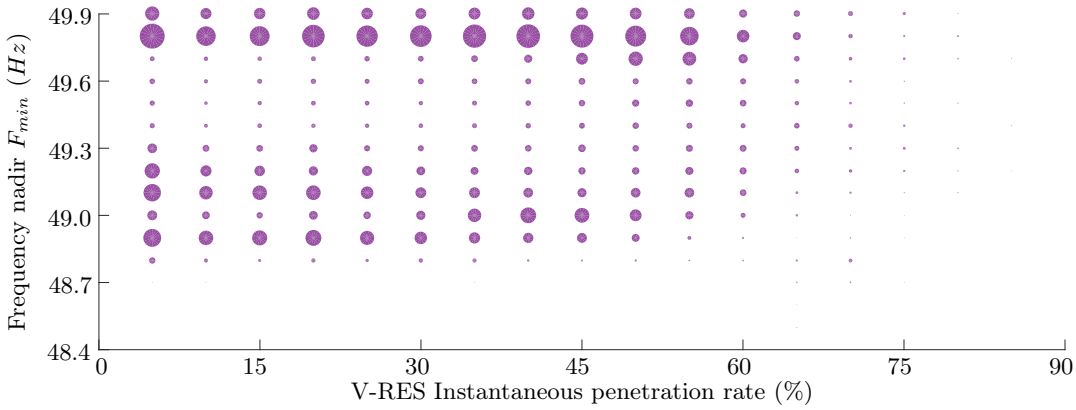

Figure 3.28: Relation between F_{min} and instantaneous penetration rates for scenario 4

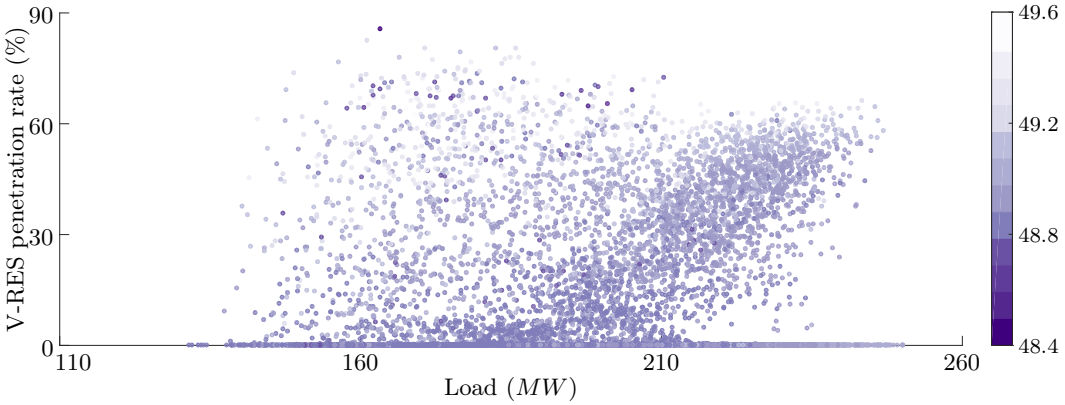

Figure 3.29: Relation between F_{min}, instantaneous penetration rates and load level

It can be noticed that dark points tend to be concentrated in the top-left side, when the load is low and the instantaneous penetration rate is high. Only the more severe contingency by time step is represented (8760 dots). Nevertheless, for equivalent load and penetration rates, different frequency minima can be found. Figure 3.30 presents the relation between the $ROCOF$ and the PV instantaneous penetration rates for scenario 4.

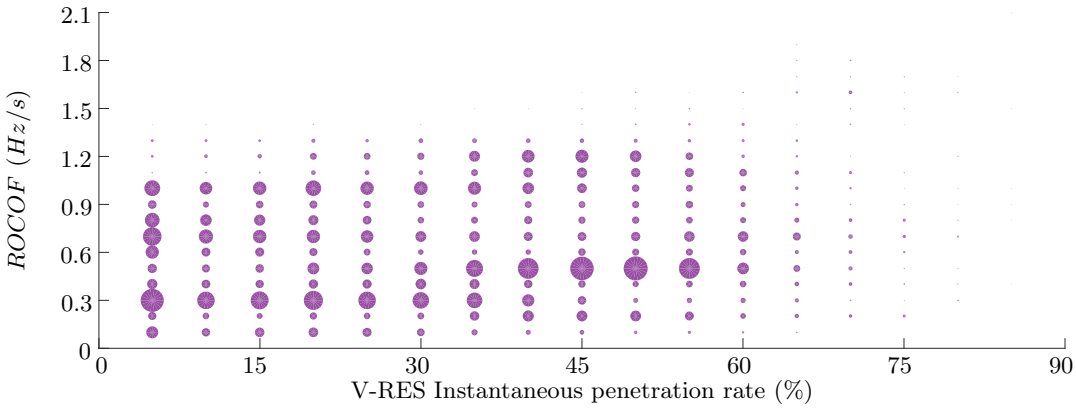

Figure 3.30: Relation between $ROCOF$ and instantaneous penetration rates (scenario 4)

It is observed that for high PV penetration levels the $ROCOF$ does tend to increase. Finally, figure 3.31 shows the relation between the frequency nadirs and $ROCOF$ for the different PV integration scenarios. Once more, this figure depicts a statistical class representation. The size of the circle indicates the portion of the simulated contingency that exhibited the frequency minimum read in the ordinate for the $ROCOF$ value observed in the abscissa. The color of the filled circle indicates the scenario.

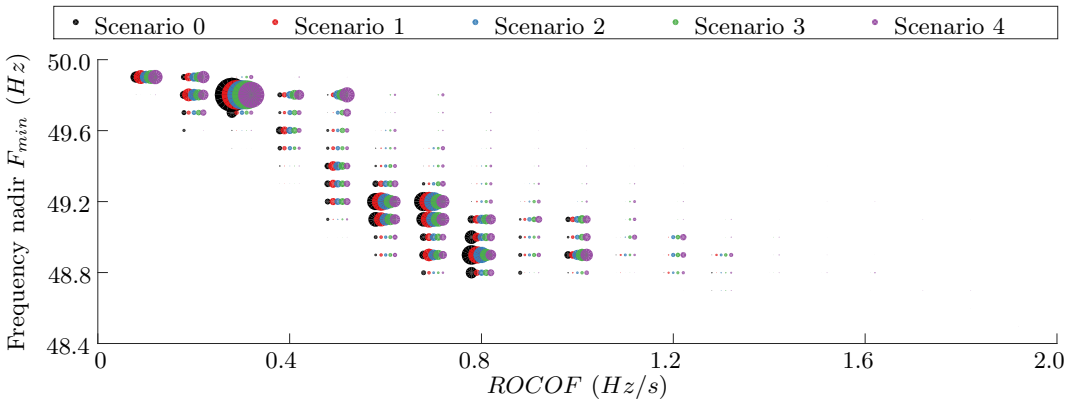

Figure 3.31: Relation between F_{min} and $ROCOF$

It is observed that low frequency nadirs tend to appear for high $ROCOF$ and the amount of cases with high $ROCOF$ increases with the installed capacity of PV, which might be related with the increase of the UFLS risk at some critical time steps. In other words, low values of $ROCOF$ are more common in scenarios with low share of no synchronous generation (see the size of the circles for $0.3Hz/s$), and vise-versa (see the size of the circles for $ROCOF \geq 1Hz/s$). Then, the frequency nadir does tend to increase for low $ROCOF$ values. This topic will be more deeply explored in the next chapter (section 4.3.2).

3.5 Conclusion

According to environmental policies, V-RES are usually prioritised in dispatch. As a consequence, conventional units are operated in a different way to compensate for the variability of non-synchronous generation and their no participation to the ancillary services. Beyond the obvious reduction of the participation to the energy mix, conventional units may experiment more cycling processes, and be committed in partially-loaded state, reducing efficiency and increasing the security cost.

Simulation results considering an isolated test system confirmed these well known features of powers system operation with V-RES. In addition, a instance with a significant instantaneous penetration level of V-RES was thoroughly discussed to provide an insight on the nature of some integration capability limits that may experiment a conventional power system regarding the provision and performance of primary frequency regulation services.

Then, a exhaustive contingency analysis was conducted for different PV integration scenarios in order to examine the evolution of the primary frequency response as the share of non-synchronous generation is increased. Classic metrics, such as the frequency nadir and gradient ($ROCOF$) were statistically characterised.
It was shown that the frequency does tend to evolve faster (higher $ROCOF$), at least for an isolated power system. However, contrary to what may be expected, the frequency nadirs tend to be, in average, less deep, due to the reduction of the units loading levels. In addition, this metric is more spread, giving place to new extreme values and increasing the risk of UFLS.
Moreover, a new metric was proposed to characterise the reduction of the power system security as a consequence of the decline of the primary frequency response. This metric is defined by the periods with an insufficient dynamic response in a simulated year (PIDR). For the test system, the PIDR started to increase after a certain level of PV integration (scenario2).
On the one hand, the models presented in chapter 2 have been validated for further studies regarding the performance of the primary frequency regulation. On the other hand, the risk and limits of the classic security constraint were unravelled, revealing the need for a more accurate representation of the primary frequency response in UC models.
Chapter 4, analyses different FCUC models, characterised by the linear formulation of certain impact mitigation measures, such as the prescription of different forms of inertia requirements. Chapter 5 proposes a new formulation of the FCUC by a decomposition approach.

Chapter 4

Limiting UFLS risk with high share of non-synchronous generation

Contents

4.1 Introduction

Variable renewable energy sources (V-RES), such as wind and solar, are generally prioritised in dispatch, even though they produce an intermittent power output that has low controllability and is only partially predictable. Moreover, they tend to be connected through power electronics, which prevent them to naturally contribute to the system inertia, and in many cases they do not participate in the provision of ancillary services.

Chapter 3 described a suitable methodology to assess the impact of some of these features on the primary frequency response of a electrical power system. A numerical implementation illustrated the effect of the increasing share of photovoltaic (PV) generation on the risk of under frequency load shedding (UFLS) in an isolated power system. **Simulation results showed an increase of the UFLS risk, as well as an uneconomic operation of the conventional thermal park, which in practice may limit the deployment of V-RES**.

In this chapter, the proposed methodological framework is used to investigate the cost and potential benefits of implementing some impact mitigation measures in order to contain the declining behaviour of the primary frequency regulation following the V-RES integration. This section discusses some recent works dealing with the contribution of different resources to the frequency regulation, and describes the proposed methodology. Section 4.2 presents the implemented model for each mitigation technique and section 4.3 analyses simulation results.

As in the previous chapter, a numerical implementation using the test system described in appendix E is provided for illustrative purposes, but the attention will be placed on the understanding of the underlying phenomena, which may provide an insight on the limitations of different impact mitigation techniques. It is acknowledged that results are strongly system dependent, however some trends can be identified thanks to parametric analyses. Finally, conclusions are drawn in section 4.4, where the need and challenges of including a more detailed representation of the primary frequency regulation process in the unit commitment (UC) model are identified.

4.1.1 Background

The primary reserve has been traditionally specified following a static reliability criterion, based on the capacity of the largest unit. This is called the $N-1$ criterion. Historically, in a system with a conventional generation mix, this security constraint allows system operators (SO) to obtain UC solutions that naturally provide an acceptable transient response, although the physical processes that enable this behaviour are not necessarily taken into account in an explicit manner. For instance, the deployment times of the primary control reserve in the European synchronous system are defined as follows [129]:

> The deployment time for 50% or less of the total primary control reserve is at most 15 seconds and from 50% to 100% the maximum deployment time rises linearly to 30 seconds.

In addition, the minimum acceptable frequency is set to $49.2Hz$. However, the expected shape of the system frequency following different generation losses, provided by the same reference through graphical representations, indicates that this frequency threshold is reached before 20 seconds for the reference incident (a loss of generation of $3GW$).

This means that, if all regulating units deploy their primary reserve at the required rate, and no more, this criterion would not be able to prevent under-frequency load shedding (UFLS). In practice, the self-regulation of the load in all synchronous areas is considered to be around $1-2\%/Hz$, which means that for a load level of $150GW$ (lowest point), the load is actually reduced by, at least, $1.5GW$ when reaching the first UFLS step (at $49Hz$).

Other constraints may be included to ensure the proper performance of the primary frequency control. For instance, in France, the transmission system operator (TSO), called RTE for its acronym in french (*Réseau de Transport d'Électricité*) indicates that a primary reserve provider cannot supply more than $150MW$ of reserve, which represents 5% of the total primary reserve provided in the European synchronous system [141]. Moreover, other allocation limits may be enforced by the generating companies (GENCOS) themselves when optimising their portfolios, depending on the physical characteristics of each unit [8]. Hence, as discussed in chapter 2, equation (2.8) enforces a reserve allocation limit (R_j^{max}) for each unit j to account for their actual capability of providing primary reserve [142].

In smaller power systems, such as the English system, the primary reserve deployment time is reduced to 10 seconds for a frequency deviation of $-0.5Hz$ [130]. However, the increasing penetration of V-RES that do not participate to the inertial response or to the frequency control, may lead to UC solutions that no longer ensure system security. As discussed in chapter 3, under this condition the frequency tends to evolve faster and the dynamic of the primary reserve deployment may become insufficient, leading to the activation of UFLS relays following single contingencies.

Therefore, different solutions have been proposed in literature to limit the risk of UFLS, such as the inclusion of enhanced security constraints when optimising the day-ahead generation schedule, as well as the consideration of new participants (different from conventional generators) to the primary frequency regulation.

In this work, the family of these modified optimisation models will be referred to as frequency constrained unit commitment (FCUC). They seek the optimal schedule that allows one to keep the frequency above a certain threshold, while respecting classical constraints. Some published works are focused on the formulation of this new set of constraints in a Mixed-Integer Linear Programming (MILP) structure to apply classic optimisation techniques.

Nevertheless, as discussed in section 2.3, power systems' dynamics are non-linear and an analytical expression of the frequency nadir is hard to obtain. To circumvent these issues, linearisation techniques have been recently proposed [85] and indirect constraints have been set over specific parameters, such as the inertia, regulation droop and response times, considering their impact on the frequency evolution [83, 86].

Enhanced security constraints

The inclusion of primary frequency regulation constraints in power generation optimisation models was first proposed for the economic dispatch problem (ED) [59, 143, 144]. The ED is defined here as the solution of a single-period optimisation, where the active power levels of on-line units are allocated to supply the load, while respecting generation capacity limits and satisfying certain security criteria at minimal cost. The main difference with the UC model is that the unit states are supposed known and inter-temporal constraints are not represented. In both cases, different constraints, such as network capacity or emissions limits, can also be included [144].

In this section, system security constraints are discussed, independently of the specific complete optimisation model used. The most basic representation of this constraint consists of the requirement of a certain amount of spare capacity: a minimal reserve requirement R_{pr}^{min}. This model was described in chapter 2 and is denoted by $\mathfrak{M}_1$.

The optimisation of the primary reserve was first proposed in [143] for a small isolated power system, following a cost/benefit approach, where an iterative process was implemented to balance the cost of providing the primary reserve and the associated risk of load shedding. The reserve requirement (R_{pr}^{min}) was sequentially increased, in a discrete way, until the risk of load shedding reached a certain threshold, where the acceptable risk was defined as a compromise between the cost and security in a specific operating condition.

Subsequently, more sophisticated methodologies were proposed, based on the off-line simulation of several scenarios in order to build linear approximations of the security constraints from a database, which could then be easily included in ED models [59, 144]. These works revealed the interest of including enhanced primary reserve constraints, representing the transient response and regulation capability of committed units, in optimisation models to compute a secure and economical schedule. However, the approaches based on off-line calculations have some drawbacks, such as the computational burden of building the database, which may need to be recalculated as some system parameters change. Following the integration of V-RES, some of these parameters may evolve almost continuously. This topic is further discussed in appendix G.

The inclusion of additional constraints in the UC model under a MILP formulation, accounting for primary regulation unit parameters was proposed in [83]. However, these constraints were written as an explicit function of the steady-state system frequency deviation considering only the governor power-frequency droop to determine if enough primary reserve was committed. The main drawbacks of this approach are:

- the absence of any consideration of the transient response, and
- the exclusive consideration of the frequency droop as the unit regulating parameter.

In fact, the frequency droop seems to be in practice the less restrictive parameter to ensure a proper allocation of the primary reserve.

The droop represents the frequency “sensibility" of the regulation and its value is usually between 3% and 8% [127]. If a unit with a droop of 4% is considered in a system whose nominal frequency is $50Hz$, this means that the unit could release 50% of its active power rating for a frequency extrusion of $1Hz$. As discussed previously, other physical constraints may limit the evolution of the output power of the unit before the droop limit is achieved. A more recent work by Ela *et al.* [86] includes the linear representation of several dynamic aspects in a market design for the primary frequency response ancillary service, such as: the system inertia, the droop curve, the frequency nadir time (when the minimum is reached), among others. However, the case study was focused on pricing and the economic incentives that generators will receive for providing frequency regulation services, while the power system security enhancement, if any, was disregarded [145].

Afterwards, Ahmadi *et al.* [85] proposed a security-constrained unit commitment model with linearised system frequency constraints. A piecewise linearisation (PWL) technique is used to approximate the frequency nadir function, allowing its integration in an MILP formulation of the UC problem. The analytical expression for the frequency nadir was deduced from a simplified equivalent machine model [127] and the response time of all generators was considered identical since its impact was found negligible.

However, as discussed in chapter 2, these hypotheses may overestimate the system response and overlook some risk, since the saturation of individual units cannot be modelled and the deployment time of the reserve might be underestimated, assuming that the regulation performs better than it actually will. Therefore, a comprehensive study on the cost, benefit and limits of such approaches becomes necessary.

Variable generation dispatch-down

Although V-RES are prioritised in dispatch, system operators (SO) may be forced to request that some V-RES facilities generate below their instantaneous available power. This action will be referred to as a dispatch-down. In the literature the term V-RES curtailment is also widely used, but it may or may not include network constraint motivation [139].

Many factors affect the need for V-RES dispatch-down in a power system. On the one hand, there is the load level and profile, the total installed V-RES, its location, technology and capacity factor. On the other hand, the flexibility and dynamic behaviour of the conventional park, its capacity to provide ancillary services, the network and interconnection capacity, the operational environment, as well as the observability and controllability of V-RES sources. Finally, the market structure may also play an important role.

In practice, the V-RES dispatch-down is generally motivated by power system limitations [139]. The nature of these limitations can be related to adequacy or security issues. Moreover, some V-RES dispatch-down may limit the increase of the security cost following a high V-RES integration. This factor will be further discussed as a potential economic motivation for V-RES dispatch-down, although in practice it may have low occurrence.

1. **Adequacy**. Sometimes, a specific system is not able to accommodate a certain level of V-RES. Therefore, SO may be forced to dispatch-down V-RES to accomplish a certain task, for example determining a day-ahead schedule that supplies the load while respecting system-wide and units constraints. This includes capacity, flexibility and exchange limits which determine the zone steady-state power balance.

2. **Security**. This factor is split in two. Local and global security issues. The former mainly concerns distribution system operators (DSO), that must ensure energy quality (*i.e.*, voltage levels) and preserve their infrastructure (lines, transformers, etc.) from overloads. The photovoltaic curtailment in Germany, for instance, is mostly due to these issues. Different mitigation techniques has been proposed in literature to limit the dispatch-down due to distribution network constraints while optimising investment cost [146], however this topic lies out of the scope of this work.

   Network constraints may also appear in the transmission system, in both normal and especially in $N-1$ condition. In this case, the main driver is the gap between the delays involved in the installation of new V-RES and transmission capacity. Hence, transmission system operators (TSO) are also authorised to dispatch-down some V-RES facilities to prevent the operation of protection devises, which may entail cascading outages. In practice, this is the reason of some wind curtailment in Germany, but also in UK and Texas. Once more, innovating mitigation techniques are proposed to limit reinforcement costs while increasing the V-RES integration capabilities, such as the use of probabilistic approaches [147], and the deployment of dynamic line rating with special protection schemes [148], which are not further discussed.

   Finally, the attention is placed in global security issues. Indeed, V-RES dispatch-down may be required to ensure the provision of ancillary services, *i.e.*, operational reserve and proper voltage control. However, alternative solutions to limit V-RES dispatch-down while optimising operational cost are less addressed in the literature. Furthermore, V-RES penetration limits may be set to prevent instability issues. In the french DOM's, the SO (EDF SEI) is authorised to disconnect V-RES generators when the instantaneous penetration rate of V-RES exceeds 30% of the load [63].

   In Ireland, the system non-synchronous penetration (SNSP) level is currently limited to 50% [48]. In addition, others system stability requirements have been defined based on the synchronous inertia for instance, which in practice imposes minimum generation requirements on the conventional (synchronous) generation portfolio and put a cap on the amount of V-RES power that can be accommodated in the system at any instant [139]. In this chapter, the cost and benefit of such kind of palliative measures will be examined.

Moreover, these solutions are put into perspective regarding the contribution of new actors, such as the use of storage or demand side management systems (DSMS), for maintaining the power system security. Finally, the potential benefits of the deployment of a more adaptive approach that enables the commitment of regulation resources according to the actual system needs will be highlighted. This initiative is consistent with the aforementioned research trends observed when dealing with network constraints following V-RES integration.

3. **Economics**. As illustrated in chapter 3, the start-up and primary reserve provision costs in the test system increased with the PV integration. In this chapter, it will be shown that optimal dispatches may entail some PV curtailment, even if they have no variable cost. Some power systems with limited flexibility may be forced to commit more expensive units for several hours in order to deal with high ramps and punctual low values of net demand, due to important minimum down times of base units for instance [34]. Hence, V-RES integration may lead to an operational cost increase.

Regulation authorities start to acknowledge the importance of V-RES dispatch-down at least for adequacy and security reasons, although they seek to limit the activation of this measure. Thus, in some countries compensation mechanisms have been deployed. Moreover, SOs are required to take corrective measures in order to prevent the increase or perpetuation of V-RES curtailments. Therefore, innovating technologies to reduce V-RES dispatch-down due to network constraints, while limiting reinforcement costs, have been proposed [146, 148]. This work offers a contribution on the optimisation of some impact mitigation techniques to face global security issues, where V-RES dispatch-down is only one of them. It will be shown that the deployment of complementary measures will help to reduce the V-RES curtailments. Conversely, the inclusion of indirect constraint on the conventional park may encourage the V-RES dispatch-down, at least for economic motivations. In some cases, risk polices may be reviewed to achieve a better trade of between renewable share and economical performance.

New providers of frequency regulation resources

Regulation is evolving in different systems to anticipate security issues as the installed capacity of V-RES continues to grow [149]. Some of them enforce V-RES constructive capability to provide certain ancillary services, or consider dedicated providers.

1. **V-RES sources.** On the one hand, wind power does possess a rotating mass that indeed stores some kinetic energy. Since they are asynchronously connected to the grid, the kinetic energy stored in wind turbines varies in a larger range as a function of their instantaneous speed. In general, the rotating speed of the blades is controlled to maximise the power conversion efficiency [150, 151].

Then, in the event of an important system power imbalance, part of the kinetic energy stored in the moving parts could be extracted from the shaft and injected into the system by controlling their speed as a function of the system frequency deviation [75, 76, 152]. In this way, wind generation could emulate the inertial response of a conventional synchronous generation. For this reason, this control scheme is referred to in the literature as “synthetic" or “virtual" inertia. In this work, this kind of solution will be considered as a fast “storage" system. It must be noted that, although the mass of wind generators may be smaller than a large conventional unit, their speed variation can be larger, making their contribution significant enough as the share of this resource increases.

On the other hand, V-RES could also participate to the provision of active reserve by injecting a derated power [72, 73, 74, 153]. The main drawback of this technique is that part of the renewable energy is constantly wasted. An interesting option could be the use of the dispatched-down V-RES (for security reasons) as reserve. However, the dispatch computation becomes more challenging, since it would require knowing, at different time scales, the available headroom capacity of V-RES, which presupposes an accurate forecast of the future maximal generation, in addition to the implementation of the suitable control schemes and communication architecture.

Finally, some V-RES generating companies may consider the integration of storage systems to their facilities in order to provide a response as a conventional power plant, *i.e.*, being able to modulate their power output and to provide ancillary services. In this work, the provision of ancillary services by a storage system, in this case for primary frequency regulation, will be considered separately as a dedicated facility.

2. **Dedicated facilities.** Some works have been published evaluating the contribution of dedicated facilities, such as centralised storage systems (pumped-storage [66], batteries [68], flywheel [77], etc.) or demand side management systems (DSMS) [78, 79, 80], including electric vehicles (V2G) [154, 155, 156], to the mitigation of V-RES impacts. Moreover, these resources have been identified as key elements in the reduction of V-RES dispath-down, since, on the one hand they can store the energy that the system is not able to accommodate at a certain instant. On the other hand, they may limit the appearance of power system limitation, such as network constraint by modulating their active and reactive power injection/consumption thanks to a fully controlled power electronic interface.

   Historically, pumped hydro (PH) has been the most deployed storage system, mainly for load levelling. Some advantages of PH are the maturity of the technology, its high efficiency and live time. However, this resource requires a specific topology, which makes it less suitable to solve local problems.

In addition, PH has a relatively slow dynamic that may not compatible for primary regulation purposes in some systems. For these reasons, batteries and flywheel are receiving more attention, despite of their cost, since they can be installed in weak network areas, offering different services [157, 158]. Moreover, some battery storage system can be modular and transportable, providing high flexibility, since they could be used to alleviate congestion in some zone, and be then mobilised to another location after network reinforcement is conducted in the first region. Of course, other drivers have influenced this trend, such as the increasing maturity level of certain technologies, as well as the deployment of some pilot project with or without some public support and the development of more sophisticates control schemes.

For instance, in France, the VENTEEA smart grid initiative was launched in November 2012 to investigate new solutions that can enable a larger integration of V-RES in distribution systems [159]. This project is supported by the French Agency for the Environment and Energy Management (ADEME). It includes a 2 MW / 1.3 MWh lithium-ion battery connected to the MV grid thanks to a 2-MVA power conversion system. The whole system was commissioned in 2015 and aims to draw technical and economic conclusions regarding the provision of multiple services, from load shifting to frequency control, to several stakeholders of the electricity value chain.

Indeed, the response time of electrochemical storage systems connected through power electronic is very fast with respect to the electromechanical dynamics of a conventional power system, which makes this technology suitable for primary frequency regulation purposes. The interest of this kind of systems, from a technical point of view has been proven, but their profitability is still under investigation. Although investment costs are coming down, concerns remain regarding their live time with respect to their operational environment, *i.e.*, charge/discharge profiles. Nevertheless, the provision of dynamic support by dedicated storage facilities starts to become a cost effective solution in isolated systems with high share of V-RES [64, 66, 68], where the variable fuel cost tends to be high, and the security cost due to the provision of the primary reserve tends to increase with the share of V-RES.

This work does not attempt to provide detailed models of the contribution of any specific resource, such as the V-RES themselves, a centralised storage system, a demand side management system (DSMS) or electric vehicles (V2G), to the primary frequency regulation. Instead, a prescriptive analysis is proposed, which means that an envelope is defined for the required performance of the new resource contribution to effectively limit the UFLS risk. A discussion on the mechanisms and specific control strategies needed to achieve this response is out of the scope of this work. But, it is known to be an active research field [68, 74, 75, 79, 156].

4.1.2 Methodology

This chapter compares the cost and effectiveness, in terms of the UFLS risk limitation following unit outages, of different impact mitigation techniques for different levels of V-RES installed capacity. The proposed methodology is based on the sequential simulation of different day-ahead scheduling models and a reduced order primary frequency response (ROSFR) model following unit outages (both described in chapter 2).
Each impact mitigation technique (or palliative measure) m is represented by a specific UC model ($\mathfrak{M}_m$), which consist in a day-ahead primary reserve & energy co-optimisation model, and it is characterised by a parameter c as represented in figure 4.1.

N	number of units	k	index of the lost unit
T	optimisation horizon	h	index of the time step
M	amount of palliative measure	m	index of the palliative measure
C	amount of parameters considered	c	index of the palliative measure parameter

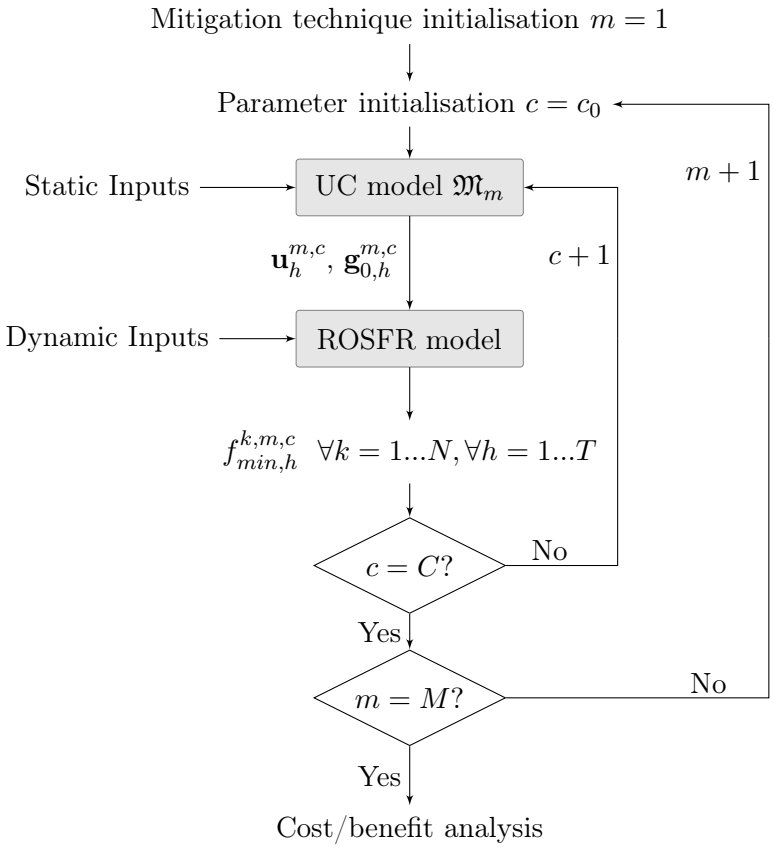

Figure 4.1: General diagram of the proposed methodology

This procedure will be then repeated for different scenarios of PV integration in an isolated power system, and for 365 days to get more representative cost/benefit indicators. The specificities of each implemented model $\mathfrak{M}_m$ are described in the next section.

4.2 Implemented models

The classic deterministic UC model described in chapter 2 and denoted by $\mathfrak{M}_1$, is the base of all the models proposed in this section for including the different impact mitigation techniques. It is recalled that model $\mathfrak{M}_1$ is given by equations (2.2)-(2.12) and enforces a fixed reserve requirement. Here, only the specific constraints that differentiate each model $\mathfrak{M}_m$ from model $\mathfrak{M}_1$ will be defined. It must be noted that, the modelling of an impact mitigation technique may imply the modification of a predefined constraint or even the objective function. The MILP structure of the UC models will be preserved.
Some numerical results for the different FCUC models are provided for illustrative purposes. In order to asses their cost and effectiveness, they are compared with the result obtained with model $\mathfrak{M}_0$. It is recalled that model $\mathfrak{M}_0$ is given by equations (2.2)-(2.13), where the latter constraint enforces a dynamic allocation of the primary reserve. In this case, the fixed reserve requirement in equation (2.12) is set to zero ($R_{pr}^{min} = 0$).
Finally, models $\mathfrak{M}_2$ and $\mathfrak{M}_3$ were introduced in chapter 2 by equations (3.1) and (3.2) respectively. It is recalled that the former enable the violation of the primary reserve constraint to a high penalty cost in order to compute a schedule whenever $\mathfrak{M}_0$ becomes infeasible. The latter authorises the dispatch down of V-RES and will be further discussed in section 4.2.2, where the impact of the penalty cost is investigated.

4.2.1 Enhanced security constraints

Before considering the participation of new actors in the frequency regulation, one can imagine that the classic (static) security criterion, applied to conventional generators could be tightened. On the one hand, the required primary reserve deployment time (*e.g.*, 30 seconds in Europe and 10 seconds in UK) could be reduced, which would prevent slower units to participate to the primary frequency regulation, and force the commitment of faster units to provide this service, even though this may increase the operational cost.
In the MILP formulation used in this work for the FCUC models this could be represented by a reduction of the R_j^{max} parameter, which represent the maximal primary reserve that can be allocated on each generating units j. However, this option will be disregarded because its representativeness of the underlying physical processes is considered insufficient for the purposes of this study and no reference was identified in literature that considers this practice.
On the other hand, the primary reserve requirement R_{pr}^{min} could be increased. This alternative has been considered for the UK system [160]. In this reference, it is explained that primary response requirements may almost double at low load levels, to ensure compliance with the security and quality of supply standards (SQSS), as the capacity of synchronous generation needed to meet the residual demand decreases.

Moreover, a minimal kinetic energy requirement may be constrained to ensure sufficient inertia and limit the speed of the frequency drop following significant power imbalances. This solution has been examined in the Irish system [84]. In this section, different models, some of them already proposed in the literature, will be detailed, in order to investigate the cost, effectiveness and limitations of the different enhanced security constraints based on linear approximations of the power system dynamics.

$\mathfrak{M}_1$: revision of the primary reserve requirement

This impact mitigation technique needs no additional constraint. However, the R_{pr}^{min} in equation (2.12) becomes a parameter that will be varied. Then, different approaches could be considered for adjusting the primary reserve requirements. In this work, R_{pr}^{min} will be considered fixed for each scenario. It is recalled that here a scenario is defined by a time series of hourly stepped demand and V-RES generation, for a given installed V-RES capacity. Therefore, model $\mathfrak{M}_1$ must be solved 1825 times (365 days and 5 scenarios) for each considered primary reserve requirement.

$\mathfrak{M}_4$: prescription of a kinetic energy requirement

Alternatively, a requirement could be enforced on the sum of the stored kinetic energy (KE_{min}) of all committed (or surviving) units j at nominal frequency, for all time steps h, as expressed in equations (4.1a)-(4.1b). The latter enforces a set of NT constraints on the kinetic energy of the system at each possible post-contingency state following the outage of each unit k, where KE_{min} is a predefined parameter that will be varied.

It is recalled that N denotes the amount of conventional units, T represents the amount of time steps of the optimisation horizon, H_j is the inertia constant of unit j, $S_{n,j}$ is the nominal apparent power of unit j and u_j^h is the UC binary optimisation variable.

$$\sum_{j=1}^{N} S_{n,j} H_j u_j^h \geq KE_{min} \qquad \forall h = 1, \ldots, T. \tag{4.1a}$$

$$\sum_{\substack{j=1 \\ j \neq k}}^{N} S_{n,j} H_j u_j^h \geq KE_{min} \qquad \forall k = 1, \ldots, N, \forall h = 1, \ldots, T. \tag{4.1b}$$

In both cases, an iterative approach could be imagined to determine the minimal value of the kinetic energy requirement by load level and V-RES penetration that limits the UFLS risk, in order to compute the kinetic energy requirement by time step (KE^h). However, in this work a parametric analysis is preferred.

$\mathfrak{M}_5$: prescription of a *ROCOF* limit

The maximal rate of change of frequency (*ROCOF*) occurs in the first instant of the disturbance and it depends only on the kinetic energy storage in the on-line units and synchronous loads, and the size of the disturbances [84], which for the purposes of this study, correspond to any possible contingency, *i.e.*, the generation of each unit g_k^h. Thus, the constraint on the maximal frequency slope is given by equation (4.2).

$$\frac{f_0 g_k^h}{2ROCOF} - \sum_{\substack{j=1 \\ j\neq k}}^{N} S_{n,j} H_j u_j^h - KE_L \leq 0 \qquad \forall k = 1,\ldots,N, \forall h = 1,\ldots,T. \tag{4.2}$$

In general, this constraint will also adapt the inertial resource at the post-contingency state as the previous one ($\mathfrak{M}_4$). Nevertheless, it may also shift the punctual system needs for inertial resource by eventually limiting the production level of certain units if this results in being more cost/effective, or some times just feasible, to satisfy the constraint. Hence, cost saving may be achieved in the start-up of extra (or more inertial) units by dispatching already committed units in a less economical way to limit the (at least the initial) speed of the frequency drop.

4.2.2 V-RES dispatch-down

Models $\mathfrak{M}_0$ and $\mathfrak{M}_1$ only considered conventional dispatchable generators in the optimisation variables and the parameter D_f^h referred to the forecasted residual demand addressed to the conventional park (see chapter 2). Model $\mathfrak{M}_3$ defined a curtailment variable VG_{dn}^h by time step in order to account for V-RES dispatch-down (see chapter 3). This variable was included in the power balance constraint (2.5) and in the objective function (2.2) as shown in equation (3.2). For this, hypothesis 1 is supposed to hold, which is consistent with current technological capability of large scale V-RES plants.

Hypothesis 1 *The V-RES dispatch-down variable is considered continuous, which means that at least part of the V-RES park can be operated at a de-rated power.*

In addition, the V-RES dispatch-down is defined positive and it must be limited to the available V-RES power, or at least to a portion Φ of it (in per unit).

$$\begin{aligned} VG_{dn}^h &\leq \Phi VG_f^h && \forall h = 1,\ldots,T, \\ VG_{dn}^h &\geq 0 && \forall h = 1,\ldots,T. \end{aligned} \tag{4.3}$$

First, the security cost entailed by the obligation to purchase V-RES can be examined by considering no V-RES dispatch-down penalty cost ($a_{vg,dn} = 0$). Then, different trade-off between limiting the V-RES dispatch-down and improving the economical performance of the dispatch could be achieved depending on the value of $a_{vg,dn}$, which represents the compensation mechanism that may be deployed for reducing V-RES dispatch-down.

4.2.3 Dynamic support from non-conventional providers

Part of the primary reserve needed to face any possible unit outage could be provided by a new actor different from conventional units. On the one hand, some saving on the dispatch cost could be achieved by considering the V-RES power already dispatched-down for other reasons, as part on the primary reserve.
On the other hand, V-RES sources could be considered as potential providers of primary reserve, leaving the optimisation to allocate this resource in V-RES by dispatching them down when this is more cost effective. Finally, part of the primary reserve could be provided by a dedicated facility that do not participate to the energy generation such as a centralised storage system. In this section, this last two cases will be considered and represented by models $\mathfrak{M}_6$ and $\mathfrak{M}_7$ respectively.

$\mathfrak{M}_6$: from de-rated V-RES sources

In this case, model $\mathfrak{M}_3$ is considered and equation (2.13) is replaced by expression (4.4). Therefore, the V-RES that are scheduled to a power level below the maximal available capacity can, in principle, participate to the provision of the primary reserve. As aforementioned, in practice it is difficult to build and maintain the scheduled primary reserve due to variability and uncertainty.

$$g_k^h - \sum_{\substack{j=1 \\ j \neq k}}^{N} r_j^{h,pr} - VG_{dn}^h \leq 0 \qquad \forall k = 1, \ldots, N, \forall h = 1, \ldots, T. \tag{4.4}$$

$\mathfrak{M}_7$: from dedicated facilities

The primary reserve constraint (2.13) is partially relaxed by a fixed parameter C, which represents the primary reserve that is provided by a dedicated facility.

$$g_k^h - \sum_{\substack{j=1 \\ j \neq k}}^{N} g_j^h - C \leq 0 \qquad \forall k = 1, \ldots, N, h = 1, \ldots, T. \tag{4.5}$$

Primary frequency regulation support

A virtual unit, with no inertia, is included in the ROSFR model to represent the participation of another resource to the primary frequency regulation. Its initial output power (g_0) is zero, and the maximum power output is the reallocated primary reserve VG_{dn}^h or C. It will respond following a proportional gain, similar to the conventional governor's droop, with a dead band as shown in figure 4.2. Finally, the impact of its time constant (τ_r) on the UFLS risk will be examined.

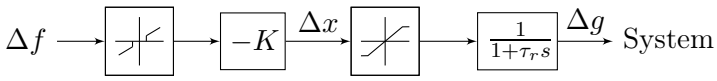

Figure 4.2: General diagram of dynamic support model

Summary of FCUC models for impact mitigation techniques

Table 4.1 summarised the main features of the implemented FCUC models based on indirect security constraints. The next section examines their cost and effectiveness in limiting the UFLS risk.

Table 4.1: FCUC models

Model	Security constraint	Description
$\mathfrak{M}_0$	(2.13)	Dynamic primary reserve requirement
$\mathfrak{M}_1$	(2.12)	Static primary reserve requirement
$\mathfrak{M}_2$	(3.1)	Relaxation of the reserve constraint with penalty cost (risk tolerance)
$\mathfrak{M}_3$	(3.2)	Relaxation of the power balance constraint with penalty cost (V-RES dispatch down)
$\mathfrak{M}_4$	(4.1b)	Prescription of a kinetic energy requirement
$\mathfrak{M}_5$	(4.2)	Prescription of *ROCOF* limit
$\mathfrak{M}_6$	(4.4)	Provision of primary reserve from de-rated V-RES sources
$\mathfrak{M}_7$	(4.5)	Provision of primary reserve from dedicated facilities

4.3 Case study

4.3.1 Primary reserve volume

First, day-ahead schedules are obtained for the test system presented in appendix E by solving model $\mathfrak{M}_1$ for different values of R_{pr}^{min}. Then, the ROSFR model described in chapter 2 is run for every possible single outage in order to compute the frequency nadirs. This procedure is repeated for the different V-RES integration scenarios also described in appendix E. It must be noted that for certain levels of PV and high values of the constraint parameter, infeasibility issues were encountered.

For the purposes of this section, it is desirable to compute a schedule, even for the initially infeasible instances. One option consists in authorising V-RES dispatch-down at a high penalty cost. This solution is considered separately in the next section.

Here, constraint (2.12) is partially relaxed by an auxiliary variable R^h_{ns} which represents the not supplied primary reserve. Then, its value can be penalised in the objective function by a high loss of load cost (VOLL). This is written in equation (4.6) and represents a theoretical worst case of fully-uncontrollable distributed V-RES generation.

$$\begin{aligned} \underset{\mathbf{u},\mathbf{g},\mathbf{R}_{ns}}{\text{minimise}} \quad & \left\{ \sum_{h=1}^{T} \sum_{j=1}^{N} C_j^h \left(u_j^h, g_j^h \right) + S_j^h \left(u_j^h, u_j^{h-1} \right) \right\} + VOLL \sum_{h=1}^{T} R_{ns}^h, \\ \text{subject to} \quad & \sum_{j=1}^{N} r_j^h + R_{ns}^h \geq R_{pr}^{min} \qquad \forall h = 1, \ldots, T. \end{aligned} \tag{4.6}$$

Figure 4.3 depicts the amount of infeasible instances for different primary reserve requirements and V-RES integration scenario when solving model $\mathfrak{M}_1$. Although high primary reserve requirements can be provided up to scenario 2 (no infeasible days for $R_{pr}^{min} < 44$ MW), the number of instances without any schedule able to supply the net demand while respecting all the system-wide constraints increases with the installed V-RES capacity.

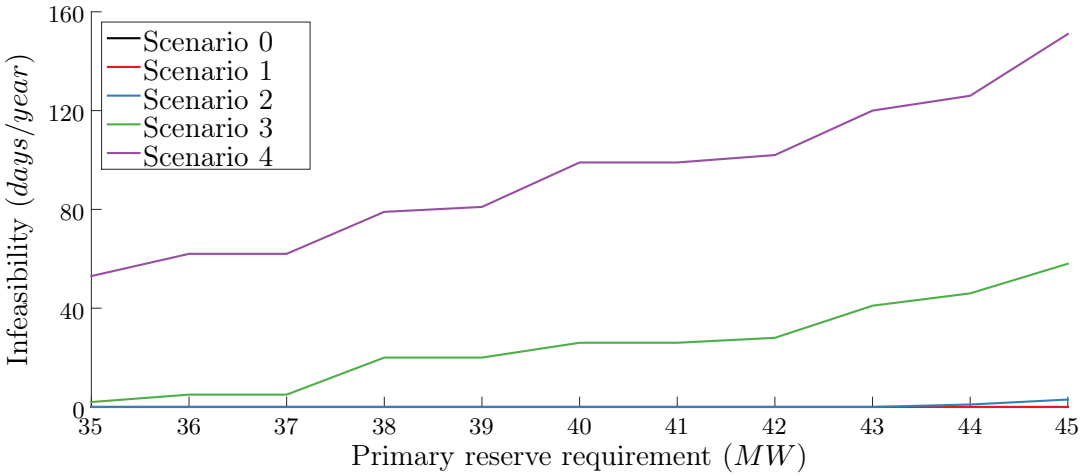

Figure 4.3: Instances where the security constraint is violated (model $\mathfrak{M}_1$)

Regarding cost and effectiveness, figure 4.4 shows the annual generation cost (dashed line) and UFLS risk (solid line) incurred to supply the load in the test system considering different primary reserve requirements. As aforementioned, the cost curve of each scenario is normalised with respect to its own annual generation cost, considering a dynamic allocation of reserve and no minimum requirement (model $\mathfrak{M}_0$). These results were discussed in chapter 3 (table 3.11). The risk curve is given by the number of periods with insufficient dynamic response (PIDR), *i.e.*, when the frequency nadir may attain the security threshold. For illustrative purposes, this value is set to $48.75Hz$ in the test system.
For a reserve requirement of $35MW$ and no PV installed (scenario 0), the annual scheduling cost is similar to the benchmark case (1 p.u.), since the average value of the total allocated primary reserve when considering a dynamic allocation model ($\mathfrak{M}_0$) is around this value.

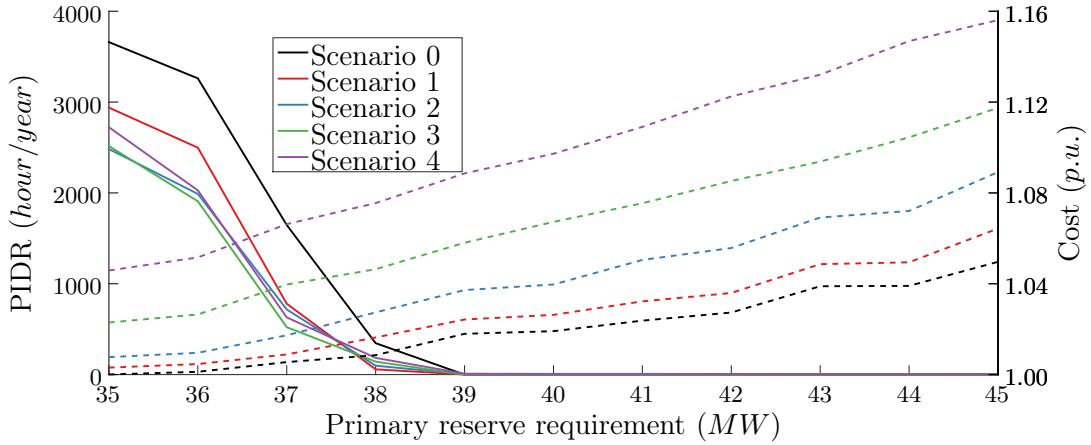

Figure 4.4: Cost and risk with fixed reserve criterion set to different values (model $\mathfrak{M}_1$)

However, the risk is considerably higher for low primary reserve requirements without constraint (2.13), since no enough reserve is necessarily provided to face the outage of any single unit. Contrary to what was expected, the risk diminishes with the development of V-RES generation for low requirements. This can be explained by the reduction of the loading level of conventional units, which limits the severity of the power imbalances.

In general, the overall security cost for providing the primary reserve increases with the installed capacity of PV. Simulation results for the test system show that for a fixed reserve requirement of $35MW$, the dispatches generated with model $\mathfrak{M}_1$ are, in average, 0.3% to 4.6% more expensive than those generated with model $\mathfrak{M}_0$, depending of the level of V-RES integration (see figure 4.4). Moreover, this value increases with the primary reserve prescription. However, in many cases this extra reserve is actually unnecessary, or at least not optimally allocated. As a consequence, increasing the reserve prescription can become extremely uneconomical and even ineffective, as illustrated in figure 4.5 (scenario 4).

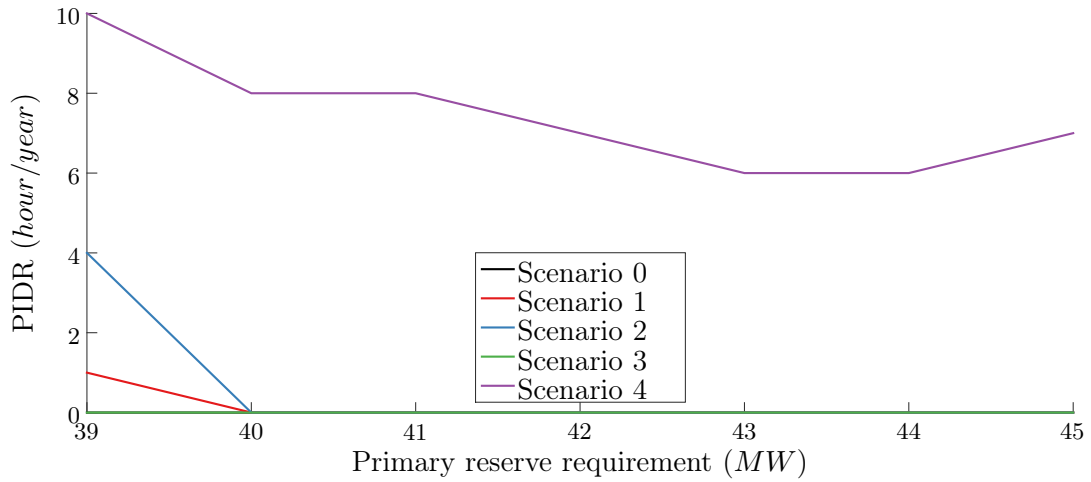

Figure 4.5: Zoom on the UFLS risk for mid-high values of primary reserve requirements

For instance, scenario 3 presents 20 infeasible days, where the primary reserve requirement is not always respected, for a R_{pr}^{min} set to 39 MW. Nevertheless, this primary reserve prescription is able to ensure a proper frequency regulation, since no periods at risk were identified, which is not the case of scenarios 1 and 2.

In addition, the risk over the year may increase at some point with the reserve requirement. Figure 4.5 shows that when the primary reserve prescription is increased from 44 to $45MW$ for scenario 4, the UFLS risk appears in at least one new hour. This may occur when changes in the commitment decisions aim to privilege units with higher power ratings, even though their contribution to the inertia or primary frequency regulation may be lower. Thus, t**he upward revision of the primary reserve prescription may become a non-viable impact mitigation measure for high V-RES penetration levels**.

Finally, an analysis of the not supplied primary reserve variable (R_{ns}) provides an insight of the system incapacity to maintain the security criteria as the share of PV increases. Figure 4.6 presents a box representation of this variable by time step, which includes the minimal, maximal and average value, for scenarios 3 and 4, over the specific infeasible days of the year (20 and 81 of 365 respectively). As expected, the system is not able to respect the primary respect constraint during sunny hours for high integration levels, which in practice may be interpreted as a limit in V-RES integration capability.

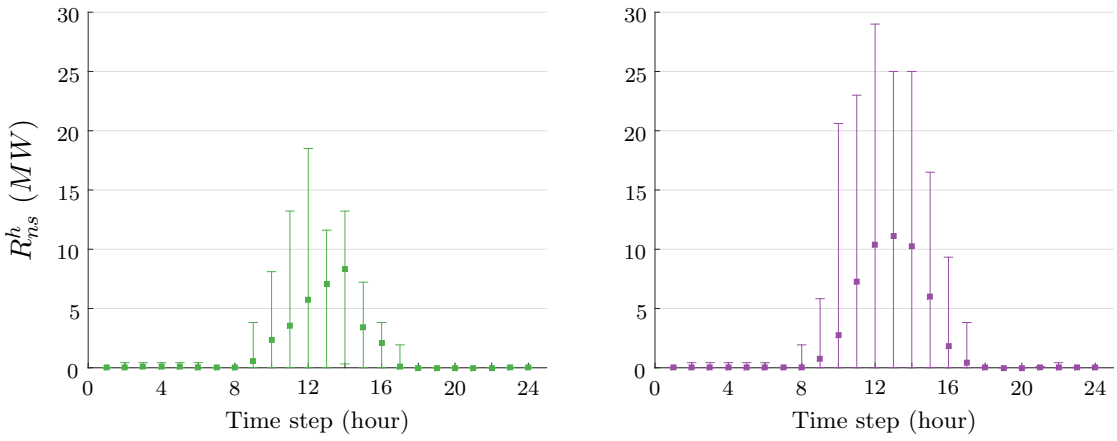

(a) Scenario 3 (b) Scenario 4

Figure 4.6: Not supplied reserve in infeasible days for $R_{pr}^{min} = 39MW$ (model $\mathfrak{M}_1$)

Cost/benefit analysis

Table 4.2 recalls the amount of (PIDR) by scenario for a UFLS threshold at $48.75Hz$, which were already discussed in chapter 3 (table 3.11). In addition, it presents the PIDR after reviewing the prescription of primary reserve (R_{pr}^{min}) to $39MW$ and $40MW$, as well as the annual supplementary cost.

Table 4.2: Periods with insufficient dynamic response and over cost

Model	Metric	Scenario 0	Scenario 1	Scenario 2	Scenario 3	Scenario 4
$\mathfrak{M}_0$	PIDR (h/y)	0	0	12	19	33
$\mathfrak{M}_1$ - $39MW$	PIDR (h/y)	0	1	4	0	10
	Over cost (%)	2	3	4	6	9
$\mathfrak{M}_1$ - $40MW$	PIDR (h/y)	0	0	0	0	8
	Over cost (%)	2	3	4	7	10

The security cost tends to increase with the primary reserve requirement and integration of non-synchronous generation. Regarding the benefits and limitation of this impact mitigation techniques, it is worth highlighting at least three points:

- For a given primary reserve requirement, the UFLS risk does not necessarily increase as the integration of V-RES progresses, since certain threshold effects may appear. This is observed in the test system for a primary reserve prescription of $39MW$, where the PIDR increases for scenarios 1 and 2, but becomes zeros for scenario 3.
- For a given scenario of V-RES integration, the UFLS risk does not necessarily diminish with the increase of the primary reserve requirement. Indeed, some changes in the commitment decisions following capacity consideration may modify the dynamic parameters of the system, such as the equivalent system inertia and the liberation rate of the allocated reserve. If these values are decreased, the frequency may drop faster and lower, even though more reserve is available. In this case, the extra volume of primary reserve is not able to compensate for the “quality" lost.
- For some V-RES penetration levels, it may be no longer possible to enforce high the primary reserve requirements.

This study revealed one of the limitations of the revision of primary reserve prescription: the low representativeness of the underlying physical processes. Feasibility issues appear as a second downside, especially in small and isolated systems with high share of V-RES.

Computational performance

One of the main advantages of the use of fixed reserve requirements is its implementation and computational simplicity. The total CPU time of the 365 day-ahead schedules is presented in figure 4.7[1]. It is observed that this metric is not strongly dependent on the value of the security parameter, *i.e.*, the primary reserve prescription. However, it does increase with the penetration of V-RES sources, which means that the dispatch becomes more “difficult" to compute.

[1] 2x8 cores Intel(R) Xeon(R) CPU E5-2690 @ 2.90GHz and 64Gb of RAM. GUROBI MIP gap = 0.1%

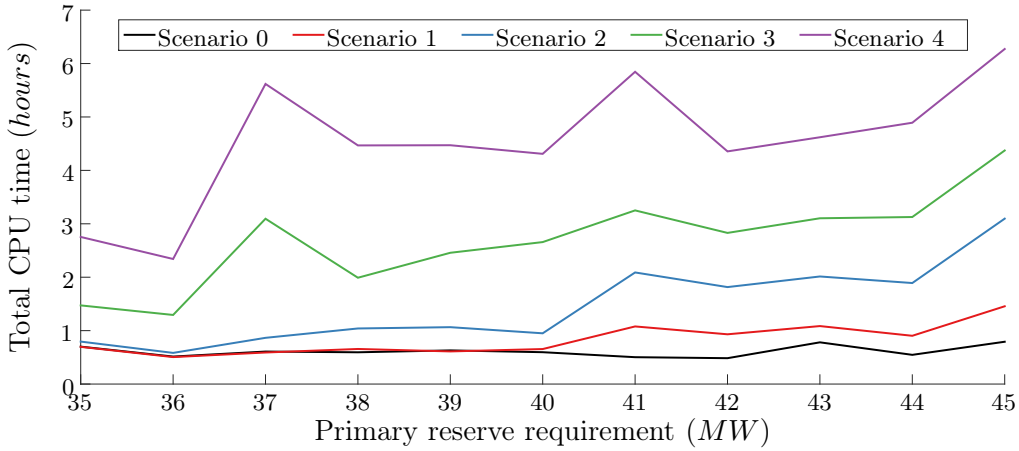

Figure 4.7: Total CPU time for the whole year day-ahead schedules with model $\mathfrak{M}_1$

4.3.2 Inertia constraints

In order to improve the representation of the physical processes behind the frequency regulation, other considerations may be included as security constraints. In this section the reserve requirement (R_{pr}^{min}) is set to zero, the constraint (2.13) is held and constraint (4.1b) is included. As previously done, day-ahead schedules are obtained for the test system presented in appendix E, this time by solving model $\mathfrak{M}_4$ for different values of KE_{min}, from 400 to $1400MWs$, which is the range of value identified in chapter 2 (see figure 2.17b). This model enforces a kinetic energy constraint in the $N-1$ state, which means that it is set over the surviving units taking into account the outage of any single unit.
Then, the ROSFR model described in chapter 2 is run for every possible single outage in order to compute the frequency nadir and determine the PIDR, where a predefined frequency threshold of $48.75Hz$ could be attained. This procedure is repeated for the different V-RES integration scenarios. Figure 4.8 shows the amount of infeasible days by parameter value and scenario, *i.e.*, when the violation of the kinetic energy constraint had to be authorised in order to compute a schedule.

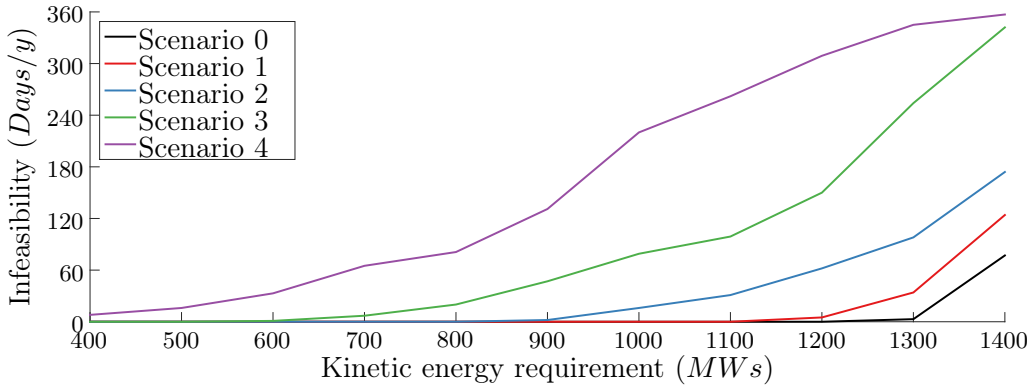

Figure 4.8: Amount of infeasible days a year for model $\mathfrak{M}_4$

Once more, it is observed that as the security criterion is tightened, infeasibility issues appear, and become more significant as the share of non-synchronous V-RES increases. For instance, this criterion is viable for scenarios 1 and 2, at least up to a KE requirement of $1200MWs$ for the considered test system. However, from a certain level of V-RES integration, feasibility issues will prevail. In practice, this means that high V-RES curtailments will be need to enforce this constraint, which will be investigated further in the next section. For the moment, the attention is placed on the cost and effectiveness of this impact mitigation technique, and infeasibility issues are handled as done previously. An auxiliary variable $KE^h_{ns,k}$ is defined to partially relax constraint (4.1b), and its value was penalised in the objective function by a high cost ($VOKE$) as shown in equation (4.7).

$$\begin{aligned} \underset{\mathbf{u},\mathbf{g},\mathbf{KE}_{ns}}{\text{minimise}} \quad & \left\{ \sum_{h=1}^{T} \sum_{j=1}^{N} C_j^h \left(u_j^h, g_j^h\right) + S_j^h \left(u_j^h, u_j^{h-1}\right) VOKE \;\; KE_{ns}^h \right\}, \\ \text{subject to} \quad & \sum_{\substack{j=1 \\ j \neq k}}^{N} S_{n,j} H_j u_j^h + KE_{ns,k}^h \geq KE_{min} \quad \forall k = 1, \ldots, N, \forall h = 1, \ldots, T. \end{aligned} \tag{4.7}$$

Figure 4.9 depicts the risk (solid line) and the annual cost (dashed line) incurred to supply power demand in the test system considering different kinetic energy requirements. As expected, the cost increases as the security criterion is tightened and the risk is reduced. Both curves may exhibit some threshold effect in small system due to the discrete nature of the possible combination of committed units. For the test system a kinetic energy requirement of $600MWs$ suffices to prevent the increase of the UFLS risk.

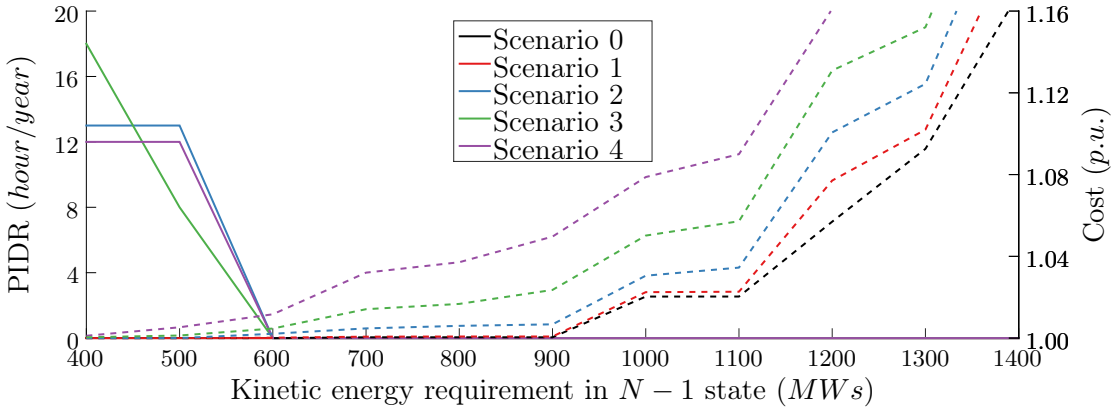

Figure 4.9: Cost and risk for different minimal kinetic energy requirements (model $\mathfrak{M}_4$)

Finally, a limitation may be set on the maximal (initial) frequency slope through model $\mathfrak{M}_5$. Results are presented in figure 4.10. It is observed that for all predefined $ROCOF$ thresholds, the UFLS risk was fully eliminated.

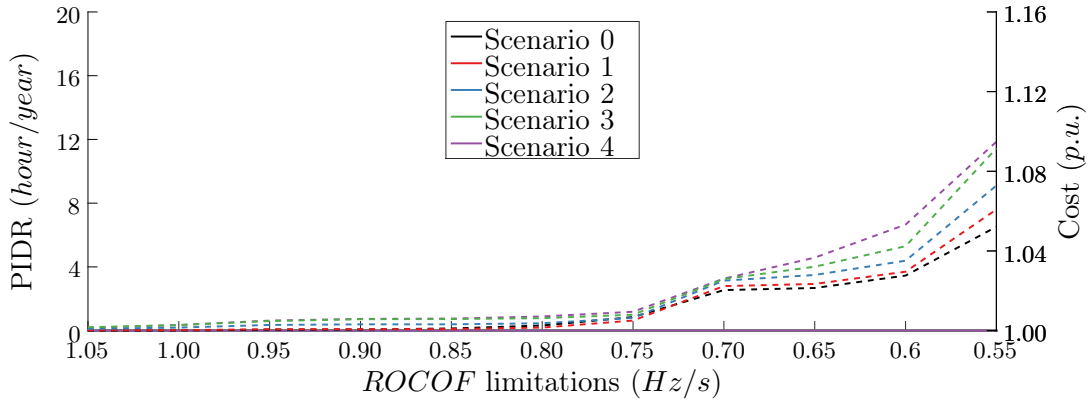

Figure 4.10: Cost and risk for different $ROCOF$ limitations (model $\mathfrak{M}_4$)

In addition, a more economical schedule can be achieved by reallocating some power instead of starting-up bigger but expensive units, since the $ROCOF$ constraint is able to adjust kinetic energy resources in the post-contingency state as well as the size of the possible contingency. Moreover, infeasibility issues are significantly reduced.

Cost/benefit analysis

Table 4.3 compares the amount of periods with an insufficient dynamic response (PIDR) by scenario for a UFLS threshold at $48.75Hz$, with and without the prescription of a certain minimal kinetic energy requirement (KE_{min}) or $ROCOF$ limit, as well as the associated annual over cost and the amount of infeasible days.

Table 4.3: PIDR, over cost and infeasibility

Model	Measure	Scenario 0	Scenario 1	Scenario 2	Scenario 3	Scenario 4
$\mathfrak{M}_0$	PIDR (h/y)	0	0	12	19	33
$\mathfrak{M}_4$ - $600MWs$	PIDR (h/y)	0	0	0	0	0
	Over cost (%)	0	≤ 0.1	0.21	0.47	1.17
	Infeasible days	0	0	0	1	33
$\mathfrak{M}_5$ - $1.05Hz/s$	PIDR (h/y)	0	0	0	0	0
	Over cost (%)	0	≤ 0.1	≤ 0.1	0.17	0.15
	Infeasible days	0	0	0	0	1

For low shares of V-RES **this family of measures provides a better trade/off between economics and security with respect to the increase of the primary reserve prescription**. In addition, secure solutions may be provided for higher levels of V-RES integration, although feasibility issues remain. However, it is observed that for parameter values presented in table 4.3 the frequency is always kept above the security threshold, even though at some instances the kinetic energy constraint was in fact not fully enforced. This feature reveals some **optimality issues**, since for some time steps the requirement is enforced unnecessarily implying an unjustified “desoptimisation" cost.

4.3.3 Relation between the V-RES dispatch-down and the UFLS risk

In this section the potential contributions of the V-RES dispatch down is examined, from both an economical and technical perspective. The objective is to provide an insight on the effects of this impact mitigation technique in the primary frequency response, as a consequence of the changes in the day-ahead scheduling.

Optimal dispatch down for different penalty cost

Here model $\mathfrak{M}_3$ is solved considering the test system described in appendix E and one year of forecasted load and V-RES generation. The reserve requirement (R_{pr}^{min}) is set to zero and the constraint (2.13) is held. Then, two cases are considered: with and without penalty cost for V-RES dispatch down. In the first case, the penalty coefficient ($a_{vg,dn}$) is defined slightly higher than the variable cost coefficient of base units. In the second case, $a_{vg,dn}$ is set to zero. The interest is placed in the amount of energy lost over the year, as well as in the dispatch cost variation. Simulation results are shown in figure 4.11 for illustrative purposes.

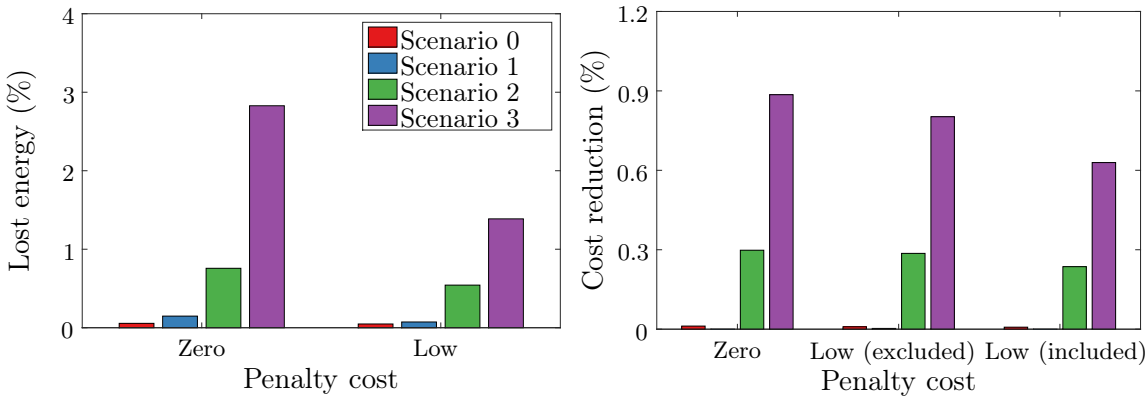

(a) V-RES dispatch down activation

(b) Cost reduction

Figure 4.11: Optimal dispatch down for different penalty cost (model $\mathfrak{M}_3$)

Figure 4.11a depicts the total energy that was dispatched-down in per cent of the total forcasted V-RES generation for the whole year. Figure 4.11b shows the cost reduction, also in per cents, this time of the annual operational cost, with respect to the cost with no V-RES dispatch down. In this last figure, the case with penalty cost is represented twice, including or not the value of the compensation.

It is observed that some PV dispatch down may indeed improve the economical performance of the schedules. For the test system, relevant cost saving (beyond the optimisation MIP gap) are verified from scenario 3, even when considering a penalty cost.

Consequence on the risk of UFLS

This section discusses the consequences of day-ahead schedule adjustments, following V-RES dispatch down on the primary frequency response. Table 4.4 compares the amount of PIDR for the schedules obtained with model $\mathfrak{M}_0$ and model $\mathfrak{M}_3$, which means with and without optimal dispatch down.

Table 4.4: Periods with insufficient dynamic response (hour/year)

Case	Scenario 1	Scenario 2	Scenario 3	Scenario 4
Without dispatch down	0	12	19	33
With dispatch down	0	13	16	30

It is observed that it is not possible to establish a direct relation between the penetration of V-RES and the risk of UFLS. Although, at high V-RES integration levels (scenario 3 and 4), the PIDR tends to decrease with the V-RES dispatch down, scenario 2 illustrates that the opposite phenomenon may occur. Moreover, the periods of time may not be the same in both cases. In order to understand the underlying processes, a close look on both phenomena is provided. The scheduling changes that entailed a security improvement are depicted in figure 4.12. A counterexample is presented in figure 4.15.

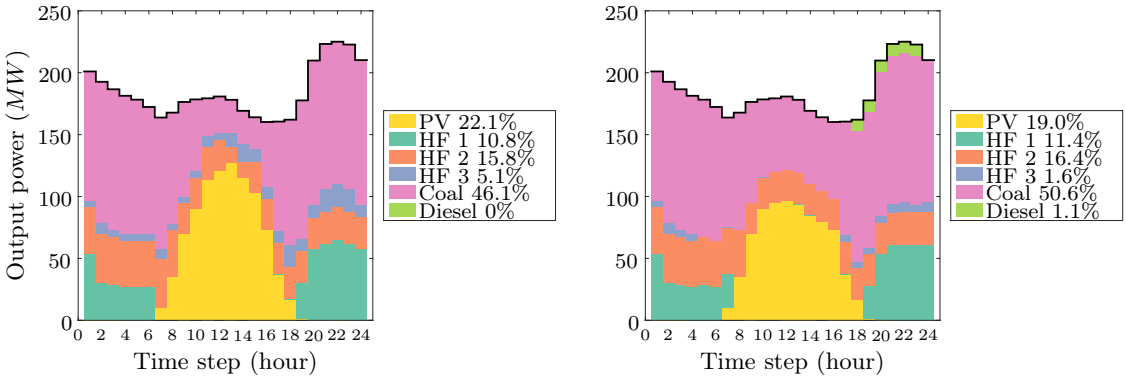

(a) Model $\mathfrak{M}_0$ (b) Model $\mathfrak{M}_3$

Figure 4.12: Dispatch change for improved dynamic response (Scenario 4)

For this particular day of low demand, the economical optimisation entailed a high PV dispatch down (14% of the generation forecast). The saving on the daily operational cost reached 4% when computing the day-ahead schedule with model $\mathfrak{M}_3$ instead of model $\mathfrak{M}_0$. A close look on the scheduling changes at hour 11 is provided in figure 4.13. It is observed that the V-RES dispatch down enabled the commitment of more base units which improved both, the economical and security performance of the dispatch. In addition, the distribution of the allocated power has been modified. Therefore it is not straightforward to compare the response of the primary frequency regulation for an equivalent outage.

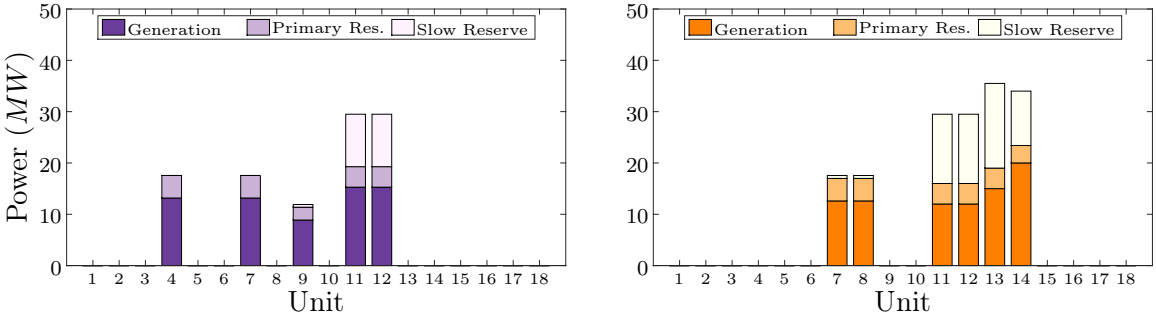

(a) Model $\mathfrak{M}_0$ (b) Model $\mathfrak{M}_3$

Figure 4.13: Detailed dispatches at hour 11 for the scenario 4

Figure 4.14 depicts the frequency trajectories for different single contingencies. It must be noted that the loss of unit 11 in the left side (schedule computed with model $\mathfrak{M}_0$) entails a power imbalance of 15.3 MW, while the output powers of units 13 and 14 in the right side (schedule computed with model $\mathfrak{M}_3$) are 15 and 20 MW respectively. Hence, the better behaviour of the frequency response is indeed related to the increased inertia and regulation capabilities.

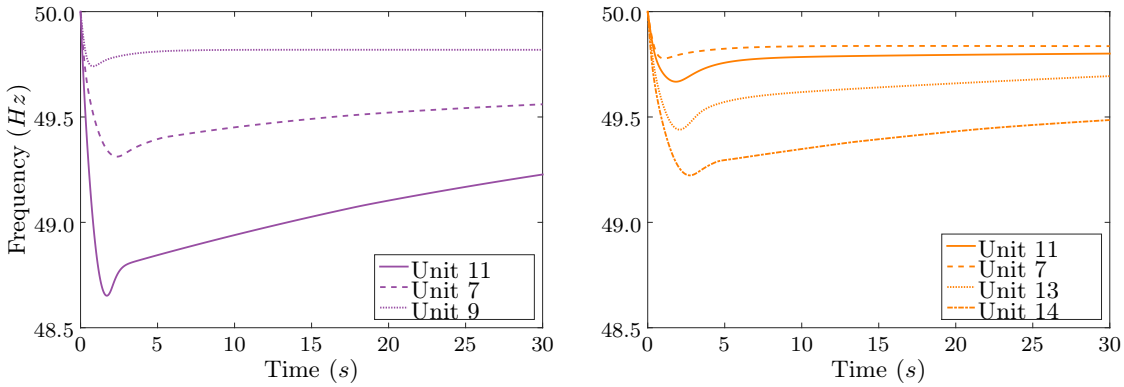

(a) For model $\mathfrak{M}_0$ schedules (b) For model $\mathfrak{M}_3$ schedules

Figure 4.14: Possible frequency trajectories at hour 11 for one instance of scenario 4

Finally, figure 4.15 presents the UC results for a different instance, where the V-RES dispatch down has actually generated an additional PIDR. For this specific example, considerable savings can be achieved with a slight V-RES dispatch down. However, the commitment changes affect the available inertia and regulating capabilities of the adjacent time steps. In fact, some PV has been curtailed at hours 12 and 13, which prevent the commitment of more expensive and flexible units for the early hours.

Figure 4.16a compares the frequency trajectory for a power loss of 25.5 MW (outage unit 11) considering the different day-ahead schedules in figure 4.15, and figure 4.16b presents the frequency trajectories for different single contingencies.

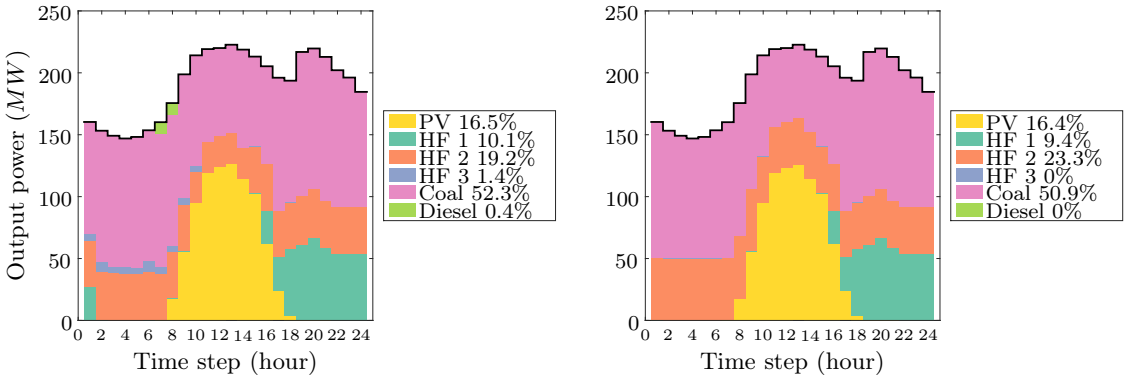

(a) Model $\mathfrak{M}_0$ (b) Model $\mathfrak{M}_3$

Figure 4.15: Dispatch change for declined dynamic response (Scenario 4)

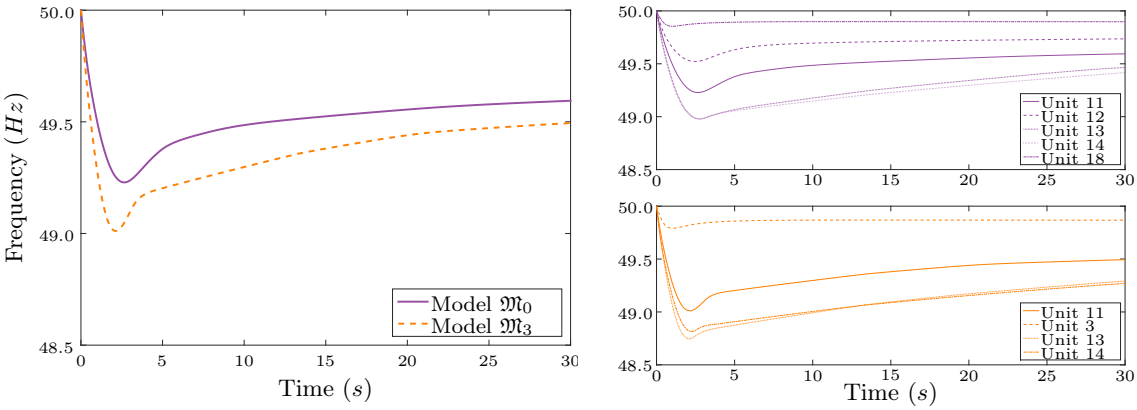

(a) Outage of unit 11 (b) By model

Figure 4.16: Possible frequency trajectories at hour 7 for one instance of scenario 4

Remark 1: The dispatch down of V-RES generation at certain specific hour may **improve the economical performance** of the dispatch by limiting some start up and shut down cost. Hence, commitment changes appear in different times steps, including those without any (or with low) V-RES contribution due to **inter-temporal constraints**. But it is difficult to anticipate the consequence of changes on the primary frequency response.

4.3.4 Contribution of frequency regulation resources by new providers

The optimisation model $\mathfrak{M}_7$ is computed for 11 different values of C, which represents the primary reserve supplied by the new participants, from 0 MW to 40 MW. As discusses in previous chapters, the provision of the primary reserve is costly in isolated systems. Figure 4.17 illustrates the potential reduction in the operational (conventional fuel) cost if part of (or all) the primary reserve was provided by other actor different from conventional units. Here only the evolution of the annual security cost is investigated, without taking into account the cost of reserve by the new provider.

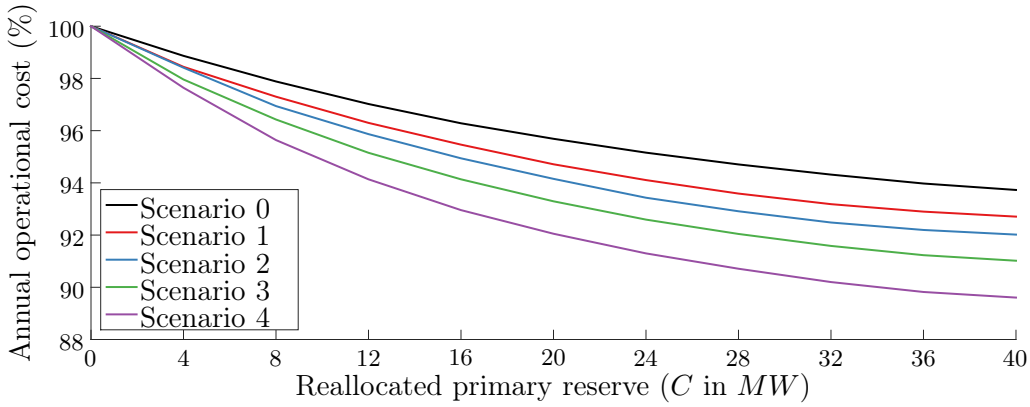

Figure 4.17: Scheduling annual cost reduction with the level of reallocated primary reserve

In this section, the interest is placed in the consequence of such a measure on the primary frequency response. For this, the evolution of the kinetic energy and headroom capacity for different values of C is examined. The evolution of the average, minimal and maximal amount of committed units and stored kinetic energy by time step for scenario 0 (without any V-RES) are presented in figure 4.18.

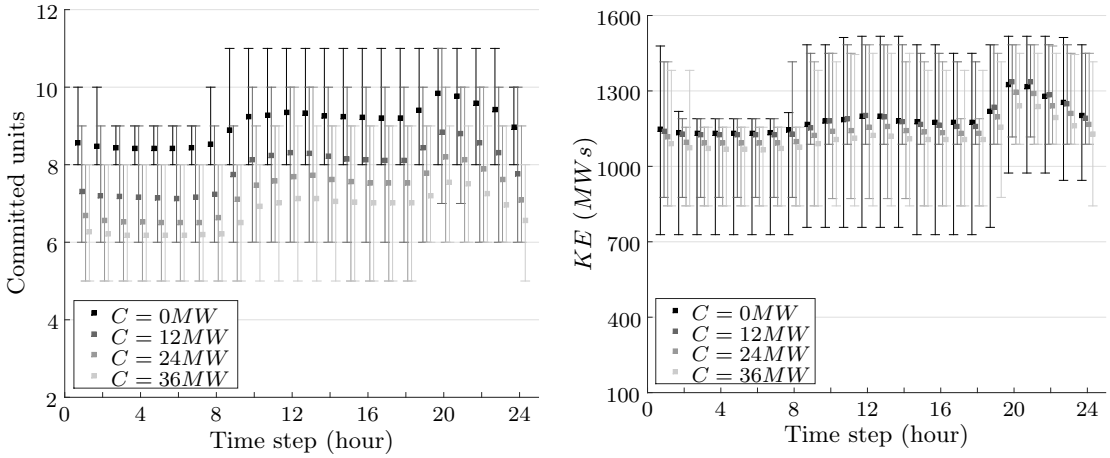

(a) Amount of committed units

(b) Stored kinetic energy

Figure 4.18: Schedules with model $\mathfrak{M}_7$ for scenario 0

It is observed that when the primary reserve is only provided by conventional units, 8 to 11 on-line units are needed to supply the demand. As the C parameter increases, less units are committed (1 to 3). Hence, the reallocation of the primary reserve will reduce the amount of committed units. As a consequence, the equivalent inertia (*i.e.*, the stored kinetic energy in rotating masses) is also diminished. Nevertheless, the reduction of the latter is not always linear since the shift to bigger units may prevail in some instants. Moreover, the dispersion of this variable may tend to decrease, since some cycling could be avoided.

For the test system, this had a reduced impact on the average stored kinetic energy (see figure 4.18b), since large base units take a higher share in the energy mix, which is consistent with the observed operational cost reduction. This is detailed in table 4.5.

Table 4.5: Energy mixes with $\mathfrak{M}_7$ for scenario 0

Type of unit	$C = 0MW$	$C = 12MW$	$C = 24MW$	$C = 36MW$
Heavy fuel 1	27%	30%	31%	32%
Heavy fuel 2	18%	10%	6%	3%
Heavy fuel 3	1 %	$\leq 1\%$	$\leq 1\%$	$\leq 1\%$
Coal	54%	59%	63%	64%
Diesel	$\leq 1\%$	$\leq 1\%$	$\leq 1\%$	$\leq 1\%$

Furthermore, conventional units tend to be more heavily loaded, which increases the need for primary frequency regulation resources, but also the severity of the power imbalance following a single unit outage. Figure 4.19a presents the box plot of the allocated primary reserve by time step including its average, minimal and maximal value over 365 days. The top of figure 4.19b depicts an histogram with a bin width of $3MW$, while the bottom part of this figure shows the cumulative distribution function (CDF).

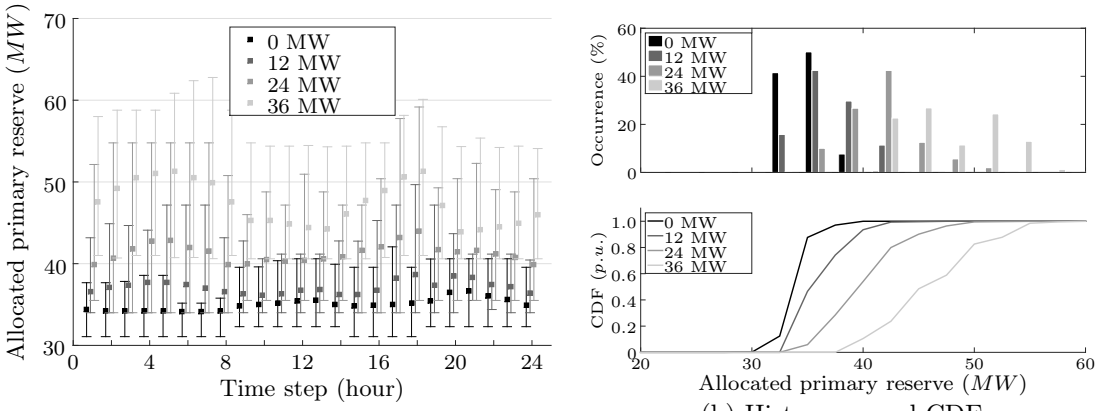

(a) By time step

(b) Histogram and CDF

Figure 4.19: Evolution of the allocated primary reserve with $\mathfrak{M}_7$ for scenario 0

It is observed that as base units are operated closer to their maximal power output, the need for primary regulation resources increases. For high values of C, the primary reserve tends to be over scheduled, since a certain spare capacity will often be available in conventional units and C was always entirely considered as part of the primary reserve.
It must be noted that for the purpose of this study, no cost was attached to the provision of the primary reserve. In addition, the provision of other services by the installed capacity C was disregarded. A different compromise may be achieved as the payments of the new ancillary services providers evolve.

Such studies, regarding optimal sizing, primary reserve bidding and multi-services operation, are beyond the scope of this work, since results may be strongly depending on cost hypotheses. Alternately, the proposed methodological framework could be suitable for a sensibility analysis on some of these topics by defining c^h in equation (4.5) as an optimisation variable and including a cost term in the objective function. Then, for a fixed installed capacity C^{max}, a study on its use may be carried out as a certain cost coefficient a_{rc}, reflecting investment and operational cost, varies. This is formally expressed in equation (4.8).

$$\begin{aligned} \underset{\mathbf{u},\mathbf{g},\mathbf{c}}{\text{minimise}} \quad & \left\{ \sum_{h=1}^{T} \sum_{j=1}^{N} C_j^h \left(u_j^h, g_j^h \right) + S_j^h \left(u_j^h, u_j^{h-1} \right) \right\} + a_{rc} \sum_{h=1}^{T} c^h, \\ \text{subject to} \quad & g_k^h - \sum_{\substack{j=1 \\ j \neq k}}^{N} r_j^h - c^h \leq 0 \qquad \forall k = 1, \ldots, N, h = 1, \ldots, T. \end{aligned} \tag{4.8}$$

It is recalled that all classic constraints described in chapter 2 must be considered, although they are not explicitly included here. Numerical results for this UC model will not be discussed, since in this section, the focus is placed on the evolution of the primary frequency response for different levels of V-RES and non-synchronous primary reserve.

Figure 4.20 shows the evolution of the frequency gradient ($ROCOF$) for scenario 0 as the C parameter is increased. It is observed that, although the stored kinetic energy was not strongly affected, the frequency tends to evolve faster following single unit outages because conventional units are more heavily loaded. The average and maximal values are higher, but also the minimal. Therefore, the degree of dispersion is not linearly increased.

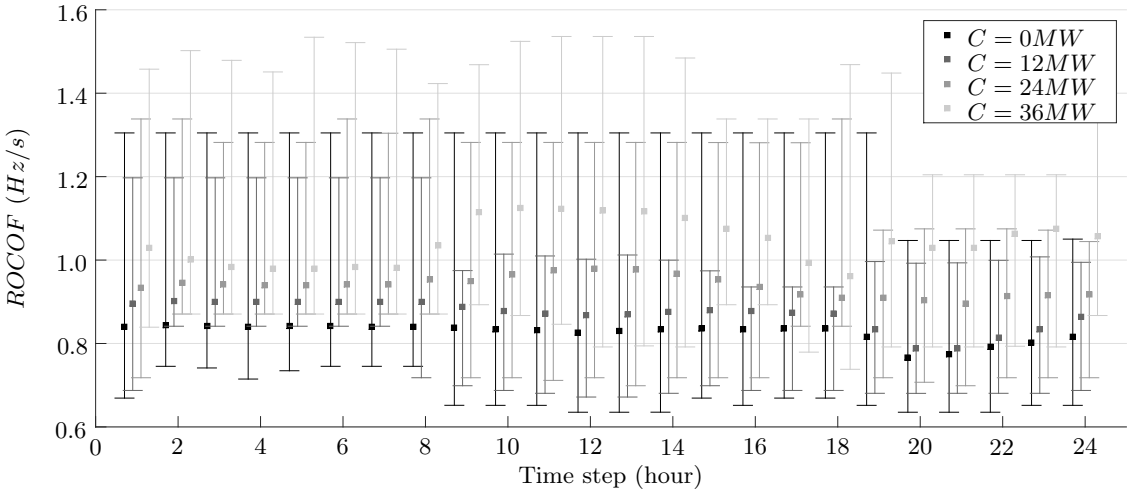

Figure 4.20: $ROCOF$ mean and dispersion by time step for different C values

A histogram representation offers more details about the distribution of this variable. Reducing the bins width and fitting the data to a normal distribution illustrate the displacement of the frequency initial gradients as the share of non-synchronous providers of frequency regulation raises. Results are presented in figure 4.21. Finally, figure 4.21c shows the CDF of this metric. Then, depending on the "quality" of the non-synchronous primary reserve different frequency nadirs can be attained.

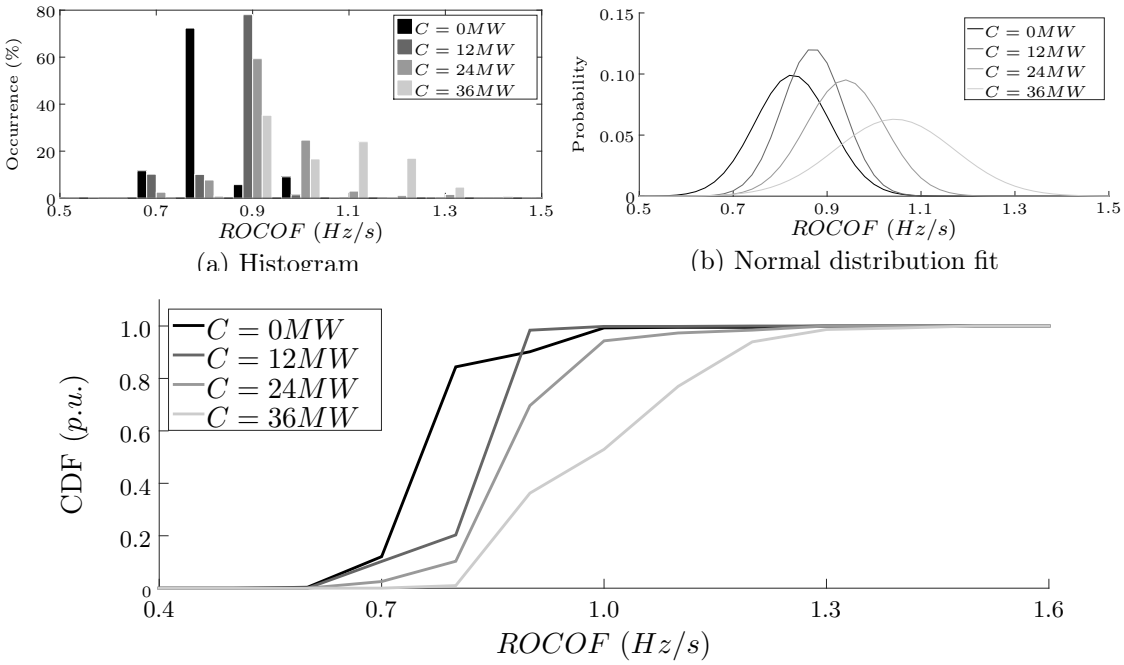

(a) Histogram

(b) Normal distribution fit

(c) Cumulative distribution function

Figure 4.21: $ROCOF$ for primary reserve allocation with model $\mathfrak{M}_7$ for scenario 0

Remark 2: The provision of the primary reserve by non-synchronous suppliers entails an inertia reduction. Moreover, conventional units tend to be more heavily loaded if the reserve constraint is partially loosed. Both trends together lead to a $ROCOF$ increase.

Effectiveness for different deployment dynamics

In this section, the impact of the response time of the regulation will be investigated. A dead-band of $200mHz$ is considered in order to limit cycling processes and, in the case of batteries, extend lifetime. The gain factor (K in figure 4.2) is adjusted for each C value in order to deploy all the allocated primary reserve for a frequency deviation of $500mHz$. First, let us consider a theoretical case, where the non-synchronous providers of primary frequency regulation services have a considerably slow dynamic, which means that their response time is larger than the equivalent primary reserve deployment time of conventional generators. In this case, it is expected that the UFLS risk increases with the participation of the former to the primary frequency regulation.

A specific day will be used to illustrate this behaviour. Figure 4.22 shows the dispatch of conventional unit for C equals to 0 and $12MW$ for scenario 0 (without V-RES). It is observed that the reallocation of $12MW$ of primary reserve reduces the day dispatch costs by 3%. Start-up operations are also reduced and the energy mix shifted to coal base units.

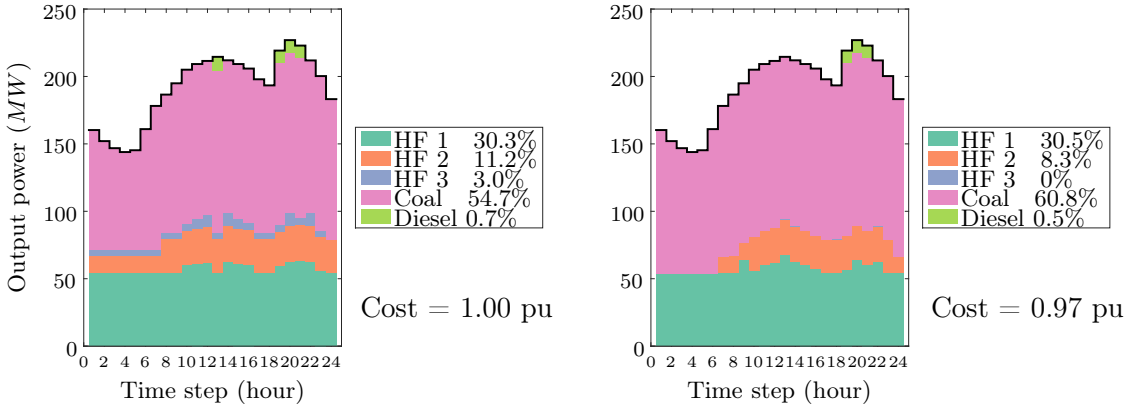

(a) Dispatch for $C = 0MW$ (b) Dispatch for $C = 12MW$

Figure 4.22: Day-ahead dispatches with and without primary reserve dedicated providers

Figure 4.23 shows the detailed power and reserve allocation at hour 13, where the (pre-contingency) system equivalent inertia is reduced by 7.4% (from 1250 to 1157 MWs), since units 10 and 17 are not longer committed. In addition, unit 12 do not participate to the frequency regulation any more.

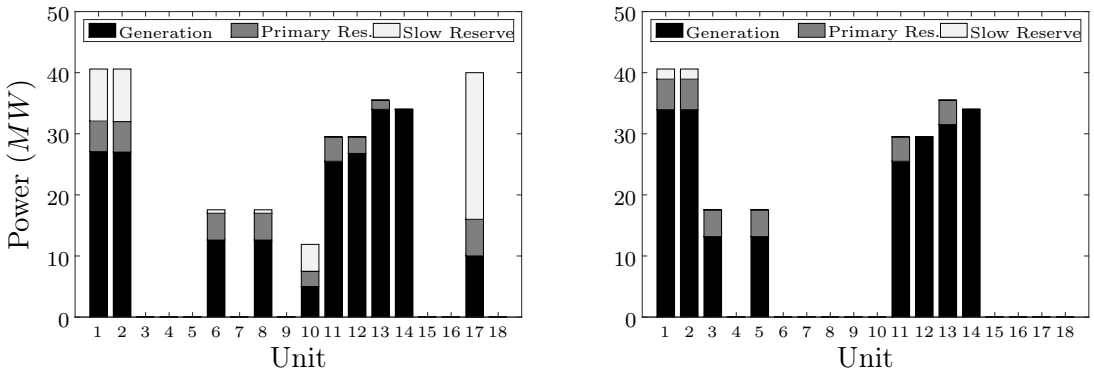

(a) Detailed dispatch for $C = 0MW$ (b) Detailed dispatch for $C = 12MW$

Figure 4.23: Detailed dispatch for hour 13 and scenario 0

Figure 4.24a compares the frequency trajectory following the outage of unit 14, which in both cases generates $34MW$, considering different time constants (τ_r) of the new provider regulation. For the chosen operational point, the time constant of the new provider of primary reserve most be lower than 1.6 seconds to outperform conventional generators, while compensating for the inertia reduction. This analysis is conducted for the 8760 time steps. The CDF of the frequency nadirs for different values of τ_r is shown in figure 4.24b.

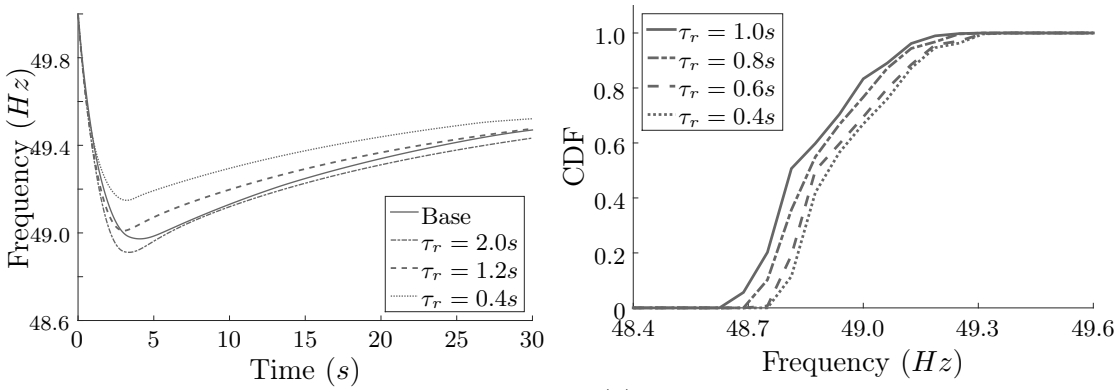

(a) Frequency trajectory

(b) CDF of frequency nadirs for one year

Figure 4.24: Frequency for the outage of unit 14 at hour 13 (Scenario 0, $C = 12$ MW)

Remark 3: Primary frequency response may be improved by non-synchronous providers as long as their **deployment dynamics compensate for the inertia reduction**.

Increasing the reallocated reserve C

Figure 4.25 presents similar results when considering C equal to 24 MW. It is observed that the further reduction of the inertia, and above all, the lack of participation of units 11 and 13 to the frequency regulation have deteriorated the primary frequency response. For the same load profile and power imbalance, a lower time constant is required to maintain the frequency nadir, at least equivalent to the system before considering new providers. For this scenario, the time constant of the new provider must be tightened to 1 second when the total installed capacity increased from $12MW$ to $24MW$.

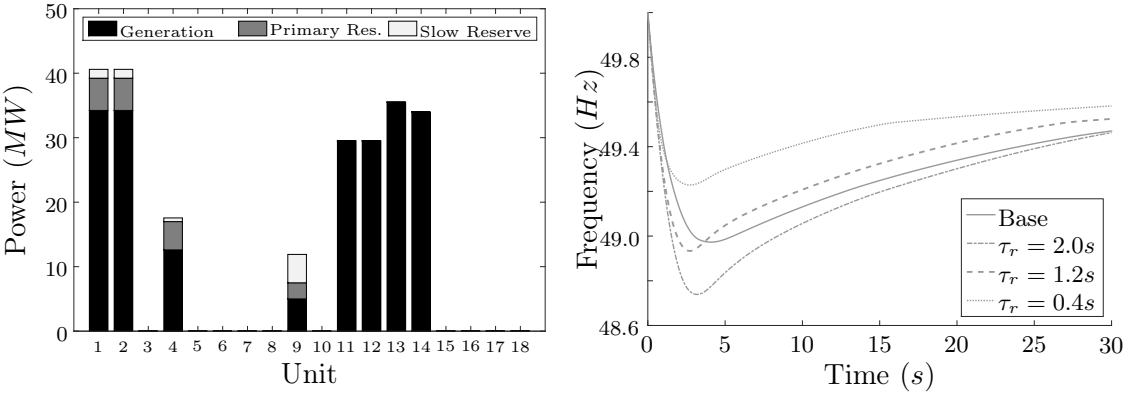

(a) Detailed dispatch

(b) Frequency after the outage of unit 14

Figure 4.25: Scenario 0 and $C = 24$ MW, typical week day at hour 13

Remark 4: The primary reserve deployment rate **must be tightened** as the penetration of non-synchronous providers increases in order to contain UFLS.

Effectiveness for different scenarios of V-RES integration

In this section, a similar analysis is conducted considering the integration of some PV in the test system. First, some attention is given to the further reduction of the stored kinetic energy, which, together with the shift of the generation mix, produces an additional increase of the frequency gradient. Then, the evolution of the PIDR is investigated, considering different primary reserve deployment dynamic from the non-synchronous provider. This paragraph determines if the prescription done for scenario 0 holds for high level of V-RES integration.

Figure 4.26 depicts the evolution of the *ROCOF* for the different scenario of PV. It is observed that both the PV capacity and the reallocation of the primary reserve make the frequency to evolve faster.

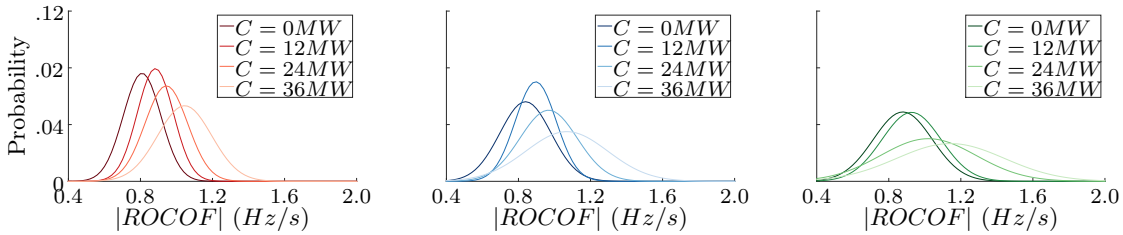

(a) Scenario 1 (b) Scenario 2 (c) Scenario 3

Figure 4.26: *ROCOF* for different scenarios of installed PV and C

Figure 4.27 depicts the UFLS risk in hours a year for different scenarios, values of C and fixed τ_r. It is observed that indeed, the risk of UFLS increases with the response time of the primary reserve provider. As expected, this becomes more important as the share of slow providers increases. Moreover, the risk may raise with the integration of V-RES. Finally, at some points the inertia reduction may prevail, entailing a non linear behaviour of the PIDR with the installed capacity of new providers (figure 4.27b).

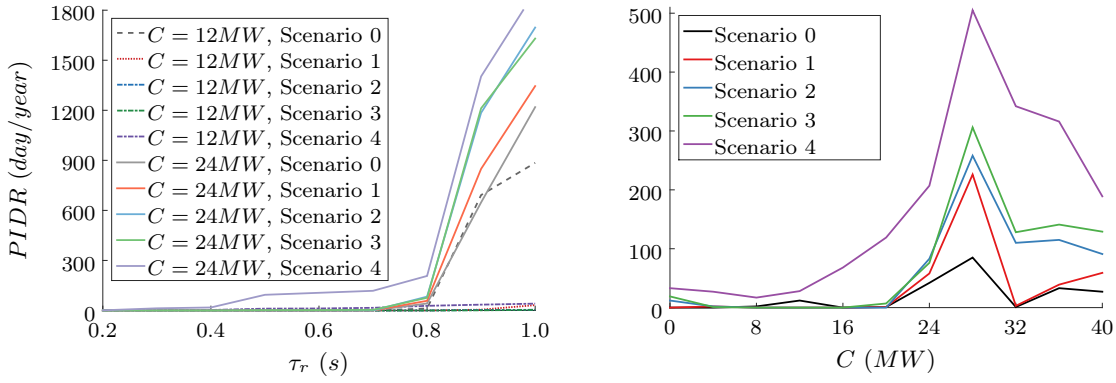

(a) *PIDR* vs. τ_r (b) *PIDR* vs. C ($\tau_r = 0.8$)

Figure 4.27: PIDR for different scenarios of installed PV, C and τ_r

4.4 Conclusion

This chapter examined the cost/benefit and limitation of some V-RES impact mitigation techniques. The main observation can be listed as follows:

1. **Increasing the basic primary reserve constraint (model $\mathfrak{M}_1$)** might indeed reduce the dynamic risk, however the opposite effect could appear due to the replacement of certain units by others having less inertia and/or regulating capabilities. Moreover, it is hard to determine how much more primary reserve should be added. If the required primary reserve is higher than actually needed, the security cost is unnecessarily increased, which entails optimality issues. Otherwise, the effectiveness of the measure may be compromised.
2. Although the **dispatch down of some V-RES (models $\mathfrak{M}_3$)** at high penetration levels may improve the primary frequency response for the specific instant, there is just not direct relation between security and dispatch down. Limiting the V-RES penetration rate at some instant may modify dispatch in adjacent time steps due to the inter-temporal dependency of the UC model, which could lead to an additional UFLS risk.
3. **Inertia constraints (models $\mathfrak{M}_4$ and $\mathfrak{M}_5$)** may provide secure solutions at high security cost for low shares of V-RES, without compromising computational tractability. However, this kind of constraint may become ineffective for higher levels of V-RES integration, mainly due to feasibility issues, which in practice would encourage V-RES dispatch-down. Afterwards, the limitation of the maximal frequency slope following a unit outage provided a more accurate model of the system kinetic energy requirements, at the post-contingency state with respect to the potential power imbalance. In this case, the power output of units can also be adjusted to limit the size of the possible power imbalance. However, other important parameters, such as the deployment time of the primary reserve can not be taken into account.
4. **The fast deployment rate of non-synchronous providers of frequency regulation services (models $\mathfrak{M}_6$ and $\mathfrak{M}_7$)** may improve the performance of the primary frequency regulation. However, at some time steps the consideration of this kind of suppliers leads to a further reduction of the system inertia.

Therefore, the ability of simple linear constraints on the primary reserve volume, the kinetic energy (KE) or the maximal frequency slope (f^{max}_{slope}) to ensure a secure schedule depends on the specific system and its operation point. One solution could be the computation of the limits of these constraints at the optimisation horizon level in a hourly basis. However, such an approach may compromise computational tractability and optimality, since the mixture of different levers seems hard to implement.

In conclusion, a new approach is needed to include a more detailed representation of the primary frequency regulation process in the unit commitment (UC) model in order to optimise the frequency regulation ancillary service, reduce cost and maximise the energy produced by renewable sources. The model should be able to:

1. Take into account the dynamic parameters affecting the frequency nadir, not only the primary reserve, inertia and size of the contingency, but also the deployment rates and saturation limits of all the available resources.
2. Handle inter-temporal dependency with respect to the frequency nadir. This means, ensuring that commitment changes meant to solve security issues in one time step will not lead to some risk in other intervals of the optimisation horizon.
3. Find a feasible solution if any, by scheduling the right combination of available frequency regulation resources.

The next chapter proposes a new formulation of the FCUC problem able to satisfy these three requirements, ensuring optimality and effectiveness.

Chapter 5

A convex formulation for the FCUC problem

Contents

5.1 Introduction

This chapter presents the formulation of a two-stage decomposition approach for the frequency constrained unit commitment problem (FCUC), based on the Benders' method since the FCUC has a structure appealing for a variable decomposition. In this section some standard definitions of convex optimisation are recalled. Then, the interest of formulating an optimisation problem as a convex one is highlighted and backgrounds on the use of decomposition methods to solve optimisation problems in power systems are provided. Subsequently, section 5.2 develops the proposed formulation for the FCUC problem and discusses some preliminary simulation results. Then, section 5.3 proposes a quadratic stabilisation of the standard Benders' method applied to the FCUC problem to improve convergence properties. Finally, section 5.4 finishes with some concluding remarks.

5.1.1 Generalities on convex optimisation

Mathematical optimisation problems are generally classed into families, characterised by particular forms of the objective and the constraint functions. In chapter 2, the classic UC problem was formulated as a Mixed-Integer Linear Programming (MILP) problem, since the objective and constraint functions were linear, some variables were binary and some others were continuous. Then, chapter 4 discussed a few FCUC formulations based on indirect constraints than enable the preservation of this structure. This section provides some definitions considering a different (wider) class of optimisation problems, called convex optimisation problems, in order to ensure the understanding of the this chapter. These definitions are mainly taken from [161].

Definition of a convex set

A set C is convex if the line segment between any two points in C lies in C, *i.e.*, if for any $x_0, x_1 \in C$ and any $\alpha \in [0, 1]$, $\alpha x_0 + (1 - \alpha)x_1 \in C$.

Definition of a convex and concave functions

A function $f : \mathbb{R}^n \to \mathbb{R} \cup \{\infty\}$ is convex if its domain $\mathbf{dom} f = \{x \in \mathbb{R}^n : f(x) < \infty\}$ is a convex set and if for all $x_0, x_1 \in \mathbb{R}^n$ and $\alpha \in [0, 1]$ the equation (5.1) below is satisfied.

$$f(\alpha x_0 + (1 - \alpha)x_1) \leq \alpha f(x_0) + (1 - \alpha)f(x_1). \tag{5.1}$$

Geometrically, inequality (5.1) means that the line segment between $(x_0, f(x_0))$ and $(x_1, f(x_1))$, which is the chord from x_0 to x_1, lies above the graph of f. Figure 5.1 illustrates the difference between a convex, a non-convex and a concave function. In practical terms, a convex function has positive curvature, it bends up, as represented in figure 5.1a. Figure 5.1b shows that the line segment between $(x_0, f(x_0))$ and $(x_1, f(x_1))$ of a non-convex function is below the graph of f for certain points $x_0, x_1 \in \mathbf{dom} f$.

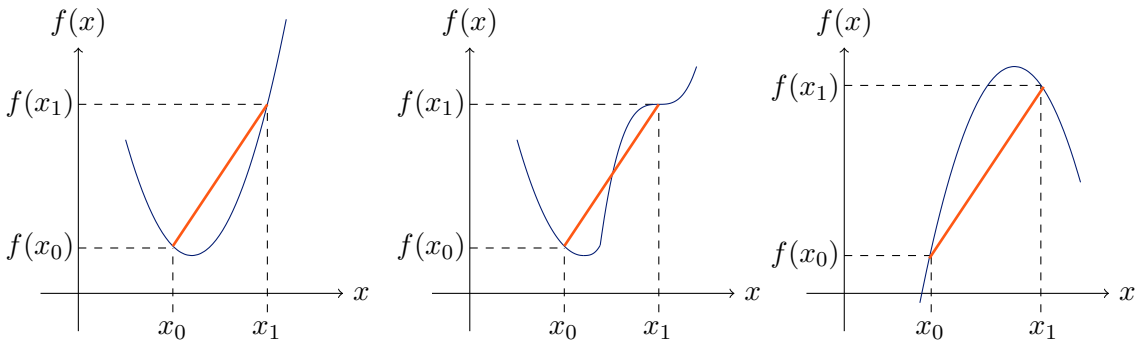

(a) Convex function (b) Non convex function (c) Concave function

Figure 5.1: Graph of a convex, non-convex and concave functions

Finally, a function f is concave if $-f$ is convex. All definitions and proprieties of convex functions hold for concave functions as well, but the sense of the inequalities is inverted. Therefore, the line segment between $(x_0, f(x_0))$ and $(x_1, f(x_1))$ for a **concave** function lies **below** the graph of f, as represented in figure 5.1c.

Properties of convex functions

- A convex function is continuous on the relative interior of its domain; it can have discontinuities only on its relative boundary.
- If a function is convex and concave, then it is affine.
- First order condition: if f is convex and differentiable, then $f(x_0) + \nabla f(x_0)^T(x_1 - x_0) \leq f(x_1), \forall x_0, x_1 \in \mathbf{dom} f$, where, the affine function of x_1 given by $f(x_0) + \nabla f(x_0)^T(x_1 - x_0)$ is the first-order Taylor approximation of f near x_0.
- Second order condition: if f is convex and twice differentiable, its Hessian or second derivative $\nabla^2 f$ is positive semidefinite ($\nabla^2 f(x) \geq 0$) for all $x \in \mathbf{dom} f$.
- Certain operations preserve convexity (or concavity), such as nonnegative weighted sums, composition with affine mappings, pointwise maximum (and minimisation).

On the one hand, the first order condition means that the first-order Taylor approximation is in fact a global under-estimator of a convex function, which is an interesting feature for solving optimisation problem. On the other hand, the second order condition offers a local convexity prove. In this applicative work, first order linearisations are required.

Definition of a convex optimisation problem

A convex optimisation problem is one of the form:

$$\begin{aligned} &\underset{x \in X}{\text{minimise}} && f_0(x) \\ &\text{subject to} && f_\imath(x) \leq b_\imath, \qquad \imath = 1, \ldots, i, \end{aligned} \tag{5.2}$$

where $X \subset \mathbb{R}^n$ ($\mathbf{dom} f$) is a convex set, and the functions $f_0, \ldots, f_i : \mathbb{R}^n \to \mathbb{R}$ are convex.

5.1.2 Interest of convex optimisation for the FCUC problem

As discussed in chapter 2, some classes of optimisation problems, such as least-squares or linear programming, can be solved in an effective and reliable way through suitable solvers. However, trying to stick to linear formulations may limit the representativeness of certain models, as illustrated in chapter 4 with the FCUC problem. Recent developments have enabled the tractability of large convex problems, although, their recognition or reformulation remain less straightforward than in the linear case [161].

In addition, there are also theoretical or conceptual advantages in formulating an optimisation problem as a convex one. For instance, the associated dual problem, defined in the next paragraph, often has an interesting interpretation in terms of the original problem, and sometimes leads to efficient and/or distributed methods for solving it. Furthermore, convex optimisation approaches can be useful, even in the case of non-convex problems. First of all, they can be used to initialise local optimisation methods, by solving an approximated, but convex, formulation of the problem. Secondly, they can provide bounds for global optimisation methods by, for example, relaxing a nonconvex constraint with a looser, but convex, constraint, or by solving the Lagrangian dual problem, which by construction is convex, and provides a lower bound on the optimal value of the nonconvex problem. Finally, through decomposition, non-convex problem can be handled partially by convex optimisation techniques as it will be discussed in section 5.1.3.

Duality

In convex optimisation the most widespread dual formulation is the Lagrangian. The idea is to relax the constraints in (5.2) and penalise them in the objective function. Hence, the Lagrangian $\mathcal{L} : \mathbb{R}^n \times \mathbb{R}^i_+ \to \mathbb{R}$ associated to problem (5.2) is defined as follows:

$$\mathcal{L}(x, \lambda) = f_0(x) + \sum_{\imath=1}^{i} \lambda_\imath (f_\imath(x) - b_\imath). \tag{5.3}$$

The variable $\lambda_\imath \geq 0$ is denoted as the Lagrange multiplier associated with the $\imath^{th}$constraint $f_\imath(x) \leq 0$, while λ is called the dual variable or Lagrange multiplier vector associated with the problem (5.2). Then, the Lagrange dual function (or just dual function) $\Theta : \mathbb{R}^i \to \mathbb{R}$ is the minimum value of the Lagrangian over x, for $\lambda \in \mathbb{R}^i$.

$$\Theta(\lambda) = \inf_{x \in X} \mathcal{L}(x, \lambda) = \inf_{x \in X} \left(f_0(x) + \sum_{\imath=1}^{i} \lambda_\imath (f_\imath(x) - b_\imath) \right). \tag{5.4}$$

An important property of dual functions is that they are concave in λ, even though the initial (or primal) problem (5.2) is not convex, since the dual function is the pointwise infimum of a family of affine functions. As aforementioned, these operations preserve concavity. In addition, the dual function yields lower bounds on the optimal value of the problem (5.2) for any $\lambda \geq 0$. Indeed, for any feasible point $\tilde{x}$, the Lagraingian $\mathcal{L}(\tilde{x}, \lambda)$ is below the function $f_0(\tilde{x})$, since each term of the sum in equation (5.5) is negative.

$$\mathcal{L}(\tilde{x}, \lambda) = f_0(\tilde{x}) + \sum_{\imath=1}^{i} \lambda_\imath (f_\imath(\tilde{x}) - b_\imath) \leq f_0(\tilde{x}), \tag{5.5}$$

It must be noted that equation (5.5) is valid for every feasible point $\tilde{x}$ and any $\lambda \geq 0$, hence it holds for the optimal point x^*.

$$\Theta(\lambda) \leq c^*, \tag{5.6}$$

where $c^* = f_0(x^*)$ is the objective value at the solution of problem (5.2).

The difference between the solution of the primal (original) and the dual functions is called the duality gap. Under certain conditions, which are called constraint qualifications, and include Slater's condition, the duality gap becomes zero. In this case, the optimal dual objective function value is equal to the primal function value at the optimal point and strong duality is said to hold.

Subgradient method in nonsmooth optimisation

The first and second order conditions suppose differentiability properties of convex functions. However, a convex function is not necessarily differentiable. A classical example of this feature is provided by the absolute value function. Nevertheless, the gradient of the function can be replaced by a similar concept, the subgradient [162, 163]. Geometrically, the "gradient" function is approximated by a cone (S_aS_b) since a unique tangent hyperplane (L_0) can not be determined for a specific point (x_0), as illustrated in figure 5.2.

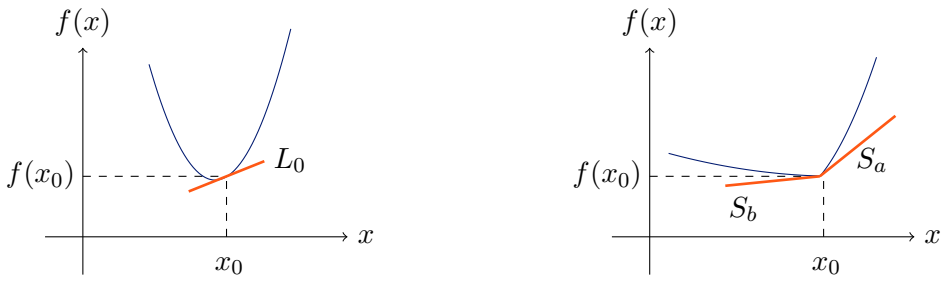

(a) Differentiable function

(b) Non differentiable convex function (in x_0)

Figure 5.2: Graph of linear and sublinear tangent

As a consequence, the "derivative" of a convex function f at $x_0 \in \mathbb{R}^n$ can be approximated by its subdifferential ∂f defined as follows:

$$\partial f(\mathbf{x}_0) = \{\mathbf{s} \in \mathbb{R}^n : f(x) \geq f(x_0) + \langle s, x - x_0 \rangle \forall x \in X\}, \tag{5.7}$$

where the vector $\mathbf{s} \in \partial f(\mathbf{x}_0)$ is called a subgradient of f at $\mathbf{x}_0$. It can be shown that for any $\mathbf{x}_0$ in the interior of the domain of f, $\partial f(\mathbf{x}_0)$ is a non empty compact convex set [163].

5.1.3 Decomposition methods

Decomposition is a general approach that has been applied in optimisation for at least 50 years [164]. As its name indicates, it consists in solving an optimisation problem by decomposing it into smaller sub-problems, that can be solved separately. Then, the solution of the initial problem is guaranteed by iteratively solving a sequence of these sub-problems. The interest of this approach is straightforward when thinking of parallelisation. Moreover, the lower complexity of the sub-problems makes them easier to solve.

For very large problems that are beyond the reach of standard techniques, decomposition methods are the only tractable option to compute a numerical solution.
More recently, the research on decentralised computation delivers new potential uses for decomposition methods. Indeed, decentralised algorithms enable the coordination of a collection of subsystem decisions to achieve global optimality, although they tend to be slower than centralised methods. Furthermore, the decomposition enables the use of convex optimisation techniques to solve problems that involve non-convex functions by reformulating them as a set of convex subproblems. Then, different techniques can be used to decompose an optimisation problem, depending on its structure.
For example, a problem may have *complicating constraints*, which means that the problem becomes easier to solve without those constraints. Alternatively, an optimisation problem may become simpler if some variable (*complicating variables*) are fixed. In the former case, a constraint decomposition method could be used, such as the Lagrange relaxation, or the Dantzig–Wolfe decomposition. In the latter case, a variable decomposition method, such as Benders, may be suitable.
These methods have proven their value in solving optimisation problems in power system applications. Examples are provided in the next paragraph. Some references are indicated for the interested reader, but details are given only for the UC problem. In this work the interest is placed in a variable decomposition method in order to handle the partially non-convex frequency nadir constraint in the FCUC problem.

Decomposition methods in power system applications

Nowadays, interconnected systems, such as continental Europe or US are large scale. As a consequence, system-wide optimisation problems, such as generation and network planning [165, 166], asset management [167], and optimal FACTS allocation [168], for instance, are extremely difficult to solve and beyond the reach of a direct attack. Hence, the aforementioned decomposition techniques have been used to solve these problems in practice. Moreover, this approach supports the formulation of operational problems [169], such as the network reconfiguration [170, 171, 172, 173], state estimation [174, 175], and short-term generation scheduling as discussed below.

Decomposition in the unit commitment problem

Historically, the UC problem has provided a major forum for the application of decomposition techniques. Initially, Lagrangian relaxation was the most wide spread decomposition method in short-term scheduling models [99, 176, 177, 178]. The Dantzig–Wolfe was proposed for the long-term UC problem [179]. In the last decade, the Benders' method has received a lot of attention [180]. In this work, the attention is placed on the latter.

Unit commitment by Benders' decomposition

The Benders' method consists in decomposing an initial multi-variable optimisation problem, as the one described by (5.8), into a sequence of two problems called master and slave problems. It is used when a complicated problem can be simplified by fixing some variables.

$$\begin{aligned} &\underset{x\in X, y\in Y}{\text{minimise}} && f_0(x,y) \\ &\text{subject to} && f_\imath(x,y) \leq b_\imath, \quad \imath = 1,\ldots,i, \end{aligned} \tag{5.8}$$

where $X \subset \mathbb{R}^{n_1}, Y \subset \mathbb{R}^{n_2} : n_1 + n_2 = n$, and y is considered to be a complicating variable, in the sense that when it is fixed the remaining sub-problems are considered more tractable. Then, figure 5.3 shows the general diagram of Benders' method applied to problem (5.8).

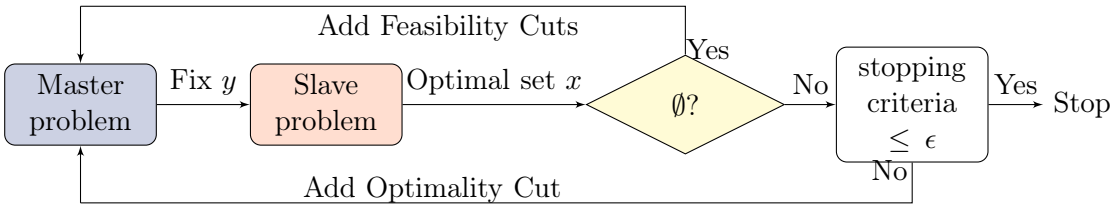

Figure 5.3: Standard Benders' decomposition schema

The decomposition of the UC problem by variable type was proposed 30 years ago in order to reduce its size [181]. However, as the capabilities of solving MILP problems increased, this technique was dropped. Several years later, Shahidehpour *et al.* [99, 179, 180] did a lot of research on the benefit that the Benders' method (and other decomposition techniques) could bring to the UC problem, specially in the topic of constraint formulation revision. For example, they propose to improve the accuracy of the UC model by including AC (alternating current) network constraints for instance [182]. More recently this work has been extended for considering uncertainty [30]. The next section details the proposed FCUC formulation, based on the Benders' decomposition method.

5.2 Benders' decomposition approach for the FCUC

For the purposes of this chapter, the optimisation problem presented in chapter 2 as model $\mathfrak{M}_0$ is written in a compact manner to simplify notation, as represented in (5.9). Here, all continuous variables, given by the power outputs and allocated reserves, are aggregated in $x \in X$, while all binary variables, given by the units state and start up/shut down decisions, are represented by $y \in Y$. As a consequence, the variable domains are $X \subseteq \mathbb{R}^{4NT}$ and $Y \subseteq \{0,1\}^{3NT}$, where N is the number of units and T is the number of time steps in the optimisation horizon.

In addition, the objective function is split in two parts and all constraints are aggregated in two mappings. In this section, a new formulation for the FCUC problem is proposed by including the frequency nadir constraints into model $\mathfrak{M}_0$, which gives the following optimisation problem:

$$\begin{aligned} \underset{x\in X, y\in Y}{\text{minimise}} \quad & f_1(x) + f_2(y) \\ \text{subject to} \quad & G(x,y) \leq 0, \\ & H(x,y) = 0, \\ & \underline{q} - q_m(x,y) \leq 0, \quad \forall m = 1,\ldots,M. \end{aligned} \tag{5.9}$$

where, $f_1 : \mathbb{R}^{4NT} \to \mathbb{R}$ is an affine function including the costs that depend on the continuous variables, *e.g.*, the variable cost of the generation and reserve. It can be represented by a piece-wise linear model. The mapping $f_2 : \mathbb{R}^{3NT} \to \mathbb{R}$ stands for the cost components that depend on the unit's states, *e.g.*, fixed, start up and shut down cost.

The mapping $G : \mathbb{R}^{7NT} \to \mathbb{R}^{\mathcal{G}}$ defines all inequality constraint, which are considered to be jointly convex in (x, y). In the UC model the inequality constraints include, among others, the technical limits and reserve requirements. The mapping $H : \mathbb{R}^{7NT} \to \mathbb{R}^{\mathcal{H}}$ defines all equality constraints, which represent the power balance equation and the auxiliary variable definitions in the basic UC model. This latter mapping H, is linear, so that $\left\{(x,y) \in \mathbb{R}^{7NT} : H(x,y) = 0\right\}$ is a polyhedral set. In model $\mathfrak{M}_0$ the dimension of the constraint function are given by $\mathcal{G} = 14NT + 3T$ and $\mathcal{H} = (N+1)T$.

Without loss of generality, G and H can include additional constraints of different variants of the deterministic UC problem. If more auxiliary variables are needed, the domain of these mappings will of course be enlarged. For example, in a classic security constrained unit commitment problem, additional constraints are included to consider line capacity or voltage limits. In that case, the bus voltages and the line currents are included in the optimisation vector x, since they are continuous. Hence, $x \in X_2 \subset \mathbb{R}^{4NT} \times \mathbb{R}^B \times \mathbb{R}^L$, where B would be the number of buses and L the number of lines. The remainder of this work holds for those cases, as long as the joint convexity hypothesis remains true and the domain of the mappings are redefined in consequence.

Finally, the frequency nadir (f_{min}) constraint is kept explicit and modelled by mapping $q : \mathbb{R}^{7NT} \to \mathbb{R}^M$, and the security threshold is denoted by $\underline{q}$. Regarding the dimension of the contingency set, M, is in principle equal to NT for the FCUC problem, since $m \in \{1,\ldots,NT\}$ represents each possible unit outage over the optimisation horizon. Then, the frequency nadir q_m is associated with the failure of a given generating unit $k(m) \in \{1,\ldots,N\}$ at a specific time step $h(m) \in \{1,\ldots,T\}$. For the purposes of this work $M = NT$, although it is acknowledged that not all contingencies necessarily produce a security violation. In fact, only few of them may be active in practice.

For fixed binary variables y, the FCUC becomes a Frequency Constrained Economic Dispatch (FCED), which is a continuous problem, much easier to solve. Therefore, the FCUC presents a structure where the Benders' method may deliver potential benefits.

5.2.1 FCUC decomposed formulation

In the proposed approach, the binary variables y are handled by the master problem, while the slave problem adjusts the generation levels of committed units x, considering a candidate solution $\bar{y}$. The frequency nadir constraints are included in the slave problem through a cutting plane model, under the hypothesis that the frequency nadir is a concave function of the power level of the generating units, for given commitment decisions.
If the slave problem is feasible, a new generation dispatch is proposed, where only the power outputs of the units committed in the first stage are adjusted in order to satisfy the frequency nadir constraints. Then, an optimality cut is added to the master problem to check that there is not another commitment state that satisfies the frequency constraints at lower cost than the initial redispatch proposed by the slave problem. If the slave problem is infeasible, a feasibility cut is added instead.
This idea can be formalised as follows:

1. The master problem (y is optimised)

$$\begin{aligned} \mathcal{C}^* = \underset{y \in Y}{\text{minimise}} \quad & \mathcal{V}(y) + f_2(y) \\ \text{subject to} \quad & G(y) \leq 0 \\ & H(y) = 0, \\ & \text{Feasibility cuts}, \\ & \text{Optimality cuts}, \end{aligned} \tag{5.10}$$

   where $\mathcal{V} : \mathbb{R}^{3NT} \to \mathbb{R}$ is defined by the slave problem.

2. The slave problem (x is optimised for $\bar{y} \in \{0,1\}^{3NT}$ fixed)

$$\begin{aligned} \mathcal{V}(\bar{y}) := \inf_{x \in X} \quad & f_1(x) \\ \text{subject to} \quad & G(x, \bar{y}) \leq 0 \\ & H(x, \bar{y}) = 0 \\ & \underline{q} - q_m(x, \bar{y}) \leq 0, \quad \forall m = 1, \ldots, M, \end{aligned} \tag{5.11}$$

where $\mathcal{C}^*$ is the original problem solution: the total minimal cost, and $\mathcal{V}(\bar{y})$ is the cost of a feasible solution minimised over x (*i.e.*, the final dispatch cost).
However, the set of non-linear frequency constraints (q_m) still needs to be handled. For that a cutting plane model is proposed in next section.

Cutting plane model for the frequency nadir

Let us consider that the frequency nadir (q_m) is a concave function with respect to the generation level of the on-line units (x), for a fixed commitment decision vector ($\bar{y}$) as illustrated in figure 5.4. Then, by concavity it is known that a cutting plane model ($\check{q}_m$) in green forms an upper model of the mapping q_m, *i.e.*, $q_m(x, \bar{y}) \leq \check{q}_m^L(x, \bar{y})\ \forall x \in X, \bar{y} \in Y$.

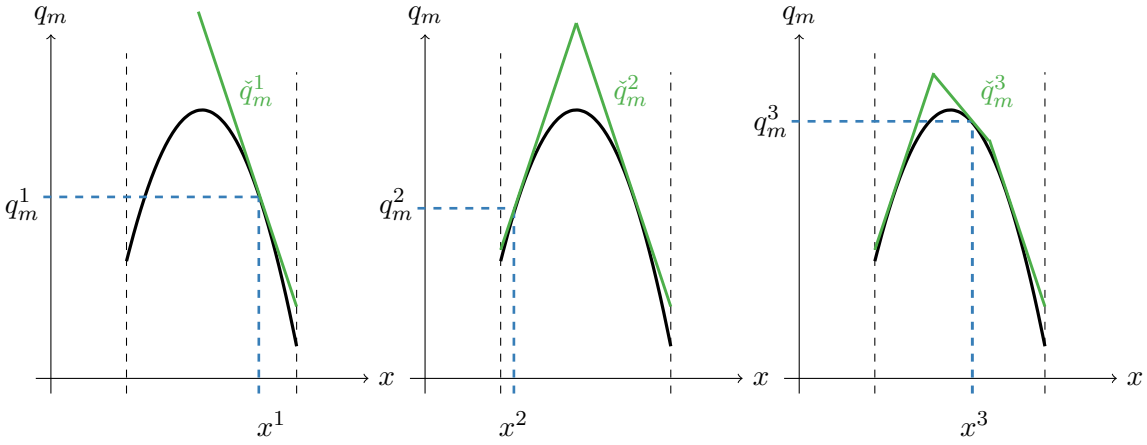

(a) Iteration 1 (b) Iteration 2 (c) Iteration 3

Figure 5.4: Cutting plane model of a concave function

The cutting plane model can be computed iteratively by solving (5.12) as illustrated in figure 5.5. For a candidate solution $(\bar{y}, x^\ell)$, a black box function, called the *Oracle* and based on the dynamic simulator described in section 2.3, provides all possible frequency nadirs q_m^ℓ and their sub-gradients in x^ℓ (s_m^ℓ). Then, $x^{\ell+1}$ is the solution of (5.12) at following iteration $\ell + 1$, where the cutting plane model at iteration L, $\check{q}_m^L$, is defined by the first order approximation of q_m as expressed in equation (5.13).

$$\begin{aligned} \mathcal{V}(\bar{y}) := \inf_{x \in X} \quad & f_1(x) \\ \text{subject to} \quad & G(x, \bar{y}) \leq 0 \\ & H(x, \bar{y}) = 0 \\ & \underline{q} - \check{q}_m^L(x, \bar{y}) \leq 0, \quad \forall m = 1, \ldots, M. \end{aligned} \tag{5.12}$$

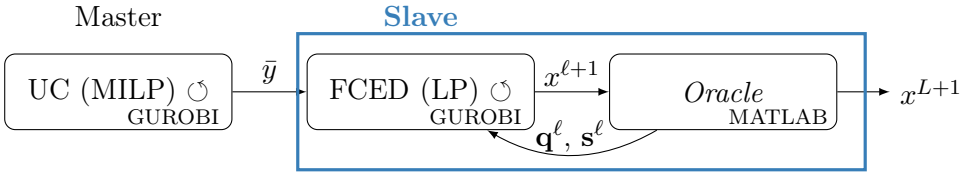

Figure 5.5: General diagram of the slave problem algorithm

$$\check{q}_m^L(x) = \min_{1 \leq \ell \leq L} \left\{ q_m^\ell + \langle s_m^\ell(x^\ell, y_{-m}), x - x^\ell \rangle \right\}. \tag{5.13}$$

Here, y_{-m} denotes the commitment decision vector at time $h(m)$, when considering the outage of unit $k(m)$: $y_{-m} = [y_1^1, \ldots, y_N^1, \ldots, y_1^h, \ldots, y_{k-1}^h, 0, y_{k+1}^h, \ldots, y_N^h, \ldots, y_1^T, \ldots, y_N^T]$. It must be noted that $\check{q}_m^L(x)$ depends on $\bar{y}_{-m}$, but it is not made explicitly dependent.
In addition, $q_m : x \mapsto q_m(x, \bar{y})$ is continuously differentiable (C^1) since for the outage of unit $k(m)$, the output power of this unit represents the power imbalance itself. As discussed in chapter 2, the frequency nadir is linearly dependent on the generation level of the lost unit x_m. Finally, $s_m(x^\ell, y_{-m})$ is computed by using finite differences:

$$\frac{\partial q_m(x^\ell, \bar{y}_{-m})}{\partial x_j} \approx \frac{q_m(x^\ell + \Delta x e_j, \bar{y}_{-m}) - q_m(x^\ell - \Delta x e_j, \bar{y}_{-m})}{2\Delta x}, \tag{5.14}$$

where e_j is a standard unit vector in $\mathbb{R}^M$ with the j^{th} components equal to one, and Δx is a small value ($1e^{-5}$ for instance).
Let x^{L+1} be the solution of (5.12). The cutting plane method stops when the estimation of the frequency nadir ($\check{q}_m$) is close enough to the simulation result (q_m), for all considered contingency $m \in M$. Hence the stopping criterion is given by equation (5.15):

$$\check{q}_m^L(x^{L+1}) - q_m(x^{L+1}) \leq \epsilon, \tag{5.15}$$

where ϵ is a given tolerance (here $1e^{-3}$). If x^{L+1} is the solution of (5.12), this optimal point is actually ϵ-feasible to (5.11). Which means that in the worst case the actual frequency nadir (q_m) can be lower than $\check{q}_m$ by ϵ. If this results is not satisfactory enough, $\underline{q}$ can be increased of ϵ in order to ensure than the frequency nadir constraint is satisfied.

Feasibility cuts

If the slave problem (5.12) is infeasible, a feasibility cut must be added to the master problem and a new candidate solution $\bar{y}^{i+1}$ will be given to the slave problem as depicted in figure 5.3. For the FCUC problem, the binary nature of the commitment decision variables (y) provides a simple feasibility constraint that enforces the change of the state of at least one unit. The feasibility cut is then written as follows:

$$\sum_{j \in \mathfrak{J}^i} \left(1 - y_j^h\right) + \sum_{j \notin \mathfrak{J}^i} y_j^h \geq 1 \quad \forall i = 1, \ldots, I^{fea}, \tag{5.16}$$

where, $\mathfrak{J}^i = \{m = \{1, \ldots, NT\} : y_m^i = 1\}$ denotes the set of committed units in the infeasible iteration i of the master problem.
The disadvantage of this approach is that the amount of feasibility cuts may become significant (increasing the size of the optimisation problem), as well as the amount of iterations needed to find a feasible point, since no information is given about the suitable direction of the decision changes. Therefore computation time can highly increase. In order to avoid this, sub-optimality cuts will be also provided as explained below. Obviously, the underlying hypotheses is that problem (5.10) admits a feasible solution.

Optimality cuts

Lets rewrite problem (5.12) one last time. In this case, the commitment decision variables will be included into the slave problem as w, but they will be fixed to the values provided by the master problem at iteration i, $\bar{y}^i$, as shown in (5.17).

$$\begin{aligned} \mathcal{V}(\bar{y}^i) := \inf_{x\in X, w\in Y} \quad & f_1(x) \\ \text{subject to} \quad & G(x,w) \leq 0 \\ & H(x,w) = 0 \\ & w = \bar{y}^i \\ & \underline{q} - \check{q}_m^L(x,w) \leq 0, \quad \forall m = 1 \dots M. \end{aligned} \tag{5.17}$$

The Lagrangian $\mathcal{L} : \mathbb{R}^{10NT} \times \mathbb{R}^{\mathcal{G}} \times \mathbb{R}^{\mathcal{H}} \times \mathbb{R}^{\mathcal{M}} \to \mathbb{R}$ associated with the problem (5.17) is defined as follows:

$$\mathcal{L}(x,w,\lambda,\pi,\nu,\upsilon) := f_1(x) + \lambda^T(\bar{y}^i - w) + \pi^T G(x,w) + \nu^T H(x,w) + \upsilon^T\left(\underline{q} - \check{q}_m^L(x,\bar{y}^i)\right), \tag{5.18}$$

where $\lambda \in \mathbb{R}^{3NT}$ denotes the set of dual variables associated to the new constraint $(w = \bar{y}^i)$. Then, the dual function, $\Theta_{\bar{y}^i} : \mathbb{R}^{3NT} \times \mathbb{R}^{\mathcal{G}} \times \mathbb{R}^{\mathcal{H}} \times \mathbb{R}^{\mathcal{M}} \to \mathbb{R}$, is defined as:

$$\begin{aligned} &\Theta_{\bar{y}^i}(\lambda,\pi,\nu,\upsilon) = \inf_{x\in X, w\in Y} \mathcal{L}(x,w,\lambda,\pi,\nu,\upsilon) = \\ &\inf_{x\in X, w\in Y} \left(f_1(x) + \lambda^T(\bar{y}^i - w) + \pi^T G(x,w) + \nu^T H(x,w) + \upsilon^T\left(\underline{q} - \check{q}_m^L(x,w)\right)\right). \end{aligned} \tag{5.19}$$

Noting that $\lambda^T\bar{y}^i$ is not optimised over, equation (5.19) can be rewritten as follows:

$$\Theta_{\bar{y}^i}(\lambda) = \lambda^T\bar{y}^i + \Theta_0(\lambda,\pi,\nu). \tag{5.20}$$

By construction the dual function is concave, even if the original function was not, and it provides a lower bound for the original problem for $\lambda \neq 0$. Then, weak duality gives $\Theta_{\bar{y}^i}(\lambda) \leq \mathcal{V}(\bar{y}^i)$. Let $y \in Y$ be arbitrary, applying (5.20) twice yields:

$$\Theta_{\bar{y}^i}(\lambda^*,\pi^*,\nu^*) = \lambda^{*T}(\bar{y}^i) - \lambda^{*T}(y) + \Theta_y(\lambda^*,\pi^*,\nu^*), \tag{5.21}$$

and weak duality gives:

$$\Theta_{\bar{y}^i}(\lambda^*,\pi^*,\nu^*) + \langle\lambda^*, y - \bar{y}^i\rangle \leq \mathcal{V}(y). \tag{5.22}$$

If moreover, strong duality holds, *i.e.*, $\Theta_{\bar{y}^i}(\lambda^*,\pi^*,\nu^*) = \mathcal{V}(\bar{y}^i)$:

$$\mathcal{V}(\bar{y}^i) + \langle\lambda^*, y - \bar{y}^i\rangle \leq \mathcal{V}(y). \tag{5.23}$$

Consequently, the Lagrange multiplier provides the subgradient of the slave problem objective ($\lambda^* \in \partial\mathcal{V}(\bar{y}^i)$). Strong duality for problem (5.19) can be ensured if some constraints qualification condition holds (and joint convexity). So a cutting plane model of the slave cost as a function of the binary decision variables can be provided by equation (5.24):

$$\check{\mathcal{V}}^I(y) = \max_{1\leq i\leq I-1} \left\{\Theta_{\bar{y}^i} + \langle \lambda^i, y - y^i\rangle\right\} \tag{5.24}$$

Figure 5.6 illustrates the way optimality cuts provide information about the dispatch cost. The underlying result is that there exists a convex mapping $\bar{\mathcal{V}}$, such that: $\check{\mathcal{V}} \leq \bar{\mathcal{V}} \leq \mathcal{V}$, which is equal to the dual function $\Theta_{\bar{y}^i}(\lambda^*)$ at each iterate and $\lambda^i \in \partial\Theta_{\bar{y}^i}(\bar{y}^i)$ [183]. If strong duality holds, then $\Theta_{\bar{y}^i}(\lambda^*) = \mathcal{V}(\bar{y}^i)$ and $\lambda^i \in \partial\mathcal{V}(\bar{y}^i)$ is the subgradient of the dispatch cost. It is highlighted that this inequality holds even if $\mathcal{V}$ is not convex in y.

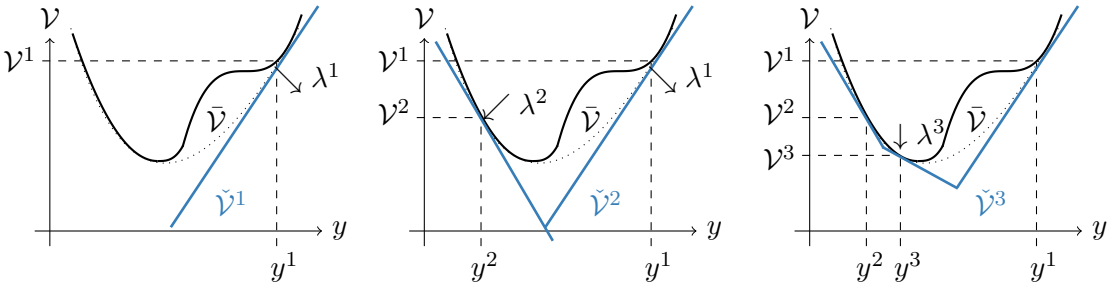

(a) Iteration 1 (b) Iteration 2 (c) Iteration 3

Figure 5.6: Illustration of the optimality cuts principle

Sub-optimality cuts

In practice, if the first proposed commitment vector is infeasible, the algorithm could spend a lot of time adding "no good" feasibility cuts, given by equation (5.16), before finding at last one feasible point. Indeed, the master objective includes only the costs that depend on the binary variables (y). To avoid this, the inclusion of sub-optimality cuts is proposed, as illustrated in figure 5.7, so that even when the proposed master solution is infeasible at the slave problem level, some information about the slave objective is given back to the master problem. This sub-optimality cuts are built from the solution of (5.17) without any frequency constraint ($L = 0$).

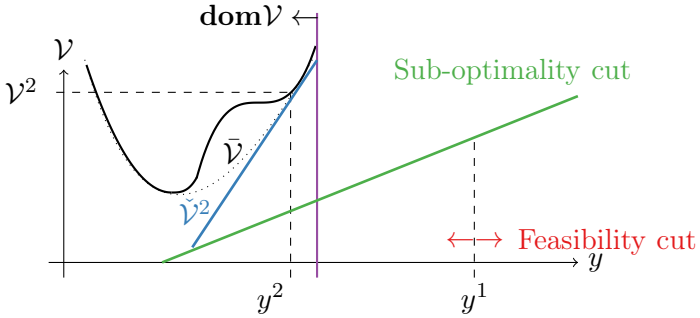

Figure 5.7: Feasibility and sub-optimality cuts at iteration 1

Therefore, $\mathcal{V}$ and λ can be calculated for all iteration i, feasible or infeasible. Moreover, the constraints in x (such as the power balance equation) will be included in the master problem in order to limit the amount of feasibility cuts.

5.2.2 Proposed algorithm

Finally, the optimisation problem is written in equations (5.25)-(5.27). Figure 5.8 shows a general diagram of the proposed method and algorithm 1 details an implementation path.

1. The master problem (y is optimised)

$$\begin{aligned} \mathcal{C}^* = \underset{y\in Y,\zeta}{\text{minimise}} \quad & f_2(y) + \zeta \\ \text{subject to} \quad & G(x,y) \leq 0 \\ & H(x,y) = 0 \\ & \sum_{j\in\mathfrak{J}^i}\left(1-y_j^h\right) + \sum_{j\notin\mathfrak{J}^i} y_j^h \geq 1 \qquad \forall i = 1\dots I^{fea} \\ & \mathcal{V}(\bar{y}^i) + \langle \lambda^i, y - \bar{y}^i\rangle - \zeta \leq 0 \qquad \forall i = 1\dots I \end{aligned} \tag{5.25}$$

   where $\zeta : \mathbb{R}^{3NT} \to \mathbb{R}$ is the cost of the second stage problem, I^{fea} are the iteration that generated infeasible solutions, and I includes all iterations, with both feasible and infeasible solutions.

   Let y^I be the solution of the master problem (5.25), the algorithm converges when equation (5.26) is satisfied, where η is a predefined tolerance.

$$\mathcal{V}(y^I) - \check{\mathcal{V}}(y^I) \leq \eta \tag{5.26}$$

2. The slave problem (x is optimised for $\bar{y}^i \in \{0,1\}^{3NT}$ fixed)

$$\begin{aligned} \mathcal{V}(y) := \inf_{x\in X, w\in Y} \quad & f_1(x) \\ \text{subject to} \quad & G(x,w) \leq 0 \\ & H(x,w) = 0 \\ & w = \bar{y}^i \\ & \underline{q} - q_m^\ell(\bar{y}_{-m}^i) - \langle s_m^\ell(\bar{y}_{-m}^i), x - x^\ell\rangle \leq 0 \quad \forall \ell = 1\dots L, \forall m = 1\dots M. \end{aligned} \tag{5.27}$$

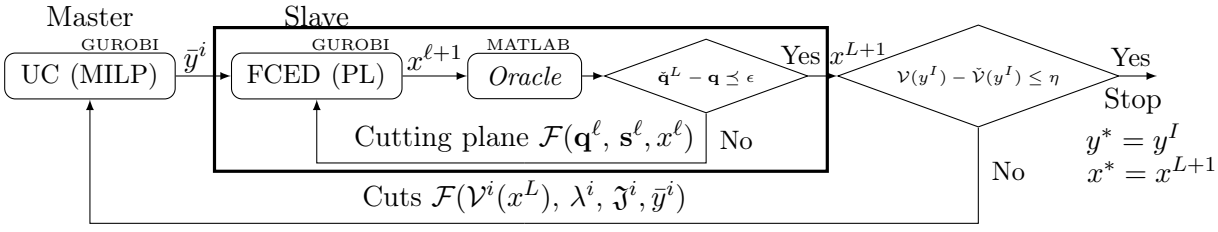

Figure 5.8: General diagram of the proposed FCUC formulation

Initialisation;
1: Define $\epsilon \geq 0$, $MIPgap \geq 0$, $\eta \geq MIPgap + \epsilon$, $AOC \geq \eta$, L^{max}, I^{max};
2: Solve model (5.9) for $M = 0$ and get y^1, x^1 and $\mathcal{C}^1$;
3: Call the oracle and get $q_m(x^1, y^1_{-m})$ and $s_m(x^1, y^1_{-m})$;
if $\underline{q} - q_m(x^1, y^1_{-m}) \leq 0 \quad \forall m = 1, \dots M$ **then**
  4: return $x^* = x^1$, $y^* = y^1$ and $\mathcal{C}^* = \mathcal{C}^1$;
else
  5: Set $\mathcal{C}^{low} \leftarrow \mathcal{C}^1(1 - MIPgap)$, $I = 0$, $I_{fea} = 0$ and $flag$ =false;
  while $flag$ =*false* & $I \leq I^{max}$ **do**
    6: $I = I + 1$;
    if $I > 1$ **then**
      Master problem;
      7: Solve model (5.25) and get y^{I+1};
      8: Solve model (5.27, $M = 0$) at y^{I+1} and get x^{I+1};
      9: Call the oracle and get $q_m(x^{I+1}, y^{I+1}_{-m})$ and $s_m(x^{I+1}, y^{I+1}_{-m})$;
    end
    10: Set $flagSlave$ =false, $L = 1$ and $x^1_s = x^I$;
    while $flagSlave$=*false* & $L \leq L^{max}$ **do**
      Slave problem;
      11: Attempt to solve model (5.27) at y^I and get x^{L+1}_s;
      if *model (5.27) is optimal* **then**
        Frequency Cutting Plane Model;
        12: Call the oracle and get $q_m(x^{L+1}_s, y^I_{-m})$, $s_m(x^{L+1}_s, y^I_{-m})$;
        13: Compute $\check{q}^L_m(x^{L+1}_s) = \min_{1 \leq \ell \leq L} \left\{ q^\ell_m + \langle s^\ell_m, x^{L+1}_s - x^\ell_s \rangle \right\}$;
        Slave stopping test;
        if $\check{q}^L_m(x^{L+1}_s) - q_m(x^{L+1}_s, y^I_{-m}) \leq \epsilon$ **then**
          14: $flagSlave$ =true;
          15: Set $\mathcal{V}^I = \mathcal{V}^{L+1}$, $\lambda^I = \lambda^{L+1}$, $\mathcal{C}^{up} \leftarrow \min_{1 \leq i \leq I} \left\{ \mathcal{V}^i + f_1(y^i) \right\}$;
          Master stopping test;
          if $I > 1$ **then**
            16: $\check{\mathcal{V}}^I(y^I) = \max_{1 \leq i \leq I-1} \left\{ \mathcal{V}^i + \langle \lambda^i, y^I - y^i \rangle \right\}$;
            if $\mathcal{V}(y^I) - \check{\mathcal{V}}^I(y^I) \leq \eta \mathcal{C}^{low}$ **then**
              17: $flag$ =true;
              18: return $x^* = x^{L+1}_s$, $y^* = y^I$ and $\mathcal{C}^* = \mathcal{V}^I + f_1(y^I)$;
            end
          end
        else
          19: $L = L + 1$;
        end
      else
        20: $flagSlave$ =true;
        21: $I_{fea} = I_{fea} + 1$, $y^{Ifea}_{infeasible} = y^I$;
        22: Solve model (5.27) at y^I for $M = 0$ and get $\mathcal{V}^I$ and λ^I (sub-optimality cut);
      end
    end
  end
end

Algorithm 1: Proposed method

5.2.3 Numerical implementation

In this section a day-ahead schedule is computed with the proposed FCUC model in order to illustrate its behaviour. The performance of the algorithm is analysed from two perspectives. First, the effectiveness and the additional security cost of the slave problem is examined for a feasible candidate solution, emphasising the accuracy of the cutting plane model of the frequency nadir ($\check{q}_m$). Then, the cutting plane model of the slave problem cost function ($\check{\mathcal{V}}$) is discussed to examine the convergence properties of the global algorithm.
The selected load profile corresponds to the week day already discussed in chapter 2, without any variable renewable sources (V-RES). It is recalled that the test system consists of 18 thermal units of different technologies. The base units are coal fired and has been denoted with the ID numbers 11 to 14. Then, there are 3 types of heavy fuel units, represented by units 1-2, 3-8, and 9-10 respectively. Finally, units 15-18 are the peaking diesel units. Their characteristics and technical limits are described in appendix E.
For the purposes of this section, ϵ and the $MIPgap$ are set to $1e^{-3}$, η is fixed to $2e^{-3}$ and the maximal acceptable over cost (AOC) at the slave level solution is defined by η. This means that if the total cost of a feasible point $\tilde{x}$ ($\mathcal{C}(\tilde{x},\bar{y}) = \mathcal{V}(\tilde{x}) + f_2(\bar{y})$) provided by the slave problem is less than 0.2% higher than $\mathcal{C}^1$, the algorithm is stopped. In this case, $\tilde{x}$ and $\bar{y}$ are considered to be the (optimal) solution of the complete FCUC problem.
The initial day-ahead schedule (y^1,x^1,$\mathcal{C}^1$) is obtained by solving model $\mathfrak{M}_0$ (line 2 in algorithm 1). Simulation results were provided in section 2.4 and are recalled in figure 5.9. The cost ($\mathcal{C}^1$) is considered to be 1 per unit.

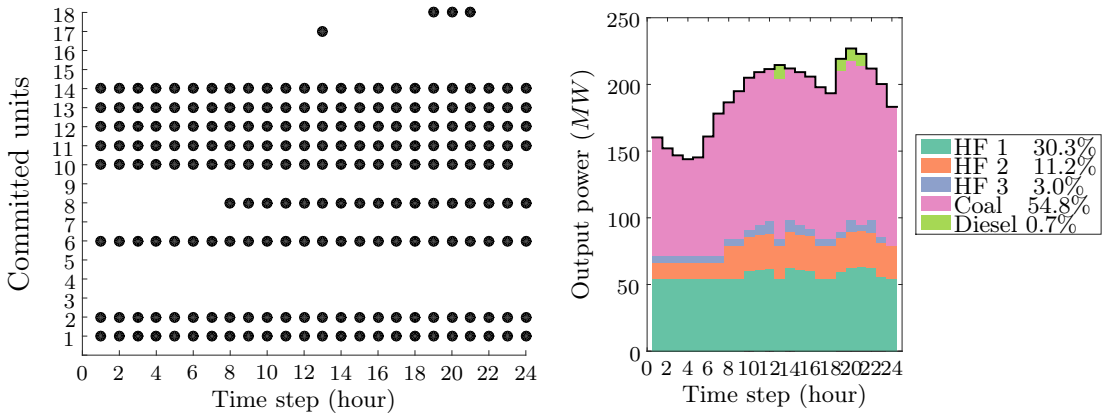

(a) Schedules (y^1) (b) Dispatch (x^1)

Figure 5.9: UC solution for a week day with dynamic allocation of reserve (model $\mathfrak{M}_0$)

Then, the oracle is called (line 3), which means that the frequency nadir $q_m(x^1, y^1_{-m})$ and its subgradient $s_m(x^1, y^1_{-m})$ are computed for every possible outage and for all time steps. Results for the frequency nadir are shown in figure 5.10 through a box plot representation. For each time step, the average, maximal and minimal values are indicated. A frequency threshold ($\underline{q}$) is set to $48.9Hz$ for illustrative purposes.

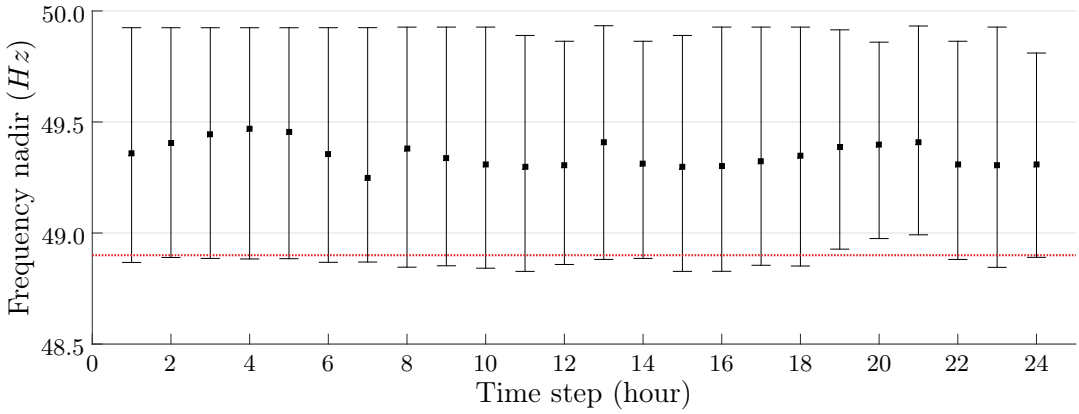

Figure 5.10: Frequency nadirs by time step (q_m) for the initial candidate solution (x^1, y^1)

Figure 5.10 shows that almost all the worst contingencies by time step entail a frequency nadir lower than the acceptable value (except from time steps 19-21). Therefore, line 10 is executed, and the slave problem (5.27) is solved for $L = 1$ in order to obtain a second dispatch x^{L+1} for the same commitment decision vector (y^1) shown in figure 5.9a.

Slave problem redispatch

The new dispatch and primary frequency response is depicted in figure 5.11. It is observed that the lower frequency nadirs start to evolve thanks to slight changes in the dispatch.

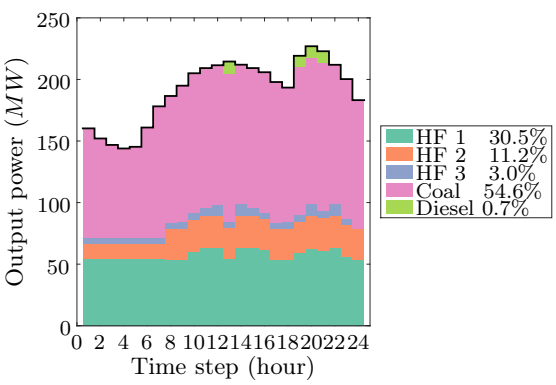

(a) Dispatch (x^2)

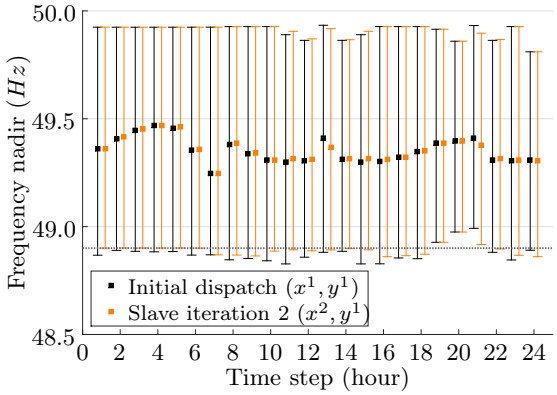

(b) Frequency nadirs (q^2)

Figure 5.11: First iteration of the slave problem (x^2 and q^2)

Figure 5.12 shows the evolution of the cost and the minimal frequency nadir of each time step by iteration. The first candidate solution $(\bar{y})$ turned out to be feasible and the slave problem converged after 8 iterations. The additional cost due to the frequency constraint is less than 0.1%. Therefore, in this case the algorithm can be stopped.

The final dispatch is presented in figure 5.13. The dispatch changes are insignificant from an energy mix perspective, but the frequency nadirs are kept above the security threshold.

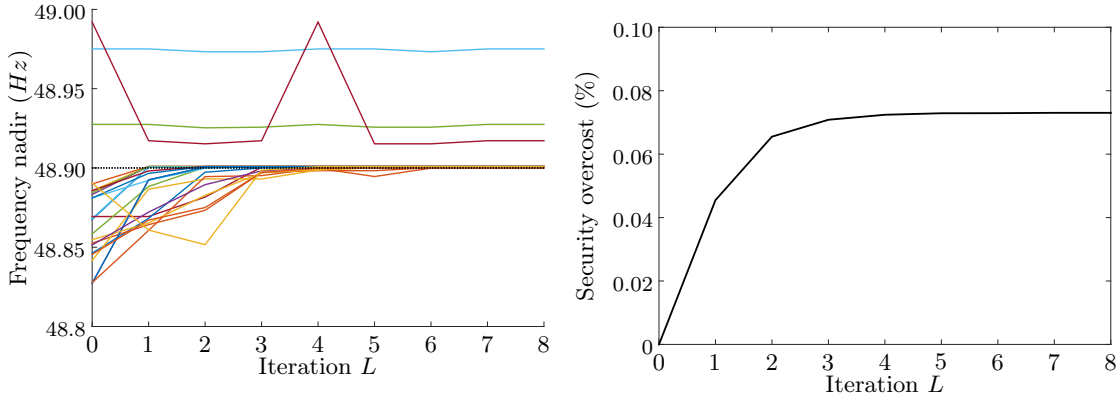

(a) Minimal frequency nadir by time step

(b) Dispatch cost

Figure 5.12: Evolution of the minimal frequency nadirs and cost with slave iterations

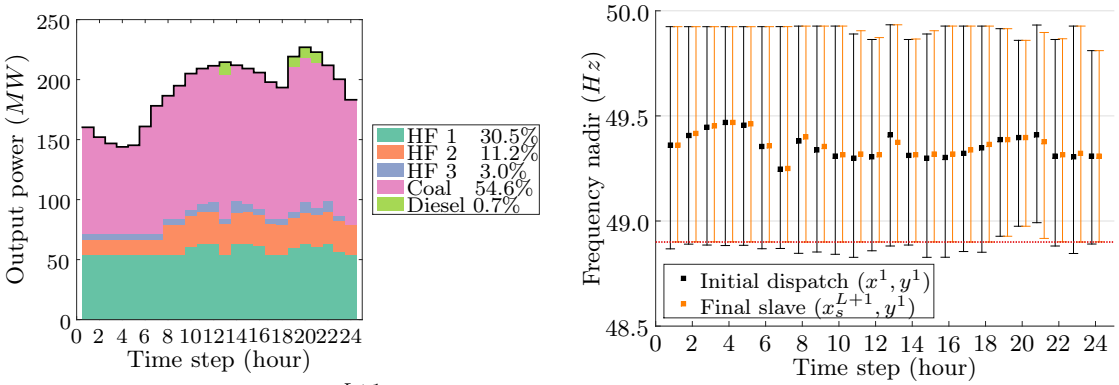

(a) Dispatch (x^{L+1})

(b) Frequency nadirs (q^{L+1})

Figure 5.13: Last iteration of the slave problem (x^{L+1} and q^{L+1})

To conclude, the cutting plane model of the frequency is accurate, converges fast, and entails a low additional security cost.

Comparing with indirect constraints. In this paragraph a comparison with the indirect constraints described in chapter 4 is introduced. As aforementioned, for the purposes of illustration the frequency threshold has been tightened to $48.9Hz$. It should be noticed that the $ROCOF$ constraint for instance (model $\mathfrak{M}_5$) is indeed able to ensure that the frequency nadir is kept above $48.9Hz$ for any single outage, and every time step of the annual time series provided in appendix E for scenario 0 (no PV generation), if the maximal frequency gradient ($|ROCOF^{max}|$) is set to $0.55Hz/s$. However, this would entail a additional security cost larger than 5% of the annual generation cost (see figure 4.10).
For the moment, let us consider only the instance presented in figure 5.9b. For this specific load profile, a $|ROCOF^{max}|$ of $0.7Hz/s$, which entailed an additional cost of 2%, suffices to ensure that no periods with insufficient dynamic response (PIDR) appear. The results are presented in figure 5.14.

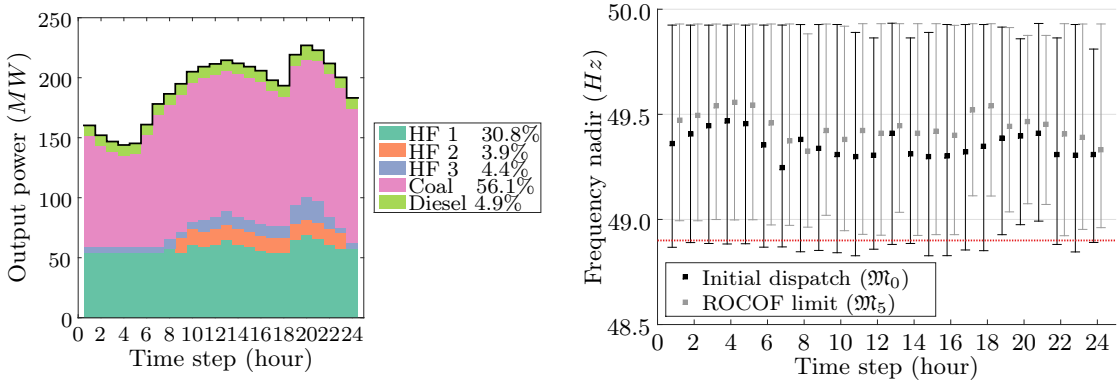

(a) Dispatch

(b) Frequency nadirs

Figure 5.14: Solution for typical week day using model $\mathfrak{M}_5$ ($|ROCOF^{max}| = 0.7Hz/s$)

Although the constraints proposed in the literature may be able to achieve day-ahead schedules that naturally provide an acceptable transient response, these schedules are not optimal because the indirect constraints do not represent the complexity of the underlying processes and end up over-scheduling primary frequency regulation resources at high security cost. Indeed, the solution proposed by the slave problem, within the proposed decomposition approach, satisfies the security constraint at an additional cost 10 times lower than the feasible point obtained with the ROCOF constaint.

In addition, indirect constraints may become ineffective in some other instances. Finally, they might overlook feasible points, in the sense that it is not possible to generate a schedule that respects all the constraints, including the indirect security one (*e.g.*, the inertia), while in practice there is a schedule able to respect the classic constraints, while keeping the frequency nadir above the predefined threshold for any single outage. The next section shows that the master problem is able to find severable feasible points when the security constraint is further tightened, while the ROCOF constraint becomes infeasible.

Comments about the subgradient calculation. The subgradient is obtained by considering an incremental and decremental power of $\Delta x = 1e^{-5}$ for each surviving unit j when considering the outage of each unit $k(m)$ at each time step $h(m)$. Then, the computation of the frequency nadir and its subgradient is done only for the committed units ($N^i_{on,h} = \sum(\bar{y}^i_h)$). Therefore, the MMR-ROSFR model is run $2\sum_{h=1}^{T} N^i_{on,h} \times (N^i_{on,h} - 1)$ times in order to compute the subgradient. For illustrative purposes, let us consider that ten units are committed by time step ($N^i_{on,h} = 10 \;\; \forall h = 1, \ldots, T,$) and that the optimisation horizon is set to 32 hourly steps.

Consequently, the oracle requires more than 6000 runs of the MMR-ROSFR model for building the first cutting plane model, based on $(q_m(x^1, y^1_{-m}), s_m(x^1, y^1_{-m}))$. On average, the computation of a frequency nadir takes about 25 miliseconds[1] (one MMR-ROSFR run).

[1] Hp EliteBook Workstation, Intel Core i5, 2.8GHz with 16GB of RAM.

Hence, the computational time of the first oracle is more than 2 minutes. In this work, the parallel toolbox of MATLAB was used, which enables increasing the computational resources up to 12 workers. When considering 4 threads, the oracle CPU time is reduced to less than 1 minute[1]. This time is further reduced when more resources are available. In the remainder of this work this time is brought down to 2-5 seconds[2]. In addition, the subgradient is computed only if the specific contingency produces a frequency nadir lower that the predefined threshold ($q_m < \underline{q}$). Thus, the CPU time of the oracle diminishes as the algorithm progresses. This is illustrated in figure 5.15.

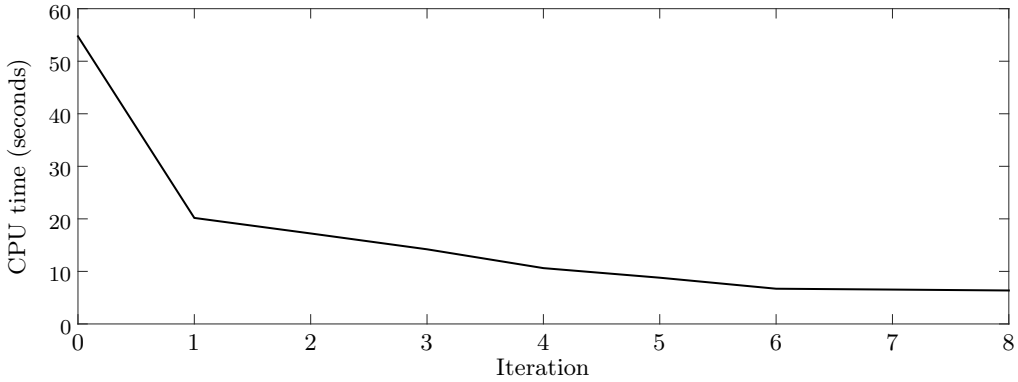

Figure 5.15: CPU time of the oracle by iterations

Comments about the concavity hypothesis. The mapping q_m is given by a "black box" model. Therefore, an analytical verification of its concavity seems unlikely. This section provides a practical analysis that illustrates why this hypothesis is reasonable. Let us consider a snapshot of the test system at one specific hour of figure 5.9b (13 hour). The power output and detailed reserve allocation of this instant were already presented in previous chapters and are recalled in figure 5.16a.

It is observed that, on the one hand, unit 14 does not participate to the primary frequency regulation, and that units 12 and 13 have an allocated primary reserve below their maximal capacity. On the other hand, the peaking unit 17 is committed to its minimum stable generation level (MSG) due to its high variable cost.

Now, let us imagine that part of the power allocated in units 12-14 is displaced to unit 17 in order to maximise the allocated primary reserve, *i.e.*, to make unit 12-14 (further) participate to primary frequency regulation, as represented in 5.16b. Then, the outage of unit 1 is simulated considering both initial conditions. Results are presented in figure 5.16c. It is observed that the frequency nadir can be significantly improved, in this case by increasing the total available reserve. However, this action has an impact on the dispatch cost. Indeed, the dispatch presented in the top-right side of figure 5.16 is 8% more expensive that the one proposed by model $\mathfrak{M}_0$ (left side).

[2] 2x8 cores Intel(R) Xeon(R) CPU E5-2690 @ 2.90GHz and 64Gb of RAM

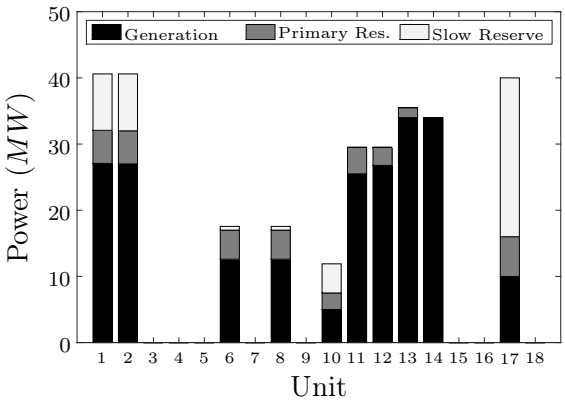

(a) Optimal dispatch with model $\mathfrak{M}_0$

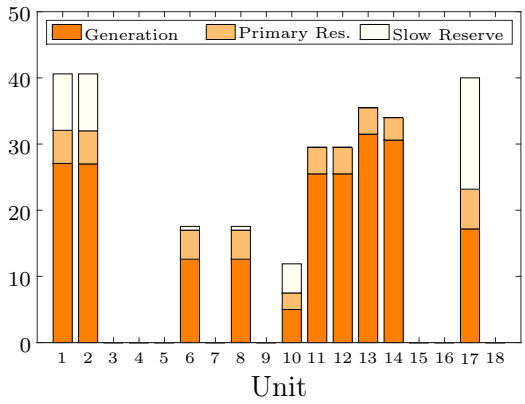

(b) Manually adjusted dispatch

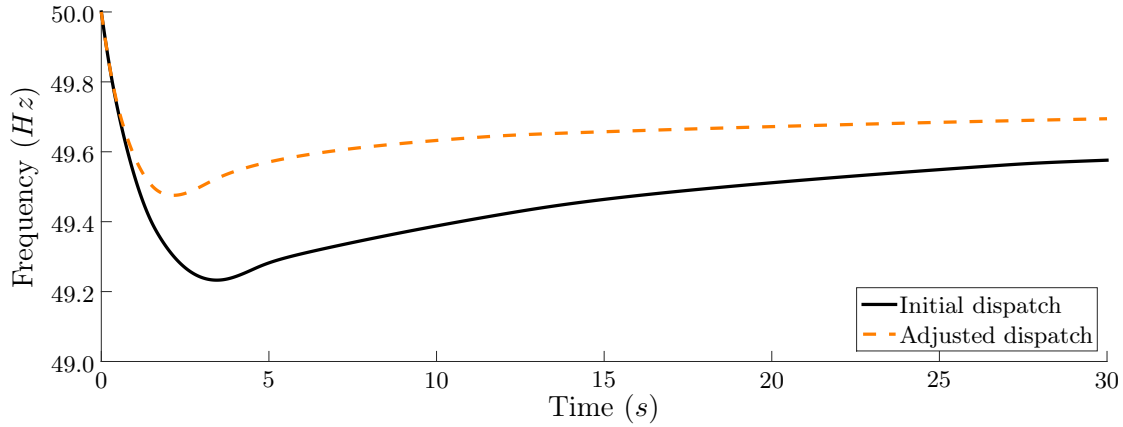

(c) Frequency evolution following the outage of unit 1 at hour 13

Figure 5.16: Evolution of the primary frequency response with dispatch changes

Moreover, the main question of how much more reserve should be cleared remains. In order to get an insight on this issue, figure 5.17 compares the cost increase and the frequency nadirs following the same contingency for different intermediate dispatches between figures 5.16a and 5.16b. The abscissa represent the amount of power that is displaced from units 12-14 to unit 17.

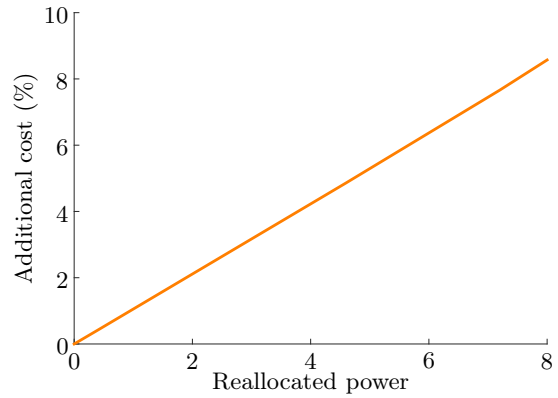

(a) Dispatch additional cost

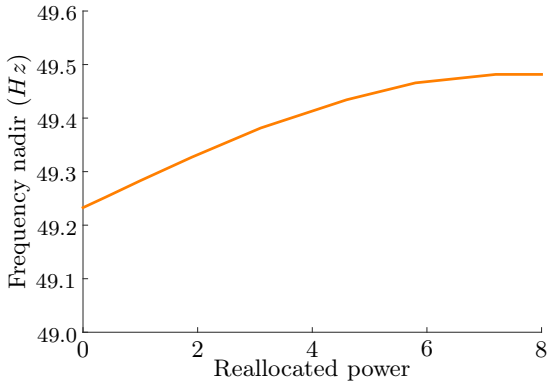

(b) Evolution of q_m

Figure 5.17: Cost and benefit of a gradual (manual) dispatch adjustment

The reader would agree that figure 5.17b does inspire a concave hypothesis on the frequency nadir (q_m) with respect to the allocated power (x). In order to verify this hypothesis, the cutting plane errors ($CPerr$), given by equation (5.15) over the iterations are examined. If q_m is concave, the cutting plane model is always above the function ($\check{q}_m^L(x^{L+1}) > q_m(x^{L+1})$). If $\check{q}_m^L(x^{L+1}) - q_m(x^{L+1})$ becomes negative, the cutting plane model cuts the function, *i.e.*, it is below the function. This may be caused by the chosen subgradient approximation or because the function is not actually concave. Figure 5.18 shows the distribution of the normalised $CPerr$ for 3 different iterations.

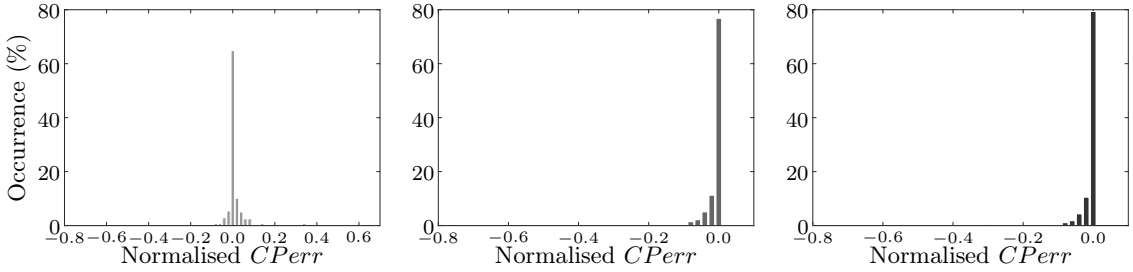

(a) Iteration 1 (b) Iteration 4 (c) Iteration 8

Figure 5.18: Normalised errors of the cutting plane model ($\frac{\check{q}_m^L(x^{L+1}) - q_m(x^{L+1})}{|q_m(x^{L+1})|}$)

It is observed that in fact the different frequency nadirs may not be all jointly concave. In some rare cases, the error may be significant, but in general it remain small and tend to converge toward zero. But what are the implications of this issue?

On the one hand, this means that the real (simulated) frequency nadir (q_{m1}) is higher than the constrained value since $q_{m1} > \check{q}_{m1} > \underline{q}$. This means that the security threshold is absolutely respected, even in the cases when the concavity hypotheses does not hold. On the other hand, this means that the frequency nadir has been reduced "beyond" the requirement, which would compromise optimality. However, as the additional security cost remains low enough, this will not be an issue.

In practice, this behaviour may be explained by the fact that another cutting plane model (the outage of a different unit, $\check{q}_{m2}$) is forcing the modification (reduction) of the output power on the unit $k(m_1)$ at $h(m_1)$ which makes the frequency nadir following the outage of unit $k(m_1)$ "better" than expected. But in reality, this is not suboptimal, this action is absolutely necessary to respect constraint $\check{q}_{m2} > \underline{q}$. Figure 5.13b shows that the worst contingency for each time step is limited the the frequency threshold ($\underline{q}$) and no more.

The master problem

For a frequency threshold ($\underline{q}$) of $48.9Hz$ the first candidate solution turned out to be feasible and optimal since the additional cost to ensure power system security was within the $MIPgap$ of the initial dispatch. In this case, solving the master problem makes no sense since it is unlikely to find a better point.

Thus, in order to illustrate the performance of the master problem, the frequency threshold ($\underline{q}$) must be tightened, until the first candidate solution becomes infeasible or significantly more expensive. For $\underline{q} = 49.0Hz$, the slave problem becomes infeasible, which means that there is not any power allocation combination ($\tilde{x}_s^1$) capable of satisfying the frequency nadir constraints for the first candidate decision vector (y^1). Then, the cost of this point is defined as a lower bound of the solution, and a feasibility (and a sub-optimality) cut are added to the master problem in order to compute a new candidate solution (y^2).
However, with only one sub-optimality cut, the master problem has limited information about the dispatch cost ($f_1(x)$). The candidate solution has minimised almost exclusively the fixed, start up and shut down costs ($f_2(y)$), and although the slave problem is feasible at the new candidate solution ($\exists\ \tilde{x}_s$ at $\bar{y}^2$), its cost is considerably high ($\mathcal{C}_2 = \mathcal{V}(\tilde{x}_s) + f_2(y^2) \gg \mathcal{C}_1$). In the example under consideration the scheduling and dispatch cost are almost 50% higher than the lower bound.
Therefore, an optimality cut is added and the algorithm proposes a third candidate solution, and so on. Figure 5.19 presents the dispatch (slave) cost $\mathcal{V}$ and the total cost ($\mathcal{C}$) of all proposed solution. **The algorithm was stopped after 500 iteration, but the convergence criterion was not reached**. For illustrative purposes the slave cost was set to zero whenever the slave problem was infeasible. A considerable number of candidate solution (y_i), more than 40%, are infeasible at the slave problem level ($\nexists\ \tilde{x}_s$ at $\bar{y}_i$). In addition, the objective function (the cost) exhibits important oscillations.

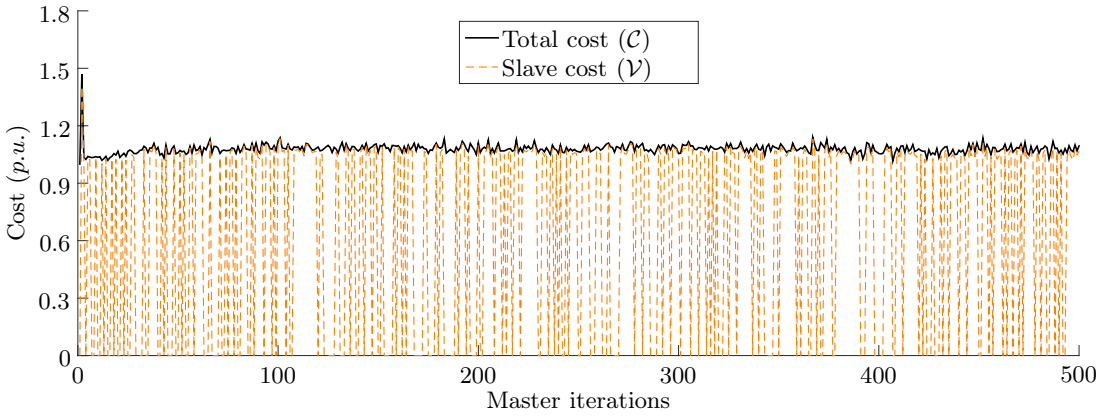

Figure 5.19: Evolution of the master problem solution with iterations

In order to improve readability and interpretation, figure 5.20a presents the additional security cost for the 294 feasible solutions. It is observed that the cost of the candidate solutions increases between 2% and 14% with respect to the lower bound.
From a practical point of view, two feasible points were found that eliminate the risk of UFLS (at 49 Hz) following any possible unit outage for security additional cost of about 2%. Figure 5.20b shows the frequency nadirs for schedule proposed at iteration 12 (6th feasible point) which is the best candidate solution and provides an upper bound.

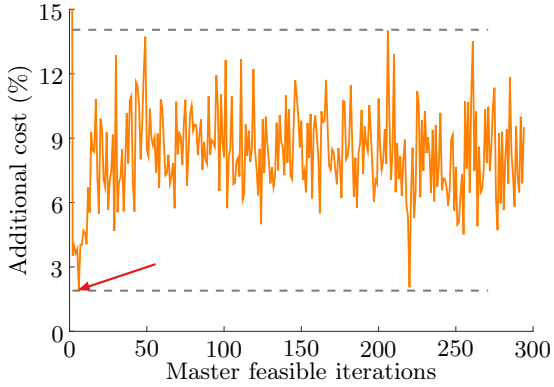

(a) Security cost of feasible points

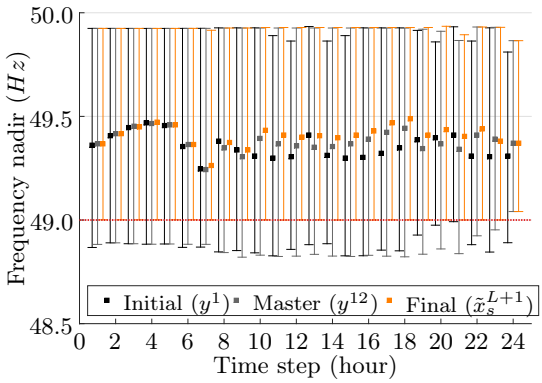

(b) Frequency nadirs at iteration 12

Figure 5.20: Cost and effectiveness of the feasible candidate solutions

From an algorithmic perspective, **the master problem did not converge within the allocated budget** (500 iterations). Figure 5.21 shows some variables that define the convergence properties of the algorithm, which is extremely slow. Figure 5.21a shows the evolution of the slave problem cutting plane model ($\check{\mathcal{V}}$), which exhibits an undesirable flat behaviour. Figure 5.21b shows the evolution of the normalised stopping criterion ($\frac{\mathcal{V}-\check{\mathcal{V}}}{\mathcal{C}^1}$).

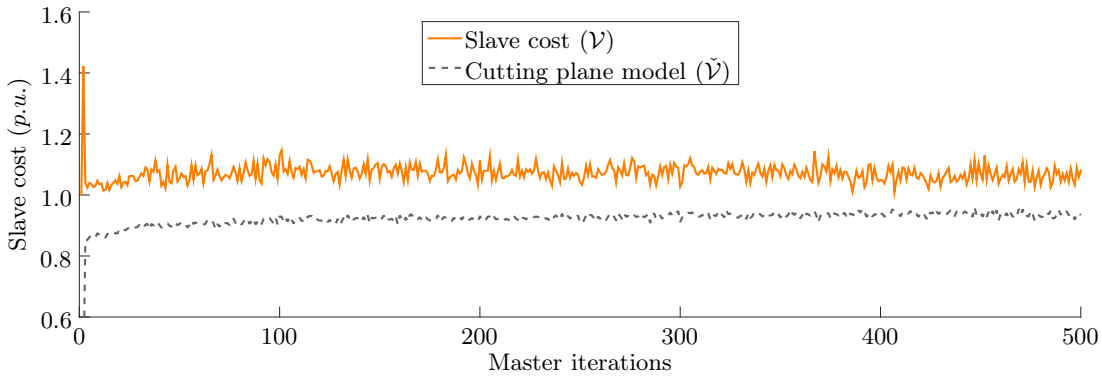

(a) Evolution of the slave cutting plane model with iterations

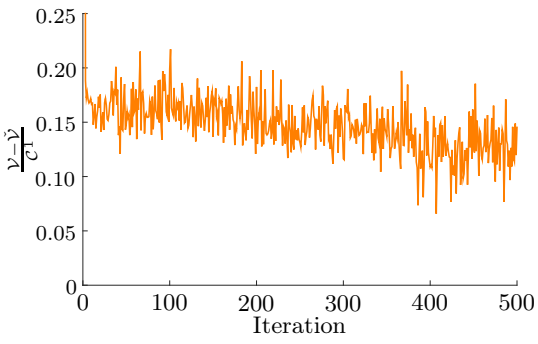

(b) Stopping criterion

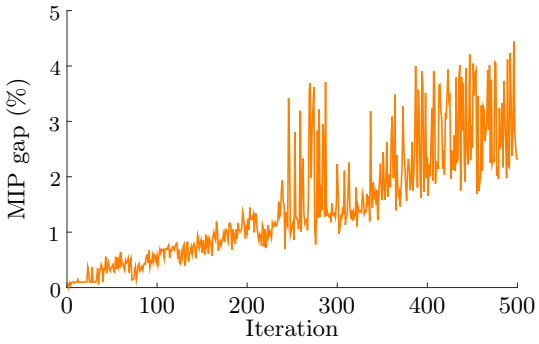

(c) MIPgap

Figure 5.21: Master problem convergence

The error of the cutting plane model oscillates between 6% and 20%, which does not provide meaningful information about the bounds of the solution.

Finally, figure 5.21c depicts the evolution of the MIP gap with the iterations. It is observed that the quality of the solution declines with iterations due to the increasing complexity of the optimisation model. After 500 iteration, no better solution has been found and the predefined $MIPgap$ (0.1%) has not been achieved before the time limit of 10 minutes is reached. After 250 iterations the error of the cutting plane model is around 15% and the $MIPgap$ exceeds the additional cost of the best candidate solution (2%), which prevent the master problem from finding a better solution.

Nonetheless, it is highlighted that the master problem is able to find several feasible points while other constraints, such as the ROCOF constraint, do not provide any schedule that satisfies the tight security threshold (49 Hz) set to the test system in this section. Moreover, a reasonable solution was found in a reduced number of iteration.

Figure 5.22 presents the distribution of the additional cost obtained at the slave problem level regarding the candidate solution proposed by the master problem at iteration i ($\Delta\mathcal{C}^i = \mathcal{C}(x_s^{L+1}, y^i) - \mathcal{C}(x_s^1, y^i)$). This value is normalised with respect to the cost of the initial (infeasible) solution, *i.e.*, the lower bound ($\mathcal{C}^1 = \mathcal{C}(x^1, y^1)$). It is observed that the additional cost generated by the slave problem to satisfy the frequency nadir constraints is lower than 0.5% for all the 294 feasible candidate solution.

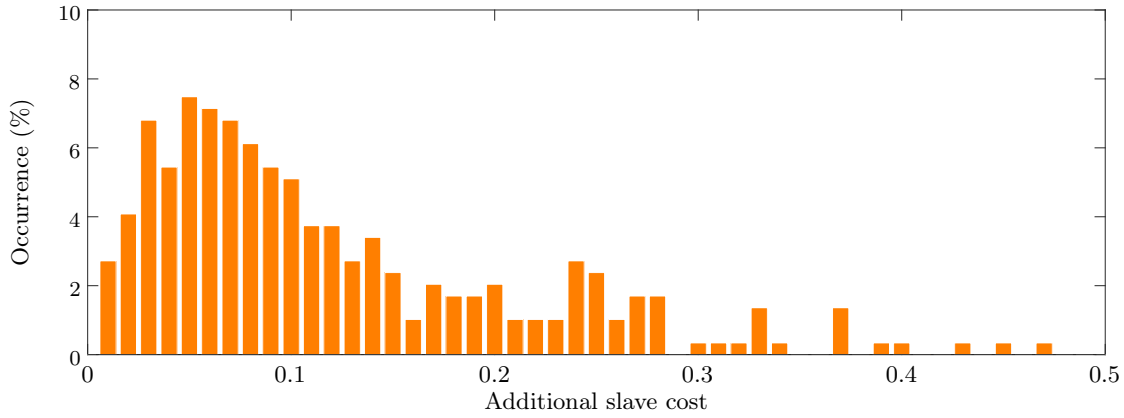

Figure 5.22: Distribution of additional cost at the slave problem level ($\frac{\mathcal{C}(x_s^{L+1},y^i)-\mathcal{C}(x_s^1,y^i)}{|\mathcal{C}(x^1,y^1)|}$)

It is worth emphasising the practical interest of using a cutting plane model to represent the security constraint. Although the concavity hypothesis on mappings q_m is not fully verified, which causes and implications should be further investigated, the solution are 100% effective (with respect to the given Oracle) and the cost is quite low (considering a $MIPgap$ of 0.1%).

Computational details. On the downside, it is acknowledge that the computation time of all those candidate solution is not compatible with real time operation. For instance, the CPU time of the computation of the fist 12 candidate solutions is about 45 minutes[3] (in average less than 4 minutes by master iteration, including the solution of each slave problem). It must be noted that this work aimed to test the interest of the method and not to develop a robust implementation. CPU time can be brought down partially with appropriate tools and resources.
Here, the computation of the frequency nadir cutting plane model was parallelised using the MATLAB *parfor*. Significant time reduction at the slave problem level are already achieved with respect to figure 5.15. Figure 5.23 presents the oracle CPU times for all the 294 feasible solutions. In addition, this figure illustrate that the frequency nadir model does converge fast. All identified candidate solution converged in less than 20 iterations.

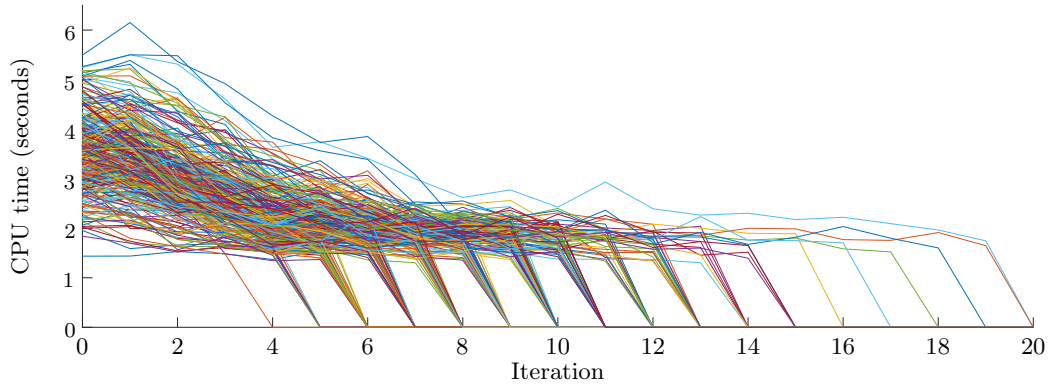

Figure 5.23: CPU time of the oracle by iterations for all feasible candidate solutions

The main issue of the method remains the slow convergence of the master algorithm. In order to tackle this issue, the last pages of this work are consecrated to the investigation of the potential benefits of bundle-like stabilisation methods [184].

5.3 Quadratic stabilisation of the Benders' method

The Benders' method is known to have slow convergence, therefore an important number of iterations may be needed. However, the preliminary results presented in section 5.2.3 show that the quality of the candidate solution degrades fast with the number of iterations. Different causes could explain this phenomenon and diverse solutions can be proposed.
On the one hand, each iteration provides a (sub)-optimality cut which enlarges the size of the master problem. Moreover, given the limited information provided by the sub-optimality cuts about the $\mathcal{V}$ space, a cutting plane model of the dispatch cost that is accurate enough may be difficult to build.

[3] 2x8 cores Intel(R) Xeon(R) CPU E5-2690 @ 2.90GHz and 64Gb of RAM

On the other hand, inherent instability of bundle methods may cause the iterates to oscillate before arriving at the optimal solution. In this section a quadratic stabilisation is propose to reduce the iterates' oscillations.

In non smooth optimisation, bundle methods have been proposed to stabilise cutting plane models [163]. The general idea is to encourage the next iterate to stay close to the best one, while decreasing the cutting plane model objective.

In this section a level-master problem [185], described in equation (5.28) is proposed to speed up convergence of the FCUC problem. The objective function is now defined by the distance between the candidate solution and the best feasible point found at each iteration, which is called "stability center" and is denoted by $\hat{y}$. The operational cost is included as a constraint. It is enforced that the cost function at the candidate solution must be lower or equal to a certain level parameter, denoted c^i_{lev}.

$$\begin{aligned} c^* = \underset{y\in Y,\zeta}{\text{minimize}} \quad & \frac{1}{2}\left\|y-\hat{y}\right\|^2 \\ \text{subject to} \quad & f_2(y)+\zeta \leq c^i_{lev} \\ & G(x,y) \leq 0 \\ & H(x,y) = 0 \\ & \sum_{j\in\mathfrak{J}^i}\left(1-y^h_j\right) + \sum_{j\notin\mathfrak{J}^i} y^h_j \geq 1 \qquad \forall i = 1\dots I^{fea} \\ & \mathcal{V}(\bar{y}^i) + \langle \lambda^i, y-\bar{y}^i\rangle - \zeta \leq 0 \qquad \forall i = 1\dots I, \end{aligned} \tag{5.28}$$

The level parameter is calculated from equation (5.29) as a function of the upper and lower bounds of the solution and a parameter denoted γ (here set to 0.2).

$$\begin{aligned} c^i_{lev} =& c^i_{lb} + \gamma\Delta c, \\ \Delta c^i =& c^i_{ub} - c^i_{lb}, \end{aligned} \tag{5.29}$$

The upper bound (c_{ub}) is given by the cost of the best feasible iterate: $f_1(\hat{y}) + f_2(x^{L+1}_s)$, and c_{lb} is a lower bound of the level-master problem. It can be computed by solving a continuous relaxation or a "fast" MILP of the standard master problem. This latter consist in solving problem (5.25) with a low time limit (here 5 seconds). Then, $c^i_{lb} = \left(f_1(y^i_{fast}) + \zeta^i_{fast}\right)\left(1 - MIPgap^i_{fast}\right)$. The algorithm stops when $\Delta c^i < \eta\mathcal{C}^1$. Figure 5.24 illustrates these elements for both feasible and infeasible cases of problem (5.28).

The optimality gap is defined by Δc which is the distance between the lower and upper bound. It provides a guarantee that the solution is within these two values. The level parameter (c_{lev}) restraints the feasible domain. If the level-master problem (5.28) remains feasible, which means that the level parameter is above the slave cost cutting plane model, the closest point (y^3) to the current best iterated (y^1) is returned as the new candidate solution as shown in figure 5.24a.

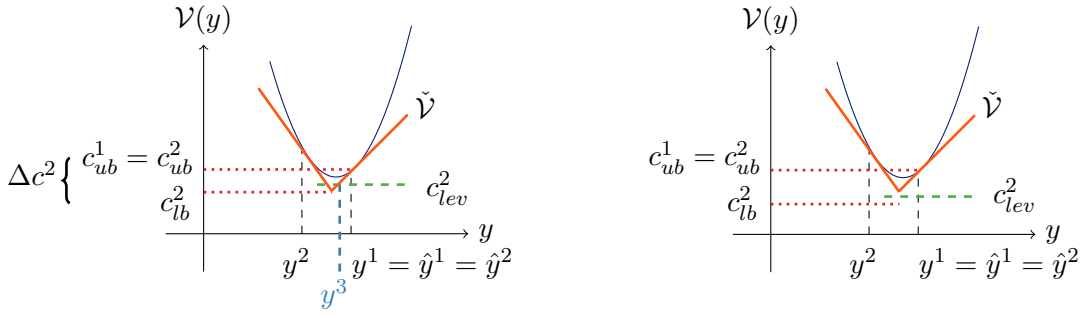

(a) Feasible case (b) Infeasible case

Figure 5.24: Illustration of the level-master principle

Otherwise, if the level parameter lays below the cutting plane model, as illustrated in figure 5.24b, the level-master becomes infeasible. In this case, c_{lev} provides a valid lower bound for problem (5.28) and c_{lb} can be actualised.

The level-master problem presented in (5.28) has a quadratic objective function and linear constraints, therefore, it has become a Mixed Integer Quadratic Programming (MIQP) problem. Nevertheless, since the optimisation variable y is binary, the master problem remains linear, since:

$$\begin{aligned} \|y - \hat{y}\|^2 &= \|y\|^2 - 2\langle y, \hat{y}\rangle + \|\hat{y}\|^2 \\ \|y\|^2 &= \sum_{j=1}^{N}\sum_{h=1}^{T}\left(y_j^h\right)^2 = \sum_{m=1}^{M} y_j^h \end{aligned} \tag{5.30}$$

The optimisation problem (5.28) can be rewritten as a linear problem as follows:

$$\begin{aligned} c^* = \underset{y\in Y,\zeta}{\text{minimize}} \quad & \left(\frac{1}{2}e - \hat{y}\right)^T y \\ \text{subject to} \quad & G(x,y) \leq 0 \\ & H(x,y) = 0 \\ & \sum_{j\in\mathfrak{J}^i}\left(1 - y_j^h\right) + \sum_{j\notin\mathfrak{J}^i} y_j^h \geq 1 \qquad \forall i = 1\dots I^{fea} \\ & \mathcal{V}(\bar{y}^i) + \langle \lambda^i, y - \bar{y}^i\rangle - \zeta \leq 0 \qquad \forall i = 1\dots I \\ & f_2(y) + \zeta \leq c^{lev}, \end{aligned} \tag{5.31}$$

where e is a standard unit column vector in $\mathbb{R}^{3NT}$ with all its components equal to one. Figure 5.25 compares the simulation results of the stabilised and the standard Benders' method. It is observed that the purple curve is below the orange one, which means that the stabilised approach is able to find better quality candidate solutions.

Figure 5.26 depicts the evolution of the slave cost cutting plane model with both formulations. It is observed that the undesirable flat behaviour of the slave cost cutting plane model ($\check{\mathcal{V}}$) is improved. Moreover, the evaluated dispatch cost ($\mathcal{V}$) is indeed diminished.

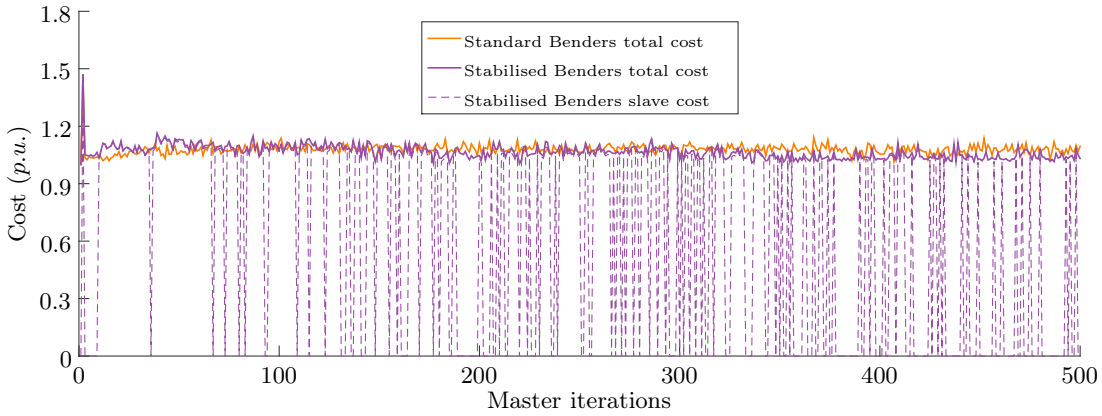

Figure 5.25: Comparison of the total cost of the master candidate solutions

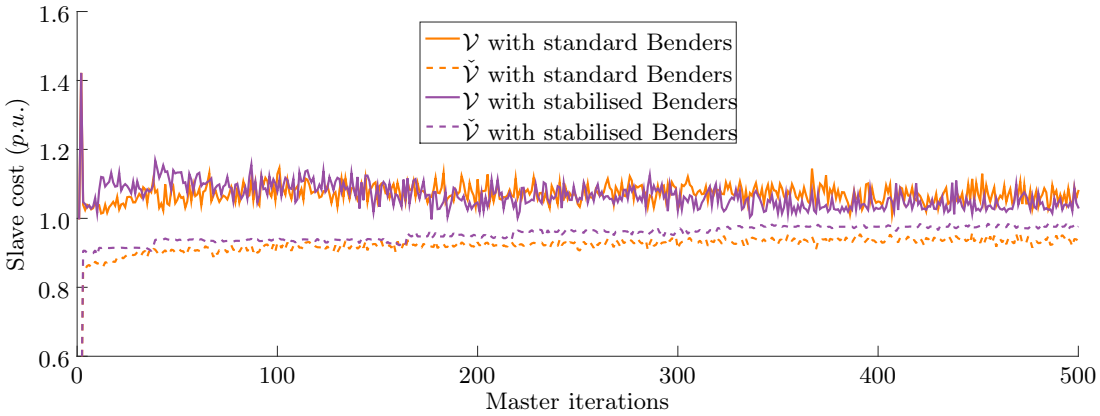

Figure 5.26: Comparison of the slave cutting plane model

Figure 5.27 examines the convergence properties of the algorithm. On the one hand, the stabilised method does progress faster towards an optimality guarantee, as illustrated in figure 5.27a, where the stopping criteria of both formulations are compared. On the other hand, the algorithm may spend a lot of time with a certain level (c^i_{lev}), unable to actually find a proper solution with the allocated CPU time budget (10 minutes), before getting an infeasibility guarantee and actualising the lower bound.

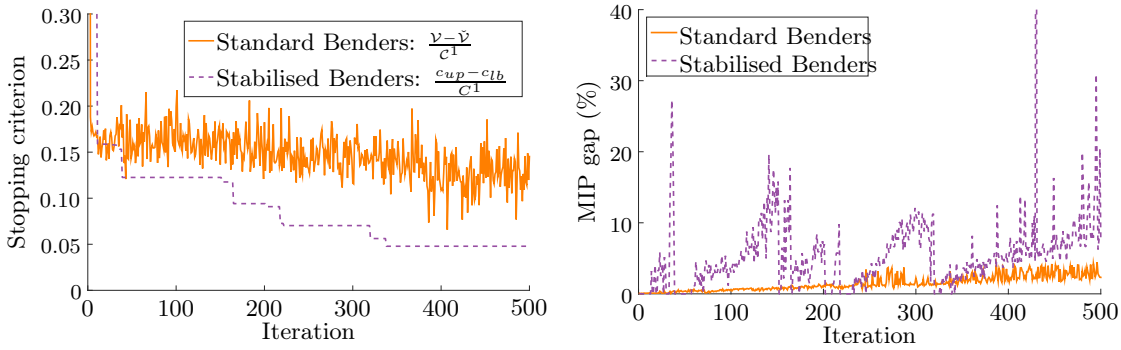

(a) Stopping criterion

(b) $MIPgap$

Figure 5.27: Master problem convergence for the stabilised formulation

This is deduced from the behaviour of the $MIPgap$ presented in figure 5.27b. It is observed that for the first c^i_{lev} the $MIPgap$ raises fast. At iteration 36 it almost reaches 30% because the first feasible point is found after several minutes, and only some seconds are in fact dedicated to optimising the problem. Then, at some point (iteration 38) the master problem became infeasible, which allows one to actualise the lower bound. This entails a reduction of the stopping criterion and the $MIPgap$. This process is repeated at iterations 164, 217 and 319 for instance. At these points, the $MIPgap$ drops, and better candidate solutions are, in general, proposed. For instance, the upper bound is actualised at iterations 221 and 337 because a better solution was found.

Finally, it is expected that this method also provides less infeasible points [184]. This feature is indeed verified for the first iterations. Before 100 iteration only 15 infeasible points are found, while with the standard Benders this value reaches 52. But unfortunately, as the algorithm progresses, the amount of candidate solutions that are declared infeasible increases, becoming slightly higher than for the standard Benders (212 vs. 206).

From a more practical point of view, figure 5.28 shows the additional security cost for the stabilised Benders regarding the standard formulation. It is observed that as the algorithm progresses the additional security cost associated to the frequency nadir constraint tends to decrease. Iteration 337 (which is the 238th feasible candidate solution) generates an additional security cost of 1.6%, which represents a cost reduction of 20% regarding the best candidate solution obtained with the standard formulation.

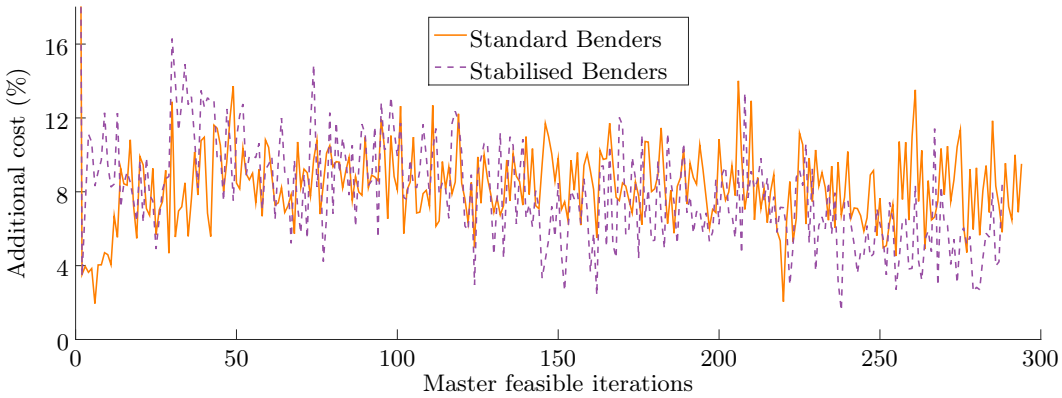

Figure 5.28: Security cost of feasible points

In conclusion, the stabilisation of the proposed FCUC formulation by bundle-like methods exhibits promising features, such as the better quality of the candidate solution, as well as the faster evolution of the stopping criterion towards the predefined threshold. However, **the level-master did not converge within the allocated budget** (500 iterations). From a practical perspective, the best feasible point identified is indeed more economical that the one found with the standard Benders' formulation, *i.e.*, it entailed an additional security cost of 1.6% instead of 2%.

It is recalled that indirect constraints are not able to find any feasible solution for the selected (tight) security threshold ($49Hz$). The main challenge remains the control of the $MIPgap$, which prevents the algorithm from converging fast. In a less constrained (more realistic) scenario, it is believed that the behaviour of the algorithm could be better, *i.e.*, it should be easer to find more good quality candidate solutions, however further investigation is required to backup such a statement.

Comments about the $MIPgap$ control. The parameter γ could be adjusted when the $MIPgap$ of a candidate solution becomes too bad. For instance, γ may be doubled (0.4) when the $MIPgap$ of the previous iteration is greater or equal to 10%. This action looses the level parameter (c_{lev}) for the next iteration in order to obtain better quality candidate solutions. Results for this case are presented in figure 5.29.

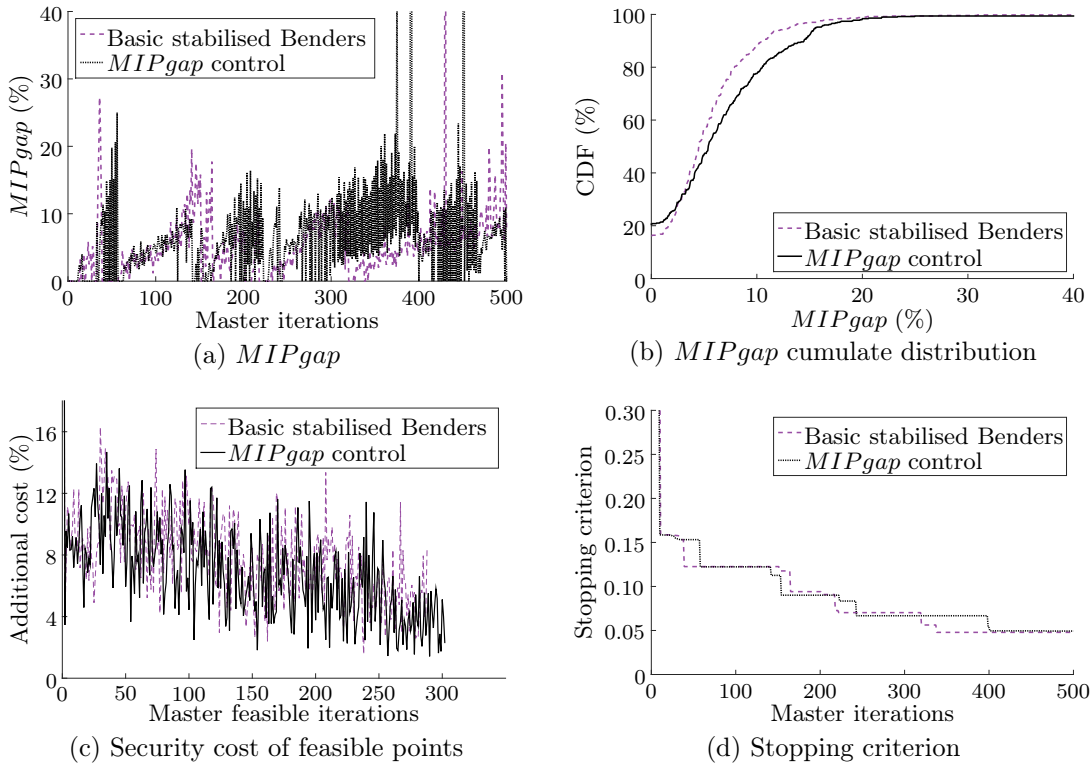

(a) $MIPgap$ (b) $MIPgap$ cumulate distribution

(c) Security cost of feasible points (d) Stopping criterion

Figure 5.29: Level-master problem convergence with $MIPgap$ control

It is observed the amount of candidate solution that converged to the predefined $MIPgap$ (0.1%) in the allocated time (10 minutes) increases (see figure 5.29b), although at some points the $MIPgap$ behaviour seems to decline (figure 5.29a). Moreover, the amount of feasible candidate solutions increases by 5% (from 288 to 302), and with it their quality. Figure 5.29c compares the additional security cost of the stabilised algorithm without and with $MIPgap$ control. It is observed that the black curve has some downward peaks, which means that several candidate solutions have low security cost.

Indeed, 11 candidate solutions exhibit a additional security cost lower than 2%. The best candidate solution entails a cost increase of 1.4 %, which represent and additional improvement of 10% for this specific example. However, the stopping criterion presents a similar shape in both cases. The evolution of the stopping criterion is shown in figure 5.29d. Finally, figure 5.30 illustrates the CDF of the additional cost for the three considered cases. More research on this topic is required.

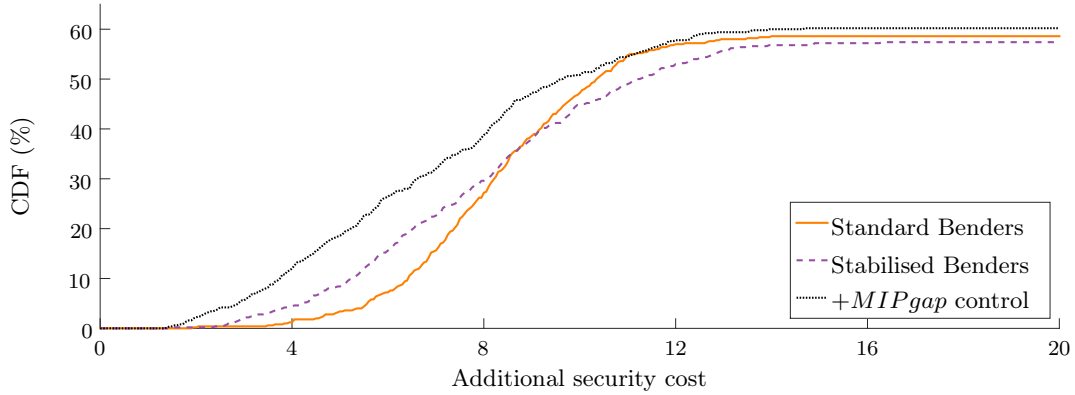

Figure 5.30: Stopping criterion

5.4 Conclusion

An original formulation for the FCUC problem, based on the Benders' method has been proposed. The FCUC has been decomposed in two subproblems. The slave problem is a multi-period FCED since only the dispatch cost is optimised and the frequency nadir constraints are enforced, through a cutting plane model, for fixed commitment decision. The master problem handles the binary variables and proposes candidate commitment decision vectors. In order to ensure that the initial problem is indeed solved, feasibility and optimality cuts are generated by the slave problem and are added to the master problem.

This innovating approach permits an accurate and simultaneous representation of all the dynamic parameters that determine the primary frequency response, while preserving the linear programming structure of the optimisation problem. Hence, the slave problem can be solved fast with available commercial solvers. If the initial candidate solution is feasible at the slave problem level, *i.e.*, a dispatch that satisfies the frequency nadir constraints can be computed, effectiveness is ensured. This means that the frequency nadir is kept above the security threshold for any single outage and all time steps. Indeed, at this level the solution is ϵ-feasible, for a frequency nadir mapping that is concave with respect to the committed units power outputs. Simulation results illustrated the interesting cost/benefit ratio of the proposed formulation that outperform the indirect methods discussed in the literature, although concavity could not be proved.

Optimality can be claimed if the additional security cost is lower or equal to the predefined $MIPgap$. Otherwise, an optimality cut is added to the master problem, which computes a new candidate solution until it is ensured that there is not another feasible point than satisfies the frequency nadir constraints at lower cost.

If a certain candidate point is infeasible at the slave problem level, a feasibility and a suboptimality cut are added to the master problem. Simulation results show that the master problem is able to provide several feasible points, some of them at reasonable cost, where existing indirect methods fails to compute at least one feasible solution.

However, the master problem exhibits slow convergence, due to the well-known tailing off effect of cutting plane methods. The master master problem did not converged with in the allocated budget (500 iteration and 10 minutes by iteration). Although several feasible points were found, the convergence criterion is still too large to claim optimality.

Therefore, the potential contribution of a bundle-like method in stabilising the FCUC problem were explored by introducing a level-master problem. Although the convergence properties were improved, the stopping criterion remained significantly higher than the required optimality gap (5% vs. 0.2%).

The formulation proposed in this work has pushed the boundaries of the existing trade-off between modelling and numerical tractability for the FCUC problem. The representation of the frequency nadir by its cutting plane model in the FCED model offers a significant breakthrough since it accounts for several aspects of the dynamic response that were historically neglected. In addition, different degrees of details can be considered in the Oracle, which provides the frequency nadir value and subgradient, and is given, in this work by the MMR-ROSFR model described in chapter 2. Besides, the FCUC by Benders makes no hypothesis on the behaviour of the frequency nadir with respect to the binary decision variables. Optimality is theoretically ensured although in practice is hard to yield. In this regard, the stabilised FCUC formulation provides encouraging results regarding the improvement of the convergence properties and sets the path for future work.

Chapter 6

General conclusions and perspectives

Providing primary frequency regulation resources entails costs for the suppliers and the system: the formers are penalised by the loss of opportunity cost, while the system pay the price of the mix desoptimisation. The primary reserve provision cost is meant to be minimised in short-term generation scheduling. However, the low representativeness of the security constraints contributes to an optimality loss and the presence of a latent risk.
This thesis proposes an original formulation for the frequency constrained unit commitment problem (FCUC), which ensures optimality and effectiveness of the security constraint, by making large use of cutting plane methods. This innovative approach outperforms existing FCUC formulations based on the inclusion of indirect security constraints.

6.1 Dissertation overview

First, the FCUC was defined as a family of optimisation problems that deals with the short-term scheduling of power generation to supply electrical demand, while preventing the under frequency load shedding (UFLS). Suitable models for characterising the relation between the commitment and dispatch variables, and the primary frequency response were established. It is highlighted that the current industrial practice for scheduling primary frequency regulation resources is based on significant modelling simplifications. Consequently, security constraints may be uneconomical in large and interconnected power systems, and ineffective in small and isolated ones.
Second, the need and challenges of improving the representation of the primary frequency response in optimisation models were identified. Nowadays, the liberalisation of the electricity sector calls for cost reductions, while the integration of variable renewable sources (V-RES) jeopardises the reliable electricity supply.
The case studies showed that the need for primary regulation resources depends on the specific operational condition and that high penetration rates of V-RES increase the risk

of UFLS. Thus, a more accurate model of the security constraint is needed for obtaining optimal schedules that provide an acceptable transient response, while minimising operational cost and maximising the share of V-RES. However, the primary frequency response is strongly non-linear with respect to the optimisation variables, while the UC problem needs to be solved in a time compatible with power system operation. These features have encouraged the use of affine approximations which enable the employment of effective mixed integer linear programming solvers.

Third, the cost, benefit and limits of enhanced security constraints proposed in literature were investigated. It is shown that the use of fixed constraints over specific parameters is not cost/effective to tackle security issues following the integration of V-RES sources. On the one hand, the enforcement of fixed security constrains (related to the primary regulation), that obviously increase the operational cost, yields sub-optimal solutions. On the other hand, these impact mitigation techniques may fail to contain the UFLS risk due to their low representativeness of the underlying processes. Moreover, the inter-temporal dependency of the optimisation variables can produce involuntary actions in adjacent time steps which may have counter-productive effects. Finally, some of them tend to encourage high V-RES dispatch down, which goes against environmental policies.

Next, a new formulation for the FCUC problem is proposed following a Benders' decomposition approach, which overcome many limitations of existing models. For instance, all the primary frequency regulation resources available at the dispatch level can be simultaneously optimised thanks to an explicit representation of the frequency nadir constraints. This is done without compromising computational tractability since the linear programming structure of the economic dispatch problem is preserved at each iteration of the slave problem. Simulation results showed that the cutting plane model of the frequency nadir is accurate, 100% effective (to the precision of the *Oracle*, as long as the commitment candidate solution is feasible) and converge fast for hundreds of these candidate solutions, entailing low additional security costs.

Finally, the master level coordination ensures that the FCUC problem is indeed solved. Once more a cutting plane model is proposed, this time to represent the optimal slave objective that is computed through the solution of a simpler optimisation problem (the slave problem). The algorithm seems to asymptomatically converge in the beginning, but as the iterations progress the quality of the solution declines, which prevent the master problem from converging fast. To tackle this issue a level-master problem is formulated based on a bundle-like method. Preliminary results are promising but further work must be carried out to improve the convergence properties of the global algorithm and make it a viable solution in an operational environment.

6.2 General remarks

The main contributions of this work, from a methodological point of view, were summarised in chapter 1 (see section 1.5). In this section some general remarks drawn for the analytical development and case studies are highlighted.

1. **UFLS risk and instantaneous penetration rate are *false friends*.** It is expected that for high load levels, higher share of V-RES can be accommodated. However, stabilising maximal instantaneous penetration rates supposes that this relation is linear, which may not be the case in practice. In this work, especially in chapter 3, the impact of having partially loaded units at high V-RES penetration levels has been taken into account as a reduction on the power imbalance generated by unit outages. Thus, although less frequency regulation resources are available at significant V-RES penetration (and low demand), in practice less of these resources may be actually required. Moreover, at an equivalent V-RES penetration rate, and high load level, the remaining conventional units may be enough to ensure frequency regulation. Furthermore, it was shown that although some V-RES dispatch down may limit UFLS risk at some instants, it may have the opposite effect at other time steps. Indeed, as this measure tend to improve the economical performance of the mix, some units may be replaced by cheaper ones. However, the latter may have lower primary reserve limits or deployment rates and/or inertia constants. In these rare cases, a slight reduction of V-RES may lead to a decline on the primary frequency response. In large interconnected systems this type of phenomenon may be smoothed by the significant amount of committed generating units.

2. **Frequency regulation requirements *depend* on the operational point.** This is: the load level, the V-RES instantaneous generation, the optimal schedule (which is as function of the load profile rather than the precise load level, due to inter-temporal dependencies), as well as the security criterion and the frequency threshold for UFLS. As discussed in the previous point, the load level (through the load frequency sensitivity) and the worst possible contingency may affect the actual system needs, and capability to provide, primary reserve. Moreover, different combinations of inertial resources and primary reserve deployment rates may be suitable to satisfy a predefined frequency security threshold following any single unit outages.

3. **Primary reserve deployment rates may be *as relevant as* inertia for primary frequency regulation purposes.** Recent contribution dealing with the FCUC problem are focused on the inertia, which is indeed an interesting lever to limit the risk of UFLS. However, chapter 2 (and appendix B) has brought forward the sensibility of the frequency nadir to the time constants of the primary reserve de-

ployment associated to different providers. Under certain conditions consistent with practical ranges, the contribution of allocating the primary reserve in faster units may be equivalent to the commitment of more inertial units regarding the limitation of the UFLS risk. This becomes obvious when thinking of the increasing room for fast contingency services [186, 187]. The reduced attention received by this lever until now is driven by its complex relation with the UC variables. In terms of cost, one lever may be more economical than the other in some instants, and vice-versa.

4. **Enforcing fixed frequency regulation requirement is *uneconomical*, and may become *ineffective* at high share of non-synchronous V-RES.** Chapter 4 thoroughly discussed the impact of different prescriptions of primary frequency regulation resources, such as the primary reserve and the inertia, on the cost and the UFLS risk. Simulation results showed that they conduct to the over-schedule of resources at some instants and to unacceptable primary frequency response at other time steps. In consequence, such security constraints lead to high (unnecessary for primary frequency regulation purposes) cost and V-RES dispatch down. Moreover, other levers, such as the reserve deployment dynamics are disregarded. Thus, different impact mitigation techniques are not competitive but complementary and their activation should be planed in the short-term by advance optimisation tools.

5. **Analytical expressions are overrated.** These words are in fact taken from S. Boyd [161], who insists that, although many optimisation problem (even those based on linear programs) cannot be solved through a simple analytical formula, there are a variety of very effective methods for solving them. This remark fits well the FCUC problem in a different sense. A lot of effort has been devoted to the formulation of the frequency constraint as an explicit analytic function of the UC variables at the expense of significant modelling simplifications. But, with current computational power, the numerical evaluation of implicit functions is perfectly viable, even in certain operational environments, as long as the number of required operations can, at least, be bounded. Several methods exits to build suitable models from the numerical evaluation of complex functions. In this work, cutting plane methods were used to preserve the linear structure of the UC problem, while taking into account complex underlying processes. The nadir function is approximated at each operational point without simplifying its modelling at a level that compromise accuracy. Indeed, here the approach was to build a model that is accurate enough to represent the phenomena of interest (chapter 2), and then a suitable method was proposed (in chapter 5) to handle the frequency nadir constraint. The simplification of the dynamic model should be driven by the acceptable trade-off between complexity and accuracy, and not by the requirements of a predefined solution method.

6.3 Perspectives

Several models were proposed in this work to study the relation between the generation schedules and the primary frequency response, and to optimise the frequency regulation resources. Some assumption and limitations of those models, and their solution methods, were acknowledged and recommendations to raise them have been already provided. The list below summarises them and provides other possible research directions.

1. First perspectives naturally follow from the work conducted during this thesis:

   - **Improving the master problem convergence.** The slow convergence of the proposed master problem formulation makes it incompatible with power system operation. In this work, a first step was proposed towards improving the convergence properties of the algorithm by a quadratic stabilisation and the formulation of a level-master problem. Main remaining issues are related to the quality of the candidate solutions. For a certain time limit the $MIPgap$ reaches high values before actualising the lower bound. An empirical simple $MIPgap$ control strategy was implemented for illustrative purposes. The potential benefits of this approach were highlighted. However, the $MIPgap$ shows a chaotic behaviour and the stopping criterion evolved similarly slow. More sophisticated formulation should be developed in order to foresee an industrial application.
   - **Deeper analysis of the concavity hypothesis on the frequency nadir with respect to the power set-points.** In chapter 5 was acknowledged that in some cases the cutting plane model of the frequency nadir cuts the original functions, which raises concerns about the validity of the concavity hypothesis. It was argued that this issue does not compromise the effectiveness of the proposed formulation to limit the UFLS risk. However, optimality could not be claimed. An practical analysis provided a preliminary explanation of this behaviour and the simulation results showed that in practice the proposed formulation outperform other FCUC models. Nonetheless, the causes and implications of this behaviour should be investigated in deep. Published works on the use of bundle method for nonconvex optimisation problems [188] may bring lights to this subject.
   - **Probabilistic security criterion**. The proposed FCUC formulation seeks to avoid UFLS at all time, at any cost. In a more prospective way, other approaches could be considered to account for a certain acceptable risk level. For instance, a chance constrained formulation would enable the definition of the security constraint as a probabilistic one in order to include differentiated weights for unit outages depending on their availability rates.

2. In this work some assumptions were made for simplicity, which may not be acceptable depending on the considered system. For example:

   - **Slower and downward reserve requirements.** Since the focus was placed on the scheduling of primary frequency regulation resources, their cost and response following unit outages, other requirements were neglected. This consideration is unrealistic, and should be changed when applying the proposed simulation tools to assess real systems. It is recalled that the simulation results have shown that, for low V-RES penetration levels, a reasonable amount of unintended downward reserve was often available. However, this was no longer the case for high V-RES penetration levels.
   - **Intra-hour variability and uncertainty.** For the same reason indicated above, here the demand was represented by a deterministic hourly stepped profile. It is supposed that secondary and tertiary reserves are continuously deployed such that the system is always at nominal frequency in the pre-contingency state, and the primary reserve is always as scheduled. In large systems, the spatial smoothing effect and the advancement on forecasting techniques may support this hypothesis for short-term scheduling [47]. However, in small systems the intra-hour variability and uncertainty is often compensated by the automatic primary reserve. As a consequence, the pre-contingency state may differ from the scheduled one, entailing an additional risk. In this case, the possible pre-contingency states should be considered in the study.
   - **Handling infeasibility.** In this work, the V-RES dispatch down was in principle forbidden, instead, the violation of the security constraint (reserve or inertia in chapter 4) was authorised (to a high penalty cost) in order to compute schedules that were infeasible otherwise. In practice, the V-RES dispatch down would be used in those case. However, considering the two previous points, the quantification of the amounts of V-RES energy not produced would be mislead. Therefore, it was preferred to statistically characterise the level of violation of the security constraint by time step to offer an insight on the additional amount of frequency regulation resources required to fully integrate the available V-RES. This information may be used to define a upper bound on investments required to ensure power system security, and roughly estimate the potential value of V-RES dispatch down.
   - **Reference incident.** The frequency regulation resources were optimised to face the outage of any single on-line unit. Depending of the system, other contingencies may define the reference incident. The different studies proposed in this work would support the definition of a wider security criterion, such as

the N-2 (prevent UFLS following the loss of 2 units), the loss of an import, the cascading outages of part the V-RES, the loss of distributed generation with circuit breaker operation, etc. In some systems, the first UFLS step is part of the primary reserve, hence, the security criterion is defined by the second UFLS step. In the new FCUC formulation proposed here, these considerations can be included by adapting the *Oracle*, which is quite flexible from a modelling point of view. When the activation of a UFLS step is authorised for certain contingencies, the validity of concavity hypothesis should be checked.

- **Network consideration.** Some heavily constrained systems need to consider voltage and line current limits at the scheduling level. A lot of work have been published on including these constraints into MILP UC formulations (SCUC). Thus, they could be included in all the models discussed in this work.
- **Diversity of generating units in the dynamic model.** An enhanced multi-machine reduced order system frequency response model (MMR-ROSFR) was proposed in this work. Several features were included: (i) the aggregated inertial response of committed units at the post-contingency state, (ii) the load frequency sensitivity and (iii) the regulation characteristic of different thermal units. This latter component included: (i) a proportional droop controller, (ii) a first order transfer function for the process, (iii) a lead-lag compensator, and (iv) a saturation of the control signal for capacity and allocated primary reserve limits. Other features may be relevant and should be included, such as a dead-band if any. Moreover, different models should be included for representing other types of units such as hydro and nuclear. Finally, for large scale system, identical units could be clustered by power plant. Attention must be paid to their dispatch. Indeed, if the different units of the power plant are dispatched differently, the aggregated model may become inaccurate since heavily loaded units may interrupt their contribution to the primary frequency regulation before the nadir is reached due to the capacity limits.

3. The review of some modelling and simulation considerations could bring improvements in the computational performance of certain parts of the proposed tools.

- **Solution method of the MMR-ROSFR model.** In this work, a fixed step numeric integration method was implemented in order to easily take into account saturation processes. However, it is well known that the frequency trajectory has a smooth behaviour, which delivers potential for variable step numeric integration methods. These methods generally reduce the computational requirements in terms of memory and number of operations.

- **Dynamic simulation approach.** A sequential execution approach was used for the analysis of the V-RES impact on the primary frequency response, and the effectiveness of the impact mitigation techniques (chapters 2-4). However, chapter 5 illustrated the reduction of computational time that could be obtained by parallel execution of the dynamic model, which is straightforward within the proposed approach. Depending on the available computational power (threads) such sequential simulation tool can be applied to quite large systems. Moreover, in this work, all possible contingency were simulated. In practice, some *umbrella contingencies* could be defined in order to reduce the amount of needed simulations. Here, the exhaustive simulation provided an insight on the reduction of the possible power imbalances, which entailed an increase on the average frequency nadirs during sunny hours. However, this analysis is unnecessary for security purposes.

Finally, these ideas should be complemented with emerging clustering and scenario reduction approaches to make this kind of formulation scalable to **larger systems**.

Bibliography

[1] F. Bouffard, F.D. Galiana, and A.J. Conejo. Market-clearing with stochastic security-part i: formulation. *Power Systems, IEEE Transactions on*, 20(4):1818–1826, Nov 2005.

[2] J. Machowski, J. W. Bialek, and J. R. Bumby. *Power System Dynamics: Stability and Control*. Wiley, Chichester, U.K., 2008.

[3] K Bhattacharya and J. Zhong. Reactive power as an ancillary service. *Power Systems, IEEE Transactions on*, 16(2):294–300, 2001.

[4] R.D. Christie and A. Bose. Load frequency control issues in power system operations after deregulation. *Power Systems, IEEE Transactions on*, 11(3):1191–1200, 1996.

[5] A. J. Wood and B. F. Wollenberg. *Power Generation, Operation and Control*. Wiley, New York, USA, 1996.

[6] Y.G. Rebours, D.S. Kirschen, M. Trotignon, and S. Rossignol. A survey of frequency and voltage control ancillary services mdash;part i: Technical features. *Power Systems, IEEE Transactions on*, 22(1):350–357, 2007.

[7] ENTSO-E. Operational reserve ad hoc team report. Technical report, ENTSO-E, Brussels, Belgium, 2012.

[8] N. Jaleeli, L. S. VanSlyck, D.N. Ewart, L.H. Fink, and A. G. Hoffmann. Understanding automatic generation control. *IEEE Transactions on Power Systems*, 7(3):1106–1122, Aug 1992.

[9] P. Kundur. *Power System Stability and Control*. McGraw-Hill, California, USA, 1994.

[10] H. E. Lokay and V. Burtnyk. Application of underfrequency relays for automatic load shedding. *Power Apparatous and Systems, IEEE Transactions on*, PAS-87(3):525–532, 1968.

[11] R. M. Maliszewski, R. D. Dunlop, and G. L. Wilson. Frequency actuated load shedding and restoration: part 1—philosophy. *Power Apparatous and Systems, IEEE Transactions on*, PAS-90(4):1452–1459, 1971.

[12] F.D. Galiana, F. Bouffard, J.M. Arroyo, and J.F. Restrepo. Scheduling and pricing of coupled energy and primary, secondary, and tertiary reserves. *Proceedings of the IEEE*, 93(11):1970–1983, 2005.

[13] Y.G. Rebours, D.S. Kirschen, M. Trotignon, and S. Rossignol. A survey of frequency and voltage control ancillary services mdash;part ii: Economic features. *Power Systems, IEEE Transactions on*, 22(1):358–366, 2007.

[14] United Nations. Kyoto protocol to the united nations framework convention on climate change. Available on http://unfccc.int/kyoto_protocol/items/2830.php, 1998. "[Online; accessed 05-August-2015]".

[15] REN21. Renewables 2015 global status report. Available on http://www.ren21.net/status-of-renewables/global-status-report/, 2015. "[Online; accessed 05-August-2015]".

[16] European Commision. The 2020 climate and energy package. Available on http://ec.europa.eu/clima/policies/package/index_en.htm, 2008. "[Online; accessed 05-August-2015]".

[17] European Commision. 2030 framework for climate and energy policies. Available on http://ec.europa.eu/clima/policies/2030/index_en.htm, 2014. "[Online; accessed 05-August-2015]".

[18] United Nations. Sustainable energy for all. Available on http://www.se4all.org/, 2012. "[Online; accessed 05-August-2015]".

[19] Sustainable Development Ministry of Ecology and Energy. The energy transition for green growth. Available on http://www.developpement-durable.gouv.fr/La-loi-transition-energetique.html, 2015. "[Online; accessed 05-August-2015]".

[20] BDEW. Erneuerbare energien und das eeg: Zahlen, fakten, grafiken (2015). Available on https://www.bdew.de/internet.nsf/id/DE_Erneuerbare-Energien, 2015. "[Online; accessed 05-August-2015]".

[21] EirGrid. All island wind and fuel mix report. Available on http://www.eirgrid.com/operations/systemperformancedata/all-islandwindandfuelmixreport/, 2014. "[Online; accessed 05-August-2015]".

[22] Red eléctrica de España. Avance del informe del sistema electrico español 2014. Available on http://www.ree.es/es/publicaciones/sistema-electrico-espanol/informe-anual/avance-del-informe-del-sistema-electrico-espanol-2014, 2014. "[Online; accessed 05-August-2015]".

[23] EnerginetDK. Electricity generation 2014. Available on http://www.energinet.dk/EN/KLIMA-OG-MILJOE/Miljoerapportering/Elproduktion-i-Danmark/Sider/Elproduktion-i-Danmark.aspx, 2014. "[Online; accessed 05-August-2015]".

[24] REN. Annual report 2014. Available on http://www.ren.pt/en-GB/, 2014. "[Online; accessed 05-August-2015]".

[25] Terna. Sustainability report 2014. Available on http://www.gse.it/it/Dati%20e%20Bilanci/Bilanci%20Gse/Pages/default.aspx, 2015. "[Online; accessed 05-August-2015]".

[26] RTE. Bilan électrique 2014. Available on http://www.rte-france.com/fr/article/bilans-electriques-nationaux, 2014. "[Online; accessed 05-August-2015]".

[27] Sustainable Development Ministry of Ecology and Energy. Bilan énergétique de la france pour 2014. Available on http://www.developpement-durable.gouv.fr/Bilan-energetique-de-la-France,44190.html, 2014. "[Online; accessed 05-August-2015]".

[28] J.C. Smith, M.R. Milligan, E.A. DeMeo, and B. Parsons. Utility wind integration and operating impact state of the art. *Power Systems, IEEE Transactions on*, 22(3):900–908, Aug 2007.

[29] R. Karki, Po Hu, and R. Billinton. A simplified wind power generation model for reliability evaluation. *Energy Conversion, IEEE Transactions on*, 21(2):533–540, June 2006.

[30] Jianhui Wang, M. Shahidehpour, and Zuyi Li. Security-constrained unit commitment with volatile wind power generation. *Power Systems, IEEE Transactions on*, 23(3):1319–1327, Aug 2008.

[31] Y.V. Makarov, C. Loutan, Jian Ma, and P. de Mello. Operational impacts of wind generation on california power systems. *Power Systems, IEEE Transactions on*, 24(2):1039–1050, May 2009.

[32] P. Meibom, R. Barth, B. Hasche, H. Brand, C. Weber, and M. O'Malley. Stochastic optimization model to study the operational impacts of high wind penetrations in ireland. *Power Systems, IEEE Transactions on*, 26(3):1367–1379, Aug 2011.

[33] R. Doherty and M. O'Malley. A new approach to quantify reserve demand in systems with significant installed wind capacity. *Power Systems, IEEE Transactions on*, 20(2):587–595, May 2005.

[34] B.C. Ummels, M. Gibescu, E. Pelgrum, W.L. Kling, and A.J. Brand. Impacts of wind power on thermal generation unit commitment and dispatch. *Energy Conversion, IEEE Transactions on*, 22(1):44–51, March 2007.

[35] F. Bouffard and F.D. Galiana. Stochastic security for operations planning with significant wind power generation. *Power Systems, IEEE Transactions on*, 23(2):306–316, May 2008.

[36] M.A. Ortega-Vazquez and D.S. Kirschen. Estimating the spinning reserve requirements in systems with significant wind power generation penetration. *Power Systems, IEEE Transactions on*, 24(1):114–124, Feb 2009.

[37] J.F. Restrepo and F.D. Galiana. Assessing the yearly impact of wind power through a new hybrid deterministic/stochastic unit commitment. *Power Systems, IEEE Transactions on*, 26(1):401–410, 2011.

[38] D.A. Halamay, T.K.A. Brekken, A. Simmons, and S. McArthur. Reserve requirement impacts of large-scale integration of wind, solar, and ocean wave power generation. *Sustainable Energy, IEEE Transactions on*, 2(3):321–328, July 2011.

[39] A. Papavasiliou, S.S. Oren, and R.P. O'Neill. Reserve requirements for wind power integration: A scenario-based stochastic programming framework. *Power Systems, IEEE Transactions on*, 26(4):2197–2206, Nov 2011.

[40] N. Navid and G. Rosenwald. Market solutions for managing ramp flexibility with high penetration of renewable resource. *Sustainable Energy, IEEE Transactions on*, 3(4):784–790, Oct 2012.

[41] E. Lannoye, D. Flynn, and M. O'Malley. Evaluation of power system flexibility. *Power Systems, IEEE Transactions on*, 27(2):922–931, May 2012.

[42] J. Ma, V. Silva, R. Belhomme, D.S. Kirschen, and L.F. Ochoa. Evaluating and planning flexibility in sustainable power systems. *Sustainable Energy, IEEE Transactions on*, 4(1):200–209, Jan 2013.

[43] P. Pinson, C. Chevallier, and G.N. Kariniotakis. Trading wind generation from short-term probabilistic forecasts of wind power. *Power Systems, IEEE Transactions on*, 22(3):1148–1156, Aug 2007.

[44] M.A. Matos and R.J. Bessa. Setting the operating reserve using probabilistic wind power forecasts. *Power Systems, IEEE Transactions on*, 26(2):594–603, May 2011.

[45] D. Bertsimas, E. Litvinov, X.A. Sun, Jinye Zhao, and Tongxin Zheng. Adaptive robust optimization for the security constrained unit commitment problem. *Power Systems, IEEE Transactions on*, 28(1):52–63, Feb 2013.

[46] T. Mai, M.M. Hand, S.F. Baldwin, R.H. Wiser, G.L. Brinkman, P. Denholm, D.J. Arent, G. Porro, D. Sandor, D.J. Hostick, M. Milligan, E.A. DeMeo, and M. Bazilian. Renewable electricity futures for the united states. *Sustainable Energy, IEEE Transactions on*, 5(2):372–378, April 2014.

[47] EDF R& D. Technical and economic analysis of the european electricity system with 60% res. Available on http://chercheurs.edf.com/fichiers/fckeditor/Commun/Innovation/departements/SummarystudyRES.pdf, 2015. "[Online; accessed 22-December-2015]".

[48] EirGrid and SONI. All island tso facilitation of renewables studies. Available on http://www.eirgrid.com/renewables/facilitationofrenewables/, 2010. "[Online; accessed 13-Octobre-2015]".

[49] ADEME. Vers un mix électrique 100% renouvelable en 2050. Available on http://www.ademe.fr/sites/default/files/assets/documents/rapport100enr_comite.pdf, 2015. "[Online; accessed 05-August-2015]".

[50] P.B. Eriksen, T. Ackermann, H. Abildgaard, P. Smith, W. Winter, and J.M. Rodriguez Garcia. System operation with high wind penetration. *Power and Energy Magazine, IEEE*, 3(6):65–74, Nov 2005.

[51] Le Xie, P.M.S. Carvalho, L.A.F.M. Ferreira, Juhua Liu, B.H. Krogh, N. Popli, and M.D. Ilic. Wind integration in power systems: Operational challenges and possible solutions. *Proceedings of the IEEE*, 99(1):214–232, Jan 2011.

[52] M.V.A. Nunes, J.A. Peas Lopes, H.H. Zurn, U.H. Bezerra, and R.G. Almeida. Influence of the variable-speed wind generators in transient stability margin of the conventional generators integrated in electrical grids. *Energy Conversion, IEEE Transactions on*, 19(4):692–701, Dec 2004.

[53] D. Gautam, V. Vittal, and T. Harbour. Impact of increased penetration of dfig-based wind turbine generators on transient and small signal stability of power systems. *Power Systems, IEEE Transactions on*, 24(3):1426–1434, Aug 2009.

[54] Wen-Tsan Liu, Yuan-Kang Wu, Ching-Yin Lee, and Chao-Rong Chen. Effect of low-voltage-ride-through technologies on the first taiwan offshore wind farm planning. *Sustainable Energy, IEEE Transactions on*, 2(1):78–86, Jan 2011.

[55] S. Eftekharnejad, V. Vittal, G.T. Heydt, B. Keel, and J. Loehr. Impact of increased penetration of photovoltaic generation on power systems. *Power Systems, IEEE Transactions on*, 28(2):893–901, May 2013.

[56] H. Bevrani, A. Ghosh, and G. Ledwich. Renewable energy sources and frequency regulation: survey and new perspectives. *Renewable Power Generation, IET*, 4(5):438–457, September 2010.

[57] UCTE. Final report system disturbance on 4 november 2006. Available on https://www.entsoe.eu/fileadmin/user_upload/_library/publications/ce/otherreports/Final-Report-20070130.pdf, 2006. "[Online; accessed 05-August-2015]".

[58] NERL. Ercot event on february 26, 2008: Lessons learned. Available on http://www.nrel.gov/docs/fy08osti/43373.pdf, 2008. "[Online; accessed 05-August-2015]".

[59] R. Doherty, G. Lalor, and M. O'Malley. Frequency control in competitive electricity market dispatch. *IEEE Transactions on Power Systems*, 20(3):1588–1596, 2005.

[60] C. Mensah-Bonsu and S. Oren. California electricity market crisis: Causes, remedies, and prevention. *Power Engineering Review, IEEE*, 22(8):4–11, Aug 2002.

[61] W. Łyżwa, B. Olek, M. Wierzbowski, and W. Mielczarski. Why do we need capacity markets? In *European Energy Market (EEM), 2014 11th International Conference on the*, pages 1–5, May 2014.

[62] Ministre de l'écologie de l'énergie du développement durable et de l'aménagement du territoire. Arrêté du 23 décembre 2010 modifiant le creux de tension fixé à l'article 14 de l'arrêté du 23 avril 2008 relatif aux prescriptions techniques de conception et de fonctionnement pour le raccordement à un réseau public de distribution d'électricité en basse tension ou en moyenne tension d'une installation de production d'énergie électrique. Available on http://www.legifrance.gouv.fr/affichTexte.do?cidTexte=JORFTEXT000023587128, 2010. "[Online; accessed 05-August-2015]".

[63] Ministre de l'écologie de l'énergie du développement durable et de l'aménagement du territoire. Arrêté du 23 avril 2008 relatif aux prescriptions techniques de conception et de fonctionnement pour le raccordement à un réseau public de distribution d'électricité en basse tension ou en moyenne tension d'une installation de production

d'énergie électrique. Available on http://www.legifrance.gouv.fr/affichTexte.do?cidTexte=JORFTEXT000018698004, 2008. "[Online; accessed 05-August-2015]".

[64] C. Bueno and J.A. Carta. Wind powered pumped hydro storage systems, a means of increasing the penetration of renewable energy in the canary islands. *Renewable and Sustainable Energy Reviews*, 10(4):312 – 340, 2006.

[65] K. Dietrich, J.M. Latorre, L. Olmos, and A. Ramos. Demand response in an isolated system with high wind integration. *Power Systems, IEEE Transactions on*, 27(1):20–29, Feb 2012.

[66] P.D. Brown, J.A. Peas Lopes, and M.A. Matos. Optimization of pumped storage capacity in an isolated power system with large renewable penetration. *Power Systems, IEEE Transactions on*, 23(2):523–531, May 2008.

[67] H. Vasconcelos, C. Moreira, A. Madureira, J.P. Lopes, and V. Miranda. Advanced control solutions for operating isolated power systems: Examining the portuguese islands. *Electrification Magazine, IEEE*, 3(1):25–35, March 2015.

[68] G. Delille, B. Francois, and G. Malarange. Dynamic frequency control support by energy storage to reduce the impact of wind and solar generation on isolated power system's inertia. *Sustainable Energy, IEEE Transactions on*, 3(4):931–939, Oct 2012.

[69] C. Cardozo, L. Capely, J. Lacoste, and P. Dessante. A statistical analysis of the frequency response in an isolated power system with an increasing share of photovoltaic generation. In *PowerTech, 2015 IEEE Eindhoven*, pages 1–6, June 2015.

[70] J. Xia, A. Dyśko, and J. O'Reilly. Future stability challenges for the uk network with high wind penetration levels. *Generation, Transmission Distribution, IET*, 9(11):1160–1167, 2015.

[71] D. Al Katsaprakakis, N. Papadakis, D. G. Christakis, and A. Zervos. On the wind power rejection in the islands of crete and rhodes. *Wind Energy-Bognor Regis*, 10(5):415–434, 2007.

[72] N. Laverdure. *Sur l'intégration des générateurs éoliens dans les réseaux faibles ou insulaires*. PhD thesis, Institut National Polytechnique de Grenoble - INPG, 2005.

[73] I. Erlich and M. Wilch. Primary frequency control by wind turbines. In *Power and Energy Society General Meeting, 2010 IEEE*, pages 1–8, July 2010.

[74] K.V. Vidyanandan and N. Senroy. Primary frequency regulation by deloaded wind turbines using variable droop. *Power Systems, IEEE Transactions on*, 28(2):837–846, May 2013.

[75] D. Gautam, L. Goel, R. Ayyanar, V. Vittal, and T. Harbour. Control strategy to mitigate the impact of reduced inertia due to doubly fed induction generators on large power systems. *Power Systems, IEEE Transactions on*, 26(1):214–224, Feb 2011.

[76] Y. Wang, G. Delille, H. Bayem, X. Guillaud, and B. Francois. High wind power penetration in isolated power systems-assessment of wind inertial and primary frequency responses. *Power Systems, IEEE Transactions on*, 28(3):2412–2420, Aug 2013.

[77] N. Lu, M.R. Weimar, Y.V. Makarov, F.J. Rudolph, S.N. Murthy, J. Arseneaux, and C. Loutan. Evaluation of the flywheel potential for providing regulation service in california. In *Power and Energy Society General Meeting, 2010 IEEE*, pages 1–6, July 2010.

[78] J.A. Short, D.G. Infield, and L.L. Freris. Stabilization of grid frequency through dynamic demand control. *Power Systems, IEEE Transactions on*, 22(3):1284–1293, Aug 2007.

[79] A. Molina-Garciá, F. Bouffard, and D.S. Kirschen. Decentralized demand-side contribution to primary frequency control. *Power Systems, IEEE Transactions on*, 26(1):411–419, Feb 2011.

[80] Zhao Xu, J. Ostergaard, and M. Togeby. Demand as frequency controlled reserve. *Power Systems, IEEE Transactions on*, 26(3):1062–1071, Aug 2011.

[81] EirGrid. Eirgrid grid code, version 6. Available on http://www.eirgrid.com/operations/gridcode/, 2011. "[Online; accessed 05-August-2015]".

[82] M. Tahanan, W. van Ackooij, A. Frangioni, and F. Lacalandra. Large-scale unit commitment under uncertainty. *4OR*, 13(2):115–171, 2015.

[83] J. F. Restrepo and F. D. Galiana. Unit commitment with primary frequency regulation constraints. *IEEE Transactions on Power Systems*, 20(4):1836–1842, 2005.

[84] R. Doherty, A. Mullane, G. Nolan, D.J. Burke, A. Bryson, and M. O'Malley. An assessment of the impact of wind generation on system frequency control. *IEEE Transactions on Power Systems*, 25(1):452–460, 2010.

[85] H. Ahmadi and H. Ghasemi. Security-constrained unit commitment with linearized system frequency limit constraints. *IEEE Transactions on Power Systems*, 29(4):1536–1545, July 2014.

[86] E. Ela, V. Gevorgian, A. Tuohy, B. Kirby, M. Milligan, and M. O'Malley. Market designs for the primary frequency response ancillary service — part i: Motivation and design. *IEEE Transactions on Power Systems*, 29(1):421–431, 2014.

[87] J. J. Shaw. A direct method for security-constrained unit commitment. *Power Systems, IEEE Transactions on*, 10(3):1329–1342, Aug 1995.

[88] Yong Fu, M. Shahidehpour, and Zuyi Li. Security-constrained unit commitment with ac constraints*. *Power Systems, IEEE Transactions on*, 20(3):1538–1550, Aug 2005.

[89] C. Cardozo, L. Capely, and P. Dessante. Frequency constrained unit commitment. *Energy Systems*, pages 1–26, 2015.

[90] C. Cardozo, L. Capely, and P. Dessante. Increasing the integration capabilities of photovoltaic generation in a small and isolated power system. In *EPEC, 2015 IEEE London*, pages 1–6, Octobre 2015.

[91] A. Lotfjou, M. Shahidehpour, Yong Fu, and Zuyi Li. Security-constrained unit commitment with ac/dc transmission systems. *Power Systems, IEEE Transactions on*, 25(1):531–542, Feb 2010.

[92] R.C. Johnson, H.H. Happ, and W.J. Wright. Large scale hydro-thermal unit commitment-method and results. *Power Apparatus and Systems, IEEE Transactions on*, PAS-90(3):1373–1384, May 1971.

[93] J. J. Shaw, R. F. Gendron, and D.P. Bertsekas. Optimal scheduling of large hydrothermal power systems. *Power Apparatus and Systems, IEEE Transactions on*, PAS-104(2):286–294, Feb 1985.

[94] C. Li, A.J. Svoboda, Chung-Li Tseng, R.B. Johnson, and E. Hsu. Hydro unit commitment in hydro-thermal optimization. *Power Systems, IEEE Transactions on*, 12(2):764–769, May 1997.

[95] A. Borghetti, C. D'Ambrosio, A. Lodi, and S. Martello. An milp approach for short-term hydro scheduling and unit commitment with head-dependent reservoir. *Power Systems, IEEE Transactions on*, 23(3):1115–1124, Aug 2008.

[96] A. I. Cohen and S.H. Wan. A method for solving the fuel constrained unit commitment problem. *Power Systems, IEEE Transactions on*, 2(3):608–614, Aug 1987.

[97] F.N. Lee. A fuel-constrained unit commitment method. *Power Systems, IEEE Transactions on*, 4(3):1208–1218, Aug 1989.

[98] S. Vemuri and L. Lemonidis. Fuel constrained unit commitment. *Power Systems, IEEE Transactions on*, 7(1):410–415, Feb 1992.

[99] S.J. Wang, S.M. Shahidehpour, D.S. Kirschen, S. Mokhtari, and G.D. Irisarri. Short-term generation scheduling with transmission and environmental constraints using an augmented lagrangian relaxation. *Power Systems, IEEE Transactions on*, 10(3):1294–1301, Aug 1995.

[100] T. Gjengedal. Emission constrained unit-commitment (ecuc). *Energy Conversion, IEEE Transactions on*, 11(1):132–138, Mar 1996.

[101] A. I. Cohen and V.R. Sherkat. Optimization-based methods for operations scheduling. *Proceedings of the IEEE*, 75(12):1574–1591, Dec 1987.

[102] G.B. Sheble and G.N. Fahd. Unit commitment literature synopsis. *Power Systems, IEEE Transactions on*, 9(1):128–135, 1994.

[103] N.P. Padhy. Unit commitment-a bibliographical survey. *Power Systems, IEEE Transactions on*, 19(2):1196–1205, 2004.

[104] I.A. Farhat and M.E. El-Hawary. Optimization methods applied for solving the short-term hydrothermal coordination problem. *Electric Power Systems Research*, 79(9):1308 – 1320, 2009.

[105] A. Bhardwaj, V.K. Kamboj, V.K. Shukla, B. Singh, and P. Khurana. Unit commitment in electrical power system-a literature review. In *Power Engineering and Optimization Conference (PEDCO) Melaka, Malaysia, 2012 Ieee International*, pages 275–280, 2012.

[106] B. Saravanan, Siddharth Das, Surbhi Sikri, and D.P. Kothari. A solution to the unit commitment problem—a review. *Frontiers in Energy*, 7(2):223–236, 2013.

[107] R. H. Kerr, J. L. Scheidt, A.J. Fontanna, and J. K. Wiley. Unit commitment. *Power Apparatus and Systems, IEEE Transactions on*, PAS-85(5):417–421, May 1966.

[108] F.N. Lee. Short-term thermal unit commitment-a new method. *Power Systems, IEEE Transactions on*, 3(2):421–428, May 1988.

[109] W. L. Snyder, H. D. Powell, and J. C. Rayburn. Dynamic programming approach to unit commitment. *Power Engineering Review, IEEE*, PER-7(5):41–42, May 1987.

[110] GUROBI. *Version 5.6*. Gurobi Optimization, Inc., 2013.

[111] IBM. *IBM ILOG CPLEX V12.1*. International Business Machines Corp., 2013.

[112] FICO ™. *Xpress-Optimizer*. Fair Isaac Corporation, 2013.

[113] W.J. Hobbs, G. Hermon, S. Warner, and G.B. Shelbe. An enhanced dynamic programming approach for unit commitment. *Power Systems, IEEE Transactions on*, 3(3):1201–1205, Aug 1988.

[114] A.K. David and Fushuan Wen. Strategic bidding in competitive electricity markets: a literature survey. In *Power Engineering Society Summer Meeting, 2000. IEEE*, volume 4, pages 2168–2173 vol. 4, 2000.

[115] T. Alvey, D. Goodwin, Xingwang Ma, D. Streiffert, and David Sun. A security-constrained bid-clearing system for the new zealand wholesale electricity market. *Power Systems, IEEE Transactions on*, 13(2):340–346, 1998.

[116] F. Zhuang and F.D. Galiana. Unit commitment by simulated annealing. *Power Systems, IEEE Transactions on*, 5(1):311–318, Feb 1990.

[117] T.O. Ting, M.V.C. Rao, and C.K. Loo. A novel approach for unit commitment problem via an effective hybrid particle swarm optimization. *Power Systems, IEEE Transactions on*, 21(1):411–418, Feb 2006.

[118] S.A. Kazarlis, A.G. Bakirtzis, and V. Petridis. A genetic algorithm solution to the unit commitment problem. *Power Systems, IEEE Transactions on*, 11(1):83–92, Feb 1996.

[119] H. Sasaki, M. Watanabe, J. Kubokawa, N. Yorino, and R. Yokoyama. A solution method of unit commitment by artificial neural networks. *Power Systems, IEEE Transactions on*, 7(3):974–981, Aug 1992.

[120] A.H. Mantawy, Y.L. Abdel-Magid, and S.Z. Selim. Unit commitment by tabu search. *Generation, Transmission and Distribution, IEE Proceedings-*, 145(1):56–64, Jan 1998.

[121] Lei Wu, M. Shahidehpour, and Tao Li. Stochastic security-constrained unit commitment. *Power Systems, IEEE Transactions on*, 22(2):800–811, May 2007.

[122] P.A. Ruiz, C.R. Philbrick, E. Zak, K.W. Cheung, and P.W. Sauer. Uncertainty management in the unit commitment problem. *Power Systems, IEEE Transactions on*, 24(2):642–651, May 2009.

[123] A. Tuohy, P. Meibom, E. Denny, and M. O'Malley. Unit commitment for systems with significant wind penetration. *Power Systems, IEEE Transactions on*, 24(2):592–601, May 2009.

[124] Tao Li, M. Shahidehpour, and Zuyi Li. Risk-constrained bidding strategy with stochastic unit commitment. *Power Systems, IEEE Transactions on*, 22(1):449–458, Feb 2007.

[125] M. Carrión and J.M. Arroyo. A computationally efficient mixed-integer linear formulation for the thermal unit commitment problem. *Power Systems, IEEE Transactions on*, 21(3):1371–1378, Aug 2006.

[126] MATLAB. *version 8.4.0 (R2014b)*. The MathWorks Inc., Natick, Massachusetts, 2014.

[127] P.M. Anderson and M. Mirheydar. A low-order system frequency response model. *IEEE Transactions on Power Systems*, 5(3):720–729, Aug 1990.

[128] D. L. H. Aik. A general-order system frequency response model incorporating load shedding: analytic modeling and applications. *IEEE Transactions on Power Systems*, 21(2):709–717, May 2006.

[129] UCTE. *Operational Handbook*. 2004.

[130] National Grid Electricity Transmission plc. *The Grid Code*. 2014.

[131] H. Bludszuweit, J.A. Dominguez-Navarro, and A. Llombart. Statistical analysis of wind power forecast error. *Power Systems, IEEE Transactions on*, 23(3):983–991, Aug 2008.

[132] B. Hodge and M. Milligan. Wind power forecasting error distributions over multiple timescales. In *Power and Energy Society General Meeting, 2011 IEEE*, pages 1–8, July 2011.

[133] I. Bremer, R. Henrion, and A. Möller. Probabilistic constraints via sqp solver: application to a renewable energy management problem. *Computational Management Science*, 12(3):435–459, 2015.

[134] Werner Römisch. Stability of stochastic programming problems. In *Stochastic Programming*, volume 10 of *Handbooks in Operations Research and Management Science*, pages 483 – 554. Elsevier, 2003.

[135] Werner Römisch. Scenario reduction techniques in stochastic programming. In Osamu Watanabe and Thomas Zeugmann, editors, *Stochastic Algorithms: Foundations and Applications*, volume 5792 of *Lecture Notes in Computer Science*, pages 1–14. Springer Berlin Heidelberg, 2009.

[136] Y. Dvorkin, Yishen Wang, H. Pandzic, and D. Kirschen. Comparison of scenario reduction techniques for the stochastic unit commitment. In *PES General Meeting | Conference Exposition, 2014 IEEE*, pages 1–5, July 2014.

[137] F. Vallée, C. Versèle, J. Lobry, and F. Moiny. Non-sequential monte carlo simulation tool in order to minimize gaseous pollutants emissions in presence of fluctuating wind power. *Renewable Energy*, 50:317 – 324, 2013.

[138] Y. Wang, V. Silva, and M. Lopez-Botet-Zulueta. Impact of high penetration of variable renewable generation on frequency dynamics in the continental europe interconnected system. *IET Renewable Power Generation*, November 2015.

[139] EirGrid and SONI. Annual wind constraint and curtailment report 2013. Available on http://www.eirgrid.com/media/Annual_Wind_Constraint_and_Curtailment_Report_2013.pdf, 2013. "[Online; accessed 12-Octobre-2015]".

[140] V. Silva. *Value of flexibility in systems with large wind penetration.* PhD thesis, Imperial College London, 2010.

[141] RTE. Règles services système. Available on http://clients.rte-france.com/htm/fr/offre/telecharge/20140701_Regles_SSY_approuvees.pdf, 2014. "[Online; accessed 13-november-2015]".

[142] D. R. Bobo, D. M. Mauzy, and F.J. Trefny. Economic generation dispatch with responsive spinning reserve constraints. *IEEE Transactions on Power Systems*, 9(1):555–559, Feb 1994.

[143] J. W. O'Sullivan and M. J. O'Malley. A new methodology for the provision of reserve in an isolated power system. *IEEE Transactions on Power Systems*, 14(2):519–524, 1999.

[144] K. A. Papadogiannis and N. D. Hatziargyriou. Optimal allocation of primary reserve services in energy markets. *IEEE Transactions on Power Systems*, 19(1):652–659, 2004.

[145] E. Ela, V. Gevorgian, A. Tuohy, B. Kirby, M. Milligan, and M. O'Malley. Market designs for the primary frequency response ancillary service — part ii: Case studies. *IEEE Transactions on Power Systems*, 29(1):432–440, 2014.

[146] H. Dutrieux. *Méthodes pour la planification pluriannuelle des réseaux de distribution. Application à l'analyse technico-économiques des solutions d'intégration des énergies renouvelables intermittentes.* PhD thesis, Ecole Centrale de Lille, 2015.

[147] H. Bayem. *Apport des Méthodes Probabilistes aux Études d'Insertion des Énergies Renouvelables dans les Système Électrique*. PhD thesis, Supélec, 2009.

[148] J. Hosek, P. Musilek, E. Lozowski, and P. Pytlak. Effect of time resolution of meteorological inputs on dynamic thermal rating calculations. *Generation, Transmission Distribution, IET*, 5(9):941–947, September 2011.

[149] M. Tsili and S. Papathanassiou. A review of grid code technical requirements for wind farms. *Renewable Power Generation, IET*, 3(3):308–332, Sept 2009.

[150] A. Miller, E. Muljadi, and D.S. Zinger. A variable speed wind turbine power control. *Energy Conversion, IEEE Transactions on*, 12(2):181–186, Jun 1997.

[151] M. Chinchilla, S. Arnaltes, and J.C. Burgos. Control of permanent-magnet generators applied to variable-speed wind-energy systems connected to the grid. *Energy Conversion, IEEE Transactions on*, 21(1):130–135, March 2006.

[152] Ping-Kwan Keung, Pei Li, H. Banakar, and B.T. Ooi. Kinetic energy of wind-turbine generators for system frequency support. *Power Systems, IEEE Transactions on*, 24(1):279–287, Feb 2009.

[153] R.G. de Almeida and J.A. Peas Lopes. Participation of doubly fed induction wind generators in system frequency regulation. *Power Systems, IEEE Transactions on*, 22(3):944–950, Aug 2007.

[154] J.R. Pillai and B. Bak-Jensen. Integration of vehicle-to-grid in the western danish power system. *Sustainable Energy, IEEE Transactions on*, 2(1):12–19, Jan 2011.

[155] M.E. Khodayar, Lei Wu, and M. Shahidehpour. Hourly coordination of electric vehicle operation and volatile wind power generation in scuc. *Smart Grid, IEEE Transactions on*, 3(3):1271–1279, Sept 2012.

[156] S. Izadkhast, P. Garcia-Gonzalez, and P. Frias. An aggregate model of plug-in electric vehicles for primary frequency control. *Power Systems, IEEE Transactions on*, 30(3):1475–1482, May 2015.

[157] G. Delille. *Contribution du Stockage à la Gestion Avancée des Systèmes Électriques, Approches Organisationnelles et Technico-économiques dans les Réseaux de Distribution*. PhD thesis, Université Lille Nord-de-France, 2010.

[158] F. Geth. *Battery Energy Storage Systems and Distribution Grid Support*. PhD thesis, KE Leuven, 2014.

[159] D. Colin, J. Lugaro, J. C. Pinna, G. Delille, B. François, C. Caton, and G. Martin. The venteea 2 mw / 1.3 mwh battery system: An industrial pilot to demostrate multi-service operation of storage in distribution grids. In *23 International Conference on Electricity Distribution*, pages 1–5, June 2015.

[160] National Grid. Frequency response workgroup report. Available on http://www2.nationalgrid.com/UK/Industry-information/Electricity-codes/Grid-code/Modifications/GC0022/, 2013. "[Online; accessed 13-Octobre-2015]".

[161] S. Boyd and L. Vandenberghe. *Convex Optimization*. Cambridge, Cambridge, U.K., 2004.

[162] N. Z. Shor. *Minimization Methods for Non-differentiable Functions*. Series in Computational Mathematics. Springer, 1985.

[163] J. B. Hiriart-Urruty and C. Lemaréchal. *Convex Analysis and Minimization Algorithms I*, volume 305 of *A Series of Comprehensive Studies in Mathematics*. Springer-Verlag, Berlin, Germany, 1996.

[164] C. Sagastizábal. Divide to conquer: decomposition methods for energy optimization. *Mathematical Programming*, 134(1):187–222, 2012.

[165] S. Binato, M.V.F. Pereira, and S. Granville. A new benders decomposition approach to solve power transmission network design problems. *Power Systems, IEEE Transactions on*, 16(2):235–240, May 2001.

[166] R. Romero and A. Monticelli. A hierarchical decomposition approach for transmission network expansion planning. *Power Systems, IEEE Transactions on*, 9(1):373–380, Feb 1994.

[167] E.L. da Silva, M.T. Schilling, and M.C. Rafael. Generation maintenance scheduling considering transmission constraints. *Power Systems, IEEE Transactions on*, 15(2):838–843, May 2000.

[168] N. Yorino, E.E. El-Araby, H. Sasaki, and S. Harada. A new formulation for facts allocation for security enhancement against voltage collapse. *Power Systems, IEEE Transactions on*, 18(1):3–10, Feb 2003.

[169] S. Abdelouadoud. *Integration of renewable energies in the electricity distribution system*. PhD thesis, Ecole Nationale Supérieure des Mines de Paris, 2014.

[170] P.M.S. Carvalho, L.A.F.M. Ferreira, and A.J.C. da Silva. A decomposition approach to optimal remote controlled switch allocation in distribution systems. *Power Delivery, IEEE Transactions on*, 20(2):1031–1036, April 2005.

[171] H.M. Khodr, J. Martinez-Crespo, M.A. Matos, and J. Pereira. Distribution systems reconfiguration based on opf using benders decomposition. *Power Delivery, IEEE Transactions on*, 24(4):2166–2176, Oct 2009.

[172] E. Nasrolahpour, Hassan Ghasemi, and M. Khanabadi. Optimal transmission congestion management by means of substation reconfiguration. In *Electrical Engineering (ICEE), 2012 20th Iranian Conference on*, pages 416–421, May 2012.

[173] S. Touré. *Optimisation des réseaux : « réseau actif et flexible »*. PhD thesis, Université de Grenoble, 2014.

[174] E. Caro, A.J. Conejo, and R. Minguez. Decentralized state estimation and bad measurement identification: An efficient lagrangian relaxation approach. *Power Systems, IEEE Transactions on*, 26(4):2500–2508, Nov 2011.

[175] A.A. El-Keib, J. Nieplocha, H. Singh, and D.J. Maratukulam. A decomposed state estimation technique suitable for parallel processor implementation. *Power Systems, IEEE Transactions on*, 7(3):1088–1097, Aug 1992.

[176] R. Baldick. The generalized unit commitment problem. *Power Systems, IEEE Transactions on*, 10(1):465–475, Feb 1995.

[177] P. Carpentier, G. Gohen, J.-C. Culioli, and A. Renaud. Stochastic optimization of unit commitment: a new decomposition framework. *Power Systems, IEEE Transactions on*, 11(2):1067–1073, May 1996.

[178] S. Virmani, Eugene C. Adrian, Karl Imhof, and Shishir Mukherjee. Implementation of a lagrangian relaxation based unit commitment problem. *Power Systems, IEEE Transactions on*, 4(4):1373–1380, Nov 1989.

[179] Yong Fu, M. Shahidehpour, and Zuyi Li. Long-term security-constrained unit commitment: hybrid dantzig-wolfe decomposition and subgradient approach. *Power Systems, IEEE Transactions on*, 20(4):2093–2106, Nov 2005.

[180] M. Shahidehopour and Yong Fu. Benders decomposition: applying benders decomposition to power systems. *Power and Energy Magazine, IEEE*, 3(2):20–21, March 2005.

[181] H. Habibollahzadeh and J.A. Bubenko. Application of decomposition techniques to short-term operation planning of hydrothermal power system. *Power Systems, IEEE Transactions on*, 1(1):41–47, Feb 1986.

[182] H. Ma and S.M. Shahidehpour. Unit commitment with transmission security and voltage constraints. *Power Systems, IEEE Transactions on*, 14(2):757–764, May 1999.

[183] W. van Ackooij and J. Malick. Decomposition algorithm for large-scale two-stage unit-commitment. *Annals of Operations Research*, 238(1):587–613, 2016.

[184] S. Zaourar. *Optimisation convexe non-différentiable et méthodes de décomposition en recherche opérationnelle*. PhD thesis, Université de Grenoble, 2014.

[185] C. Lemaréchal, A. Nemirovskii, and Y. Nesterov. New variants of bundle methods. *Math. Programming*, 69(1):111–147, 1995.

[186] National Grid. Enhanced frequency response. Available on http://www2.nationalgrid.com/Enhanced-Frequency-Response.aspx, 2015. "[Online; accessed 10-January-2016]".

[187] Energy Storage Update. Pjm leads us fast-frequency regulation market. Available on http://analysis.energystorageupdate.com/market-out-look/pjm-leads-us-fast-frequency-regulation-market, 2015. "[Online; accessed 10-January-2016]".

[188] W. Hare and C. Sagastizábal. A redistributed proximal bundle method for nonconvex optimization. *SIAM J. on Optimization*, 20(5):2442–2473, June 2010.

[189] Katsuhiko Ogata. *Modern Control Engineering*. Aeeiz, New Jersey, USA, 2002.

[190] P. Daly, D. Flynn, and N. Cunniffe. Inertia considerations within unit commitment and economic dispatch for systems with high non-synchronous penetrations. In *PowerTech, 2015 IEEE Eindhoven*, pages 1–6, June 2015.

Appendix A

Analytical expression of the equivalent machine ROSFR model

A.1 Time domain solution of the frequency

The time domain expression of equation (2.21b) can be found using the inverse Laplace transformation. The inverse Laplace transformation is defined here by [189]:

$$\mathcal{L}^{-1}\left[F(s)\right] = f(t) = \frac{1}{2\pi i}\int_{c-i\infty}^{c+i\infty} F(s)e^{st}ds \qquad \forall t > 0, \tag{A.1}$$

where c, the abscissa of convergence, is a real constant and is chosen larger than the real parts of all singular points of F(s). In engineering, transformation tables are generally used by expressing transfer functions in specific forms as follows [189]:

$$\mathcal{L}^{-1}\left[\frac{\omega_n^2}{s^2 + 2\xi\omega_n s + \omega_n^2}\right] = \frac{\omega_n}{\sqrt{1-\xi^2}}e^{-\xi\omega_n t}\sin(\omega_r t), \tag{A.2}$$

where,

$$\omega_r = \omega_n\sqrt{1-\xi^2}. \tag{A.3}$$

And,

$$\mathcal{L}^{-1}\left[\frac{\omega_n^2}{s(s^2 + 2\xi\omega_n s + \omega_n^2)}\right] = 1 - \frac{1}{\sqrt{1-\xi^2}}e^{-\xi\omega_n t}\sin(\omega_r t + \phi), \tag{A.4}$$

where,

$$\phi = \tan^{-1}\left(\frac{\sqrt{1-\xi^2}}{\xi}\right) \qquad \forall(0 \leq \xi \leq 1), (0 \leq \phi \leq \pi/2). \tag{A.5}$$

Therefore,

$$\Delta\omega(t) = \frac{P_{step}R}{DR + K_m}\left[1 + \frac{e^{-\xi\omega_n t}}{\sqrt{1-\xi^2}}\left(\omega_n\tau_r\sin(\omega_r t) - \sin(\omega_r t + \phi)\right)\right]. \tag{A.6}$$

Equation (A.6) can be further simplified to:

$$\boxed{\Delta\omega(t) = \left(\frac{P_{step}R}{DR + K_m}\right)\left[1 + \alpha e^{-\xi\omega_n t}\sin(\omega_r t + \phi')\right]}. \tag{A.7}$$

A.2 Steady state frequency

The determination of the steady state frequency is quite straightforward from equation (2.20a) when $s = 0$ ($P_{sp} = 0$):

$$\boxed{\omega_{ss} = \lim_{t\to+\infty}\Delta\omega(t) = \lim_{s\to 0}\Delta\omega(s) = \frac{RP_{step}}{DR + K_m}} \tag{A.8}$$

A.3 The maximal frequency gradient

To obtain the frequency slope one must derive equation (A.6) as follows:

$$\begin{aligned}\frac{d\Delta\omega}{dt} = {} & \frac{P_{step}R\omega_n}{DR + K_m}\frac{e^{-\xi\omega_n t}}{\sqrt{1-\xi^2}} \\ & \left(\tau_r(\omega_r\cos(\omega_r t) - \xi\omega_n\sin(\omega_r t)) - \sqrt{1-\xi^2}\cos(\omega_r t + \phi) + \xi\sin(\omega_r t + \phi)\right)\end{aligned} \tag{A.9}$$

To get the maximal frequency slope, equation (A.9) is evaluated for $t = 0$:

$$\frac{d\Delta\omega}{dt}|_{t=0^+} = \frac{P_{step}R}{DR + K_m}\frac{\omega_n}{\sqrt{1-\xi^2}}\left(\tau_r\omega_r - \sqrt{1-\xi^2}\cos(\phi) + \xi\sin(\phi)\right) \tag{A.10}$$

If ϕ we replaced in equation (A.10) for equation (A.5) and taking in to account that:

$$\sin(\tan^{-1}(x)) = \frac{x}{\sqrt{x^2+1}} \qquad \cos(\tan^{-1}(x)) = \frac{1}{\sqrt{x^2+1}}$$

$$\frac{d\Delta\omega}{dt}|_{t=0^+} = \frac{P_{step}R}{DR + K_m}\frac{\omega_n}{\sqrt{1-\xi^2}}\left(\tau_r\omega_r - \sqrt{1-\xi^2}\xi + \xi\sqrt{1-\xi^2}\right)$$

$$\boxed{\frac{d\Delta\omega}{dt}|_{t=0^+} = \frac{P_{step}R}{DR + K_m}\frac{\tau_r\omega_r\omega_n}{\sqrt{1-\xi^2}} = \frac{P_{step}R\tau_r\omega_n^2}{DR + K_m} = \frac{P_{step}}{2H}} \tag{A.11}$$

A.4 The frequency nadir

The time of the frequency nadir, t_z, is found when equation (A.9) is equal to zero. From equation (2.22), the derivative is expressed as follows:

$$\frac{d\Delta\omega}{dt} = \frac{P_{step}R\alpha\omega_n}{DR+K_m}e^{-\xi\omega_n t}\left(\sqrt{1-\xi^2}\cos(\omega_r t+\phi') - \xi\sin(\omega_r t+\phi')\right) \tag{A.12}$$

And according to [127]:

$$\frac{d\Delta\omega}{dt}|_{t=t_z} = -\frac{\alpha R\omega_n P_{step}}{DR+K_m}e^{-\xi\omega_n t_z}\sin(\omega_r t_z+\phi_1) = 0 \tag{A.13}$$

Equation (A.13) is equal to zero when the sinus passes through zero:

$$t^z = \frac{n\pi-\phi 1}{\omega_r} \tag{A.14}$$

For $n=0$:

$$\boxed{t^z = -\frac{\phi_1}{\omega_r} = -\frac{1}{\omega_r}\tan^{-1}\left(\frac{\omega_r\tau_r}{1-\xi\omega_n\tau_r}\right) = \frac{1}{\omega_r}\tan^{-1}\left(\frac{\omega_r\tau_r}{\xi\omega_n\tau_r-1}\right)} \tag{A.15}$$

Therefore, the frequency nadir can be expressed in an analytical form evaluating equation (A.6) at t_z (eq: A.15) as follows:

$$\Delta\omega_{min} = \Delta\omega(t_z) = \frac{P_{step}R}{DR+K_m}\left[1+\frac{e^{-\xi\omega_n t_z}}{\sqrt{1-\xi^2}}\left(\omega_n\tau_r\sin(\omega_r t_z) - \sin(\omega_r t_z+\phi)\right)\right]$$

$$\Delta\omega_{min} = \frac{P_{step}R}{DR+K_m}\left[1+\frac{e^{\frac{\xi\omega_n\phi_1}{\omega_r}}}{\sqrt{1-\xi^2}}\left(\omega_n\tau_r\sin(-\phi_1) - \sin(-\phi_1+\phi)\right)\right]$$

$$\Delta\omega_{min} = \frac{P_{step}R}{DR+K_m}\left[1+\frac{e^{\frac{\xi\phi_1}{\sqrt{1-\xi^2}}}}{\sqrt{1-\xi^2}}\left(\omega_n\tau_r\sin(-\phi_1) - \sqrt{1-\xi^2}\cos(-\phi_1) - \xi\sin(-\phi_1)\right)\right] \tag{A.16}$$

$$\sin(-\phi_1) = \sin\left(\tan^{-1}\left(\frac{\omega_r\tau_r}{\xi\omega_n\tau_r-1}\right)\right) = \frac{\omega_r\tau_r}{\sqrt{\omega_n^2\tau_r^2-2\xi\omega_n\tau_r+1}}$$

$$\cos(-\phi_1) = \cos\left(\tan^{-1}\left(\frac{\omega_r\tau_r}{\xi\omega_n\tau_r-1}\right)\right) = \frac{\xi\omega_n\tau_r-1}{\sqrt{\omega_n^2\tau_r^2-2\xi\omega_n\tau_r+1}}$$

$$\boxed{\Delta\omega_{min} = \frac{P_{step}R}{DR+K_m}\left(1+e^{\frac{\xi\phi_1}{\sqrt{1-\xi^2}}}\sqrt{\omega_n^2\tau_r^2-2\omega_n\tau_r\xi+1}\right)} \tag{A.17}$$

Appendix B

Parametric analysis of the equivalent machine ROSFR model

This appendix includes a parametric analysis of the analytic expressions obtained with the equivalent machine ROSFR model by a numerical implementation. The base parameters of the test system, as selected in [127], are presented in table B.1.

Table B.1: Parameters for the equivalent machine model of the test system

Name	Variable	Value
Droop	R	0.05 pu
Inertia Constant	H	4.0 s
Response time	τ_r	8.0 s
Damping factor	D	1.0 pu
Fraction of the power without delay	F_H	0.3 pu
Mechanical power gain factor	K_m	0.95 pu

These parameters are in per unit. The frequency in hertz is obtained by multiplying the per unit angular speed ω with the nominal frequency f_0 (50 Hz).

$$f(t) = f_0(1 + \Delta\omega_{pu}(t)) \tag{B.1}$$

First of all, the model presented in section 2.3.2 is evaluated at different values of the disturbance power. The evolution of the frequency is computed with equation (A.6). Results are presented in figure B.1.

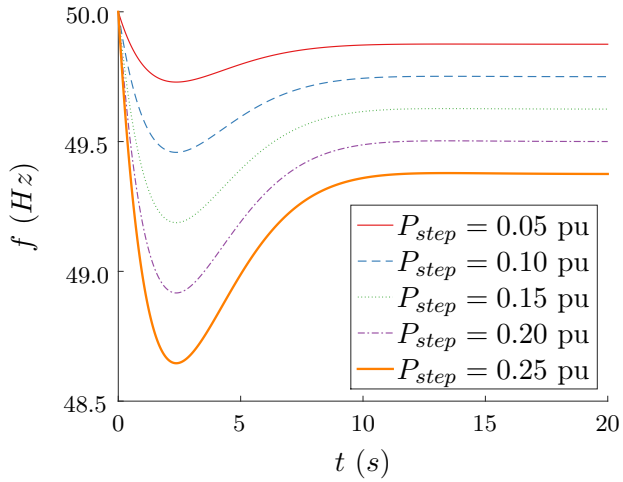

Figure B.1: Frequency for different disturbance power

It is observed that the time of the minimum (t_z) does not depend directly on the size on the disturbance (P_d), while the frequency nadir (f_{min}, eq. A.17), the steady state frequency (f_{ss}, eq. A.8) and the maximal gradient of the frequency drop (f_{slope}^{max}, eq. A.11) are linearly dependent of the size of the power imbalance, as shown in figure B.2.

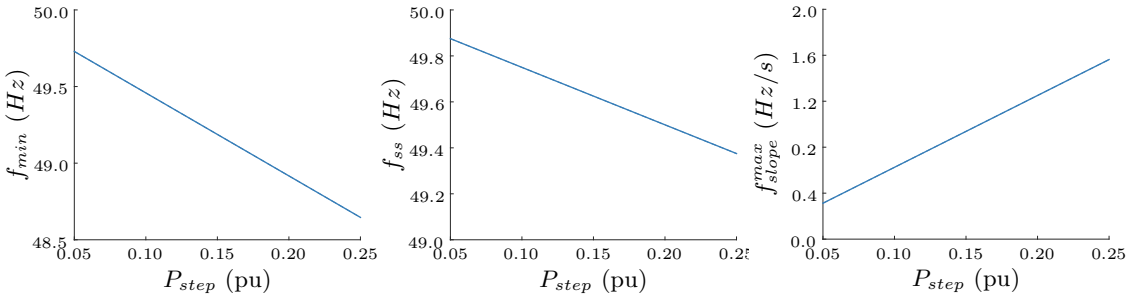

(a) f_{min} for different P_{step} (b) f_{ss} for different P_{step} (c) f_{slope}^{max} for different P_{step}

Figure B.2: Metrics of the frequency behaviour for different disturbance power

Figure B.3 illustrates the impact of different parameters of the equivalent system on the frequency nadir, when keeping all other parameters to the values specified on table B.1.

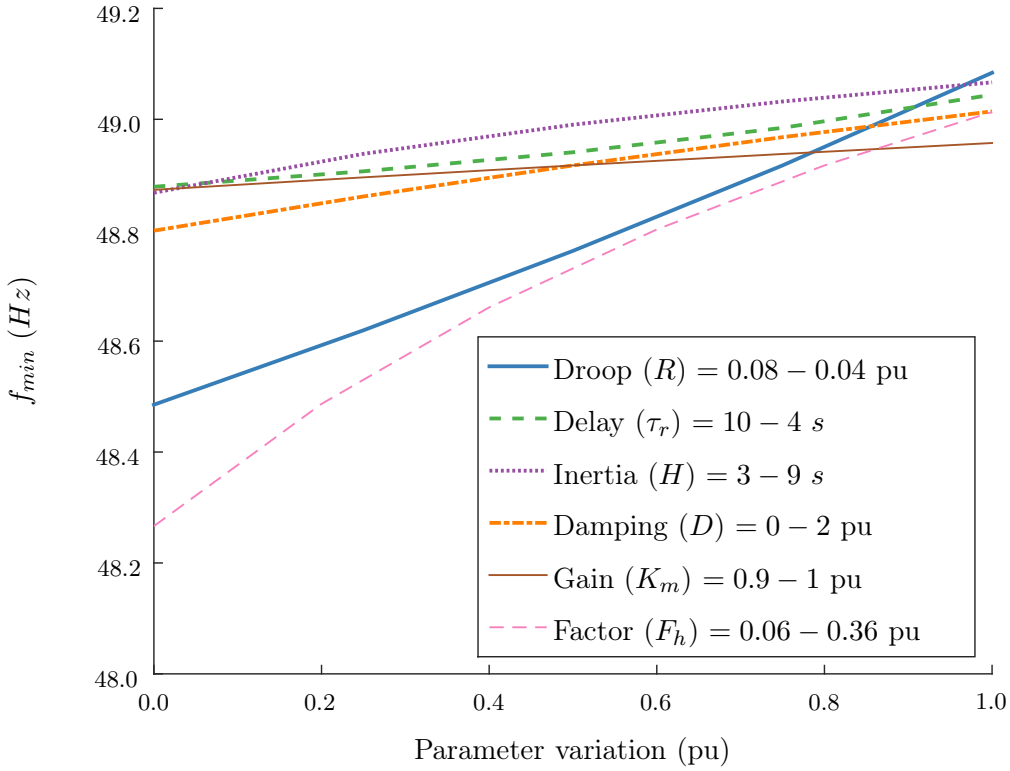

Figure B.3: Frequency nadir for different parameters variation for $P_d = 0.2$

The droop (R) and the F_h factor are the equivalent unit parameters with higher impact on the frequency nadir. For $F_h = 0$ the test system (parameters in table B.1) is badly damped, while it becomes overdamped for $F_h > 0.3655$ since $\xi > 1$. When this occurs the frequency response is not longer given by equation (A.6), but by a combination of exponentials:

$$\Delta\omega(s) = \left(\frac{\tau_1\tau_2 R\omega_n^2}{DR + K_m}\right)\left(\frac{(1+s\tau_r)P_{step}}{s(1+\tau_1 s)(1+\tau_2 s)}\right) \tag{B.2}$$

$$\Delta\omega(t) = \left(\frac{\tau_1\tau_2 R\omega_n^2 P_{step}}{DR + K_m}\right)\left[1 + \frac{\tau_1 - \tau_r}{\tau_2 - T1}e^{-t/\tau_1} + \frac{\tau_2 - \tau_r}{\tau_2 - T1}e^{-t/\tau_2}\right] \tag{B.3}$$

Alternatively, the mechanical power gain have a limited impact on the frequency nadir, therefore for the purpose of our study this parameter will be neglected $(K_m = 1)$. Finally, **the influence of the damping factor and the response time are comparable to that of the inertia constant**.

Appendix C

Limits of ROSFR models

This appendix includes a numerical implementation of the three considered ROSFR models to illustrate the impact of certain hypotheses. For this, let us consider a theoretical system of 10 identical thermal unit. Their parameters are presented in table C.1.

Table C.1: Parameters for the theoretical 10 units system

Name	Variable	Value
Maximal power	G^{max}	20 MW
Maximal reserve	$R^{pr,max}$	5 MW
Droop	R	5%
Inertia Constant	H	4.0 MWs/MVA
Lag time	τ_r	8.0 s
Lead time	τ_a	2.0 s
Mechanical power gain factor	K_m	1
Damping factor	D	2 %

It will be considered that the 10 units are supposed to supply a load of $180MW$ at a given time, and that the $N-1$ criteria must be respected, which means that the available reserve will be, at least, the capacity of the largest unit ($20MW$). If the production costs of all units are identical, it can be imagined that the scheduled power of each unit is $18MW$ (case 1). Finally, let us considered a sudden load increase of $20MW$.
The frequency evolution is computed in hertz using the equivalent machine ROSFR (EM-ROSFR) model and the multi-machine one (MM-ROSFR). As discussed in section 2.3.2, one of the drawback of the EM-ROSFR model is the calculation of the equivalent machine parameters. Here, all parameters, presented in table C.1 are maintained for the equivalent machine, except for the inertia constant. In deed, this can be done as long as all units are identical, for instance, the equivalent droop can be determined by (C.1) [85].

$$\frac{1}{R_{em}} = \sum_{j=1}^{N} \frac{1}{R_j} \tag{C.1}$$

while the equivalent inertia constant is calculated by (C.2).

$$H_{em} = \frac{\sum_{j=1}^{N} H_j S_{n,j}}{S_{em}} \tag{C.2}$$

Hence, an adjustment is done on the equivalent inertia with respect to the the base power of the system. If the units are considered to have a power factor of 0.8, their nominal apparent power ($S_{n,j}$) is set to 25 MVA, while the system base will be fixed to 200 MVA, such that the load increased is set to 0.1 pu and the damping factor is 1 pu. Therefore, for the EM-ROSFR model, $H_{em} = 5s$. Nevertheless, the time constants of the an equivalent lead-lag transfer function are more difficult to determine, reason why it is usually assumed that they are equal for all unit [85], which in practice is hardly the reality.
Simulation results are presented in figure C.1. The red curve represents the result of the EM-ROSFR model and the other two are obtained by the numeric integration of the MM-ROSFR model. The blue one considers that the response time of all units are the same, while the green dotted one considers that 5 units respond faster that the others. The time constant (initially fixed a 8 seconds), are set to 6 seconds for 5 unit and to 10 seconds for the remaining ones.

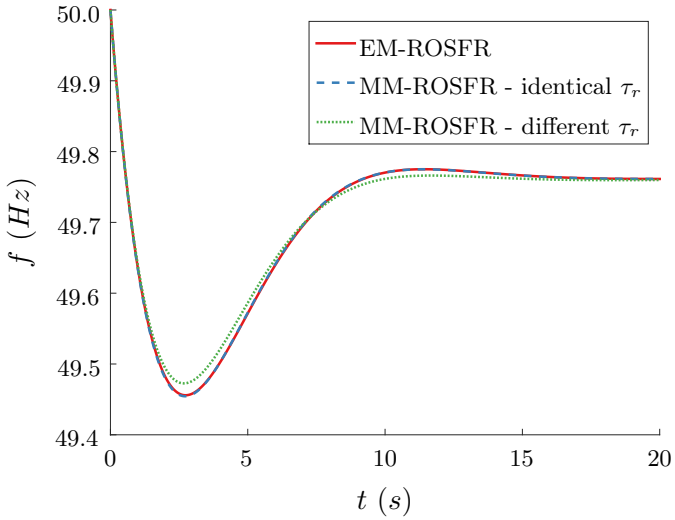

Figure C.1: Frequency for different ROSFR models

It is observed that for the case with identical time constants the curves of both models are overlapped. Therefore the EM-ROSFR model offered a good approximation of the average frequency response for a lower computational cost (0.25 ms vs. 150 ms[1]).

[1]Hp EliteBook Workstation, Intel Core i5, 2.8GHz with 16GB of RAM.

However, if the heterogeneous dynamic behaviour of different units are considered, the accuracy of the equivalent machine approximation is compromised. In addition, if the disturbance is a unit outage, instead of a load increase, the resulting system has a reduced inertia and loses the contribution of the faulted unit to the regulation process. Figure C.2 compares the frequency evolution for a load increase of $18MW$ $(0.9pu)$ and a unit outage.

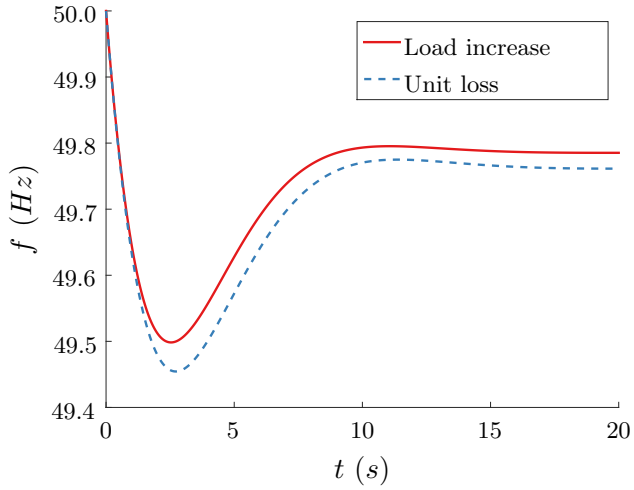

Figure C.2: Power output for different time constants

If the units have different sizes, inertia constant, and regulation parameters, this effect can be more or less important. This could be included in a EM-ROSFR model if the equivalent parameters are recalculated, however the issues of identifying the lead-lad time constants remains. Furthermore, until now all kind of saturation has been neglected. Figure C.3 shows the resulting output powers computed with the MM-ROSFR model when considering identical and differentiated time constants for a load increase on $20MW$.

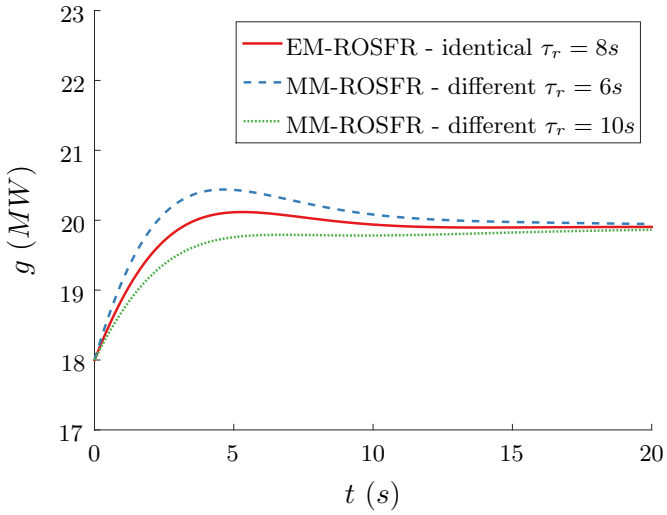

Figure C.3: Power output for different time constants

It is observed that in some cases the output power is greater than the capacity limit of the units ($20MW$). Figure C.4 illustrates the difference between the MM-ROSFR model, wiht and without capacity limits consideration.

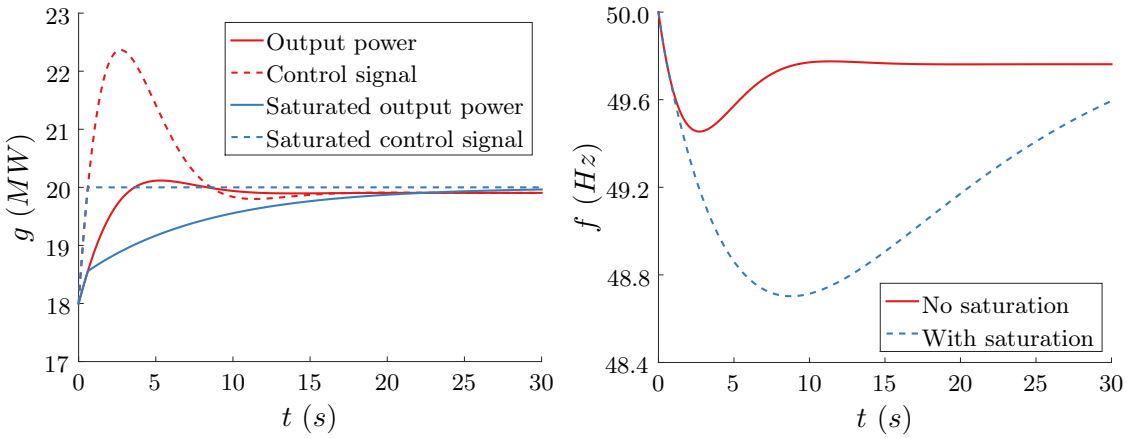

(a) Power output saturation (b) Frequency with saturation

Figure C.4: Effect of saturation in the MM-ROSFR model

The the saturation of the control signal in the frequency regulation have a significant impact on the frequency nadir, for the purposes of this study it can not be neglected. Finally, one can imagine that a certain set of 5 units are more expensive that the other 5 (case 2), such that the former set is scheduled to $16MW$, while the latter (base units) will be composed of units producing up to their capacity limit $20MW$. It must be noted that the two aforementioned constraint are respected, the produced total power is $180MW$, and the $N-1$ criteria is respected, and that, in general, the difference between case 1 and 2 can not be represented by the EM-ROSFR model. Figure C.5 compares the frequency trajectory for a load upset of $20MW$. It is shown that some risk may be overlooked.

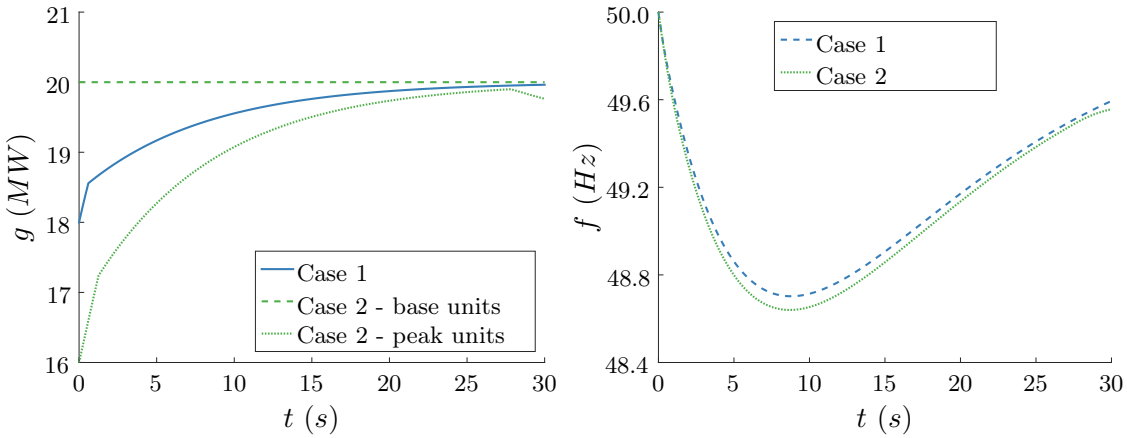

(a) Power output saturation (b) Frequency with saturation

Figure C.5: Effect of different initial dispatch in the MM-ROSFR model

Appendix D

Solution method of the implemented ROSFR model

D.1 The method - Explicit Euler

Let us consider a function $y : \mathbb{R} \to \mathbb{R}$ and its derivative $v : \mathbb{R} \to \mathbb{R}$.

$$\frac{dy(t)}{dt} = v\left(t, y(t)\right), \tag{D.1}$$
$$y\left(t_0\right) = y_0. \tag{D.2}$$

The interest is place on the temporal evolution of y in a time span of $[t_0, T_f]$. This time vector can be discretised in M intervals of length Δt. Then, the value of the solution at each point m can be found based on the values of y and h at $m-1$, such that:

$$y^{m+1} = y^m + \Delta t \times v\left(t^m, y^m\right) \qquad \forall m = 1 \ldots M-1. \tag{D.3}$$

where M is the size of the temporal discretisation vector, m is the index of the temporal discretisation, Δt is the numeric integration step in seconds, t_0 is the initial time of the numeric integration, and T_f is the final time of the numeric integration, both in seconds.

D.2 The swing equation

The kinetic energy stored on the system at specific time step h is is given by:

$$E_c = \sum_{j=1}^{N} \left(u_j^h H_j S_{n,j}\right) \tag{D.4}$$

where u_j is the binary variable defining the state of unit j (off-line= 0, on-line= 1), and E_c is kinetic energy of the system in Ws. Applying (D.3) to (2.19), the frequency evolution can be expressed as follows:

$$f^{m+1} = f^m + \Delta t \frac{f_0^2}{2E_c f^m} \left(\sum_{i=1}^{N} P_{m,j}^m - P_c^m \right) \tag{D.5}$$

D.3 The primary frequency regulation

In general, the units with the constructive capability of contributing to the primary frequency regulation respond to a proportional droop:

$$P_{m,j}(t) = P_{m0,j} - K_j \left(f(t) - f_0 \right) \tag{D.6}$$

where f_0 is the nominal frequency in Hz and K_j is the proportional controller gain of unit j in W/Hz, which is related to the power/frequency droop R in per unit, as follows:

$$K_j = \frac{G_j^{max}}{f_0 R} \tag{D.7}$$

which means that for a frequency droop of 4% and a nominal frequency $50Hz$, the regulation will ask for a deployment of half of the capacity of the unit. In general, some sort of saturation may be reached before.

The control dynamic

It is also possible to include the delay introduced by the control system:

$$X_j(s) = \frac{1 + \tau_{ac,j} s}{1 + \tau_{rc,j} s} \left(P_{m0,j} - K_j \left(f(s) - f_0 \right) \right) \tag{D.8}$$

where $\tau_{ac,j}$ is the lead phase of control system, $\tau_{rc,j}$ is the time constant of control system both in seconds, and X_j is the control signal of primary regulation proportional controller of unit j in watts. Then,

$$\Delta X_j(t) = X_j(t) - X_{0j} \tag{D.9}$$

$$\Delta P_{m,j}(t) = P_{m,j}(t) - P_{m0j} \tag{D.10}$$

$$\Delta f(t) = f(t) - f_0 \tag{D.11}$$

The time domain form of equation (D.8) can be rewritten as follows:

$$\Delta X_j(t) + \tau_{rc,j} \frac{d\Delta X_j(t)}{dt} = -K_j \left(\Delta f(t) + \tau_{ac,j} \frac{d\Delta f(t)}{dt} \right) \tag{D.12}$$

Applying (D.3) the primary frequency controller signal can be expressed as follows:

$$\Delta X_j^{m+1} = \Delta X_j^m + \frac{\Delta t}{\tau_{rc,j}} \left(-\Delta X_j^m - K_j \left(\Delta f^m + \tau_{ac,j} \frac{d\Delta f^m}{dt} \right) \right) \tag{D.13}$$

The derivative of Δf^m can be approximated as follows:

$$\frac{d\Delta f^m}{dt} = \frac{f^{m+1} - f^m}{\Delta t} \tag{D.14}$$

Finally,

$$\Delta X_j^{m+1} = \Delta X_j^m \left(1 - \frac{\Delta t}{\tau_{rc,j}}\right) - \Delta f^{m+1} \frac{K_j \tau_{ac,j}}{\tau_{rc,j}} - \Delta f^m \left(\frac{K_j \left(\Delta t - \tau_{ac,j}\right)}{\tau_{rc,j}}\right) \tag{D.15}$$

D.3.1 The primary driver dynamic

Analogously, the delay introduced by the primary driver system can be represented by a first order function.

$$P_{m,j}(s) = \frac{1 + \tau_{ag,j} s}{1 + \tau_{rg,j} s} X_j(s) \tag{D.16}$$

where $\tau_{ag,j}$ is the lead phase of primary driver system, and $\tau_{rg,j}$ is the time constant of primary driver system, both in seconds. In the same way, equation (D.8) can be rewritten in its time domain form:

$$\Delta P_{m,j}(t) + \tau_{rg,j} \frac{d\Delta P_{m,j}(t)}{dt} = \Delta X_j(t) + \tau_{ag,j} \frac{d\Delta X_j(t)}{dt} \tag{D.17}$$

And, after applying euler equation (D.3), the previous expression can be rewritten as:

$$\Delta P_{m,j}^{m+1} = \Delta P_{m,j}^m \left(1 - \frac{\Delta t}{\tau_{rg,j}}\right) + \Delta X_j^{m+1} \frac{\tau_{ag,j}}{\tau_{rg,j}} + \Delta X i^m \left(\frac{\Delta t - \tau_{ag,j}}{\tau_{rg,j}}\right) \tag{D.18}$$

Finally, the total power output of each unit at $t = \Delta t(m+1)$ can be found:

$$P_{m,j}^{m+1} = P_{m0,j} + \Delta P_{m,j}^{m+1} \tag{D.19}$$

D.4 The load damping

One way to represent the load dependency with frequency is presented in equation (D.20).

$$P_c(t) = P_{c0} \left(\frac{f(t)}{f_0}\right)^{\gamma} \tag{D.20}$$

where P_{c0} is the total power demand at nominal frequency in watts, and γ is the load frequency dependency factor. Then, the electric power demand is calculated step by step during the numeric integration process.

$$P_c^{m+1} = P_c^m \left(\frac{f^{m+1}}{f^m}\right)^{\gamma} \qquad \forall m = 1 \ldots M-1. \tag{D.21}$$

D.5 The Algorithm

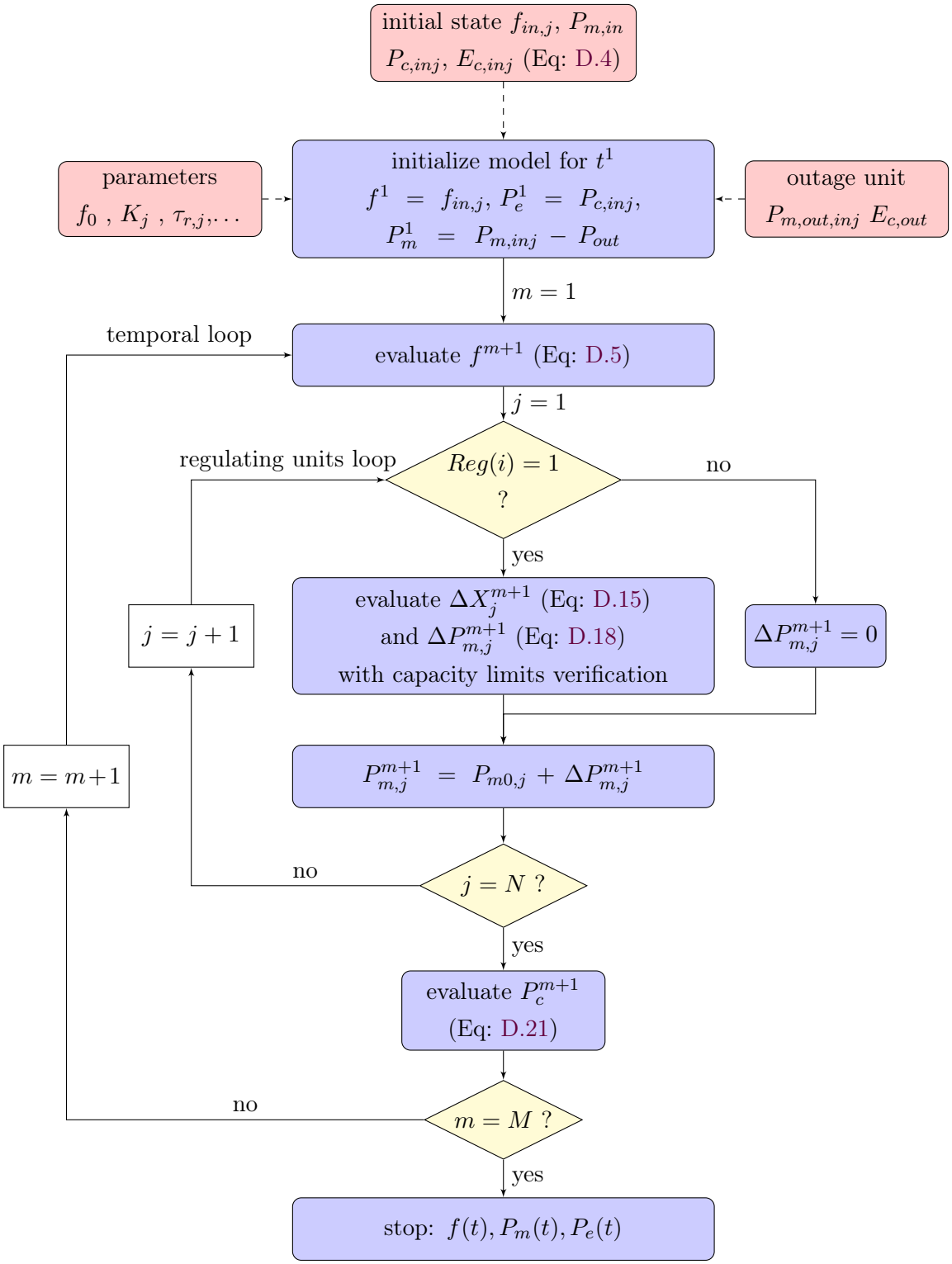

Appendix E

Test system

E.1 System load and parameters

A small power system with a peak load of 250 MW and 18 thermal units is considered. A one unique demand time series of 8760 hourly steps, showed in figure is used. It is built from historical measurement.

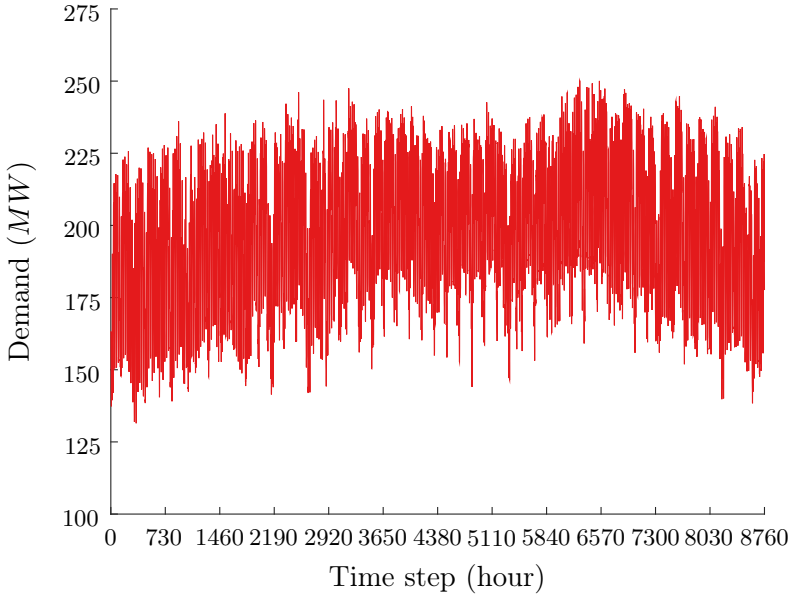

Figure E.1: Demand time series

The thermal mix is constituted by 4 coal units (base), 10 heavy fuel units (semi-base) and 4 diesel units (peaking). The static and dynamic parameters are detailed in tables E.1 and E.2 respectively. The generation park of the test system is inspired on existing units in different French Non Interconnected areas (ZNI, by its French acronym), to ensure representativeness of the results, but it does not correspond the energy mix of any real system.

Table E.1: Static parameters of the test system

Unit	G^{max} (MW)	G^{min} (MW)	$R^{pr,max}$ (MW)	R^{up} (MW)	R^{dn} (MW)	T^{up} (hours)	T^{dn} (hours)
1	40.60	27.0	5.00	27.0	27.0	2	2
2	40.60	27.0	5.00	27.0	27.0	2	2
3	17.56	12.6	4.39	12.6	12.6	2	2
4	17.56	12.6	4.39	12.6	12.6	2	2
5	17.56	12.6	4.39	12.6	12.6	2	2
6	17.56	12.6	4.39	12.6	12.6	2	2
7	17.56	12.6	4.39	12.6	12.6	2	2
8	17.56	12.6	4.39	12.6	12.6	2	2
9	11.90	5.0	2.50	6.9	6.9	2	2
10	11.90	5.0	2.50	6.9	6.9	2	2
11	29.50	12.0	4.00	17.5	17.5	2	2
12	29.50	12.0	4.00	17.5	17.5	2	2
13	35.50	15.0	4.00	20.5	20.5	2	2
14	34.00	20.0	3.40	20.0	20.0	2	2
15	19.60	10.0	6.00	10.0	10.0	1	1
16	27.00	7.0	6.00	20.0	20.0	1	1
17	40.00	10.0	6.00	30.0	30.0	1	1
18	40.00	9.0	6.00	31.0	31.0	1	1

Table E.2: Dynamic parameters of the test system

Unit	S_n (MVA)	H (MWs/MVA)	R (%)	$\tau_{r,c}$ (s)	$\tau_{r,c}$ (s)	$\tau_{a,c}$ (s)	$\tau_{a,g}$ (s)	$Rate^{sec}$ (MW/s)
1	56.10	4.370	8	15.5	7.52	3.0	0.0	0.1015
2	56.10	4.370	8	15.5	7.52	3.0	0.0	0.1015
3	23.53	1.440	4	3.0	0.10	0.0	0.0	0.0439
4	23.53	1.440	4	3.0	0.10	0.0	0.0	0.0439
5	23.53	1.440	4	3.0	0.10	0.0	0.0	0.0439
6	23.53	1.440	4	3.0	0.10	0.0	0.0	0.0439
7	23.53	1.440	4	3.0	0.10	0.0	0.0	0.0439
8	23.53	1.440	4	3.0	0.10	0.0	0.0	0.0439
9	14.00	2.077	4	9.5	0.50	2.0	0.0	0.0298
10	14.00	2.077	4	9.5	0.50	2.0	0.0	0.0298
11	35.56	3.357	4	44.0	0.18	51.0	0.0	0.0492
12	35.56	3.357	4	44.0	0.18	51.0	0.0	0.0492
13	47.00	3.815	4	44.0	0.18	51.0	0.0	0.0592
14	47.00	3.815	4	5.0	0.10	0.0	0.0	0.0567
15	29.40	7.170	4	2.5	0.20	0.0	0.0	0.0490
16	36.00	1.020	4	0.85	0.10	0.0	0.0	0.0675
17	50.40	1.265	4	1.2	0.10	0.0	0.0	0.1000
18	52.50	5.600	4	7.5	0.50	2.0	0.0	0.1000

E.2 PV integration scenarios

A unique hourly stepped load factor time series is used, which is built from normalized measurement of more than a hundred facilities in a DOM (French over sea territories). This curve is presented in figure E.2.

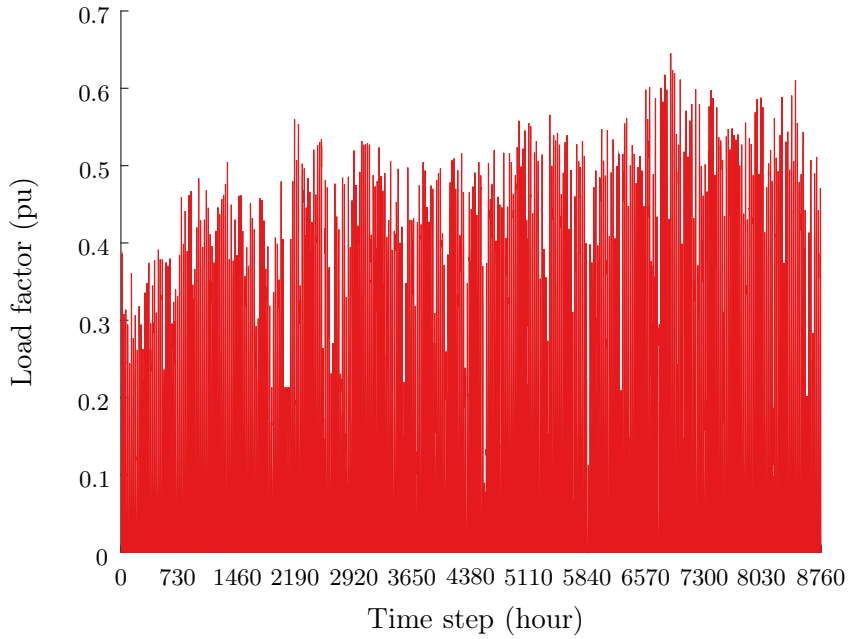

Figure E.2: PV load factor time series

Appendix F

Test system primary reserve deployment

This appendix includes a comprehensive analysis of the primary reserve deployment of the different regulating units of the test system detailed in appendix E, following the contingency considered in section 2.4.2. The load is considered to be 214.6MW (week day at 13 h, see figure 2.10). The outage of unit 1 (27MW) is simulated, when considering that schedule presented in figure 2.19a. Results are recalled in figure F.1.

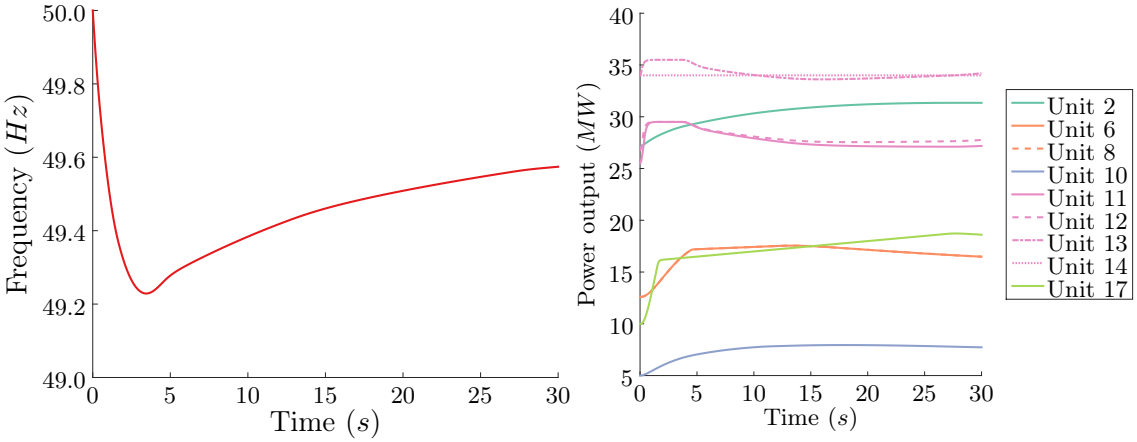

(a) Frequency response after the outage of unit 1 (b) Primary reserve deployment (week day)

Figure F.1: Deployment of the frequency containment reserve

It is observed that each unit exhibits a specific dynamic when deploying the primary reserve, depending on the parameters used to model the regulation response. Let us consider first units 2 and 10. Their response follows a classical first order shape. Looking at table E.2 it can be noted that they are dominated by relatively high lag time constants, while their lead phase is quite low ($\tau_a \leq 0.2\tau_r$). In addition, as showed in figure F.2, they do not reach any power output saturation, because they have enough head room capacity.

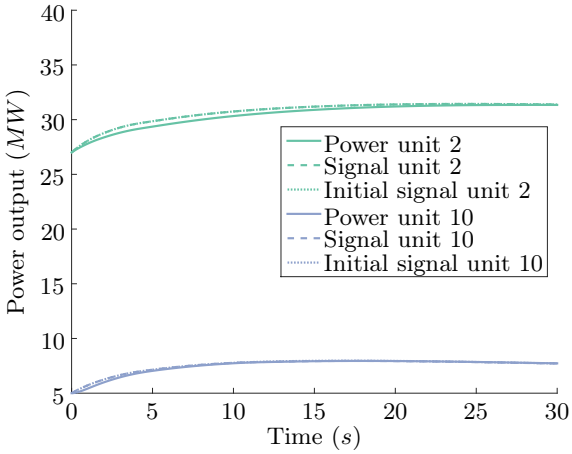

Figure F.2: Deployment of the primary reserve of units 2 and 10

Secondly, attention will be place on units 6 and 17. Looking at table E.2 it is noted that they have no lead constant, and they exhibit a behaviour typical of second order systems. This means, they are characterized by an zero initial tangent and they are faster than the former units. However, any overshoot is prevented by the saturation of the regulation when the maximal allocated primary reserve is reached as illustrated in figure F.3. The “initial" signal represent the unsaturated theoretical power reference send by the regulation of the actuators of the turbine.

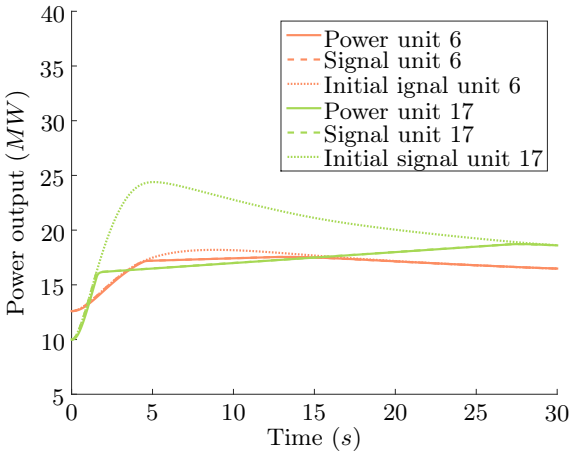

Figure F.3: Deployment of the primary reserve of units 6 and 17

Once the primary reserve saturation is reached, the output power can continue to increase following a linear ramp, which is fixed to $0.1MW/s$ for unit 17. Once the initial signal decreases the output power and the frequency stabilises. Finally, let us analyse the regulation characteristic of the base coal units. Looking at table E.2, one can observe that the lead time constant is higher than the lag time. The impact of this parameter on the power output can be analysed from figure F.4.

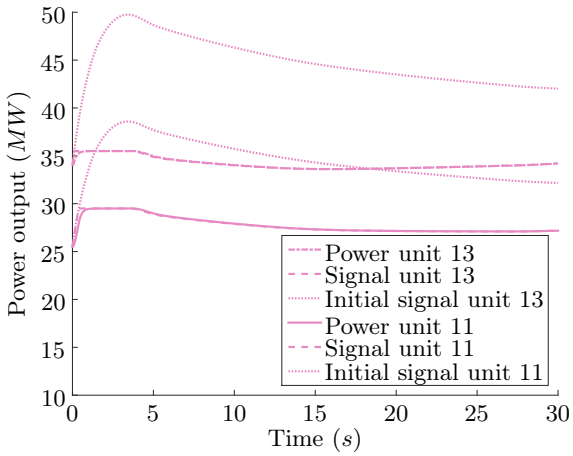

Figure F.4: Deployment of the primary reserve of base coal units

It is observed that these units stop participating to the frequency regulation faster than the others. In fact, the primary frequency control is mainly a proportional controller, which makes the control signal to evolve linearly with the frequency deviation. In this work, the units are also equipped with a lead-lag controller. This means that the control signal will also depend on the frequency gradient (see equation D.15). The idea is to reduce the action of the droop controller as the frequency drop slows down.

The coal units of the test system have a high lead time constant, therefore, when the gradient of the frequency becomes positive, and the frequency deviation has been reduced to some extend, the derivative component of the controller becomes larger than the proportional part ($\tau_a \frac{d\Delta f^m}{dt} \geq \Delta f^m + Const$). This makes the primary regulation process to stops, since the nadir has been reached.

Appendix G

Review of the frequency constrained economic dispatch problem

In [144] this kind of approach was considered for the Crete power system, where the dynamic constraints were deduced from a set of 15.000 operating points (600 load levels and 25 reserves levels) using a decision tree algorithm (DT). Complete dynamic simulation of two types of disturbance were performed: the outage of the largest/more loaded unit and a three-phase short circuit at a critical bus. The learning set included 24.000 dynamic simulations that allowed the identification of 15 attributes for a system of 7 equivalent units, given by the generation and reserve level of each unit and the total reserve level.
The constraint sets were built by looking into the chain rule that led to secure operation. Secure operation was declared if the minimal frequency following disturbance was above a certain threshold ($49Hz$). Then, the power and reserve limits of each unit, as well as the total reserve requirement, were adjusted to respect security limits deduced from the decision tree. For example, the reserve requirement and limits presented in equations (2.12), (2.6) and (2.8) were rewritten as follows:

$$\begin{aligned} R_{pr}^{min}(DT) &\leq \sum_{j=1}^{N} r_j &&\leq R_{pr}^{max}(DT), \\ R_j^{min}(DT) &\leq r_j &&\leq R_j^{max}(DT), \\ G_j^{min}(DT) &\leq g_j &&\leq G_j^{max}(DT). \end{aligned} \tag{G.1}$$

Where g_j is the power output of each unit j. The limits R_{pr}^{min}, R_{pr}^{max}, R_j^{min}, R_j^{max}, G_j^{min} and G_j^{max} are taken from the chain rule leading to secure leaves in the decision tree.
A different version was proposed in [59] for the Irish system. In this case, a simplified dynamic model was used and only unit outages were considered, which allowed approximating the set of dynamic constraints in terms of the power output of the unit lost and the reserve allocated in the remaining (*surviving*) units.

Then, two types of constraints were added to the ED model: one for limiting the maximum rate of change of frequency ($ROCOF^{max}$) and the other one for limiting the maximum frequency drop (f_{min}). Secure operation was declared if the minimal frequency following unit outage was above a certain threshold ($49,3Hz$) and if the $ROCOF$ following a unit outage was slower that $0,25Hz/s$.

The first set of constraints was imposed on the kinetic energy provided by the surviving conventional units (KE_j), following each possible contingency (outage of unit k) as a function of the specified $ROCOF^{max}$. The load contribution to the system kinetic energy (KE_L) was considered known.

$$\sum_{\substack{j=1 \\ i\neq k}}^{N} KE_j \geq \frac{f_0}{2ROCOF^{max}} g_k - KE_L \qquad \forall k, i = 1, \dots N. \tag{G.2}$$

Hence, with certain simplifications on the dynamic model, the $ROCOF$ constraint has been approximated by a set of linear relations. However, the constraint for minimal frequency is still non-linear. To circumvent this problem a database was built, this time 20.000 dynamic simulations were carried out for different sizes of contingency, load and reserve values. Then, the kinetic energy was altered through an iterative process until the desired dynamic performance was achieved. In the simplified dynamic model the load response to the frequency drop was supposed known (2.5% for $1Hz$). Finally, linear coefficients were found by minimising the error between linear approximation and actual data.

A set of linear constraints was written once more for the system post-contingency kinetic energy as a function of the power output of each unit (possible contingency g_k), the reserve allocated in the remaining ones (r_j), the load level (D) and a constant as follows [59]:

$$\sum_{\substack{j=1 \\ j\neq k}}^{N} KE_j \geq C_{i,1}D + C_{i,2}g_k + C_{i,3}\sum_{\substack{j=1 \\ j\neq k}}^{N} r_j + C_{i,4} \qquad \forall k = 1, \dots N, \forall i = 1, \dots I. \tag{G.3}$$

In the proposed model C is a 5×4 matrix, which means that the minimum frequency constraint for each possible contingency (k) is approximated by five separated four-dimensional linear functions. This model provided an interesting linear constraint over the maximal initial gradient of frequency ($ROCOF^{max}$) shown in equation (G.2). Moreover, the minimal frequency constraint accounts for load response to avoid primary reserve over-scheduling, the decision variable defining the size of the worst possible contingency (g_k) and the reserve allocation (r_j) in the post-contingency system. However, as aforementioned, this coefficient may need to be recalculated as the power system evolves.

Moreover, the constraints are expressed as a function of the kinetic energy of the system

in the post-contingency state, but this value is actually a function on the inertia constant (H) and nominal apparent power (S_n) of on-line units, which are set values for the ED model. If not enough inertial resource was committed in the scheduling process, the only possible actions at the ED level are to reallocate the reserve or to limit the possible worst contingency (g_k), which means, limiting the power output of every single unit. This could generate a really expensive or even infeasible dispatch. A more suitable approach would be the inclusion of this kind of constraint in the UC model, to allow the commitment of additional units when more inertial response is required to avoid load shedding, as was modelled in this, and other more recent works [89, 190]. Finally, the impact of this kind of constraint on the scheduling cost will be further discussed.

université PARIS-SACLAY | ÉCOLE DOCTORALE Physique et ingénierie : électrons, photons, sciences du vivant (EOBE)

Titre: Optimisation de la sûreté d'un système électrique en présence des énergies renouvelables intermittentes

Mots clés: Régulation primaire de fréquence, placement de production, PLNE, décomposition de Benders, méthodes de plans sécants.

Résumé: Le placement de production (UC pour *Unit Commitment*) est une famille de problèmes d'optimisation qui déterminent l'état et la puissance de consigne des groupes de production pour satisfaire la demande électrique à moindre coût.
Cette thèse définit formellement une sous-famille des problèmes UC : le problème FCUC (*Frequency Constrained Unit Commitment*) qui vise à maintenir la fréquence au-dessus d'un certain seuil, et éviter ainsi le délestage, en ajoutant un ensemble de contraintes de sécurité « renforcées ».

1. La formulation du problème FCUC a été définie grâce à une étude de la relation entre la fonction du creux de fréquence et les variables de décision du problème UC.
2. En second lieu, l'impact des ENR variables sur la régulation primaire de la fréquence a été étudié, ce qui met en évidence le besoin de formuler des modèles de FCUC plus fidèles.
3. Par la suite le coût, les bénéfices et les limitations des modèles FCUC simplifiés ont été étudiés. La nécessité de nouvelles méthodes pour prendre en compte la contrainte sur le creux de fréquence est mise en avant.
4. Enfin, une nouvelle formulation du problème FCUC a été proposée suivant une approche de décomposition qui offre des résultats plus performants que ces prédécesseurs en termes d'optimalité et efficacité.

Title: Optimisation of power system security with high share of variable renewables.

Keywords: Primary frequency regulation, unit commitment, MILP, Benders' decomposition, cutting plane methods.

Abstract: The Unit Commitment problem (UC) is a family of optimisation models for determining the optimal short-term generation schedule to supply electric power demand.
In this work we address a subfamily of this problem, called the frequency constrained UC problem (FCUC), which aims to keep the frequency above a certain threshold in order to avoid load shedding.

1. First, we attempt to formulate the frequency minimum constraint for the FCUC problem by examining the relation of the frequency and the decision variables of the UC problem.
2. Second, we investigate the impact of V-RES sources on the primary frequency response. We highlight the need and challenges of formulating more accurate FCUC models.
3. Third, we examine the cost/benefit and limitation of simplified FCUC models based on indirect constraints over certain dynamic parameters of the generating units. We show the need for new methods to properly handle the frequency minimum constraint in order to ensure optimality, without compromising tractability.
4. Finally, we propose a new formulation of the FCUC problem following a decomposition approach, which reaches a better trade-off between cost and risk.

Université Paris-Saclay
Espace Technologique / Immeuble Discovery
Route de l'Orme aux Merisiers RD 128 / 91190 Saint-Aubin, France